Technical Report Documentation Page

1. Report No.	2. Government Accession No.	3. Recipient's Catalog No.
FHWA/TX-06/0-4470-2		

4. Title and Subtitle	5. Report Date
Development Of Design Criteria For CCTV Camera Poles	September 2005
	6. Performing Organization Code

7. Author(s)	8. Performing Organization Report No.
Ali Abolmaali, Siamak Ardekani, and Jiwon Jung	0-4470-2

9. Performing Organization Name and Address	10. Work Unit No. (TRAIS)
Structural Engineering Laboratory and Structural Simulation Laboratory Department of Civil and Environmental Engineering The University of Texas at Arlington 416 Yates St. Arlington, Texas 76019	11. Contract or Grant No. Research Project 0-4470

12. Sponsoring Agency Name and Address	13. Type of Report and Period Covered
Texas Department of Transportation Research and Technology Implementation Office P. O. Box 5080 Austin, TX 78763-5080	Technical Report February 2003 - August 2005
	14. Sponsoring Agency Code

15. Supplementary Notes

Project performed in cooperation with the Texas Department of Transportation and the Federal Highway Administration

16. Abstract

Abstract: Design equations for steel and FRP CCTV camera poles are developed using full scale experimental testing and detailed finite element model analyses.

17. Key Word	18. Distribution Statement
Key Words: Tapered Poles, CCTV, Steel Poles, FRP Poles.	No restrictions. This document is available to the public through the National Technical Information Service, Springfield, Virginia 22161, http://www.ntis.gov

19. Security Classif. (of this report)	20. Security Classif. (of this page)	21. No. of Pages	22. Price
Unclassified	Unclassified	182	

DEVELOPMENT OF DESIGN CRITERIA FOR CCTV CAMERA POLES

by

Ali Abolmaali, Ph.D., P.E.
Research Supervisor

Siamak Ardekani, Ph.D., P.E.
Researcher

and

Jiwon Jung, Ph.D.
Research Associate

Structural Engineering Laboratory
and
Structural Simulation Laboratory

Technical Report 0-4470-2

Research Project Number 0-4470
Project Title: Development of Standard CCTV Camera Structures

Performed in cooperation with the
Texas Department of Transportation
and the
Federal Highway Administration

September 2005

Department of Civil and Environmental Engineering
The University of Texas at Arlington
Arlington, Texas 76019

ACKNOWLEDGEMENTS

The authors would like to express their sincere gratitude to the Texas Department of Transportation for their financial support of this study. The authors also wish to thank Tom Yarbrough (Project Coordinator), Ronald Medlock (Project Coordinator), Jim Yang (Project Director), and Charles Koonce (Project Monitoring) of the Texas Department of Transportation who were involved with this project and provided invaluable assistance. The support of the Department of Civil and Environmental Engineering at The University of Texas at Arlington (UTA) is greatly appreciated. In addition, the authors wish to thank JEM Engineering of Tulsa, OK and Shakespeare Composite Inc. of Newberry, SC for providing the steel and fiber reinforced polymer poles test specimens, respectively.

August 24, 2005

ABSTRACT

This study presents the development of three-parameter load-deflection models for steel and FRP poles commonly used to support closed circuit television cameras. An experimental investigation is carried out to obtain static load-deflection characteristics of tapered octagonal steel cross section and circular FRP cross section poles. Numerical results generated from three-dimensional isoparametric finite element model (FEM) considering coupled nonlinear algorithms for material, geometric, contact, and pre-tensioning effects are compared with those obtained experimentally. Eight-node elsto-plastic solid element is employed to model the pole, end-plate, bolts, concrete base, and laboratory reaction floor. The laboratory reaction floor is modeled with a thick plate having infinite stiffness. The pre-tensioning effect is modeled by using a pre-tension element. A surface-to-surface contact algorithm is used to simulate the interaction between contact surfaces of bolt head, shank, and nut with end-plate and bolt holes. Newton-Raphson scheme is used in the nonlinear regime, and convergence is checked using Hilbert L-2 norm and energy-based convergence.

A parametric study is conducted to verify the validity of the FEM and the analysis algorithms by observing the effects of the geometric and force-related variables, one at the time, on the load-deflection characteristics of the poles. The three-parameter power model is selected to mathematically model the load-deflection of the hollow poles. For this, two matrices of test cases are developed for steel and FRP poles by varying their geometric and force-related variables within their practical ranges. The load-deflection plots obtain from the FEM analysis of the aforementioned test case are fitted to the three-parameter power model and the three parameters of ultimate load, reference plastic deflection, and rigidity parameter are determined. Nonlinear regression analyses are conducted to obtain prediction equations for the parameters of the three-parameter power model in terms of the pole's geometric variables. To obtain a reasonable value for coefficient of multiple determination, R^2, for the rigidity parameter, a "characteristic load" concept is proposed. The predicted load deflection

plots are compared with these of experiments and FEM results. Error band and sensitivity analyses are conducted to check equations' accuracy and parameter sensitivity, respectively.

TABLE OF CONTENTS

LIST OF ILLUSTRATIONS

LIST OF TABLES

Table Page

CHAPTER 1
INTRODUCTION

1.1 Introduction

In recent years there has been a considerable increase in the use of tapered steel and fiber reinforced polymer (FRP) poles in structural engineering applications. This is primarily due to their superior material properties such as light weight and corrosion resistance. It is anticipated that the use of steel and FRP as structural components will increase as more knowledge of their structural performance is obtained and design guidance is developed.

One of the applications of steel and FRP hollow poles is in poles supporting Closed Circuit Television (CCTV) cameras. These poles are commonly installed on interstate highways and bridges, which are one of the key parts of an intelligent transportation system. Many states have begun to use CCTV cameras to aid in the efficiency of their respective highway systems. These camera systems would make it possible for departments of transportations to capture transportation related information for viewing in transportation management centers where this information is shared with both the public and private sectors in order to increase the mobility, safety, and efficiency of the transportation system. The poles must be designed to minimize vibration and deflection.

The stiffness and strength of supporting poles are important parameters for stabilization of the images transmitted by the cameras. Wind induced deformation of each pole is a function of the pole's geometric variables and loading which vary immensely for different regions and applications. For example, commonly used tapered pole's height may vary from 20 ft (6.1 m) to 65 ft (19.8 m) depending on the applications, which in turn would cause variation of other parameters such as base diameter, top diameter, pole thickness, end-plate thickness, bolt diameter, etc. Also, the wind loads vary in different regions and sessions, and the bridge vibrations caused by vehicle traffic would effect poles' deflections and ultimately the images transmitted by

the cameras (McDonald et al., 1995). Thus, the stiffness and strength characteristics of the poles have been under scrutiny and the need for an in-depth investigation have been recognized by Texas Department of Transportation as reported by Abolmaali et al. (2004b).

Traditionally, CCTV cameras in use have been supported by wood, concrete, and steel. Recently Fiber Reinforced Polymer (FRP) poles have gained popularity (Lacoursiere, 1999). The main disadvantage of concrete poles is in their relative weight, which drastically increases transportation and erection costs. Chemical influences on the concrete surfaces due to environmental impact can also affect their long term performance. Also concrete poles are subjected to corrosion of the steel reinforcement, resulting in further deterioration which leads to expensive maintenance. However, steel poles are the most commonly used tapered poles on or at the vicinity of bridge and transportation infrastructures by the state Departments of Transportations (DOTs) in general, and Texas Department of Transportation in particular (Abolmaali et al., 2004b). California Department of Transportation has recently installed several FRP poles on its infrastructures at different locations. The understanding of stiffness and strength of steel and FRP poles has gained immense popularity among Department of Transportation officials, construction industry, and consumers (Ibrahim et al., 1999; Polyzois et al., 1999).

1.1.1 Characteristics of steel poles

Steel poles are commonly used nationwide in several regions for transportation infrastructure system, which are designed and manufactured to be equivalent in load carrying capacity to wood poles under National Electrical Safety Code Grade "B" criteria (IEEE, 2002). Figure 1.1 shows the typical steel poles in use. Some advantages of steel poles are as follows:

1) Design flexibility
2) High strength
3) Long life
4) Factory pre-drilling

5) Reduced maintenance costs

6) No damage due to woodpeckers, pole rot or fires

7) Aesthetically pleasing

8) Environmentally friendly, can be made from recycled steel

9) Superior life cycle costs compared to wood and concrete.

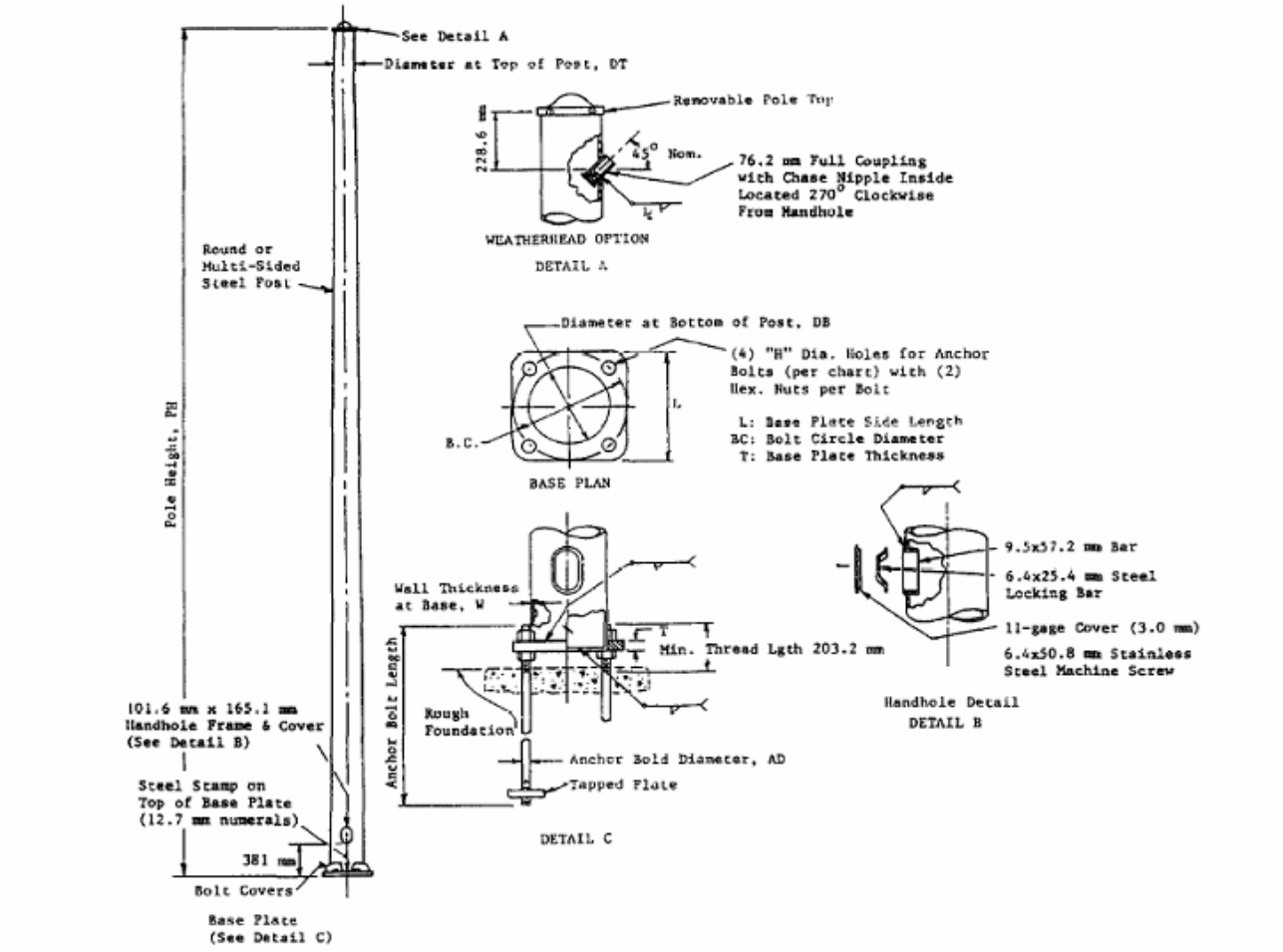

Figure 1.1 Typical signal pole supplied to NYSDOT

There are also some important environmental benefits associated with the steel poles among which are recyclables and no hazardous waste disposal or soil remediation costs are in forefronts. However, there are some concerns associated with the hot dipped galvanize coating applied to steel poles to protect it from corrosion. Some researcher

suggest that the galvanize coating degrade with time, and it can contaminate ground water. Galvanized steel will vary by the quality of the galvanizing, even the best quality may start to show rust after 5-7 years. As steel pole's weight increases the safety issue becomes more predominant over the other advantages. There are two incidences of steel pole collapse in the recent years in Central California and state of Wyoming due to strong wind.

Prediction of the fatigue life in poles under wind-induced vibration is a complex problem. Because of the relatively low stiffness and damping ratio of these structures, mild wind can cause significant vibration of the cantilever element, which causes variable-amplitude stresses to develop in the Pole. The vibration occur at relatively low wind speeds causing many cycles at moderate stress ranges to develop in a short period of time. It is possible that these poles are experiencing large numbers of cycles in a moderate wind speed. Research studies conducted by McDonald et al. (1995) indicate that the primary contributor to pole vibrations is galloping during the wind speeds in the range of 10-30 mph. Galloping is an aerodynamic phenomenon that causes the tip of the pole to displace vertically. The steel poles tend to vibrate predominately in the first mode as a single degree of freedom structure with the maximum displacement occurring at the tip of the cantilever.

1.1.2 Characteristics of FRP poles

The use of Fiber Reinforced Polymer-Composite material in civil infrastructure viewed as a potential solution to many civil engineering problems. Other incentives for using FRP Poles include the material's inherent high strength to weight ratio. According to a study conducted by The Federal Highway Administration's (FHWA) applied program for using composite materials in highway structures and the Civil Engineering Research foundation (CERF), FRP-Composite materials have the potential to be the civil engineering material of the twenty-first century. These materials have the potential to solve many of the problems that have plagued the civil structural engineer for a long time.

Structural components made of advanced composite materials offers several advantages which makes them as an interesting alternative over other traditional materials. Studies on the FRP composites concluded that composite materials make it possible to optimize the design of structures beyond strictly mechanical performance. Typical FRP poles used in industry are shown in Figure 1.2. Some advantages of FRP composite pole are as follows:

1) Light in weight
2) High strength to weight ratio
3) Reduction in transportation and construction cost
4) Corrosion Proof
5) Can be made stiffness tailored
6) Ease in Installation
7) No environmental issues
8) Aesthetically pleasing
9) No maintenance cost
10) Ease in foundation and erection

Composites encompass a wide range of materials where two or more, physically distinct and mechanically separable, components are combined together to form a new material which possesses properties that are notably different from those of its individual constituents. Composites, in general, are classified into particulate composites and fibrous composites. Historically, fibrous composites have been the predominant of the two categories. It is seen that fibrous composites have been used by nature since the creation of life form on earth, and by mankind since the first straw reinforced clay bricks were used for buildings.

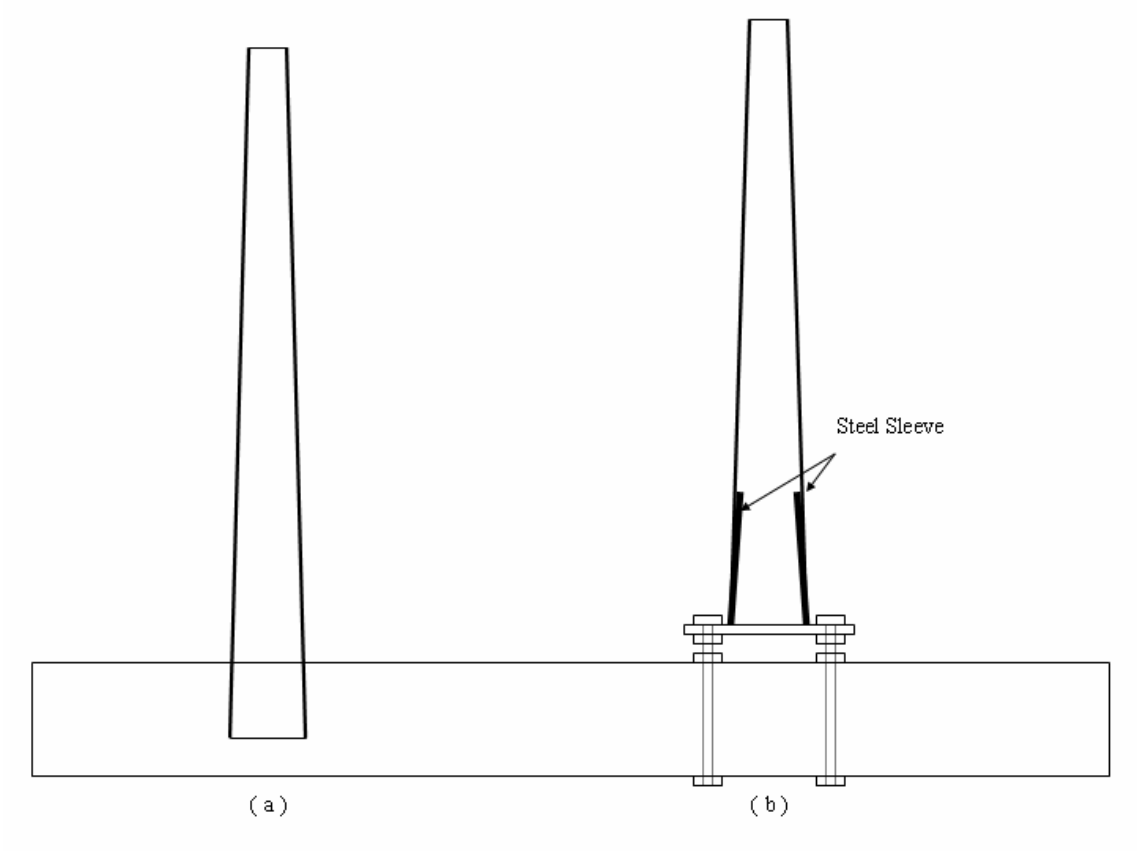

Figure 1.2 Typical Fiber Reinforced Polymer poles used in industry:
(a) Direct burial type; (b) Bolt connection type

1.2 Objectives and scope

Currently, there are no design guidelines and specifications for design of CCTV camera poles in the State of Texas. Thus, the main objective of this study aims at addressing the above needs by developing load-deflection model equations for typically used steel and FRP poles. To achieve this objective the following are at forefronts:

1) Static loading tests are performed on steel and FRP poles in order to obtain their load vs. deflection characteristics.
2) This model is analyzed using a coupled nonlinear algorithm which employs geometric, material, and contact nonlinearities.
3) Finite Element Method (FEM)-based model for steel and FRP poles are developed so as to compare the test results obtained from the experiments.
4) The experimental results are compared with the results of finite element studies conducted on the steel and FRP poles.
5) Practical range of possible geometric and force-related variables for the model poles are identified to be numerically tested using the FEM model.
6) FEM load-deflection analysis on the test cases selected is conducted.
7) Prediction equations for the load deformation characteristics of the steel and FRP poles are developed as a function of their geometric variables.
8) Error band and sensitivity analyses are conducted in order to observe the deviation of the predicted results from the actual values and examine whether the predicted equations correctly depict the behavior of the camera poles.

To achieve these objectives, full-scale experimental programs as well as numerical studies were performed on the tapered steel and FRP poles in this study. Geometric nonlinearity is considered and arbitrary large displacements, contact surface, and pretension load are included in the numerical analysis.

This study consists of five chapters. Chapter 1 is an introduction which presents the current circumstance of the research, literature review and objectives of the research. Chapter 2 describes the experimental test program of steel and FRP poles. These tests were conducted in the Engineering Laboratory Building at the University of

Texas at Arlington. Chapter 3 is dedicated to the finite element modeling which represents the specimens tested. Emphasis is placed on the effect of the bolt. This semi-rigid connection causes the structure to move in a more complicated manner. The mathematical representation of the contact between the surfaces is taken into account in the finite element model. Three-parameter power model equations are developed in Chapters 4 and 5 for load-deflection of both steel and FRP poles. Finally, in Chapter 6 the general conclusions and recommendations are presented.

1.3 Literature review

In an effort to provide an organized view of the previous literature available on the analysis and design of steel and FRP poles, this literature review is separated into two sections: steel and FRP pole, and bolted connection. The section on bolted connection is necessary since the connection of the pole to the end-plate and end-plate to concrete base is the same as those of beam-to-column and column-to-beam plate connections.

1.3.1 Steel and FRP poles

Several investigations on the steel and FRP poles have been performed to predict their load-deflection behavior. Single-pole transmission structures made of wood were studied by Vanderbilt and Criswell (1988). The analysis of the transmission poles utilized Newmark numerical technique for providing the exact solution to the differential equation for large deflections. A computer program was developed for the design and analysis of wood poles. Design equations based on the load resistance factor design (LRFD) format were presented.

Lin (1995) investigated the linear static analysis of taper FRP poles in terms of various material configurations, geometries, loading condition and boundary conditions. Large deflection analysis was also performed by the finite element model presented. In the linear static analysis, shear strains were not very significant if the pole was in bending, and the layer with the longitudinal fiber orientation would resist most of the load. This study found that the greater the taper ratio, the better the performance was in

the practical range, and fibers oriented at an angle (0 to 45 degree) with respect to the longitudinal direction resulted in economic design.

Kocer and Arora (1996, 1997) developed the optimal design process for steel transmission poles. The geometric properties such as outside diameter at the top of the pole, thickness of the first and second piece, and tapering of the pole were used for design variables. To conduct the design process, the design moment, compressive stress, bending stress, shear stress, and deflection were calculated. It was concluded that as the pole tapering increased other design variables decreased for the optimal design. This study also developed optimal design methods for standardization of steel poles which was developed by discretizing the design variables such as geometric dimensions of the poles, cross-sectional shape, material properties and steel grade, for the pole structure.

Dicleli (1997) investigated the optimum design of steel pole structures. Simple equations and charts for the design of tubular telescopic steel poles of various steel grade and length were automatically obtained by the developed program. The pole structures were considered to be subjected to concentrated loads and moments. The program used the unit dummy load method to determine the displacements of the structures.

Polyzois et al. (1998) investigated the dynamic analysis of tapered composite poles with hollow circular cross section produced by filament wound technique. The natural frequency and period were performed by modal analysis. An analytical model was developed with tapered beam elements including shear effects, which showed good correlation with the finite element results.

Polyzois et al. (1999) presented the results of twelve glass fiber reinforced plastic poles with various thickness and fiber orientations under cantilever loading. The objective of their study was to compare the analytical results obtained in the study to those of experiments in order to design a series of FRP poles with different safety factors. Modulus of elasticity, Poisson's ratio and shear modulus was calculated by the rule of mixture (Daniel and Ishai, 2005) and Tsai-Hahn approach. The correlation

between the analytical and experimental results was reasonable. It was concluded that a lower factor of safety of 4, can be used for the design of FRP poles.

Ovalization behavior of tapered fiber-reinforced polymer (FRP) poles was presented by Ibrahim and Polyzois (1999). The parameters used in the study were wall thickness and fiber angle. Brazier's modified equation was used to account for the orthotropic properties of FRP poles. This study concluded that the behavior of the FRP poles was non-linear and the critical ovalization load decreased with an increase in the fiber angle.

As a continuation of the work by Polyzois et al. (1999), Ibrahim et al. (2000) conducted twelve full-scale tests on tapered Glass Fiber Reinforced Plastic (GFRP) poles with hollow circular cross section subjected to cantilever bending. Those specimens were made of polyester resin reinforced with E-glass fibers by filament winding process. Theoretical models developed for evaluating the ultimate load was used to determine the optimal cross section of the poles. Fiber orientation and the number of layers were included in the parametric study.

1.3.2 Bolted connection

Limited number of literature exists on the experimental and finite element analysis (FEA) of tapered poles. However, the literature is rich for experimental testing and FEA of beam-to-column steel connection assembly which is similar in geometry and behavior to the pole's assembly. For example, in the testing for moment-rotation behavior of steel connection a beam is welded to an end-plate (or angles), which is bolted to column flange. This is similar to the pole assembly in which a pole is welded to an end-plate that is bolted to the concrete base.

An early study by Krishnamurthy et al. (1979) and Krishnamurthy (1980) presented the finite element modeling of bolted connections with varying geometric parameters, support conditions, loading sequence, and material properties. They also compared the results obtained from both 2- and 3-dimensional models.

Raj et al. (1987) conducted an analytical study of the behavior of the contact zone and pressure distribution between two circular flat plates connected by a circular

bolt. The analytical study included a parametric study. The parameters used in this study were as follows: elastic properties of bolt and materials, bolt head diameter and thickness of the plates. It was shown that the elasticity of the bolt and the thickness of the plates played an important role in the load transfer and the consequently the contact pressure distribution between the plates.

Stallings and Hwang (1992) presented a simple bolt pretension model in finite element analyses of bolted connections by using temperature changes for the bolts modeled with rod elements. They suggested that two methods presented could be used to produce the desired bolt pretensions without elaborate algorithms.

Kulak and Birkemoe (1993) conducted field studies on bolt pretension. This study showed that actual pretensions were 35% greater than specified minimum pretensions. Therefore, bolt pretension would be at least 70% of the ultimate tensile strength of the bolt known as proof load.

Choi and Chung (1996) investigated the effect of bolt pre-tensioning and the shapes of the bolt shank, head, and nut on the behavioral characteristics of the end-plate connections. In order for the model to simulate the interaction between the end plate and column flange, a contact algorithm with gap elements was employed.

Chutima and Blackie (1996) investigated the effect of pitch distance, row spacing, end distance and bolt diameter on composite laminate plate joints subjected to tensile loading to consider the effect on the local contact stress distribution.

Wanzek and Gebbeken (1999) emphasized the importance of through-thickness deformation in the analysis of steel end-plate connections by using three layers of elements through the thickness of the end-plate. The effects of friction and slip on the response of connections were also considered.

Yang et al. (2000) studied the effect of angle thickness of double angle connections subjected to axial tensile loads, shear loads, and the combined loads. The loads were increased monotonically and an elastic-perfectly plastic constitutive law was utilized. The force-displacement curves for axial loading and the moment-rotation curves for shear loading showed good correlation with those from the three-dimensional

finite element analysis (Yang, 1997). They concluded that the thickness of the angles had a huge influence on the response of the connection. The initial stiffness increased significantly as the angle thickness increased. The final portions of the curves were almost parallel, but the level of the load or moment increased greatly as the thickness of the angles was increased.

Bahaari and Sherbourne (2000) investigated nonlinear behavior of bolted connections considering plasticity of the material and changes in the contact area. They presented three-dimensional spar elements to model the bolt shank which were provided to find both the magnitude and distribution of the bolt force within the section. A325 slip critical bolts were used to assemble the connections. Pre-stressing of the bolt shanks was introduced by means of equivalent initial strain. It was shown that preloading was advantageous in improving connection stiffness and in maintaining relatively constant bolt stresses until yield occurred.

Harte and Cann (2001) used finite element analysis to determine the moment-rotation behavior of the pultruded fiber reinforced plastics beam-to-column connections. The model included bolted assembly, prestress forces and contact surfaces. They stated that the connection stiffness increase as the number of link elements increases, and the rotational stiffness was within 3% of the experimentally obtained. Because of plane elements used in the model of bolt, web cleats could not be considered. As a result it was suggested that a three-dimensional model of the connection use to be provided for both the flange and the web cleats.

Kishi and Yabuk (2001) used nonlinear finite element analysis to develop prediction equations based on the power model (Richard and Abbott, 1975; Kishi and Chen, 1990) for the top- and seat-angle connections. The power model contained the three parameters: initial connection stiffness, ultimate moment capacity, and shape parameter. All components of the model were completely independent from each other as assemblages in a real connection. Special attention was given to the bolts which were modeled with eight-node solid elements and divided to consider the effect of shank,

head and nut elements on connection behavior. Bolt pretension load was 70% of minimum tensile strength of bolt obtained from test data.

Citipitioglu et al. (2002) used parametric three-dimensional analysis of finite element studies to predict the overall moment-rotation response of partially-restrained bolted steel beam-to-column connections. It was shown that friction and slip in the model along with the simplicity of changing mesh geometry had more effect on the response of connections with higher moments and stiffer connecting elements. The effect of pretension of the bolts in the model was shown to be relatively important, which can vary the ultimate moment by 25 percent. Force-displacement curves were generated in terms of each bolt size and varying total plate thicknesses. Finally, a parametric study was conducted in order to investigate the effects of friction and pretension of the bolts on the connection behavior.

Gantes and Lemonis (2003) studied the impact of bolt length considered in the finite element model. They showed that the required correction in the bolt length is heavily dependent on both the applied preload level and the developed failure mechanism.

Komuro and Kishi (2003) derived the initial connection stiffness and the ultimate moment capacity of top- and seat- angle connections. Three specimens subjected to both monotonic and cyclic loading with different length of web-angle. It was concluded that the initial connection stiffness is evaluated by using the prediction equation and the ultimate moment capacity predicted was almost the same with the experimental result.

Gun (2004) evaluated a boundary element method for covering several types of elasto-plastic contact interface; infinite friction, frictionless and Coulomb friction.

Yorgun et al. (2004) presented finite element modeling of bolted connections by considering three-dimensional elements. Brick elements, Solid 45 in ANSYS (2004), were used in three-dimensional modeling of the structural components except for bolts which was modeled with Solid 92 elements. Material nonlinearity with strain hardening also was taken into account. Contact model was applied between contact pair surfaces

of all connecting elements: between the bolts, double channels, and the column section. These contact surfaces were meshed with contact element, CONTA 174 in ANSYS, and target elements, TARGE 170 in ANSYS. By considering experimental observations, the friction coefficient between steel contact surfaces was assumed as 0.2. Good correlation with test results was shown.

1.4 Chapter summary

The use of tapered steel and FRP poles in structural engineering applications has been increased in a few decades. It is because of their superior material properties over other traditional materials. Among the advantages of steel poles, the following are in forefront when compared to those of conventional concrete and wood: high strength; long lift; factory pre-drilling; reduced maintenance costs; no damage due to woodpeckers, pole rot or firs; aesthetically pleasing; environmentally friendly; usage of recycled steel; and superior life cycle costs compared. Some characteristics of FRP poles which are superior to those of steel are: light in weight; high strength to weight ratio; reduction in transportation and construction cost; corrosion proof; stiffness tailored capability; ease in installation; environmentally friendly; aesthetically pleasing; no maintenance cost; and ease in foundation and erection.

The deflection of the pole is the main concern and it is based on not only the stiffness of the pole, but also the overall load on the pole. These factors need to be taken into account in the design, installation, and implementation.

CHAPTER 2
EXPERIMENTAL PROGRAM

2.1 Introduction

This chapter presents the experimental testing program undertaken to study the load deformation behavior of tapered steel and FRP poles. Three full-scale experimental bending tests have been conducted on one tapered octagonal cross section steel poles, and two circular cross section FRP poles to identify the load deformation characteristics when subjected to monotonically increasing load.

The pole used in the laboratory was 20 and 25 feet long, the average pole being about 3 times this size, but these dimensions are sufficient for the task at hand. With the verification of a Finite Element Model (FEM) using these 20 and 25 feet poles, the application to poles with other geometric variables follows. These results would then represent what could be expected of other laboratory models, which will in turn allow for the development of a design criteria for steel and FRP poles in general.

To describe the testing program in detail, test specimens, test setup and testing procedure, instrumentation used, and the results are provided.

2.2 Experimental test specimens

The experimental portion of this research consists of cantilever testing of the tapered steel and FRP poles. This test is required in order to evaluate the strength and stiffness characteristics of the poles subjected to unidirectional loading. The configuration and dimensions of the specimens tested are shown in Figures 2.1 and 2.2 for steel and FRP poles, respectively.

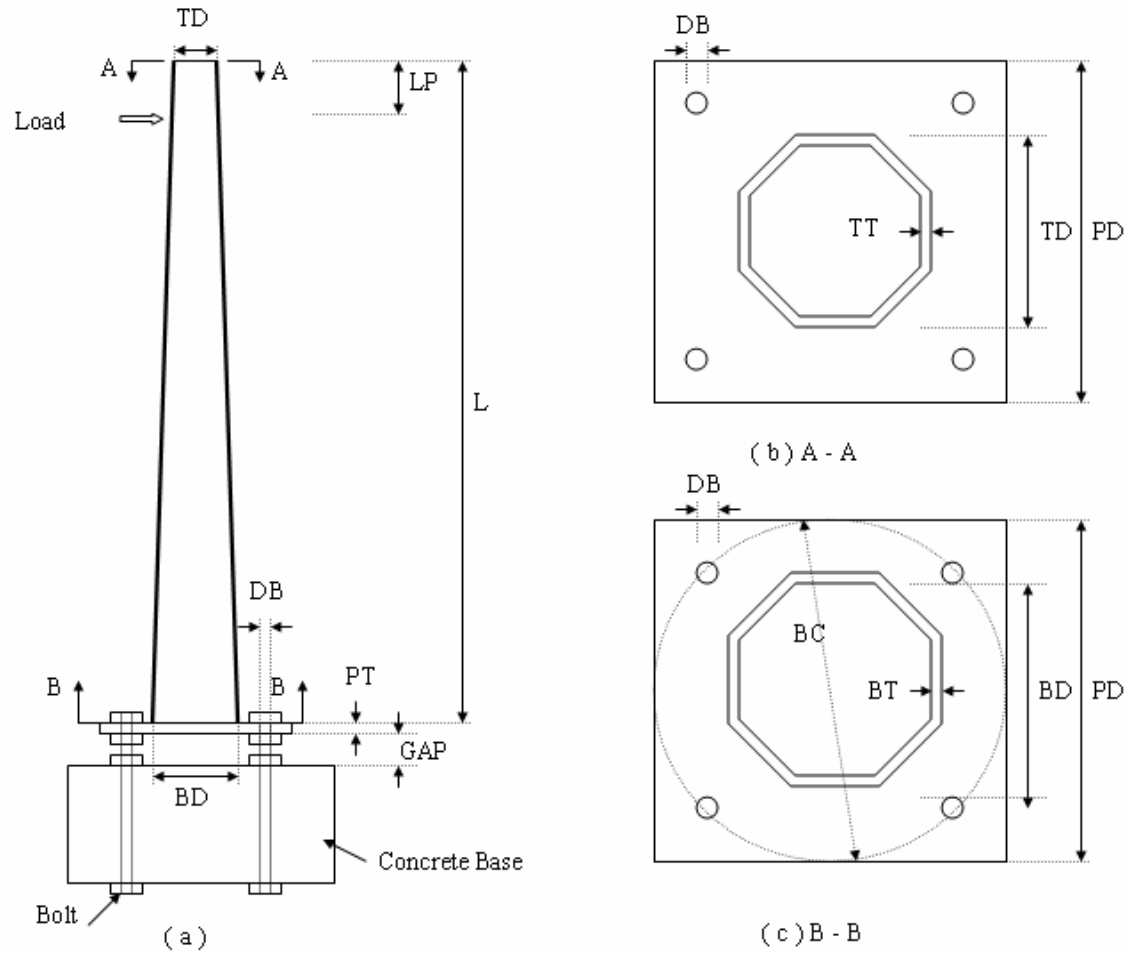

Figure 2.1 Dimensions of steel pole tested:
(a) Front view; (b) Section A-A; (c) Section B-B

The designation of the pole specimens is as follows: L, pole height; LP, height of loading point; TD, outer diameter at the pole's top; BD, outer diameter at the bottom of pole; DB, bolt diameter; BH, bolt hole diameter; TT, thickness at the top of pole; BT, thickness at the bottom of pole; PT, thickness of end-plate; PD, side length of square end-plate; BC, bolt circle diameter; LS, height of steel sleeve inserted.

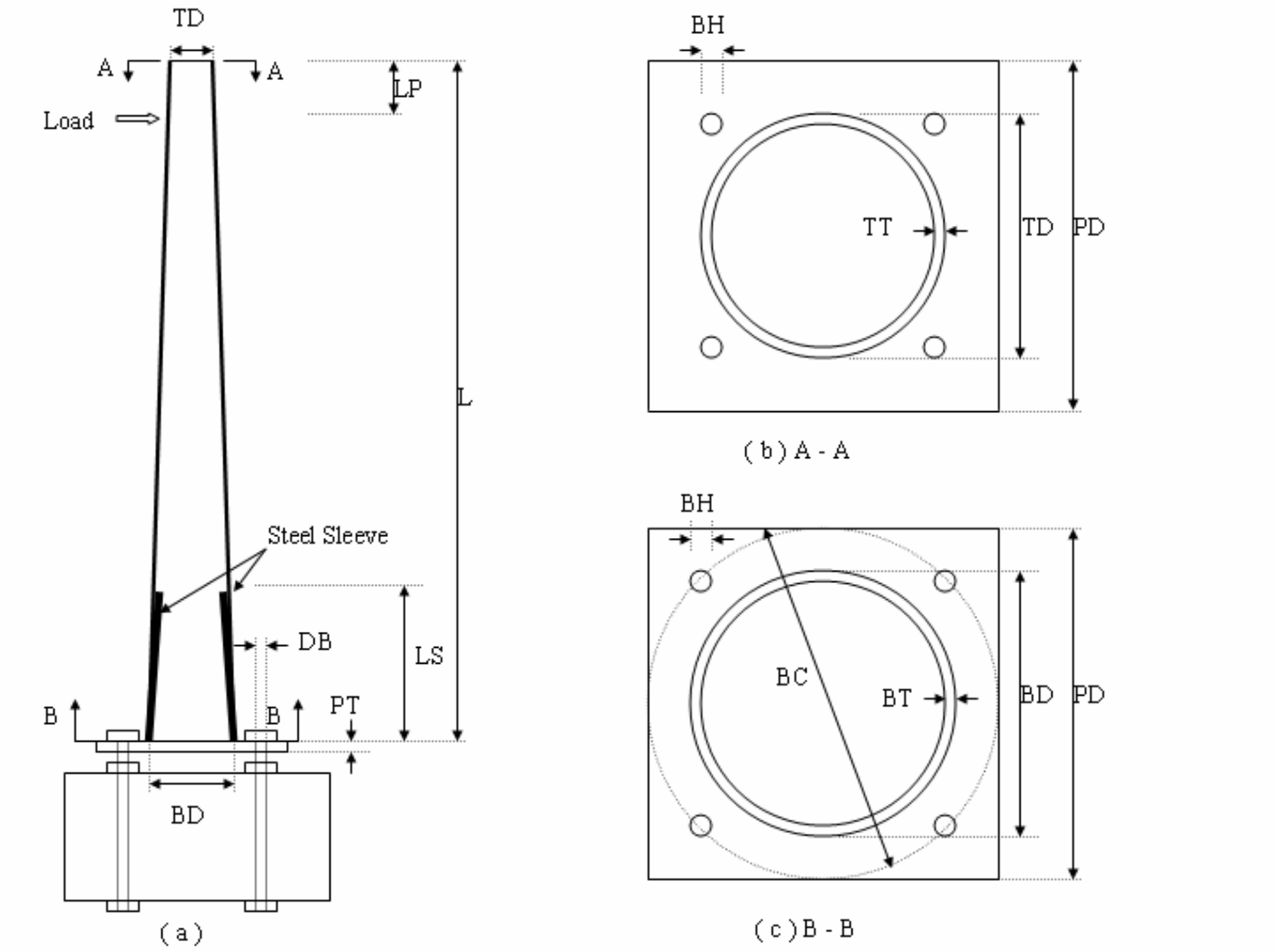

Figure 2.2 Typical dimensions of FRP poles tested:
(a) Front view; (b) Section A-A; (c) Section B-B

The numerical values of the geometric dimensions of steel and FRP poles are presented in Table 2.1. As shown, the length of steel pole was 20 ft (6.1 m) and the octagonal cross section was welded to their respective base end-plate (Figure 1), which was bolted to concrete base using four $^{1}/_{2}$ in. (13 mm) threaded rods. The steel pole had a wall thickness of $^{1}/_{8}$ in. (3 mm) and its outer base and top diameters were 5.2 in. (132 mm) and 3.3 in. (84 mm), respectively. The base end-plate was squared with 8.7 in. (221 mm) long, and its thickness was 0.42 in. (10.7 mm).

Table 2.1 Geometric properties of test specimens; in. (mm)

Specimen	Steel	FRP1	FRP2
L	240 (6096)	240 (6096)	300 (7620)
LP	18 (460)	18 (460)	22 (570)
LS		24 (610)	24 (610)
TD	3.3 (84)	10.2 (259)	9.6 (244)
BD	5.2 (132)	12 (305)	12 (305)
DB	0.5 (13)	1.125 (29)	1.125 (29)
BH	0.55 (14)	1.18 (30)	1.18 (30)
TT	0.125 (3)	0.375 (10)	0.375 (10)
BT	0.125 (3)	0.45 (11)	0.475 (12)
PT	0.42 (11)	1.25 (32)	1.25 (32)
PD	8.7 (221)	13.6 (346)	13.6 (346)
BC	7.2 (183)	15 (381)	15 (381)

Table 2.1 also shows that the height of FRP poles were 20 ft (6.1 m) and 25ft (7.6 m). The FRP poles were fabricated by a filament winding process which was made of polyester reinforced with E-glass fibers. The poles were composed of 30 % unsaturated polyester resin and 70 % standard electrical glass fiber, also known as E-glass by weight. A 24 in. (610 mm) long and $^{1}/_{4}$ in. (6 mm) thick steel sleeve was inserted in the pole and welded to the steel end-plate as shown in Figure 2, which was bolted to the concrete base by $1^{1}/_{2}$ in. (29 mm) A-325 threaded rods. The gap distance between the end-plate and concrete base was $2^{1}/_{2}$ in. (64 mm) as shown in Figures 2.1 and 2.2, and Table 2.1. The reason for this gap was to place the leveling nuts between the end-plate and concrete base in order to facilitate the adjustments of the pole during installation. The FRP poles were tapered with their dimensions given in Table 2.1. The thickness of the pole was varied such that their cross sectional area remained constant in order to meet manufacturer's standards and specifications which complied with certain FRP poles used by the California Department of Transportation. For example, the

thickness of the first FRP test specimen was varied from $^3/_8$ in. (10.7 mm) at the bottom to 0.45 in. (11.4 mm) at the top. Finally, the material properties of steel and FRP poles are presented in Tables 2.2 and 2.3, respectively.

Table 2.2 Material properties for steel poles

Material Properties	Plate (A36)	Bolt (A325)
E_x	30 Msi (206 GPa)	30 Msi (206 GPa)
F_y	36 ksi (248 MPa)	92 ksi (634 MPa)
υ	0.3	0.3
E_t	0.3 Msi (2 GPa)	0.3 Msi (2 GPa)
μ	0.2	0.2

Table 2.3 Material properties for FRP poles

Material Properties	E_x Msi (GPa)	F_y ksi (MPa)	G Msi (GPa)	ρ lb/in^3 (kg/m^3)	υ	w_f (%)	v_f (%)	δ_u (%)
E-glass	10.5 (72.4)	500 (3448)	4.4 (30)	0.09 (2540)	0.2	70	50	4.8
Polyester	0.46 (3.2)	8.7 (65)	0.2 (1.38)	0.039 (1090)	0.36	30	50	4.2

The material configuration are designated as followed: E_x for tensile modulus, E_t for tangent modulus; F_y for tensile strength, G for shear modulus, ρ for density, υ for poisson's ratio, μ for friction coefficient, w_f for fiber weight fraction, v_f for fiber volume fraction, and δ_u for ultimate elongation ratio. The fiber volume fraction was measured during the manufacturing process by determining the weight of the fiber and resin used as well as the weight of the finished FRP pole to determine the amount of resin was

wasted during the manufacturing process. Those weights are transformed into volume fractions.

Equation 2.1 shows the conversion between fiber weight fraction and fiber volume fraction where ρ_f and ρ_c is the density of fiber and FRP-composite, respectively (Jones, 1999; Daniel and Ishai, 2005).

$$w_f = \left[\frac{\rho_f}{\rho_c}\right] v_f \tag{2.1}$$

The conversion between resin weight fraction (w_m) and resin volume fraction (v_m) is also presented in Equation 2.2 where ρ_m is the density of resin.

$$w_m = \left[\frac{\rho_m}{\rho_c}\right] v_m \tag{2.2}$$

2.3 Instrumentation

Monotonically increasing static load was applied through hydraulic pressure pump, Enerpac PER 3042. This is used to raise the attached hydraulic cylinder, Enerpac RC 5013 and thereby apply the load to the testing pole (Figure 2.3). Enerpac PER 3042 can generate maximum pressure of up to 10,000 psi. (68.9 MPa) The cylinder has a 110 kips (50 ton) load capacity and exerts a perpendicular load. The main instrumentation consists of digital position transducer to calculate the relative displacement, digital controller and software to acquire data, input channels for load, and load cell. The load cell which is capable of measuring pressure up to 2,500 lbf (11,125 N) is rested on the cylinder and made physical contact with the pole. This sensor measures how much load is applied to the pole. This information is then transferred to the precise digital controller for storing. The digital controller is attached to digital position transducer which is capable of measuring displacement up to 50 in. The position transducer has a position signal sensitivity of 623.94 pulses per inch. The precise digital controller is used to indicate load, load rate, load position, and strain. This digital controller is

capable of plotting load, position or strain in real time with the help of RS 232 data port and WinCom software. Precise digital controller is designed for tension and compression testing. The controller features high resolution, high accuracy, fast sampling rates, large data storage capability, and it is designed for high reliability and ease of use. Precise digital controller can store up to six load cell calibrations for multiple load cell systems, with its accuracy exceeding ASTM E 4 standards (Figure 2.4).

Figure 2.3 Test apparatus

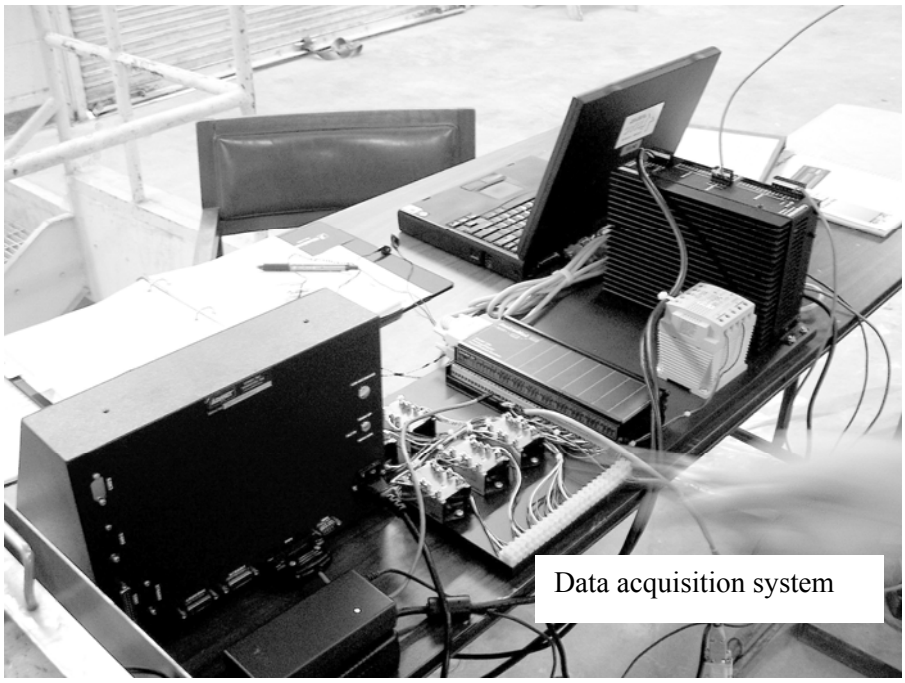

Figure 2.4 Electric test instrumentation

2.4 Test setup and procedure

The four full-scale tapered steel / FRP poles were tested in the Engineering Laboratory Building at University of Texas at Arlington. The typical configuration of the test setup is shown in Figure 2.5. The concrete base support was bolted to the 2 ft (61 cm) concrete reaction floor using $1^1/_2$ in. (38 mm) diameter rods as shown in Figure 2.6. The boundary conditions for the concrete base were considered fully restrained. The test poles were bolted to the 3 ft (91 cm) wide, 3ft (91 cm) thick by 4 ft (122 cm) long concrete base support having an average of 3,480 psi (24 MPa) of compressive strength which was over the required standard tensile strength of 3,000 psi (20.7 MPa). No general sequence for bolt tightening was used. The general sequence was to tighten the most rigid part of the joint connection first and the least rigid portions last. Two complete cycles of bolt tightening are typically required to pull the plies of the connection together and to maintain the bolt pretension. A monotonically increasing load was applied through a hydraulic pump (Enerpac P-80) vertically to the loading point for simulating the load classification test (ASTM, 2005). A hydraulic cylinder

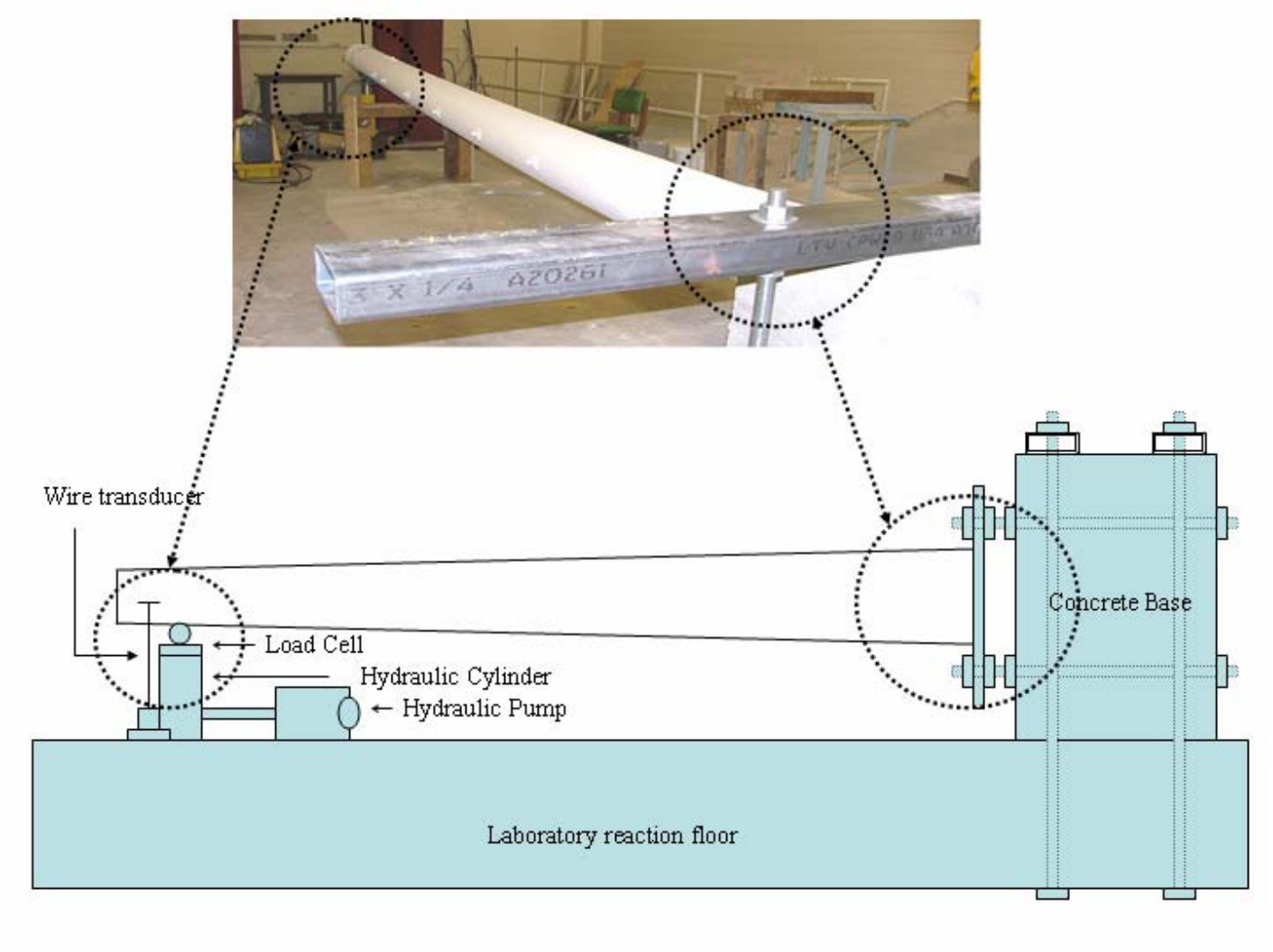

Figure 2.5 Configuration of test setup

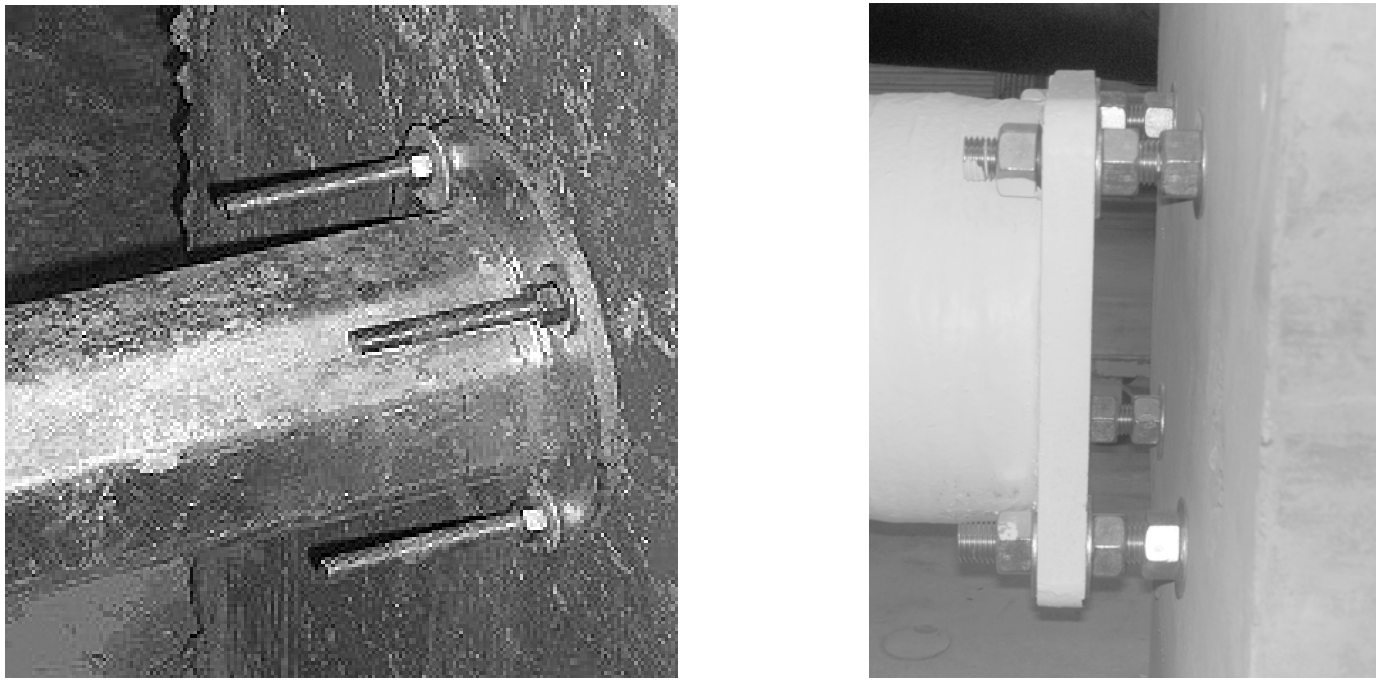

(a) (b)

Figure 2.6 Photographs of end-plate connection: (a) Steel pole; (b) FRP pole

(Enerpac RC 5013) was used to apply load to the pole. The cylinder had a 110 kips (490 N) load capacity and exerted a perpendicular load at the loading point. A load cell was mounted on the hydraulic cylinder, which measured the applied load and transferred the information to the precise digital controller for storing. The deflection of the pole was measured by using a position transducer which was attached to the loading point. During the test, lateral braces were not provided at the end of the test pole to release out-of -plane buckling of the test specimen in order to capture the actual field condition.

Figure 2.7 shows a typical incremental loading history, which was employed to apply the load in increments of approximately 4.5 lb (20 N) per second. At the end of each load increment the specimens were unloaded to zero in order to capture possible nonlinear and inelastic type behavior due to material and/or geometry.

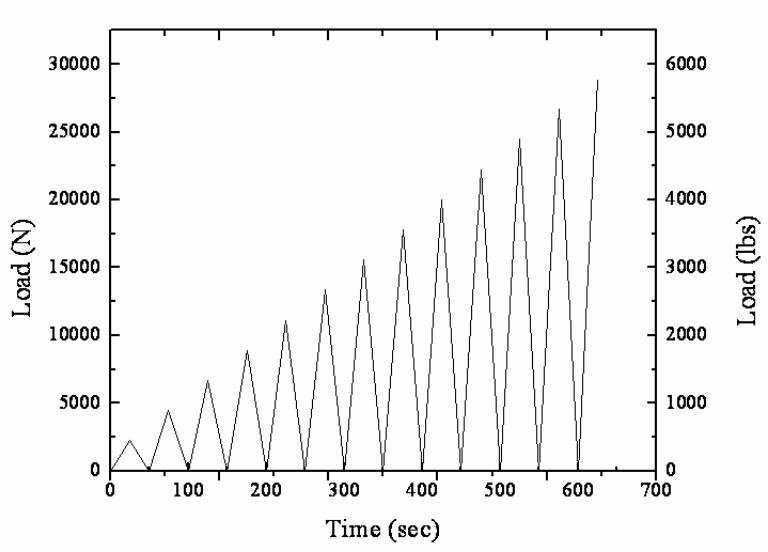

Figure 2.7 Loading history

In addition, this pseudo-cyclic loading would introduce fatigue effects in the pole during the testing.

2.5 Test results and discussion

The experimentally obtained load-deflection test sheet of the tapered steel and FRP poles are presented in Table 2.4 and the typical load deflection graph is plotted in Figure 2.8, which shows that the FRP pole with 25 ft (7.6 m) in length is more flexible than the one with 20 ft (6.1 m) in length. Also, this Figure shows that the load-deflection for steel pole is the most flexible among the three. This is due to the fact the

Table 2.4 Load and deflection of specimens experimentally tested

Test Specimens	Load, lbs (N)	Deflection, in. (cm)
Steel 20 ft (6.1 m)	505 (2247)	29.63 (75.25)
FRP 20 ft (6.1 m)	2742 (12200)	20.72 (52.63)
FRP 25 ft (7.6 m)	2889 (12856)	43.71 (111.02)

steel pole's thickness was much less than that of the FRP poles. For example, steel pole's thickness at the top is about 33% of that of FRP. The load deflection curve is observed to behave elasto-plastically and the failure mode for steel poles was determined to be excessive tip deflection. Also, yielding at steel poles' end-plate was observed which was accompanied with permanent elongation of the bolts in the tension region. Figure 2.9 shows the end-plate deformation of the steel pole at the maximum loading. However, no yielding was detected throughout the pole's length in any of the steel test pole (Figure 2.10).

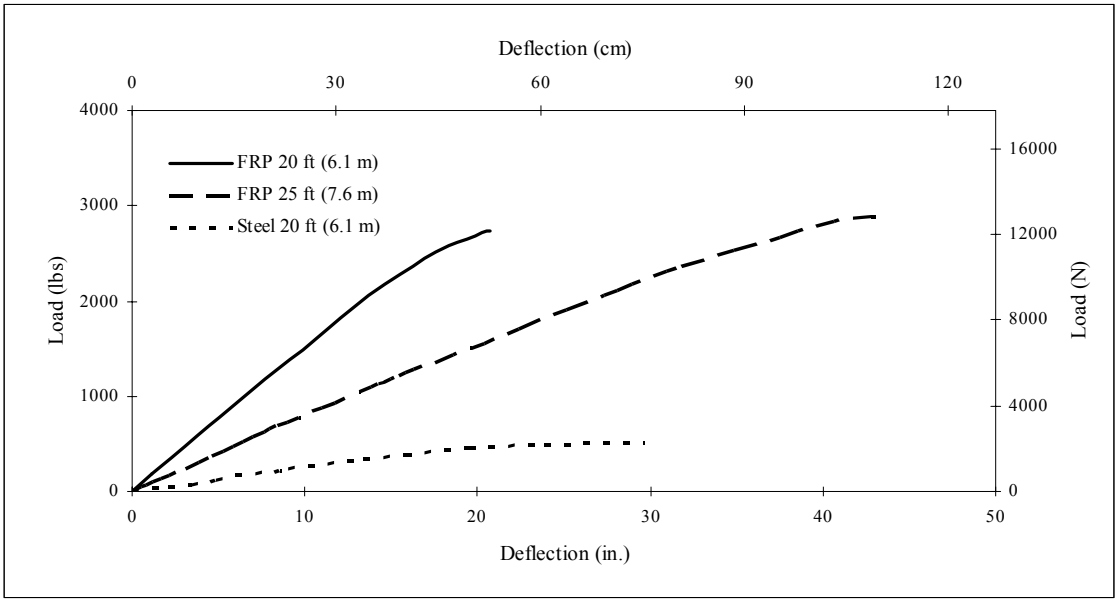

Figure 2.8 Experimental load-deflection curves

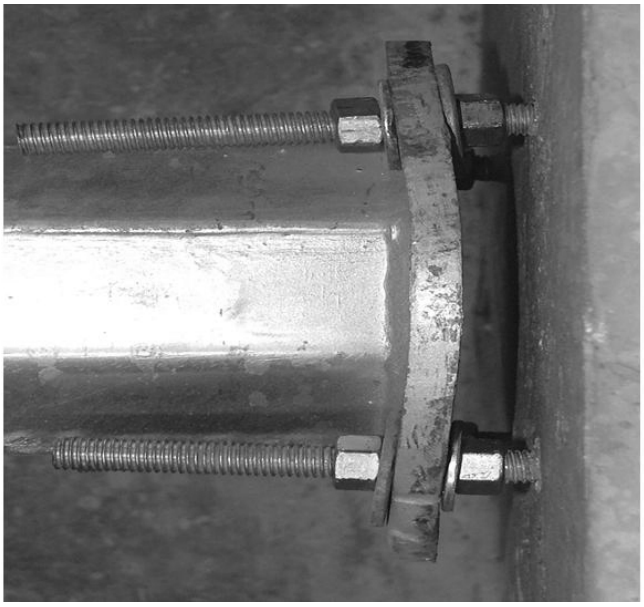

Figure 2.9 End-plate deformed shape

Figure 2.10 Overall view of steel pole tested

FRP poles also experienced excessive tip deflection and permanent bolt elongation in the tension region, however, no yielding of their end-plate was observed due to their relatively thick end-plate ($1^1/_2$ in. (29 mm)). In both tests for the FRP poles, initial superficial cracks formed at early stage of loading (i.e. 600 lbs (2670 N)). However, the initial cracks did not cause noticeable degradation in the stiffness of the FRP test poles. Figures 2.11 and 2.12 show the pole's deflection shapes on the loading level of 1 kips (4450 N) and 2 kips (8900 N), respectively. As shown in Figure 2.13, there was no yielding on the end-plate and bolts.

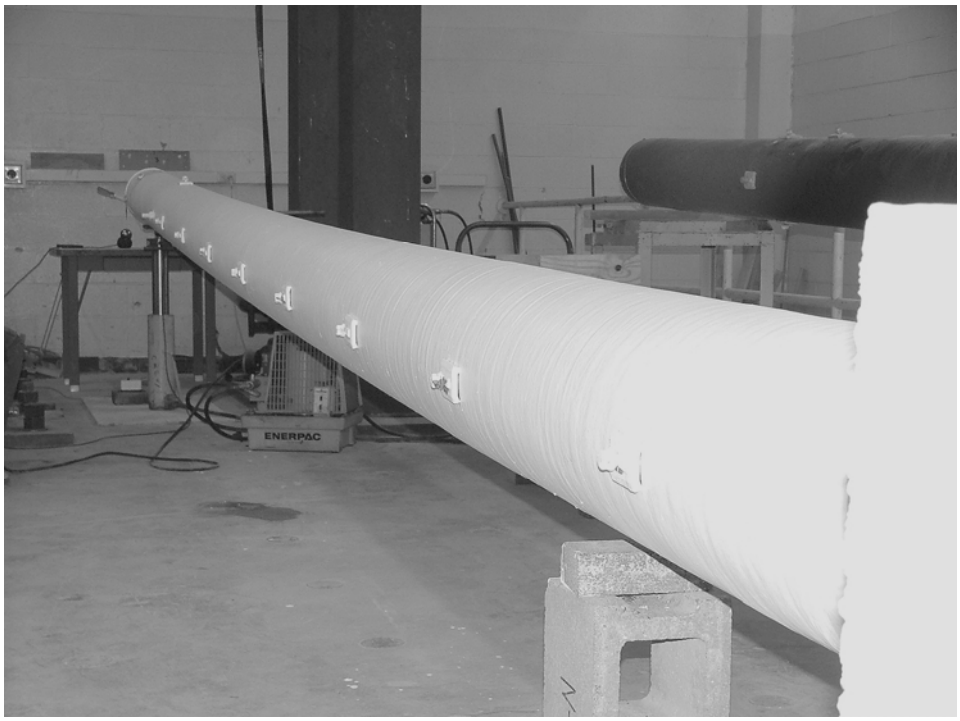

Figure 2.11 FRP pole deformed at 1 kips (4450 N)

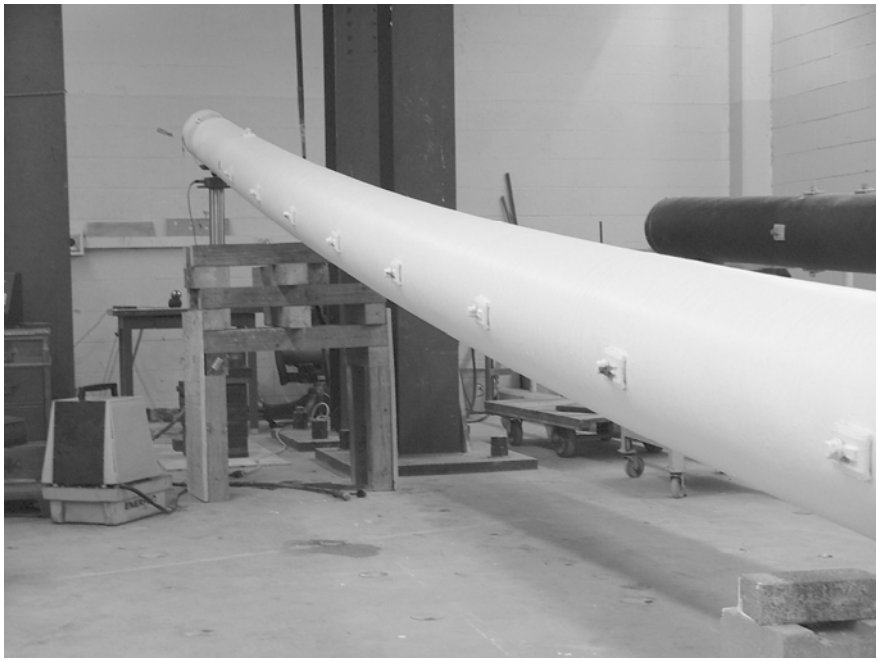

Figure 2.12 FRP pole deformed at 2 kips (8900 N)

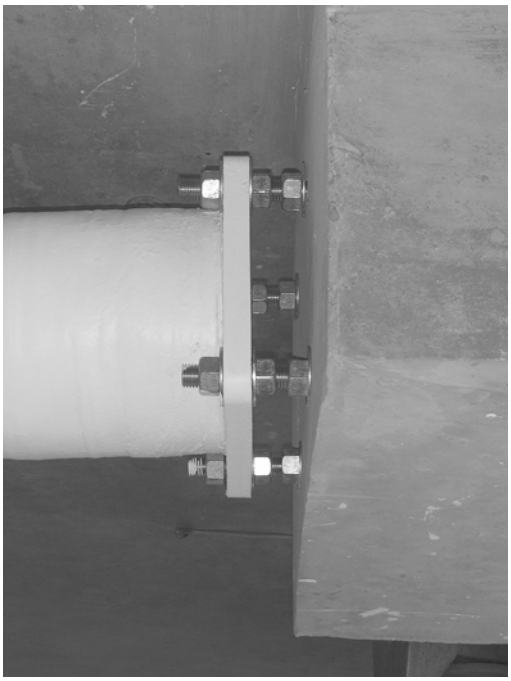

Figure 2.13 Bolt deformation at ultimate state

2.6 Chapter summary

The purpose of the second chapter is to present experimental qualifications performed for steel and FRP poles. A steel pole with octagonal cross section and two circular cross sectional FRP poles were tested to determine their stiffness and strength characteristics. Test setup was designed to mimic the actual field condition and consisted of the test pole welded to the end-plate, which was bolted to the concrete base. Instrumentation consisted of a load cylinder, load cell, wire potentiometer, and digital data acquisition system. A pseudo cyclic loading history was applied to each test pole until failure and the load versus tip deflection plots were obtained.

The failure mode for all the test specimens was determined to be excessive deflection. However, end-plane yielding of the connections of the steel poles was observed at approximately 450 lbs (2,003 N). Also, for the FRP poles, superficial cracks at 600 lbs (2,670 N) were detected accompanied with delamination of fibers. No end-plate connection yielding was observed in any of the FRP test specimens.

CHAPTER 3
FINITE ELEMENT MODELING

3.1 Introduction

Full-scale experimental testing of structural systems are time consuming, cost prohibitive, and data gathered from them are limited to surface measurements. The use of finite element method (FEM) has gained abundant popularity in recent years due to advances in high-speed computers. Also, in order to investigate the effect of force and geometric variables on certain response of structures, the researcher has employed FEM model analysis for parametric studies. It is essential to note that any FEM model analysis results should be compared and verified with selected experimental results. In cases where experimental results are unavailable or impossible to conduct, the independent variables should be varied such that the behavior of the model is intuitively evaluated.

Since FEM represents upper bound solutions the accuracy and convergence of models needs to be checked for problem in hand. The convergence behavior of the model should be check through P-, H-, or P-H convergence (Reddy, 1993). H convergence is tested by increasing the degree-of-freedom (DOF) of the model by decreasing element size. In P-convergence, higher order polynomials are used in defining assumed displacement function, which is equivalent in using higher order element. The P-H convergence employed both P and H methods. Since convergence of nonlinear problems is monotonically not guaranteed, energy-based convergence is more desirable to be adopted.

This chapter presents the FEM models and their analysis techniques used to predict and analyze the behavior of tapered steel and FRP hollow poles. The first step in the modeling process was to define the geometric shape of the pole; the discritization process was performed to subdivide the pole into an equivalent finite element. Since a refined finite element mesh leads to more accurate results (i.e. H-convergence), a fine mesh was used in the vicinity of end-plate and a bolt assemblage. Three dimensional

FEM models of steel and FRP poles are developed by making several attempts in selecting the type of elements for the analysis. Since plane of symmetry with respect to geometry and load exists, one-half of the entire poles were modeled using ANSYS version 9.0 (2004). The pole model includes pole length, end-plate, bolt assemblage, and pre-tensioning effects. The analysis algorithm employs coupled incremental material, geometric, and contact nonlinearities. The H-convergence for each model is checked by using Hilbert L-2 norm coupled with equating external virtual worked done to internal strain energy at each load increment in the Newton-Raphson marching scheme (Crisfield, 1997).

3.2 FEM model of steel pole

The FEM model of the pole tested in the experimental program was developed. A 20 ft (6.1 m) long tapered steel pole with octagonal cross section was used for the model. The geometric variables describing the configuration of a typical steel pole used are shown in Table 3.1. The connection bolts were $1^{1}/_{8}$ in. diameter, A325 strength bolts. To isolate the behavior of the pole, the concrete base was modeled with infinite stiffness. The effect of welds was not included since it is assumed that welds are designed such that they would not fail before end-plate yielding or bolt fracture. Although it seems

Table 3.1 Geometric properties used in FEM analysis for steel poles

Size	L ft (cm)	LP in. (cm)	TD in. (cm)	BD in. (cm)	DB in. (cm)	BH in. (cm)	TT in. (cm)	BT in. (cm)	PT in. (cm)	PD in. (cm)	BC in. (cm)
Steel	20 (610)	18 (460)	3.3 (84)	5.2 (132)	0.5 (13)	0.55 (14)	0.125 (3)	0.125 (3)	0.42 (11)	8.7 (221)	7.2 (183)

justifiable to use two-dimensional shell elements for the pole, early studies showed that such a solution would suffer significantly in simulating the evolution of internal stresses in plasticity zones, yielding unacceptable results (Gantes and Lemonis, 2003).

3.2.1 Finite element modeling

Thus, three-dimensional solid finite elements were used to model the pole, end-plate, and bolt assemblage. In general, higher order elements offer better accuracy per DOF but they require laborious mesh implementations. In addition, their efficiency in plasticity zones, which normally occur in the model, is questionable compared to this of the first order elements (Gantes and Lemonis, 2003) As a results, plastic quadrilateral eight-node solid elements, SOLID45 in ANSYS, were used to model steel pole, steel plate, bolt head and nut, and concrete base. This element has three translational degrees of freedom, u_x, u_y and u_z at each node which is depicted in Figure 3.1. The element has the capability to accept algorithms for material, contact, and geometric nonlinearities. This element also uses full integration i.e. eight Gauss points (Bathe, 1996).

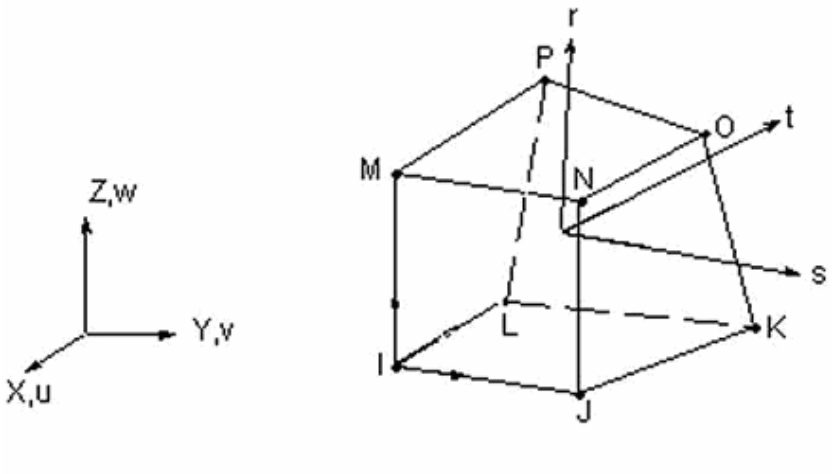

Figure 3.1 Solid eight-node element

Since a plane of symmetry exists along a section through the longitudinal axis of the pole, end-plate, and concrete base, one-half of the pole and its connection assembly were modeled for analysis as shown in Figure 3.2. Thus, all nodes which lie on the plane of symmetry are constrained not to move in the direction normal to the plane of symmetry. Typical finite element meshes for this problem used nearly 24,000 to 28,000 degrees of freedom. The finite element model used was checked for convergence by refining the finite element mesh (H-convergence). The complex interaction between the contact pair surfaces were modeled with the three-dimensional

eight-node surface-to-surface contact and target elements. The effect of plasticity and the pre-tensioning of the bolts were also included in the model. Pretension effect of the bolts was modeled with the three-dimensional pretension elements. All components including bolts were completely independent from each other as assemblages in real connection.

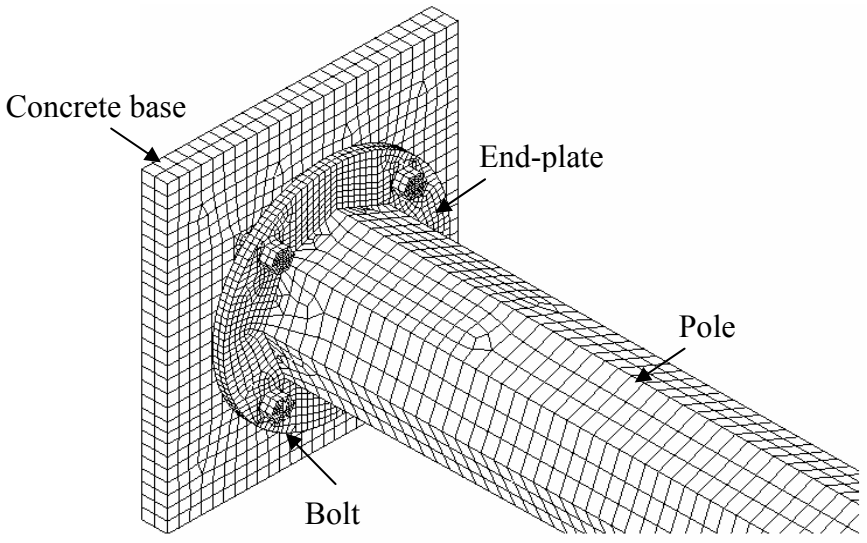

(a)

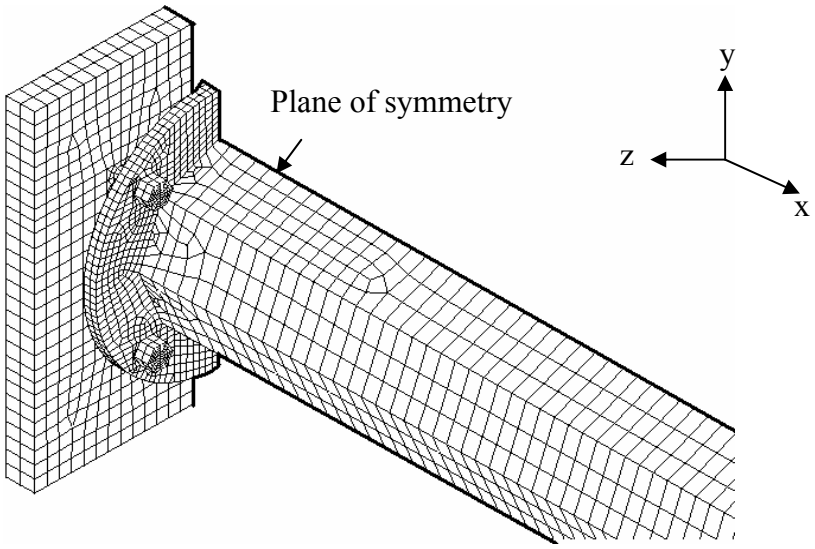

(b)

Figure 3.2 Typical FEM model for steel poles:
(a) Converged full model; (b) Converged half model

3.2.2 Bolt model

Bolts were more precisely constructed using eight-node solid elements and were divided into bolt shank, head, and nut elements in order to consider their individual effects on the pole behavior as shown in Figure 3.3. Similar bolt model was used by Choi and Chung (1996), Kishi et al., (2001), Gantes and Lemonis (2003). To include the effect of bolt bending, a three dimensional bolt model was presented in which bolt shank was assumed to behave as a beam element connected to bolt head and bolt nut. Where members are bolted together, the overall structural strain would create high local forces as the bolts tried to make one bolted member's strain match the other bolted member's strain. The bolt hole was made $^{1}/_{16}$ in. bigger than the bolt diameter (AISC, 1999). This is based on the experiments conducted by Azizinamini (1985).

Slip critical type of bolted connections were considered in this study, which is commonly used for moment connections (i.e. end-plate connections). This means that the shear load transfer is only through the friction and not through bolt shear. Therefore, bolt shear in the formulation of the three-dimensional bolt model was not included.

3.2.3 Pretension element

In the early FEM modeling of bolted connections such as those conducted by Azizinamini (1985), and Choi and Chung (1996), pretension effects in the bolts caused by the tightening of each bolt were simulated by applying compressive forces equivalent to proof load (70% of bolt's ultimate tensile strength) to the end-plate at the location of bolt head and nut. These compressive forces were equivalent to the bolt pretension force (proof load) per AISC (1995).

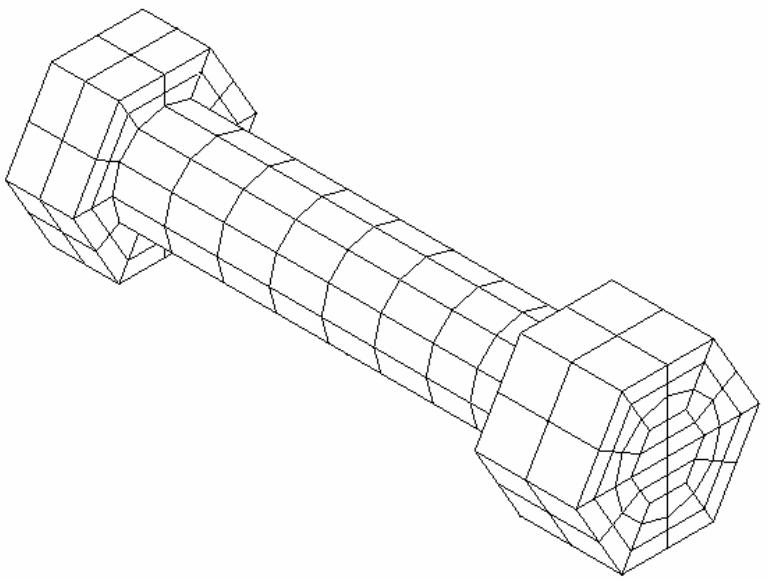

(a)

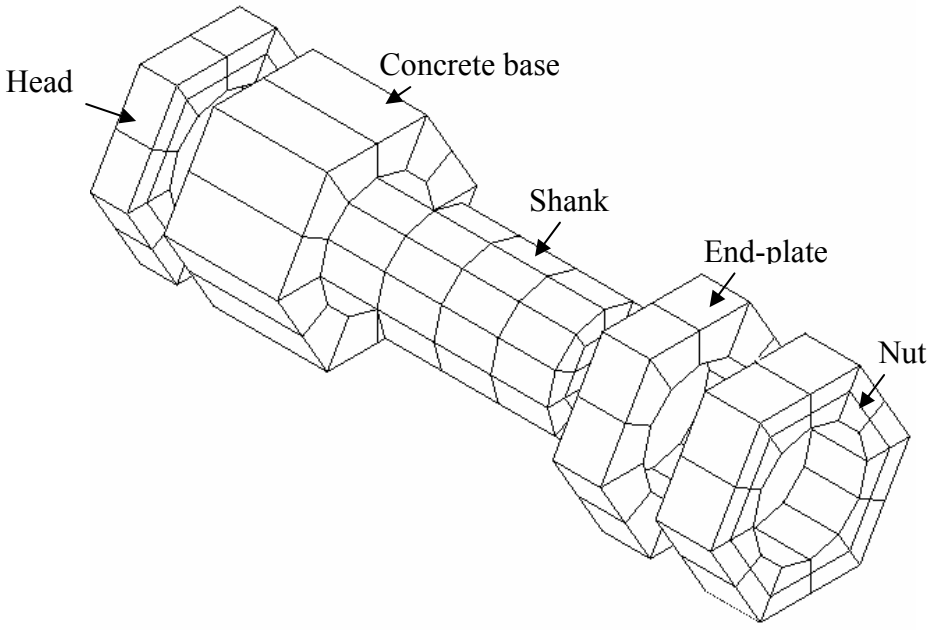

(b)

Figure 3.3 Bolt model used in analysis:

(a) Bolt mesh pattern; (b) Configuration of bolt model

This type of bolt modeling would introduce difficulties in monitoring the variation of the bolt forces during the analysis. Thus, bolt pretension element in ANSYS was used, which is a three-dimensional line element that acts as a connecting element to connect the two imaginary parts of the bolt shank. The pretension element, as shown in Figure 3.4 contains nodes "I" and "J" located at an arbitrary section through the bolt shank length which are connected with a link element. The aforementioned section is selected arbitrary in order to comply with different mesh configuration. Node K is the pretension node with one degree of freedom, u_x, with the actual line of action in the pretension load direction. The underlying bolt elements can be solid, shells, or beam elements, of any order of polynomial. When the pretension is applied on the node K, the link element joining nodes I and J will be in tension, this in turn pulls the two imaginary sections of the bolt towards each other to compress the connecting surfaces. During the pretension of a physical bolt, turning of the nut reduces the unstretched grip length of the bolt, thereby inducing pretension. When the desired pretension is achieved and the wrench is removed, the new unstretched grip length becomes locked. The pretension element used applies the same procedure during the loading in the same sequence: First, the specified pretension load is applied incrementally to capture contact nonlinearity, and possible nonlinearities induced by material yielding. At this point in the analysis, the pretension section displacement is locked for the pre-tensioned bolt. Once all bolts are pre-tensioned and locked, external load is applied incrementally to capture nonlinearities due to material, geometric, and contact. Thus, the analysis is based on non-propositional loading. Since the monotonic convergence of nonlinear problems by FEM in general is problem dependent and not guaranteed. Improved convergence was obtained with an energy based method coupled with Hilbert L-2 norm.

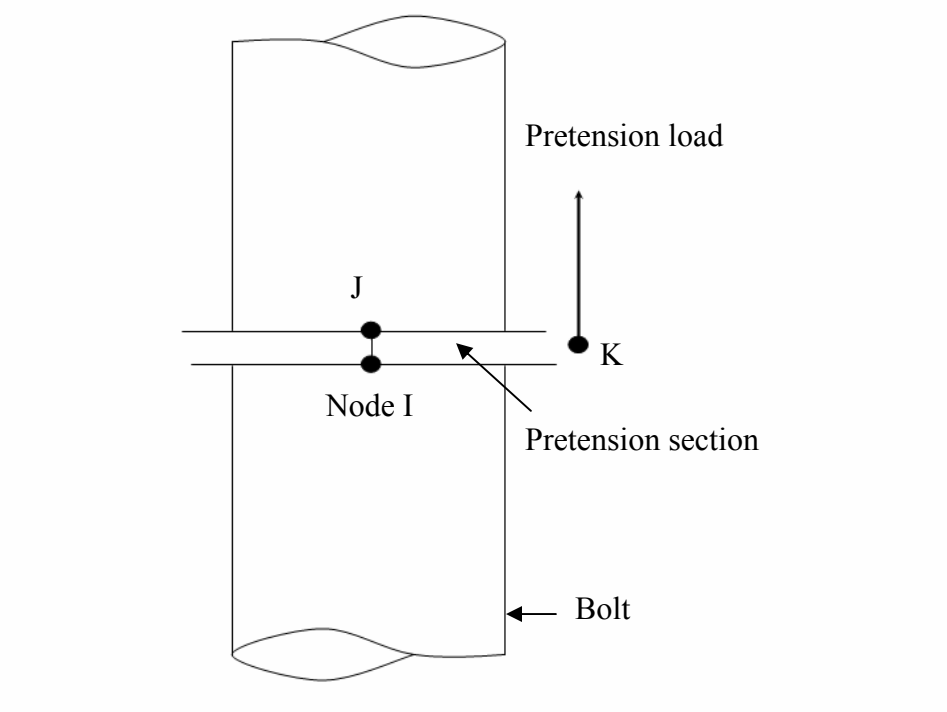

Figure 3.4 Pre-tensioning section

3.2.4 Contact element

To avoid numerical penetration between the connecting surfaces and to model friction for transferring forces between the surfaces, contact elements were used between the end-plate and concrete base as well as between the bolt head/nut and end-plate/concrete base. Contact model with small sliding option was applied between contact pair surfaces, one of which is defined as master surface and the other as slave surface. Contact pair surfaces are as follows as shown in Figure 3.5: (1) bolt shanks and bolt holes, (2) bolt head/nut and connecting components; and (3) between end-plate and concrete base. The two complex interacting surfaces were modeled using contact element (CONTA 174) and target element (TARGE 170). Master surfaces of contact fair options represent the surfaces of bolt shanks and nuts, whereas the surfaces interfacing master surfaces are defined as slave surfaces. CONTA 174 provides an option for defining the maximum equivalent shear so that, regardless of the magnitude of the contact pressure, a sliding will occur when the magnitude of the equivalent shear stress reaches its maximum. An adequate mesh density was required for regions

undergoing plastic deformations to allow contact stresses to be distributed in a smooth fashion. The friction would be a dominant parameter of stiffness at the initial stage of loading. Surface-to-surface and flexible-to-flexible contact type were used in the FEM analysis algorithm since contacts between surfaces were deformable finite elements. A coefficient of friction of 0.2 which indicates the roughness of the surfaces was used as observed by Yorgun et al. (2004).

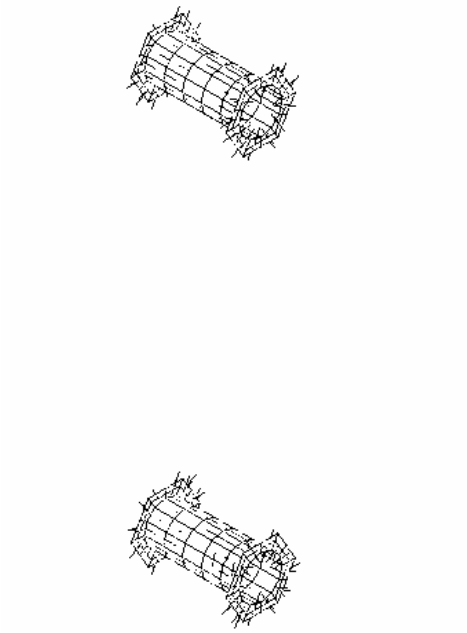

Figure 3.5 Contact pairs

3.2.5 Material model

In general, a complete plasticity theory has three components: (1) a yield criterion that defines the combination of stress components in which initial yielding occurs, (2) a flow rule that deals with the way plastic deformation occurs, and (3) a hardening rule that predicts changes in the yield surface due to the plastic strain.

The material behavior for each pole, end-plate, and bolt was described by bilinear stress-strain curves the properties of which are defined in Tables 3.2 and Figure 3.6, having a modulus of elasticity of 30,000 ksi (206 GPa), 36 ksi (248 MPa) yield stress, and a Poisson's ratio of 0.3. An isotropic type material was chosen with plasticity-based isotropic hardening rule. These options are often preferred for large

strain analysis. For steel elements the Von Mises yield criterion is well suited and was adopted in order to obtain the response of the pole in the inelastic region. The initial slope of the curve was taken as the elastic modulus, E, of the material. After several trials to best calibrate the FEM model with the experimental results obtained, the post yield stiffness identified as tangent modulus, E_t , was taken as 1 % of the initial stiffness (E_t = 0.01 E). The tangent modulus cannot be less than zero nor greater than the elastic modulus.

Table 3.2 Material properties for steel poles used in analysis

Material Properties	Pole & End-plate (A36)	Bolt (A325)
Modulus of elasticity (E)	30 Msi (206GPa)	30 Msi (206 GPa)
Yield stress (F_y)	36 ksi (248 MPa)	92 ksi (634 MPa)
Poisson's ratio (υ)	0.3	0.3
Tangential modulus (E_t)	300 ksi (2 GPa)	300 ksi (2 GPa)
Friction coefficient (μ)	0.2	0.2

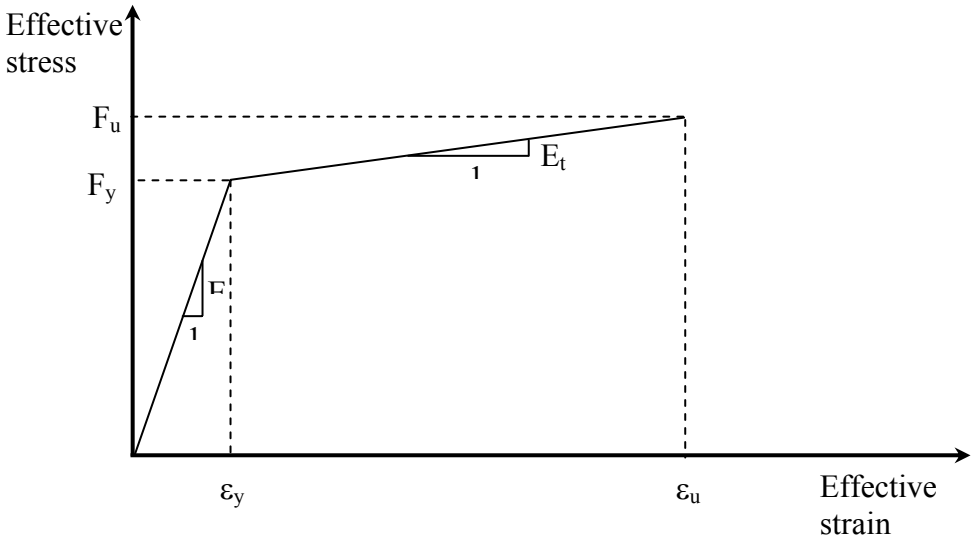

Figure 3.6 Nonlinear stress-strain relationship

The stress-strain relationship for the material was elastic-plastic strain hardening. Material plasticity and the partial changes over the contact area between the pole, end-plate and bolts are the causes of nonlinear behavior of bolted connections. For simplicity and ease of post-processing, the external load on the pole was applied in a force-driven manner. The loads were applied gradually in increments to characterize actual load history, and then multiple iterations per load step were conducted. Bilinear isotropic hardening option was used for describing the plastic behavior in which the Von Mises criterion is coupled with the isotropic work hardening. In this study, assumptions made regarding to the material modeling was one of the parts. Large plastic deformations were expected and observed, thus geometric nonlinearities were incorporated as large strain analysis that accounts for the stiffness changes resulting from the shape and orientation changes in elements. The large strain procedure places no theoretical limit on the total deformation or strain experienced by an element, but requires incremental loading to restrict strains for maintaining accuracy in the computations.

The loads were applied incrementally using the full Newton-Raphson method. Newton-Raphson procedure was employed for nonlinear analysis where the load is divided into series of load increments applied in several load steps. Before each solution step, out-of-balance load vector which is the difference between the restoring forces corresponding to element stresses and the applied loads was evaluated. Then, a linear solution was carried out using out-of-balance loads and convergence was checked. When the convergence criteria were not satisfied, out-of-balance load was reevaluated, the stiffness matrix was updated and a new solution was obtained as shown in Figure 3.7. This iterative procedure continued until the solution converges.

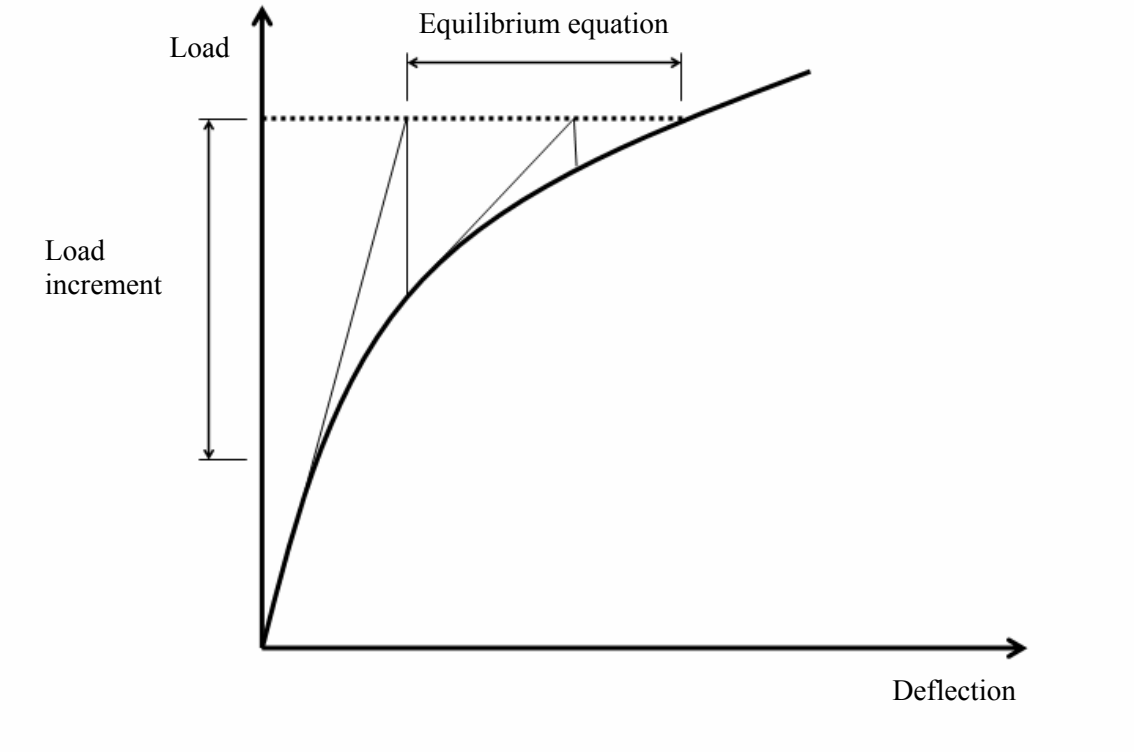

Figure 3.7 Newton-Raphson scheme

3.2.5.1 Yield criteria

Several theories of failure for yielding are discussed in mechanics of materials text books (Chen and Han, 1988; Bathe, 1996; Crisfield, 1997; and Morozov, 2004). In one-dimensional problem, yielding can be identified with comparison of just one stress component with the yield strength. In multi-axial problems there should be a general statement showing what combination of stress components causes yielding. The stress applied to a material can be broken into the hydrostatic pressure and the deviatoric stress. Some materials are pressure dependent, while some are pressure independent materials in which yield criteria do not depend on first stress invariant, and they are only defined in terms of second deviatoric stress invariant. Among the pressure independent criteria, one can name Maximum shear stress and the Von Mises which is called octahedral shearing stress or maximum strain energy of distortion. Von Mises

criterion indicates that yielding happens when the octahedral shear stress reaches a critical value. The approach of the Von Mises yield criterion is as follows:

$$(\sigma_1 - \sigma_2)^2 + (\sigma_2 - \sigma_3)^2 + (\sigma_3 - \sigma_1)^2 > 2\sigma_y^2 \tag{3.1}$$

$$\sigma_{eff} = 1/\sqrt{2}\left\{(\sigma_1 - \sigma_2)^2 + (\sigma_2 - \sigma_3)^2 + (\sigma_3 - \sigma_1)^2\right\}^{1/2} > \sigma_y \tag{3.2}$$

where $\sigma_1, \sigma_2,$ and σ_3 are the principal stresses ($\sigma_1 > \sigma_2 > \sigma_3$) and σ_y is the yield stress of material obtained from a uni-axial tensile test. When $\sigma_{eff} > \sigma_y$, then the element is said to have yielded. To consider the nonlinear behavior, it is convenient to convert stresses to strains, since for the plate material, the stresses remains constant upon yielding. The principal stresses are transferred to principal strains by the following relationships:

$$\sigma_1 = \mu\{(1-\nu)\varepsilon_1 + \nu\varepsilon_2 + \nu\varepsilon_3\} \tag{3.3}$$

$$\sigma_2 = \mu\{\nu\varepsilon_1 + (1-\nu)\varepsilon_2 + \nu\varepsilon_3\} \tag{3.4}$$

$$\sigma_3 = \mu\{\nu\varepsilon_1 + \nu\varepsilon_2 + (1-\nu)\varepsilon_3\} \tag{3.5}$$

where ν is the Poisson's ratio and μ is calculated using the following relationship:

$$\mu = E / \{(1+\nu)(1-2\nu)\} \tag{3.6}$$

and $\varepsilon_1, \varepsilon_2$ and ε_3 are the principal strains ($\varepsilon_1 > \varepsilon_2 > \varepsilon_3$). Substituting Equation 3.3 to 3.5 into Equation 3.2 gives

$$(\sigma_1 - \sigma_2)^2 + (\sigma_2 - \sigma_3)^2 + (\sigma_3 - \sigma_1)^2 = \left\{\frac{E}{1+\nu}\right\}^2 \left\{(\varepsilon_1 - \varepsilon_2)^2 + (\varepsilon_2 - \varepsilon_3)^2 + (\varepsilon_3 - \varepsilon_1)^2\right\} \leq 2(\varepsilon_y)^2 \tag{3.7}$$

or

$$\frac{\sqrt{2}}{2(1+\nu)}\left\{(\varepsilon_1 - \varepsilon_2)^2 + (\varepsilon_2 + \varepsilon_3)^2 + (\varepsilon_3 - \varepsilon_1)^2\right\}^{1/2} \leq \varepsilon_y \tag{3.8}$$

where ε_y is the yield strain of the material from a uni-axial tensile test. Taking $\nu = 0.5$ for the plastic region, Equation 3.8 reduces to

$$\frac{\sqrt{2}}{3}\left\{(\varepsilon_1-\varepsilon_2)^2+(\varepsilon_2-\varepsilon_3)^2+(\varepsilon_3-\varepsilon_1)^2\right\}^{1/2} \le \varepsilon_y \tag{3.9}$$

Therefore, the effective strain, ε_{eff} in any element of the end-plate is calculated in terms of principal strains of the element, as follows:

$$\varepsilon_{eff} = \frac{\sqrt{2}}{3}\left\{(\varepsilon_1-\varepsilon_2)^2+(\varepsilon_2-\varepsilon_3)^2+(\varepsilon_3-\varepsilon_1)^2\right\}^{1/2} \tag{3.10}$$

If ε_{eff} is found to be greater than ε_y, then the element is said to have yielded. Von Mises yield criterion is based on this alternative. It has the simple form

$$f(J_2) = J_2 - k^2 = 0 \tag{3.11}$$

or, written in terms of principal stresses,

$$J_2 = \frac{1}{6}\left[(\sigma_1-\sigma_2)^2+(\sigma_2-\sigma_3)^2+(\sigma_3\sigma_2)^2\right] = k^2 \tag{3.12}$$

where k is the yield stress in pure shear. When J_2 exceeds k^2 yielding occurs.

3.2.5.2 Flow rule

Flow rule relates the plastic strain increments to the stress increments after initiation of yielding. It gives the ratio or the relative magnitudes of the components of the plastic strain increment. Plastic deformation occurs as long as the stress point is on the yield surface, and the additional loading $d\sigma_{ij}$ must move along the tangential direction. Thus, the condition for further plastic flow is

$$f(\sigma_{ij}, k) = 0 \text{ and } df = \frac{\partial f}{\partial \sigma_{ij}} d\sigma_{ij} = 0 \tag{3.13}$$

in which σ_{ij} is stress vector in stress space, and $d\sigma_{ij}$ is stress increment vector in stress space. The concept of plastic potential function is used to determine the direction of plastic strain increments.

3.2.5.3 Hardening rule

The phenomenon whereby yield stress increases with further plastic straining is known as work hardening or strain hardening. Unlike an elastic-perfectly plastic material in which yield strength remains constant in loading, unloading, and reloading cycles, for a material with hardening property, yield strength changes with load cycles. In other words, load history affects the yield strength of the material and loading, unloading, and reloading cycles change the elastic region for the subsequent loading cycles.

There are three different theories under a reversed loading condition regarding the way a material shows hardening in a multi-axial state of stress: isotropic hardening, kinematic hardening, and independent hardening. In isotropic hardening, the reversed loading condition is assumed equal to the tensile yield stress. In other words, the yield surface expands about its origin. Thus, the isotropic hardening rule neglects completely the Bauschinger effect. In the case of multi-axial stress, the boundary between elastic and elasto-plastic behavior, defines a surface called the yield surface. Based on isotropic hardening model, the yield surface expands symmetrically about the origin and increases the range of elastic loading for the subsequent loading cycles. This phenomenon is shown in Figure 3.8.

Isotropic hardening is valid as long as the yield surface is expanding under primary monotonic loading. When a stress reversal occurs, a kinematic yield surface is developed. In this theory, hardening in one direction, equally lowers the yield strength of the material, in the other direction. In other words, the elastic range is assumed to be unchanged during hardening. Thus, the kinematic hardening rule considers the

Bauschinger effect to its full extent. The effect of kinematic hardening model on yield surface is shown in Figure 3.9. Finally, independent hardening rule is assumed the material to be hardened independently in tension and in compression.

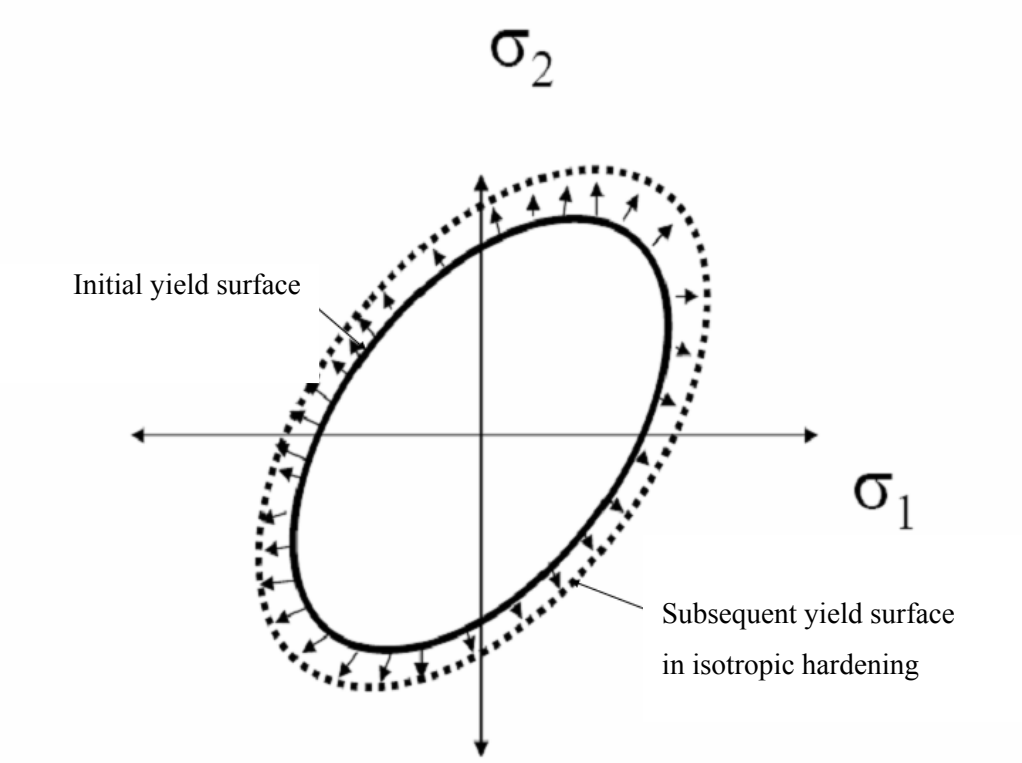

Figure 3.8 Effect of isotropic hardening model on yield surface

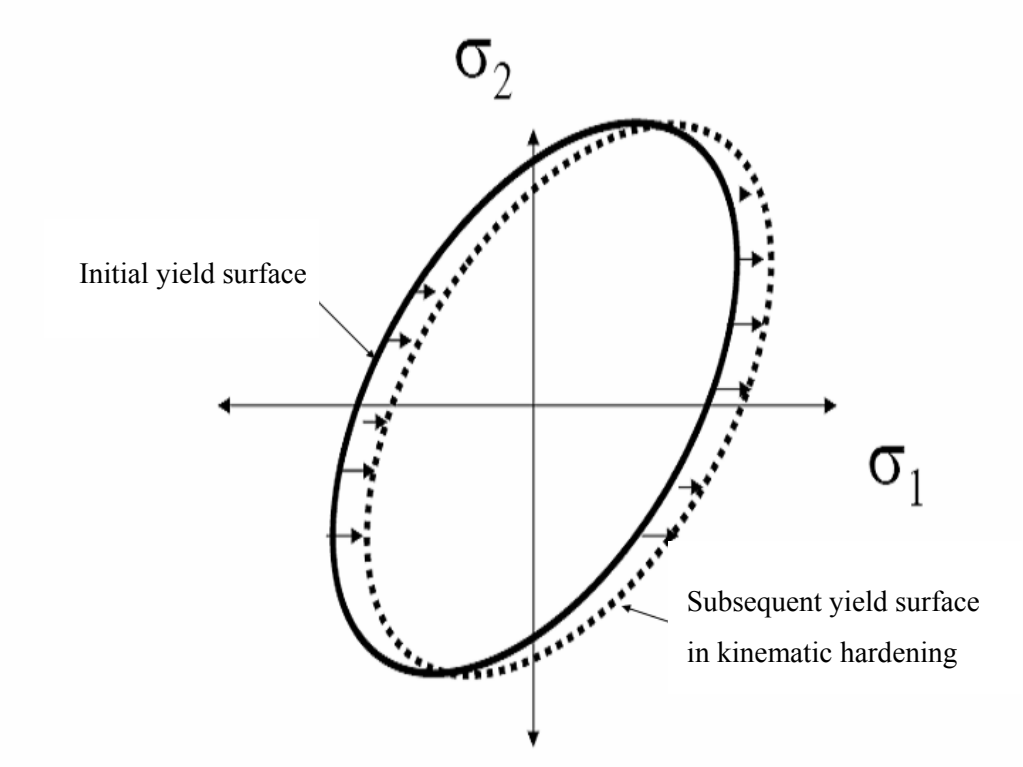

Figure 3.9 Effect of kinematic hardening model on yield surface

3.3 FRP pole modeling

A 20 ft (6.1 m) and a 25 ft (7.6 m) long tapered circular FRP poles were used for the FEM model. The geometric variables describing the configuration of typical FRP poles used in finite element modeling are shown in Table 3.3. A three-dimensional FEM of the test specimens was developed using ANSYS Software. Three-dimensional isoparamteric solid elements were used to model the pole, end-plate, bolts, and the concrete base as shown in Figure 3.10. Since a refined finite element mesh leads to more accurate results, a fine mesh was used in the connection region of the pole, which is a more stressed region.

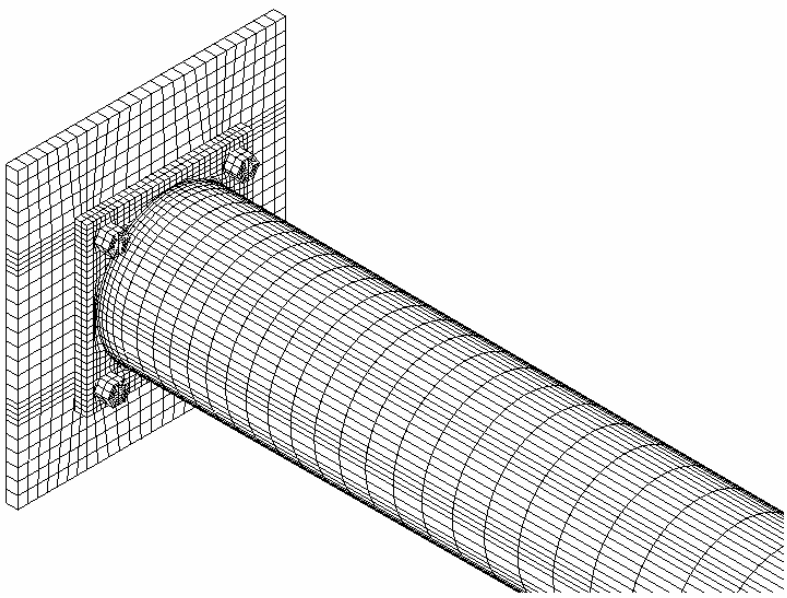

(a)

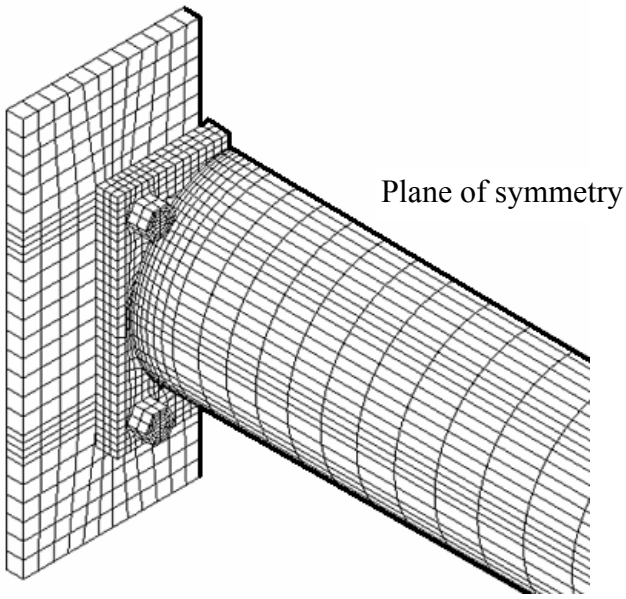

(b)

Figure 3.10 Typical FEM model for FRP poles:
(a) Converged full model; (b) Converged half model

Table 3.3 Dimensions used in FEM analysis for FRP poles

FRP	LP in. (cm)	LS in. (cm)	TD in. (cm)	BD in. (cm)	DB in. (cm)	BH in. (cm)	TT in. (cm)	BT in. (cm)	PT in. (cm)	PD in. (cm)	BC in. (cm)
20ft	18	24	10.2	12	1.13	1.18	0.38	0.45	1.25	13.6	15
	(460)	(610)	(259)	(305)	(29)	(30)	(10)	(11)	(32)	(346)	(381)
25ft	22	24	9.6	12	1.13	1.18	0.38	0.48	1.25	13.6	15
	(570)	(610)	(244)	(305)	(29)	(30)	(10)	(12)	(32)	(346)	(381)

The surface-to-surface contact algorithm was employed to model the contact surfaces between the end-plate and the concrete base in addition to the contact between the bolt hole and the bolt shank. To capture nonlinearity and inelasticity effects, incremental plasticity algorithms using Tsai-Wu failure criterion (Tsai and Wu, 1971) is considered because it accounts for the interaction between different stress components. The external load is incrementally increased, and the converged solution in each load step is obtained through an iterative procedure by updating the tangential stiffness in accordance with the flow rule. Expressions for deflection of the pole in the x- , y- and z-directions are

$$\delta_x = \int_0^L \frac{1}{EI} M_z x dx \tag{3.14}$$

$$\delta^2 = \delta_x^2 + \delta_y^2 + \delta_z^2 \tag{3.15}$$

3.3.1 Material model

Because of the high axial stiffness of the fibers, the stiffness of a unidirectional fiber reinforced polymer material is very high in the fiber direction and relatively low in the directions which are perpendicular to the fibers. Hence a unidirectional fiber reinforced polymer composite material is not isotropic. The stiffness properties are

approximately the same in the y- and z- directions, but these properties are different than those in the x- direction. This type of material is classified as transversely isotropic. The material properties used in analysis are shown in Table 2.3.

However, these FRP poles' fibers can be assumed to be approximately randomly oriented in the matrix because of filament winding technique in which fibers orient 0, 45, and 90 degrees. Then, the composite acts as an isotropic material and the properties are obtained using the following formulas (Morozov, 2004).

$$E = \frac{3}{8}E_1 + \frac{5}{8}E_2 \tag{3.16}$$

$$G = \frac{1}{8}E_1 + \frac{1}{4}E_2 \tag{3.17}$$

$$\nu = \frac{E}{2G} - 1 \tag{3.18}$$

where, E_1 and E_2 are longitudinal tensile modulus and transverse tensile modulus, respectively. The coefficients E_1 and E_2 are defined as

$$E_1 = E_f v_f + E_m v_m \tag{3.19}$$

$$\frac{1}{E_2} = \frac{v_f}{E_f} + \frac{v_m}{E_m} \tag{3.20}$$

where E_f, E_m, v_f and v_m are longitudinal fiber tensile modulus, longitudinal resin (matrix) tensile modulus, fiber volume fraction, and resin volume fraction, respectively.

3.4 Comparison to test results

The finite element analysis results are presented in comparison with those of experiments in Table 3.4, and in Figures 3.11 and 3.12 for steel and FRP poles, respectively. Due to the interaction effects on bolts and contact surfaces, the ultimate loads obtained from FEM analysis dropped after yielding point in both cases. However, as shown in Figures 3.11 and 3.12, the initial stiffness of the poles was predicted well by the proposed model. The ultimate load was assumed as the excessive yielding around the bolt holes from the Von Mises equivalent stress distributions to reduce the

computational effort. The nonlinear model was analyzed until excessive yielding around the bolt holes, which was taken as $2\sigma_y$. The ultimate deflection was measured at the same point as the experiments.

Table 3.4 Comparison experimental results to FEM results

Test Specimens	Load lbs (N)			Deflection in. (cm)		
	Exp.	FEM	Exp./ FEM	Exp.	FEM	Exp./ FEM
Steel 20 ft (6.1m)	505 (2247)	524 (2332)	0.964	29.63 (75.25)	30.39 (77.18)	0.975
FRP 20 ft (6.1 m)	2742 (12200)	2806 (12485)	0.977	20.72 (52.63)	20.98 (53.28)	0.988
FRP 25 ft (7.6 m)	2889 (12856)	3000 (13350)	0.963	43.71 (111.02)	42.88 (108.67)	1.019

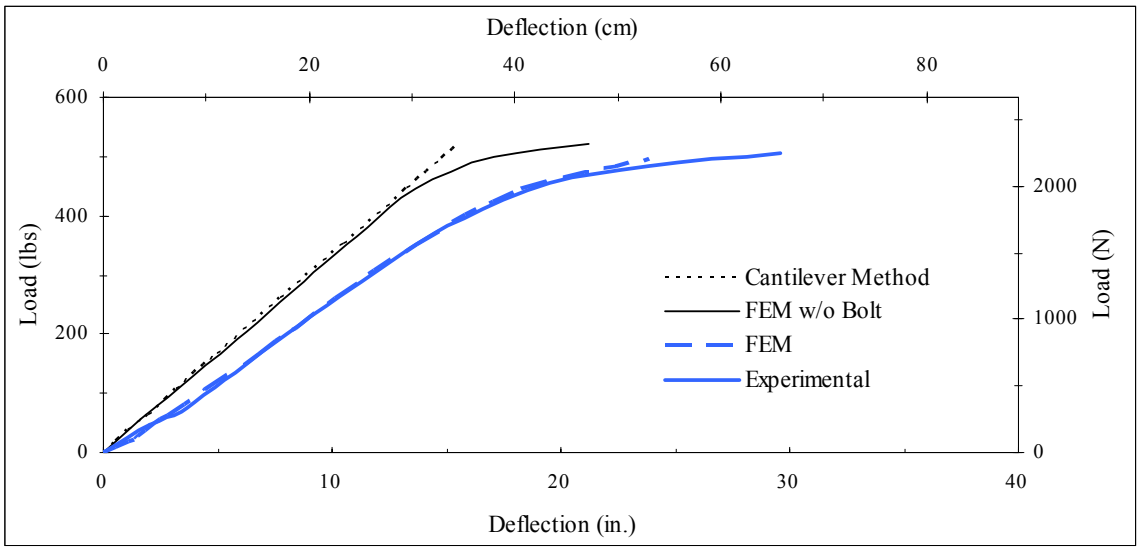

Figure 3.11 Deflection vs. load for steel poles

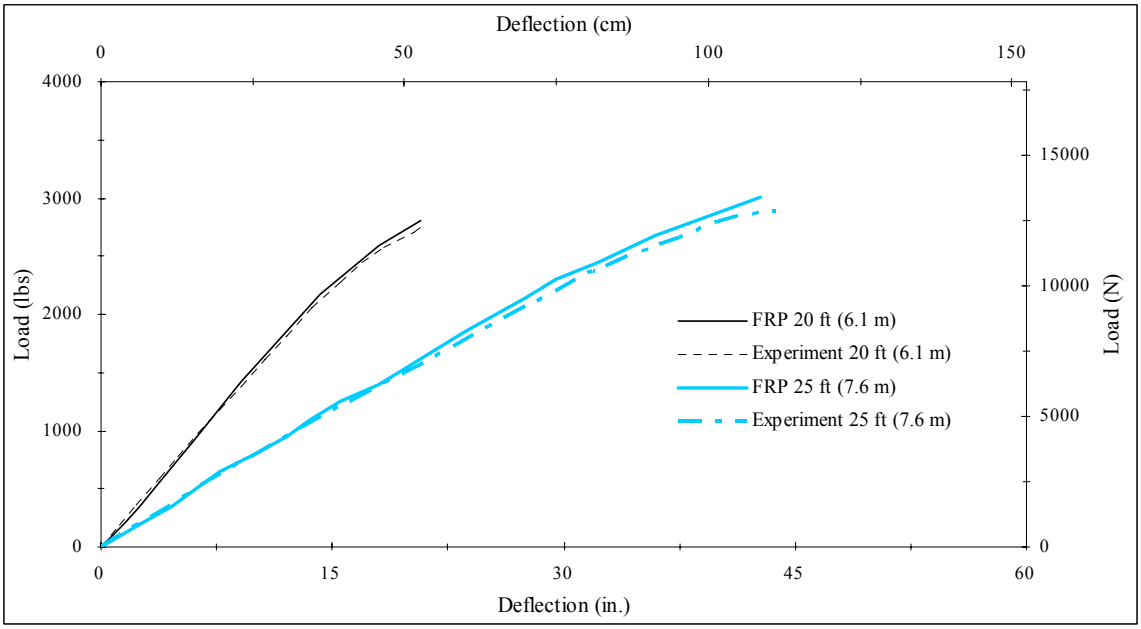

Figure 3.12 Deflection vs. load for FRP poles

Figure 3.11 presents the comparison of the ultimate load versus ultimate deflection results for the steel pole obtained from the experiment, FEM analyses, and classical structural analysis techniques (i.e. classical cantilever method). This figure shows that the FEM mimics the experimental results accurately during the early stage of loading (up to 390 lbs (1736 N)) while slight deviations are observed at a later stage. This is attributed to the fact that the contact algorithm of the FEM model is highly sensitive to the separation of the end-plate from the concrete base, and it contributes significantly to the overall pole tip deflection. These types of micro measurements are not normally easily achievable in the experimental measurements. Also, load-deflection results of the classical method and FEM without bolt are much stiffer than that of the FEM with bolts. This is due to the fact that classical cantilever method assumes elastic material properties, and the boundary condition between end-plate and concrete base was fixed. Also, the effect of bolt pre-tensioning, and contact surfaces were not adopted in classical method and FEM without bolt models. The figure also shows that the discrepancies on ultimate load capacity and ultimate deflection for steel pole between

experimental and FEM results are within 3.6 % and 2.5 %, respectively. The Von Mises equivalent strain distributions were the similar at the elastic range. Finally, the nonlinear FEM pole model with bolt and contact model behaves slightly stiffer than the behavior of the pole tested experimentally. This is due to the fact that FEM solutions are upper bound and should behave in a stiffer manner. The deformed shape of entire pole and bolt model are shown in Figures 3.13 (a) and (b), respectively.

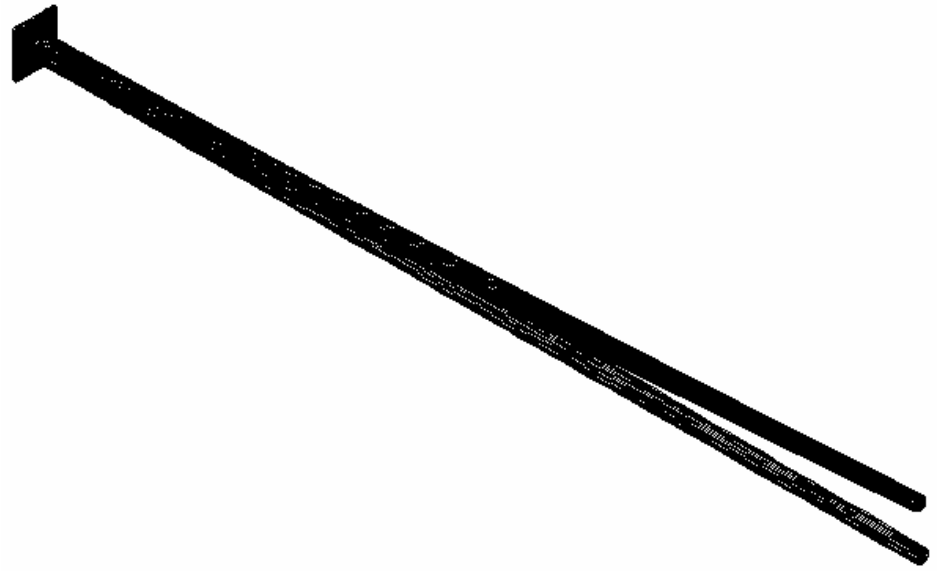

(a)

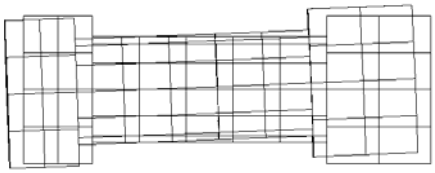

(b)

Figure 3.13 Deformed shapes of steel poles at ultimate state:
(a) Entire pole; (b) Bolt

For FRP poles, the experimental and FEM curves have also a linear form in the elastic range as shown in Figure 3.12. After the load-deflection curves began to deviate

from being linear, the high strains were observed in the bolt. From Table 3.4 and Figure 3.12, it is evident that the FEM predicted the FRP pole's behavior closely with maximum errors ranging from 2.3 % to 3.7 % for the ultimate load, and ranging from 1.2 % to 1.9 % for ultimate deflection. The result on stress in bolt and end-plate (Figure 3.14 (b)) confirms that tensile stress distributes uniformly in the whole bolt head/nut, and the maximum stress which exists through the bolt shank is greater than the yielding limit.

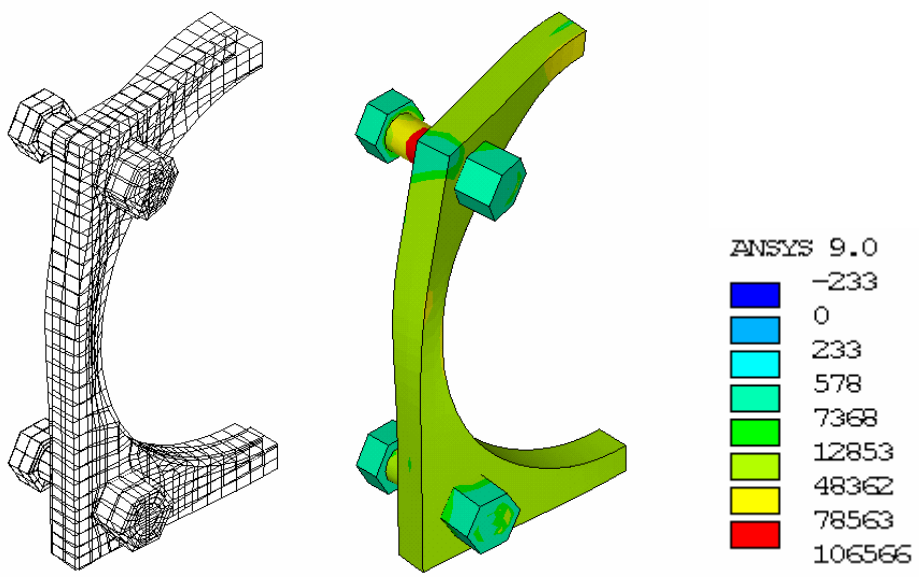

(a) (b) (unit: psi)

Figure 3.14 FEM results of FRP poles:
(a) Deformed shape; (b) Stress contour plot

To further verify the FEM, a preliminary parametric study was conducted by varying pole's end-plate and wall thickness one at a time and keeping other variables constant. The load-deflection results obtained from Figures 3.15 and 3.16 shows that FEM produced the expected and intuitive results.

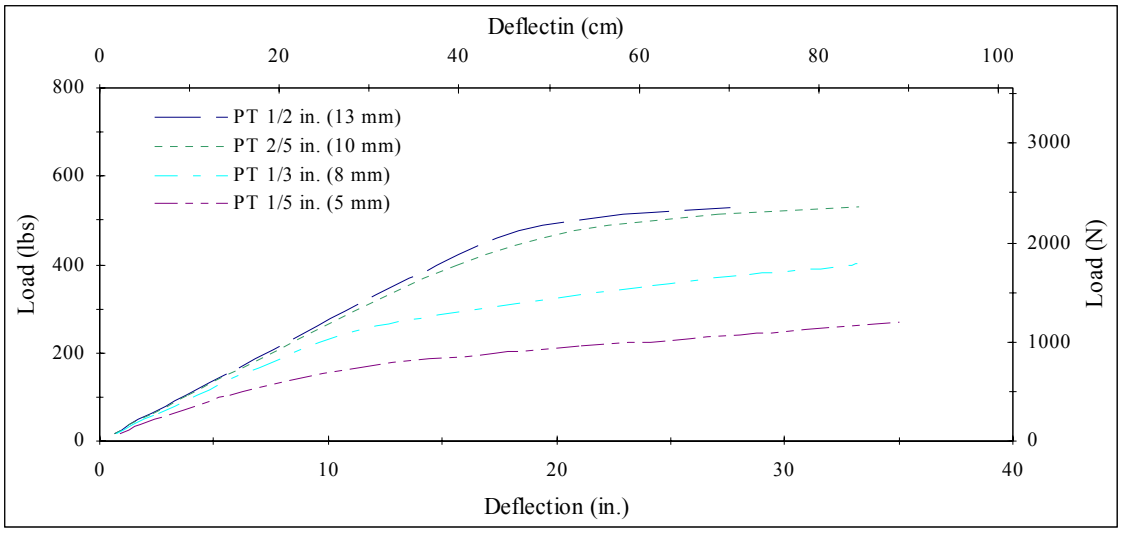

Figure 3.15 Effect of variation of end-plate thickness on load-deflection characteristics for steel pole

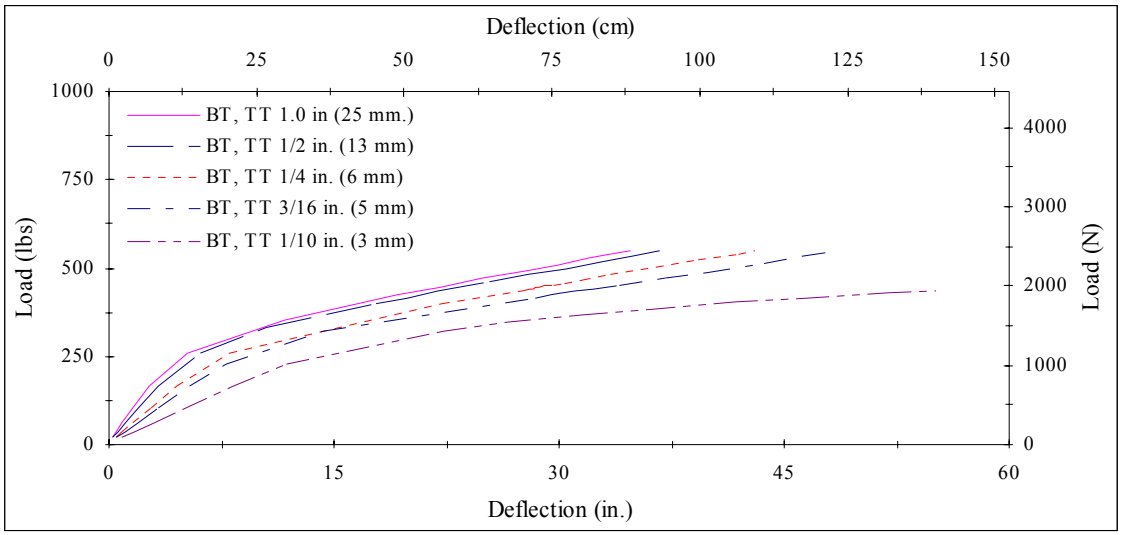

Figure 3.16 Effect of variation of wall thickness on load-deflection characteristics for steel poles

3.5 Chapter summary

In this chapter, a finite element model was developed using three-dimensional isoparametric solid elements, which included algorithms for contact, geometric, and material nonlinearities during the stress analysis. Since a plane of symmetry existed along a section through the longitudinal axis of the pole, one-half of the pole and its connection assembly were modeled.

Three dimensional solid elements were used to model the entire pole, end-plate, bolt assemblage, and concrete base. Bilinear stress-strain curves were used for steel and FRP. Transversely isotropic behavior of FRP pole was considered and the equivalent modulus was obtained for the analysis. Due to nonlinear system equation behavior, the full Newton-Raphson iteration was adopted and the convergence was obtained by using Hilbert L-2 norm coupled with equating external virtual work done to internal virtual strain energy.

The FEM produced load-deflection plots indicated close correlation with the experimental results for most regions of loading. The maximum differences between the FEM and experimental results for steel poles ranged from 1.2 % to 2.5 %. Also, the maximum differences between FEM and experimental results for FRP poles were 2.3 % to 3.7 % and 1.2 % to 1.9 % for stresses and strains, respectively.

To further verify the developed models, the end-plate and wall thickness were varied one at the time while other geometric and force related variables were kept constant. The load-deflection plots showed that FEM models followed the trend that agrees with engineering intuition.

CHAPTER 4
DEVELOPING OF MATHEMATICAL MODELS

4.1 Introduction

The load-deflection curves of the steel and FRP poles behave in a nonlinear fashion from early stage of loading for both steel and FRP poles. This phenomenon was observed both during testing and the FEM analysis of several poles with varying their force and geometric parameters. Figure 4.1 shows the configuration of a typical load-deflection plot for steel and FRP poles. This figure shows three distinct parameters that define the load-deflection curve. These parameters are: ultimate load, P_u; reference plastic deflection, δ_u; and rigidity parameter, n.

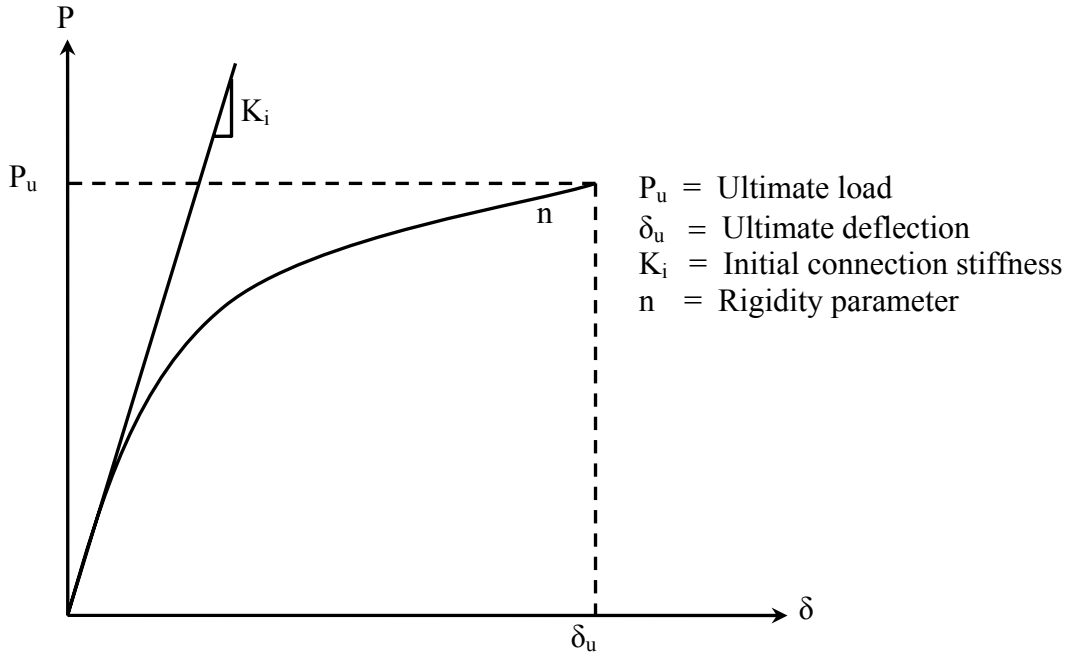

Figure 4.1 Typical load-deflection curve for poles

Several bilinear and nonlinear models are developed by researchers to represent load-deflection characteristics of different problem. Some examples of these models

include polynomial (Sommer, 1969; Frye and Morris, 1975), Cubic B-spline (Jones, Kirby, and Nethercot, 1980, 1981), three-parameter power (Colson and Louveau, 1983; Chen and Kishi, 1987; Kishi et al., 1988a, 1988b; Kishi and Chen, 1990), exponential (Lui and Chen, 1986; Yee and Melchers, 1986; Wu and Chen, 1990), Ramberg-Osgood (Ramberg and Osgood, 1943; Richard and Abbott, 1975; Ang and Morris, 1984), and Richard-Abbott (Richard et al., 1980; Attiogbe and Morris, 1991; Bahaari and Sherbourne, 1997). Among the aforementioned models the Ramberg-Osgood and three-parameter power model have gained abundant popularity among three parameter models. The polynomial model may give a discontinuous connection stiffness or negative stiffness. Although the Cubic B-spline model gives an excellent fit to the experimental data, it requires huge data in the curve-fitting process. Kishi and Chen (1990), Kishi et al. (1991) used three-parameter power model to represent moment-rotation behavior of double web angle connections. Abolmaali et al. (2004a) used both Ramberg-Osgood and three-parameter power model to predict the moment-rotation (M-θ) behavior of the flush end-plate connection. This study showed that three-parameter power model more accurately modeled the M-θ of the connection.

Since the behavior of the load-deflection curves for steel and FRP was similar to those of M-θ of steel connections as reported by Abolmaali et al. (2004a), three-parameter power model was adopted for this study. The finite element model described in chapter 3 was used as experimental data. Each 55 and 61 cases were examined to determine the effects of the variables on the deflection of the modeled pole with a corresponding load for steel and FRP poles, respectively.

4.2 Three-parameter power model

A three-parameter power model proposed by Richard and Abbott (1975) is used to predict the load-deflection characteristics of steel and FRP poles. In this model the load-deflection formula is given by:

$$P = \frac{K_i \delta}{\left[1 + \left(\frac{\delta}{\delta_0}\right)^n\right]^{\frac{1}{n}}} \tag{4.1}$$

where, P is the load capacity, K_i the initial pole stiffness, δ_o the reference plastic deflection, and n the rigidity parameter. The corresponding tangent stiffness, K_t is

$$K_t = \frac{dP}{d\delta} = \frac{K_i}{\left[1 + \left(\frac{\delta}{\delta_0}\right)^n\right]^{\frac{n+1}{n}}} \tag{4.2}$$

and the reference plastic deflection, δ_0 is

$$\delta_0 = \frac{P_u}{K_i} \tag{4.3}$$

Figure 4.2 shows a typical three-parameter power model for load-deflection curves and the influence of rigidity parameter to the shape of the model. This power model gives a smooth curve without abrupt change of slope. From this figure, it is recognized that the larger the power index n, the steeper the curve.

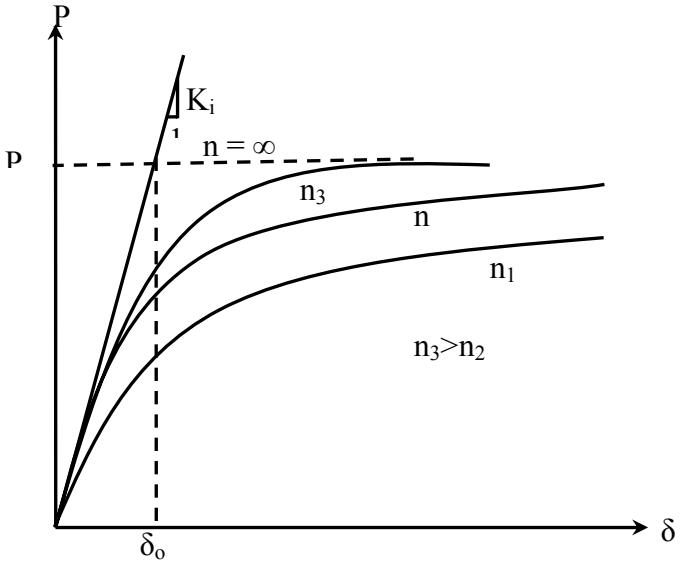

Figure 4.2 Three-parameter power model

4.3 Selection of test cases

In order to develop regression equation for parameters of three-parameter model (P_u, δ_0, and n) as functions of steel and FRP poles' geometric and force-related variables (Chapter 5), several test cases were selected for FEM analysis. These test cases were based on practical range of geometric and force-related variables adopted by the Texas Department of Transportation, which are: L; PT; TT; BT; DB; BD; TD; BC; PD; GAP; F_p; F_y; and E. These variables are defined in Chapter 2 and for convenience are repeated here:

- L = Pole length
- PT = Thickness of end-plate
- TT = Pole thickness at the pole's top
- BT = Pole thickness at the pole's bottom
- DB = Bolt diameter
- BD = Outer diameter at the bottom of pole
- TD = Outer diameter at the top of pole
- BC = Bolt circle
- PD = Side length of square end-plate
- GAP = Distance between the bottom of the end-plate lip and the nearest side of the concrete base
- F_p = Pre-tension load
- F_y = Yield stress
- E = Elastic modulus

The following procedure was adopted to select the test matrix:

1) Pole height (L) was ranged from 20 ft (6.1 m) to 60 ft (18.3 m) based on the practical design. Generally, less than 20 ft (6.1 m) high pole is installed by a direct burial. The height was increased by 5 ft (1.5 m).
2) Plate thickness (PT) was ranged from 0.5 in. (12.7 mm) to 1.75 in. (44.5 mm).

3) The pole thickness at top (TT) and bottom (BT) of the pole was ranged from 0.1 in. (2.5 mm) to 0.3 in. (7.6 mm) for steel, and from 0.2 in. (5.1 m) to 0.5 in. (12.7 mm) for FRP poles, which was based on the practical design.
4) Bolt diameter (DB) was adopted from LRFD codes (AISC, 1999) which varied between $^{3}/_{4}$ in. (19.1 mm) and 2 in. (50.8 mm)
5) The pole was considered to be tapered with cross-sectional area being a maximum at the bottom and minimum at the top.
6) Installation gap was used to give adequate space for leveling nuts. This gap was not less than two times nut thickness due to the double nut configuration.
7) The tensile strength for steel (F_y) was limited to $F_y \leq 65$ ksi (448 MPa).
8) End-plate side length (PD) and bolt circle (BC) was based on the practical design. However, the distance between the center of bolt and side end of end-plate is recommended to be more than $1^{1}/_{2}$ times bolt diameter (1.5 DB) in order to avoid end-plate rupture failure.
9) For FRP poles, the elastic modulus will be changed by altering the fiber orientation, the number of fiber layers, and fiber volume fraction which is out of this study. Thus proportional increment ranging from 3.5 Msi (24.1 GPa) to 5.5 Msi (37.9 GPa) based on rule of mix [24 and 35] was used for E values.
10) The connection bolts were assumed to be snug-tight which was in the condition of a specific percentage of the LRFD minimum specified pretension force depending on the bolt diameter (AISC, 1999). Keating et al. (2004) reported laboratory studies involving the large-diameter anchor bolts (1 in. to 3 in.) with double-nut configuration. According to the study, the extent of turn-of-the-nut mainly affects the pretension load. In this study, for the value of pretension load, the average stresses of $^{1}/_{6}$ turn-of-the-nut were adopted under the limitation of $F_p \leq$ LRFD minimum specified pretension force.

Tables 4.1 and 4.2 show the selected test case based on the aforementioned variation of variables for steel and FRP poles, respectively.

Table 4.1 Independent parameters used for steel poles

Test Case	L ft	PT in.	TT in.	BT in.	DB in.	BD in.	TD in.	GAP in.	F_y ksi	BC in.	PD in.	F_p kips
1	20	0.5	0.1	0.15	0.75	9	4	2	36	12	11	28
2	20	1	0.15	0.15	0.75	7	4	2	40	10	9.5	25
3	20	1	0.15	0.15	1	7	3	2.75	45	10.5	9.5	51
4	20	1	0.15	0.15	1.25	11	5	2.75	40	15.5	14	55
5	25	0.75	0.15	0.2	1.25	12	6	2.75	45	16.5	15	70
6	25	0.75	0.3	0.3	0.75	7	5	2.75	36	10	10	28
7	25	1	0.15	0.15	1	8	5	2.5	40	11.5	11	45
8	25	1	0.15	0.2	0.75	7	4	2	50	10	9	25
9	25	1	0.2	0.2	1	8	4	3	55	11.5	10.5	51
10	25	1.25	0.15	0.15	1.25	11	6	2.5	36	15.5	14	60
11	30	0.75	0.15	0.15	1.25	12	7	2.75	40	16.5	15	35
12	30	0.75	0.2	0.2	1.5	14	6	3.5	36	19	17	85
13	30	1	0.15	0.15	1.25	11	6	3.25	40	15.5	15	50
14	30	1.25	0.15	0.15	1	7	4	2.75	45	10.5	10	40
15	35	1	0.2	0.2	1.25	11	7	3	40	15.5	17	70
16	35	1	0.3	0.3	1.75	12	6	3.75	50	18	17	100
17	35	1.25	0.15	0.2	1.5	12	8	3.5	36	17	16.5	90
18	35	1.25	0.2	0.3	1.25	11	6	3.5	50	15.5	15	100
19	35	1.5	0.2	0.3	1.25	11	6	3	45	15.5	14	80
20	35	1.75	0.3	0.3	1	7	4	3	55	10.5	11	45
21	40	1	0.2	0.2	1.25	12	6	3	50	16.5	15	65
22	40	1	0.2	0.3	1.25	11	7	3	45	15.5	14	80
23	40	1	0.3	0.2	1.5	12	6	3.75	40	17	17	95
24	40	1.25	0.2	0.2	1.25	11	6	3.5	36	16	15	55
25	40	1.25	0.2	0.25	1.5	14	8	3.5	40	19	18	90
26	40	1.5	0.2	0.25	1.75	12	6	3.75	45	18	18	128
27	40	1.5	0.25	0.25	1.5	16	9	3.25	45	22	20	80

Table 4.1 – *Continued*

Test Case	L ft	PT In.	TT in.	BT in.	DB in.	BD in.	TD in.	GAP in.	F_y ksi	BC in.	PD in.	F_p kips
28	40	1.5	0.25	0.3	1.25	12	7	2.75	45	16.5	16	50
29	45	1	0.2	0.25	1.25	12	5	3	36	16.5	14.5	65
30	45	1	0.25	0.25	1.5	12	5	3.25	50	17	17.5	85
31	45	1	0.3	0.3	1.5	12	5	3.5	50	17	19	85
32	45	1.25	0.2	0.2	1.25	11	4	2.75	36	16	16	50
33	45	1.25	0.2	0.3	1.5	12	6	3.5	36	17	17	103
34	45	1.25	0.3	0.2	1.25	11	8	3	50	15.5	14.5	80
35	45	1.5	0.2	0.2	1.25	11	8	3	40	15.5	15	80
36	45	1.5	0.3	0.3	1.75	13	8	4	40	19	18	130
37	45	1.5	0.3	0.4	1.25	11	6	3.75	50	16	14	55
38	45	1.75	0.2	0.2	1.5	14	7	3.5	45	19	17	95
39	50	1	0.2	0.25	1.5	14	7	3.5	45	19	17.5	75
40	50	1.25	0.15	0.2	1.5	12	7	3.25	40	17	15	65
41	50	1.25	0.2	0.2	1.25	11	6	3.5	40	15.5	15	70
42	50	1.25	0.3	0.4	1	11	6	3	36	15	14	40
43	50	1.5	0.25	0.25	2	18	9	4.25	45	26	26	105
44	50	1.5	0.3	0.3	2	18	10	4.5	45	26	26	140
45	50	1.75	0.3	0.3	1	7	5	3	50	10.5	9.5	60
46	50	1.75	0.3	0.2	1.75	14	7	4	50	20	18	120
47	55	1.25	0.3	0.2	1.25	11	5	3	36	15.5	14	80
48	55	1.5	0.2	0.2	1.5	12	8	3.5	36	17	16	80
49	55	1.75	0.25	0.25	2	15	9	4.5	36	22	21	140
50	60	1.25	0.2	0.25	1.5	16	9	3.25	50	22	19.5	85
51	60	1.5	0.2	0.3	1	7	5	3.5	40	10.5	10.5	50
52	60	1.5	0.3	0.3	1.75	14	8	3.5	36	20	18	120
53	60	1.75	0.25	0.25	1.5	16	8	3.5	36	22	19	95
54	60	1.75	0.3	0.3	1.5	12	8	3.5	36	17	15.5	103
55	60	1.75	0.3	0.3	1.75	16	8	3.5	40	23	21	110

Table 4.2 Independent parameters used for FRP poles

Test Case	L ft	PT in.	TT in.	BT in.	DB in.	BD in.	TD in.	GAP in.	BC in.	PD in.	P_p kips	E Msi
1	20	0.5	0.2	0.2	0.75	6	3.5	1.5	8	7.5	28	4.5
2	20	0.75	0.25	0.275	0.75	7.5	5	1.75	10	10	25	3.5
3	20	0.75	0.275	0.25	0.75	8	5.5	1.5	10	9	10	4
4	20	0.75	0.275	0.3	1	8	3.5	2.5	10.7	10.5	40	4.5
5	20	0.75	0.3	0.3	1	8	5	2.5	10.7	10.2	40	5
6	20	1	0.25	0.225	1	10	7	2.5	13.5	12	50	4.5
7	25	0.5	0.25	0.25	1	8	4.5	2.5	10.6	10	45	5.5
8	25	0.75	0.275	0.25	1.25	10	6	2.75	13.2	13	70	4.5
9	25	0.75	0.3	0.3	0.75	7	4	2	9.5	8.5	28	5
10	25	0.75	0.3	0.325	0.75	9.5	5	1.75	12	10.5	20	4.5
11	25	1	0.275	0.275	1	7.5	4.5	2.5	10	10	51	5.5
12	25	1	0.325	0.35	1	8.5	5.5	2.25	11.5	10.5	40	5
13	25	1.25	0.3	0.325	1	10	6	2	13.5	12.5	35	5
14	30	0.75	0.275	0.275	1	8	4	2.5	10.6	10	40	3.5
15	30	0.75	0.35	0.35	1.125	8.5	5	2.5	11.5	10.5	45	3.5
16	30	1	0.3	0.275	1	9	5	2.25	11.5	11	45	5
17	30	1	0.325	0.3	1.25	11	6	2.5	14.5	13.5	71	4
18	30	1	0.325	0.325	1.125	12	7	2.25	16	14	56	5.5
19	30	0.75	0.3	0.3	1	9	4	2.5	12	11	40	4.5
20	35	0.75	0.325	0.35	1	10	5.5	2.5	13.7	13.5	51	4
21	35	1	0.275	0.275	1.125	12	6.5	2.75	16	15	50	3.5
22	35	1	0.3	0.3	1.25	12	7	2.5	16.2	15.7	56	5
23	35	1	0.35	0.35	1	10	5	2.5	13.5	12.5	41	4.5
24	35	1.25	0.325	0.325	1.5	13	8	3	17.5	16	90	4
25	35	1.25	0.35	0.325	1.25	12	7	2.75	16	14.5	65	5.5
26	35	1.25	0.35	0.35	1.125	12	7.5	2.5	16	15	48	5
27	35	1.5	0.375	0.375	1	13	8	2	17	15.5	45	5.5
28	40	0.75	0.3	0.3	1	10.5	5	2.5	14	12.5	40	5
29	40	1	0.275	0.3	1.125	11	5.5	2.75	14.5	13	50	4
30	40	1	0.3	0.325	1.25	12.5	6	3	16.5	15	60	3.5
31	40	1	0.325	0.325	1	9	4.5	2.25	12	10.5	45	5
32	40	1	0.35	0.325	1.5	12	6.5	3.25	16.5	15	95	4
33	40	1.25	0.375	0.35	1	10.5	6	2.5	14	12.5	43	5.5
34	40	1.25	0.375	0.375	1.5	14	7.5	3	18.5	16.5	85	4
35	45	1	0.325	0.35	1.125	12.5	5	2.5	16.2	14.5	40	5

Table 4.2 – *Continued.*

Test Case	L ft	PT in.	TT in.	BT in.	DB in.	BD in.	TD in.	GAP in.	BC in.	PD in.	P_p kips	E Msi
36	45	1	0.35	0.375	1.5	14	7.5	3.5	18.2	16.2	85	5.5
37	45	1	0.4	0.4	1.25	13	6.5	2.75	17.5	15	50	4
38	45	1.25	0.375	0.4	1.25	12.5	6	2.75	16.5	14.5	55	4.5
39	45	1.5	0.4	0.4	1.5	16	10	3	20	18	95	4.5
40	50	0.75	0.35	0.35	1.125	12	5	2.5	16	15	45	4
41	50	1	0.35	0.375	1.5	14	7	3.5	19	17	75	4.5
42	50	1	0.375	0.4	1.25	16.5	9	2.75	21	19.5	71	3.5
43	50	1.125	0.375	0.375	1.25	16.5	9	2.75	21	19	90	4
44	50	1.5	0.4	0.425	1.75	16	9	3.75	22.5	21	93	4
45	50	1.25	0.4	0.425	1.75	16	8	3.5	22.5	21	93	4
46	50	1.125	0.375	0.375	1.75	16	8	3.5	22.5	21.5	108	3.5
47	50	1.5	0.425	0.45	1.5	17.5	10	3.5	23	20	87	4.5
48	55	1	0.45	0.45	1.25	16	8.5	2.75	20	18.5	45	3.5
49	55	1.25	0.425	0.45	1.5	18	10	3.25	24	22	103	4
50	55	1.25	0.45	0.475	1.25	15.5	8	2.75	19.5	17.5	71	5.5
51	55	1.125	0.45	0.45	1.5	14	6	3.5	18.5	17.5	60	4
52	55	1.5	0.375	0.4	1.75	16	8.5	3.25	22	19	85	5
53	55	1.5	0.45	0.425	1.5	18	10.5	3.5	24	21	90	4.5
54	60	1	0.425	0.45	1.5	16	8	3.25	22	19.5	85	5
55	60	1.25	0.45	0.45	1.75	17.5	9	3.5	23.5	22	101	4
56	60	1.5	0.425	0.4	2	18	9.5	3.75	24	22	90	5
57	60	1.5	0.425	0.425	1.75	16.5	8	3.5	21.5	20	67	5.5
58	60	1.125	0.45	0.45	1.5	17	7.5	3.5	21.5	19	103	3.5
59	60	1.125	0.475	0.5	1.5	15	6.5	3.25	20	18.5	95	3.5
60	60	1.25	0.5	0.5	2	20	11.5	4	27.0	24.0	79	4.5
61	60	1.5	0.45	0.45	2	20	10	4.25	27.0	25.0	110	4

4.4 Fitted three-parameter power model

The curve-fitting of the load-deflection curves with the three-parameter power model will be discussed. The parameter power model equation was fitted to the data obtained for load-deflection from FEM analysis of each test case. The parameters of this model (P_u, δ_0, and n) were determined using a least square technique solved in a nonlinear fashion using Newton and Conjugate Newton techniques. This process minimizes the squares of the summation of differences by varying the three aforementioned parameters.

The three parameters obtained from the fitting of the load-deflection curve for the selected steel and FRP test cases are shown in Tables 4.3 and 4.4, respectively. The test designations shown in these tables are to be interpreted as follows: S or F-L-PT-TT-BT-DB-BD-TD-GAP-BC-PD-F_p-F_y, respectively, where S or F stands for steel or FRP pole and the other variables are previously defined. For example, S-20-0.5-0.1-0.15-0.75-9-4-2-36-12-11-28 represents steel test pole with L = 20 ft; PT = 0.5 in.; TT = 0.1 in.; BT = 0.15 in.; DB = 0.75 in.; BD = 9 in.; TD = 4 in.; GAP = 2 in.; BC = 12 in.; PD = 11 in.; F_p = 11 kips; and F_y = 28 ksi.

Table 4.3 Parameters obtained from steel FEM model

Test ID	P_u, lbs	δ_0, in.	n
S20-0.5-0.1-0.15-0.75-9-4-2-36-12-11-28	1595.5	19.3	3.37
S20-1-0.15-0.15-0.75-7-4-2-40-10-9.5-25	1338.7	22.0	4.73
S20-1-0.15-0.15-1-7-3-2.75-45-10.5-9.5-51	1515.6	22.8	2.55
S20-1-0.15-0.15-1.25-11-5-2.75-40-15.5-14-55	3066.1	13.3	7.80
S25-0.75-0.15-0.2-1.25-12-6-2.75-45-16.5-15-70	4925.7	24.3	1.52
S25-0.75-0.3-0.3-0.75-7-5-2.75-36-10-10-28	2242.0	41.8	1.64
S25-1-0.15-0.15-1-8-5-2.5-40-11.5-11-45	1444.4	21.2	2.94
S25-1-0.15-0.2-0.75-7-4-2-50-10-9-25	1758.7	45.4	4.30
S25-1-0.1-0.2-1.25-11-6-3-55-15.5-14.5-70	2718.1	43.9	2.75
S25-1-0.15-0.2-1-10-6-2.5-40-14-13-35	2337.4	15.1	4.97
S30-0.75-0.15-0.15-1.25-12-7-2.5-40-16.5-15-35	2569.8	26.1	4.30
S30-0.75-0.2-0.2-1.5-14-6-3.5-36-19-17-85	4300.6	21.5	1.45
S30-1-0.15-0.15-1.25-11-6-3.25-40-15.5-15-50	2125.2	25.5	7.92
S30-1.25-0.15-0.15-1-7-4-2.75-45-10.5-10-40	1007.0	39.5	4.06
S35-1-0.2-0.2-1.25-11-7-3-40-15.5-17-70	2589.4	34.2	3.51
S35-1-0.3-0.3-1.75-12-6-3.75-50-18-17-100	6277.7	36.4	1.48
S35-1.25-0.15-0.2-1.5-12-8-3.5-36-17-16.5-90	2731.1	22.6	2.90
S35-1.25-0.2-0.3-1.25-11-6-3.5-50-15.5-15-100	4686.1	55.4	2.94
S35-1.5-0.2-0.3-1.25-11-6-3-45-15.5-14-80	3998.6	50.1	4.31
S35-1.75-0.3-0.3-1-7-4-3-55-10.5-11-45	2324.9	89.7	2.67
S40-1-0.2-0.2-1.25-12-6-3-50-16.5-15-65	3318.3	56.6	3.44
S40-1-0.2-0.3-1.25-11-7-3-45-15.5-14-80	4900.2	47.1	1.00
S40-1-0.3-0.2-1.5-12-6-3.75-40-17-17-95	2712.7	38.5	3.82
S40-1.25-0.2-0.2-1.25-11-6-3.5-36-16-15-55	2072.8	31.5	2.23

Table 4.3 – *Continued*.

Test ID	P_u, lbs	δ_0, in.	n
S40-1.25-0.2-0.25-1.5-14-6-3.5-40-19-18-90	4328.3	39.0	4.49
S40-1.5-0.2-0.25-1.75-12-6-3.75-45-18-18-128	3350.5	48.8	7.27
S40-1.5-0.25-0.25-1.5-16-9-3.25-45-22-20-80	6536.2	38.5	4.39
S40-1.5-0.25-0.3-1.25-12-7-2.75-45-16.5-16-50	5114.0	31.9	1.25
S45-1-0.2-0.25-1.25-12-5-3-36-16.5-14.5-65	2595.7	47.1	1.79
S45-1-0.25-0.25-1.5-12-5-3.25-50-17-17.5-85	3562.0	75.1	3.76
S45-1-0.3-0.3-1.5-12-5-3.5-50-17-19-85	4125.7	78.6	4.62
S45-1.25-0.2-0.2-1.25-11-4-2.75-36-16-16-50	1578.9	55.2	5.04
S45-1.25-0.2-0.3-1.5-12-6-3.5-36-17-17-103	3010.5	49.4	2.56
S45-1.25-0.3-0.2-1.25-11-8-3-50-15.5-14.5-80	2540.2	62.6	5.46
S45-1.5-0.2-0.2-1.25-11-8-3-40-15.5-15-80	2029.4	52.1	3.98
S45-1.5-0.3-0.3-1.75-13-8-4-40-19-18-130	4025.0	47.5	6.81
S45-1.5-0.3-0.4-1.25-11-6-3.75-50-16-14-55	5205.5	87.0	2.26
S45-1.75-0.2-0.25-1.5-12-7-4-45-18-16-110	3092.3	57.9	7.57
S50-1-0.2-0.25-1.5-14-7-3.5-45-19-17.5-75	3238.7	62.0	13.24
S50-1.25-0.15-0.2-1.5-12-7-3.25-40-17-15-65	1980.7	61.7	6.96
S50-1.25-0.2-0.2-1.25-11-6-3.5-40-15.5-15-70	1843.6	65.6	2.86
S50-1.25-0.3-0.4-1-11-6-3-36-15-14-40	3081.8	92.0	3.66
S50-1.5-0.25-0.25-2-18-9-4.25-45-26-26-105	6215.9	59.8	14.62
S50-1.5-0.3-0.3-2-18-10-4.5-45-26-26-140	7880.8	58.9	6.27
S50-1.75-0.3-0.3-1-7-5-3-50-10.5-9.5-60	1531.3	139.0	2.66
S50-1.75-0.3-0.2-1.75-14-7-4-50-20-18-120	3578.4	63.5	7.15
S55-1.25-0.3-0.2-1.25-11-5-3-36-15.5-14-80	3364.5	78.2	2.08
S55-1.5-0.2-0.2-1.5-12-8-3.5-36-17-16-80	1767.5	53.0	3.49
S55-1.75-0.25-0.25-2-15-9-4.5-36-22-21-140	3459.2	51.0	3.18
S60-1.25-0.2-0.25-1.5-16-9-3.25-50-22-19.5-85	3338.6	64.7	4.61
S60-1.5-0.2-0.3-1-7-5-3.5-40-10.5-10.5-50	813.4	159.0	15.87
S60-1.5-0.3-0.3-1.75-14-8-3.5-36-20-18-120	3476.3	55.3	1.95
S60-1.75-0.25-0.25-1.5-16-8-3.5-36-22-19-95	3397.5	64.8	5.06
S60-1.75-0.3-0.3-1.5-12-8-3.5-36-17-15.5-103	2697.7	60.5	1.53
S60-1.75-0.3-0.3-1.75-16-8-3.5-40-23-21-110	4579.5	74.1	4.93

Table 4.4 Parameters obtained from FRP FEM model

Test ID	P_u, lbs	δ_0, in.	n
F20-0.5-0.2-0.2-0.75-6-3.5-1.5-8-7.5-28-4.5	531.7	155.3	5.97
F20-0.75-0.25-0.275-0.75-7.5-5-1.75-10-10-25-3.5	1196.6	58.0	3.02
F20-0.75-0.275-0.25-0.75-8-5.5-1.5-10-9-10-4	922.5	37.7	4.86
F20-0.75-0.275-0.3-1-8-3.5-2.5-10.7-10.5-40-4.5	1647.5	66.6	4.31
F20-0.75-0.3-0.3-1-8-5-2.5-10.7-10.2-40-5	1485.5	44.9	4.27
F20-1-0.25-0.225-1-10-7-2.5-13.5-12-50-4.5	1705.7	32.5	4.07
F25-0.5-0.25-0.25-1-8-4.5-2.5-10.6-10-45-5.5	861.4	62.6	2.99
F25-0.75-0.275-0.25-1.25-10-6-2.75-13.2-13-70-4.5	1658.6	61.1	4.57
F25-0.75-0.3-0.3-0.75-7-4-2-9.5-8.5-28-5	675.3	59.7	4.83
F25-0.75-0.3-0.325-0.75-9.5-5-1.75-12-10.5-20-4.5	796.6	33.8	4.73
F25-1-0.275-0.275-1-7.5-4.5-2.5-10-10-51-5.5	1274.1	78.9	5.49
F25-1-0.325-0.35-1-8.5-5.5-2.25-11.5-10.5-40-5	1541.0	61.8	5.79
F25-1.25-0.3-0.325-1-10-6-2-13.5-12.5-35-5	2174.0	58.5	4.56
F30-0.75-0.275-0.275-1-8-4-2.5-10.6-10-40-3.5	1012.9	157.3	11.00
F30-0.75-0.35-0.35-1.125-8.5-5-2.5-11.5-10.5-45-3.5	1156.6	117.2	5.94
F30-1-0.3-0.275-1-9-5-2.25-11.5-11-45-5	1357.2	98.4	7.65
F30-1-0.325-0.3-1.25-11-6-2.5-14.5-13.5-71-4	1926.9	89.4	6.23
F30-1-0.325-0.325-1.125-12-7-2.25-16-14-56-5.5	1637.4	43.3	4.58
F30-0.75-0.3-0.3-1-9-4-2.5-12-11-40-4.5	996.8	93.6	5.99
F35-0.75-0.325-0.35-1-10-5.5-2.5-13.7-13.5-51-4	1120.3	101.4	3.17
F35-1-0.275-0.275-1.125-12-6.5-2.75-16-15-50-3.5	1568.2	111.4	6.33
F35-1-0.3-0.3-1.25-12-7-2.5-16.2-15.7-56-5	1872.7	86.0	5.37
F35-1-0.35-0.35-1-10-5-2.5-13.5-12.5-41-4.5	1270.5	105.5	5.70
F35-1.25-0.325-0.325-1.5-13-8-3-17.5-16-90-4	2669.4	103.3	6.27
F35-1.25-0.35-0.325-1.25-12-7-2.75-16-14.5-65-5.5	2065.9	80.0	6.27
F35-1.25-0.35-0.35-1.125-12-7.5-2.5-16-15-48-5	2079.4	76.4	4.54
F35-1.5-0.375-0.375-1-13-8-2-17-15.5-45-5.5	2295.9	58.1	4.46
F40-0.75-0.3-0.3-1-10.5-5-2.5-14-12.5-40-5	753.5	3.1	2.66
F40-1-0.275-0.3-1.125-11-5.5-2.75-14.5-13-50-4	1204.7	143.5	7.60
F40-1-0.3-0.325-1.25-12.5-6-3-16.5-15-60-3.5	1587.0	140.1	8.29
F40-1-0.325-0.325-1-9-4.5-2.25-12-10.5-45-5	915.2	147.1	7.31
F40-1-0.35-0.325-1.5-12-6.5-3.25-16.5-15-95-4	1854.5	144.3	5.94
F40-1.25-0.375-0.35-1-10.5-6-2.5-14-12.5-43-5.5	1331.9	102.5	5.30
F40-1.25-0.375-0.375-1.5-14-7.5-3-18.5-16.5-85-4	2551.8	114.3	7.01

Table 4.4 – *Continued*.

Test ID	P_u, lbs	δ_0, in.	n
F45-1-0.325-0.35-1.125-12.5-5-2.5-16.2-14.5-40-5	1227.5	119.9	6.69
F45-1-0.35-0.375-1.5-14-7.5-3.5-18.2-16.2-85-5.5	1877.0	96.3	5.13
F45-1-0.4-0.4-1.25-13-6.5-2.75-17.5-15-50-4	1296.4	110.4	5.25
F45-1.25-0.375-0.4-12.5-6-2.75-16.5-14.5-55-4.5	1738.7	142.9	8.67
F45-1.5-0.4-0.4-1.5-16-10-3-20-18-95-4.5	2992.6	97.1	5.31
F50-0.75-0.35-0.35-1.125-12-5-2.5-16-15-45-4	932.2	165.9	4.18
F50-1-0.35-0.375-1.5-14-7-3.5-19-17-75-4.5	1644.3	145.8	5.63
F50-1-0.375-0.4-1.25-16.5-9-2.75-21-19.5-71-3.5	1626.4	98.7	5.05
F50-1.125-0.375-0.375-1.25-16.5-9-2.75-21-19-90-4	1695.9	91.0	5.09
F50-1.5-0.4-0.425-1.75-16-9-3.75-22.5-21-93-4	3651.8	178.9	4.83
F50-1.25-0.4-0.425-1.75-16-8-3.5-22.5-21-93-4	3016.9	167.5	4.88
F50-1.125-0.375-0.375-1.75-16-8-3.5-22.5-21.5-108-3.5	2784.5	191.0	4.56
F50-1.5-0.4-0.4-1.5-17.5-9-3.75-23-20-79-3.5	2816.3	96.2	4.95
F55-1-0.45-0.45-1.25-16-8.5-2.75-20-18.5-45-3.5	1327.1	111.0	5.71
F55-1.25-0.425-0.45-1.5-18-10-3.25-24-22-103-4	2394.2	111.8	4.96
F55-1.25-0.45-0.475-1.25-15.5-8-2.75-19.5-17.5-71-5.5	1743.5	95.5	4.98
F55-1.125-0.45-0.45-1.5-14-6-3.5-18.5-17.5-60-4	2078.2	232.5	8.32
F55-1.5-0.375-0.4-1.75-16-8.5-3.25-22-19-85-5	2636.5	157.7	7.00
F55-1.5-0.45-0.425-1.5-18-10.5-3.5-24-21-90-4.5	2655.1	108.7	4.22
F60-1-0.425-0.45-1.5-16-8-3.25-22-19.5-85-5	1626.7	115.8	2.14
F60-1.25-0.45-0.45-1.75-17.5-9-3.5-23.5-22-101-4	2642.0	179.1	7.22
F60-1.5-0.425-0.4-2-18-9.5-3.75-24-22-90-5	3387.0	179.2	6.22
F60-1.5-0.425-0.425-1.75-16.5-8-3.5-21.5-20-67-5.5	3013.5	190.3	7.00
F60-1.125-0.45-0.45-1.5-17-7.5-3.5-21.5-19-103-3.5	1796.1	165.5	7.28
F60-1.125-0.475-0.5-1.5-15-6.5-3.25-20-18.5-95-3.5	1935.6	235.0	6.44
F60-1.25-0.5-0.5-2-20-11.5-4-27-24-79-4.5	3126.2	124.2	4.44
F60-1.5-0.45-0.45-2-20-10-4.25-27-25-110-4	3806.6	173.8	6.72

4.5 Chapter summary

In this chapter, the mathematical models used to curve fit the experimental load-deflection curves are presented. There are several mathematical models used for representing the load-deflection curves of connections such as linear, bilinear, polynomial, Cubic B-spline, the three-parameter power, exponential, Ramberg-Osgood and Richard-Abbott models. Based on accuracy of three-parameter power model reported in literature, for similar cases, three-parameter power model was adopted as tool to develop prediction equations for load-deflection of steel and FRP poles.

Geometric and force-related parameters of the pole were varied within their practical ranges, and based on the recommendation of the Texas Department of Transportation; matrices of test cases were developed.

Fifty five test cases for steel and sixty one test cases for FRP poles were identified after careful consideration of all the varied parameters discussed above, which included elimination of impractical cases. Finite element analyses were conducted on the selected test cases and the three parameter power model equation was fitted to the data obtained from the FEM results.

CHAPTER 5
REGRESSION ANALYSIS

5.1 Introduction

Three-parameter power model described in Chapter 4 was used to predict load-deflection characteristics of steel and FRP poles. The parameters defining the three parameter model equation are: (1) ultimate load; (2) reference plastic deflection; and (3) rigidity parameter. Thus, it was decided to obtain regression equation for three parameters (dependent variables) in terms of geometric and force-related parameters of the steel and FRP poles (independent variables). The material-related variables consist of elastic modulus and yield stress of the material. The geometric parameters include variables such as pole's height, thickness, end-plate geometry, and bolt size.

The predicted load-deflection plots compared with the FEM and experimental results. A sensitivity study is conducted by varying one parameter at the time and keeping other parameters in their intermediate values.

5.2 Regression analysis

In statistics, regression equations are developed from sample data collected from numerous experiments conducted to determine the values of the dependent parameters for predetermined values of independent parameters. However, the finite element analysis is not physical experiments in the true sense; it is analytical process for experiments. Since the results for each case are completely deterministic and reproducible.

To perform the regression analysis, it is a common procedure to represent the response of dependent parameter as functions of the independent parameters. In the parametric study, the three parameters of the pole are the response measured as functions of the independent parameters. These independent parameters for the 55 and 61 cases selected, as described in Tables 4.1 and 4.2, were the input data to the computer program, ANSYS, which eventually were solved for the load deflection. Thus, the objective of the regression analysis was to develop equations for parameters

defining load-deflection of the pole as functions of geometric and force-related parameters of the pole. For example, the following would be the form of the equation which is a function of certain parameters:

$$K = f\left(L, PT, TT, BT, DB, BD, TD, BC, TD, BC, PD, GAP, F_p, F_y\right) \tag{5.1.a}$$

or

$$K = f\left(L, PT, TT, BT, DB, BD, TD, BC, TD, BC, PD, GAP, F_p, E\right) \tag{5.1.b}$$

Determination of the function f_1 is discussed in general terms as follows. Let

$$x = f(X_1, X_2, X_3, ...X_n) \tag{5.2}$$

be a function of n independent parameters, intended to fit data collected from a study. A linear (or summation) regression model for the function is written as

$$\begin{aligned} x = C_0 + C_1X_1 + C_2\ X_2 + C_3X_3 + ... + C_nX_n + C_{12}X_1X_2 \\ + C_{23}X_2X_3 + ... + C_{n1}X_nX_1 + C_{123}X_1X_2X_3 + ... \\ + C_{123.....n}(X_1X_2X_3 .....X_n) \end{aligned} \tag{5.3}$$

This techniques yield information on the relative significance of not only the main parameters $X_1, X_2, ..., X_n$, but also the interactions between these same parameters $X_1X_2X_3, ..., (X_1X_2...X_n)$. However, in most practical problems, such as the one studied, many of the higher-order interactions may be eliminated on the basis of physical and intuitive considerations. Probable interactions must, however, be included in the model. The behavior of the pole seems to be a simple solution considering the cantilever profile of the member, but there are many more parameters that can be considered in an analytical study and regression analysis. For example, bolt diameter, base diameter, base condition and connection, yield stress, plate thickness, and tapering can be factors contributing to the outcome. This possibility makes this type of an analytical study and regression analysis a complex and interesting study, but does not facilitate the complete defining of all the interactions.

If a linear regression model is not found satisfactory, an alternative method is the product regression model of the form:

$$x = C_0 X_1^{C_1} X_2^{C_2} \ldots X_n^{C_n} \tag{5.4}$$

This nonlinear regression method was used in this project because of the complexity of the interactions involved. This may be reduced to a linear regression model if logarithms are taken of both sides as shown below:

$$\ln x = \ln C_0 + C_1 \ln X_1 + C_2 X_2 + \ldots + C_n \ln X_n \tag{5.5}$$

Denoting the logarithms of the various parameters by prime superscripts, Equation 5.5 becomes

$$x' = C_0' + C_1 X_1' + C_2 X_2' + \ldots + C_n X_n' \tag{5.6}$$

This is similar to the first group of terms in Equation 5.2. It should be noted that in Equation 5.6 product terms of the form X_1', X_2', X_3', etc., do not occur, so no interactions are present.

In this study, the coefficient C_0' and the exponents $C_1, C_2, \ldots, C_n$ in Equation 5.5 are determined by multiple regression analysis, so as to obtain the best least square fit to the data. With this method, the best fit regression equation is taken as the one which minimizes the sum of the squares of the deviations of the data points from the equation fitted to the data. To demonstrate the basic principles, say that the value of the dependent variable predicted from the best fit equation is x_i', for any particular set of values, $X_{1i}', X_{2i}', X_{3i}', \ldots, X_{ni}'$ while it is measured (or directly determined) value is $\bar{x}_i$. Deviation of the predicted value from the measured value is given by

$$\bar{x}_i - x_i' = \bar{x}_i - \left(C_0' + C_1 x_{1i}' + C_2 x_{2i}' + \ldots + C_n x_{ni}'\right) \tag{5.7}$$

The sum of the squares, S for m number of data is given by

$$S = \sum_{i=1}^{m} \left(\bar{x}_i' - x_i'\right)^2 \tag{5.8}$$

The unknown coefficients $C_0', C_1, C_2, ..., C_n$ are determined by minimizing the quality S with respect to each coefficient, in other words by setting it equal to zero as shown below.

$$\frac{\partial S}{\partial C_0'} = \frac{\partial S}{\partial C_1} = \frac{\partial S}{\partial C_2} = ... = \frac{\partial S}{\partial C_n} = 0 \tag{5.9}$$

This will result in $(n+1)$ linear simultaneous equations from which the coefficients $C_0', C_1, C_2, ..., C_n$ can be determined. To determine C_0 the anti-logarithm of C_0' must be found.

A "goodness of fit" of the prediction equation is a comparison of S, the sum of the squares, and the deviations for the constant term C_0 above. The constant term model is

$$S = C_0' \tag{5.10}$$

and the sum of the squares of this model can be written as

$$S_0 = \sum_{i=1}^{m} \left(\bar{x}_i' - x_0' \right)^2 \tag{5.11}$$

in which x_0' is the mean. The difference between S_0 and S is called as "sum of squares due to regression" and the ratio $\frac{(S_0 - S)}{S_0}$ is called as "coefficient of multiple determination", R^2 which can also be written:

$$R^2 = 1 - \frac{S}{S_0} \tag{5.12}$$

A value of $R^2 = 1$ implies that S is zero and the regression prediction equation passes through all the data points. A value of $R^2 = 0.80$ means that 80 % of the sum of squares of the deviations of the observed (or directly determined) $\bar{x}_i'$ values about their x_0' can be explained by the prediction equation obtained.

In the parametric study conducted, all the cases considered had the independent parameters inputted into the finite element computer program, ANSYS, and the output

was the response of the dependent parameters. Therefore, a rerun of the same case would have same quantitative response, thus, not providing any information regarding the realistic variance in the response. The coefficient of multiple determination R^2 was the unique criterion used to measure the accuracy of the prediction equations to characterize the behavior of the typical pole.

5.3 Proposed characteristic load

Initial attempts were made to obtain regression equations for parameters of the load-deflection for the three parameter model equations (i.e. P_u, δ_0, and n) in terms of pole's geometric and force-related variables. In obtaining prediction equation for rigidity parameter, n, it was challenging to obtain an acceptable value for the coefficient of multiple determination (R^2). After eliminating several data points, this value at best was R^2=0.5508 and 0.6633 for steel and FRP cases, respectively, which is neither practical nor desirable. Thus, an additional independent parameter was proposed which improved the value of R^2 for parameter defining the three parameter power model significantly. This independent parameter is introduced as the "characteristic load".

The characteristic load for each FEM test cases was obtained by drawing a tangent line to the load-deflection plot at the point of ultimate load, such that it covered most points on the region of the graph at the vicinity of ultimate load. The intersection of this line and line of initial stiffness was graphically identified. The coordinates of this point was called characteristic load (P_c) and characteristic displacement (δ_c) as shown in Figure 5.1.

The value of P_c for all the FEM test cases were graphically obtained from the load-deflection plot of each case, which was then incorporated as an independent variables in the regression analysis.

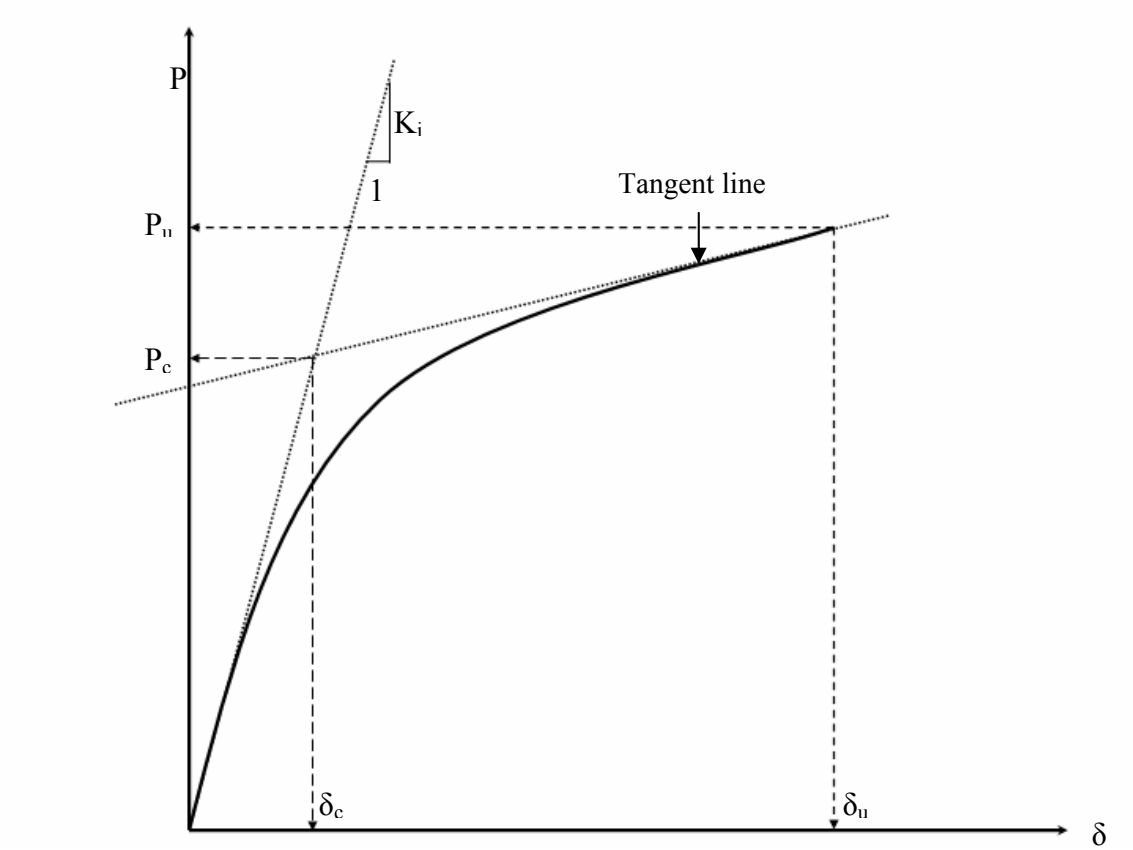

Figure 5.1 Proposed characteristic load and displacement

5.4 Comparison of predicted and FEM results

The results from the FEM test cases were regressed using the nonlinear regression analysis as explained in Section 4.2 to develop prediction equations for parameters defining the three parameter load-deflection model. Equations 5.1 through 5.10 present the prediction equations for these parameters: (1) ultimate load; (2) reference plastic deflection; and (3) rigidity parameter, for steel and FRP poles as functions of their geometric and force-related variables. Tables A.1 and A.2 of Appendix A show the comparison of the values of ultimate load, reference plastic deflection, and rigidity parameter obtained from the regression equation and the FEM results. These tables show that the ratio of the FEM to prediction is in most cases close to 1.0 for P_u and δ_0. However, this ratio fluctuates more profoundly for the rigidity parameter, n. The percentage differences between aforementioned parameters are also

presented. Tables 5.1 and 5.2 summarize the values of the power of independent variables for steel and FRP poles. The coefficient of multiple determination, R^2, is calculated for every regression equation and is used to examine its accuracy. Figures B-1 through B-14 and C-1 through C-16 of Appendix B and C present the comparison between the predicted and numerically obtained load-deflection plots for steel and FRP poles, respectively.

Table 5.1 Coefficients for the prediction equations for steel poles

Parameter	P_u, lbs	δ_0, in.	n	P_c	K_i
e	6.9290	-6.7295	7.4278	6.4261	9.7484
L	-1.0089	1.6480	-2.4001	-1.1809	-2.5836
PT	-0.0886	-0.0209	0.8623	0.0709	0.1197
TT	0.4525	-0.0026	0.0887	0.5424	0.3202
BT	0.8511	0.2370	-0.3284	0.6788	0.3447
DB	0.1552	-1.3363	1.1209	0.0352	0.7823
BD	1.8577	-0.9284	0.5812	2.1860	2.9977
TD	0.0471	-0.4106	0.7411	0.1878	0.2426
BC	0.1908	0.7893	0.2910	-0.1753	-0.7868
PD	-0.5032	0.3174	1.2278	-0.2886	-0.1011
GAP	-0.2793	0.5968	-0.3210	-0.3249	-0.3354
F_p	0.1360	0.0802	-0.3288	0.1758	-0.0031
F_y	0.7120	1.1058	-0.0616	0.7379	-0.0939
P_c			-1.2805		
K_i			1.6781		
P_u			-1.2531		
δ_0			2.6611		
R^2*	0.9399	0.9476	0.8539	0.9506	0.9715

*R^2 = 1.0 corresponds to a perfect fitting

Table 5.2 Coefficients for the prediction equations for FRP poles

Parameter	P_u	δ_0	n	P_c	K_i
e	9.6090	9.8391	9.7360	9.0505	0.6696
L	-1.0148	-1.0733	-0.2105	-1.1733	-0.0638
PT	0.8899	0.9675	1.0765	1.0788	0.0956
TT	-0.1178	-0.1013	-0.2606	0.0025	-0.0039
BT	0.4416	0.4041	-0.1280	0.2883	0.0001
DB	1.1316	1.1496	1.6709	0.9034	0.0953
BD	0.3911	0.6686	3.4301	1.1921	0.2084
TD	-0.0600	-0.0891	-0.5338	-0.2356	-0.0178
BC	-1.5253	-1.7787	-3.2081	-1.4716	-0.3423
PD	1.8761	1.9003	-0.6766	1.2234	0.1658
GAP	-0.0493	-0.0708	-0.1120	0.0314	-0.0364
F_p	-0.0044	0.0030	-0.1397	0.1095	-0.0030
E	-0.0139	-0.0303	-0.6668	0.2018	-0.0493
K_i		-1.0141	2.4710		
P_c			0.6914		0.0967
P_u			-3.6981		0.8577
δ_0			2.6733		-0.9948
R^2*	0.9898	0.9946	0.8974	0.9526	0.9989

*R^2 = 1.0 corresponds to a perfect fitting.

The comparison of the FEM results with predicted three-parameter power model obtained from Equations 5.1 through 5.5 for steel poles are shown in Figures B-1 through B-14 of Appendix B. It can be seen from these figures that the predicted curves give acceptable results in the elastic and plastic regions. However, in cases such as

Prediction equation for steel poles

$$p_u = e^{6.9290}(L)^{-1.0089}(PT)^{-0.0886}(TT)^{0.4525}(BT)^{0.8511}(DB)^{0.1522}(BD)^{1.8577}(TD)^{0.0471}(BC)^{0.1908}(PD)^{-0.5032}(GAP)^{-0.2793}(F_P)^{0.1360}(F_y)^{0.7120} \quad (5.1)$$

$$\delta_0 = e^{-6.7295}(L)^{1.6480}(PT)^{-0.0209}(TT)^{-0.0026}(BT)^{0.2370}(DB)^{-1.3363}(BD)^{-0.9284}(TD)^{-0.4106}(BC)^{0.7893}(PD)^{0.3174}(GAP)^{0.5968}(F_p)^{0.0802}(F_y)^{1.1058} \quad (5.2)$$

$$n = [e^{7.4278}(L)^{-2.4001}(PT)^{0.8623}(TT)^{0.0887}(BT)^{-0.3284}(DB)^{1.1209}(BD)^{0.5812}(TD)^{0.7411}(BC)^{0.2910}(PD)^{1.2278}(GAP)^{-0.3210}(F_p)^{-0.3288}(F_y)^{-0.0616}$$
$$(P_c)^{-1.2805}(K_i)^{1.6781}(P_u)^{-1.2531}(\delta_0)^{2.6611}] \quad (5.3)$$

where,

$$p_c = e^{6.4261}(L)^{-1.1809}(PT)^{0.0709}(TT)^{0.5424}(BT)^{0.6788}(DB)^{0.0352}(BD)^{2.1860}(TD)^{0.1878}(BC)^{-0.1753}(PD)^{-0.2886}(GAP)^{-0.3249}(F_P)^{0.1758}(F_y)^{0.7358} \quad (5.4)$$

$$k_i = e^{9.7484}(L)^{-2.5836}(PT)^{0.1197}(TT)^{0.3202}(BT)^{0.3447}(DB)^{0.7823}(BD)^{2.9977}(TD)^{0.2426}(BC)^{-0.7868}(PD)^{-0.1011}(GAP)^{-0.3354}(F_P)^{-0.0031}(F_y)^{-0.0939} \quad (5.5)$$

Prediction equation for FRP poles

$$p_u = e^{9.6090}(L)^{-1.0148}(PT)^{0.8899}(TT)^{-0.1178}(BT)^{0.4416}(DB)^{1.1316}(BD)^{0.3911}(TD)^{-0.0600}(BC)^{-1.5253}(PD)^{1.8761}(GAP)^{-0.0493}(F_p)^{-0.0044}(E)^{-0.0139} \quad (5.6)$$

$$\delta_0 = e^{9.8391}(L)^{-1.0733}(PT)^{0.9675}(TT)^{-0.1013}(BT)^{0.4041}(DB)^{1.1496}(BD)^{0.6686}(TD)^{-0.0891}(BC)^{-1.7787}(PD)^{1.9003}(GAP)^{-0.0708}(F_p)^{0.0030}(E)^{-0.0303}(K_i)^{-1.0141} \quad (5.7)$$

$$n = [e^{9.7360}(L)^{-0.2105}(PT)^{1.0765}(TT)^{-0.2606}(BT)^{-0.1280}(DB)^{1.6709}(BD)^{3.4301}(TD)^{-0.5338}(BC)^{-3.2081}(PD)^{-0.6766}(GAP)^{-0.1120}(F_p)^{-0.1397}(E)^{-0.6668} (P_c)^{0.6914}(K_i)^{2.4710}(P_u)^{-3.6981}(\delta_0)^{2.6733}] \quad (5.8)$$

where,

$$p_c = e^{9.0505}(L)^{-1.1733}(PT)^{1.0788}(TT)^{0.0025}(BT)^{0.2883}(DB)^{0.9034}(BD)^{1.1921}(TD)^{-0.2356}(BC)^{-1.4716}(PD)^{1.2234}(GAP)^{0.0314}(F_p)^{0.1095}(E)^{0.2018} \quad (5.9)$$

$$k_i = [e^{0.6696}(L)^{-0.0638}(PT)^{0.0956}(TT)^{-0.0039}(BT)^{0.0001}(DB)^{0.0953}(BD)^{0.2084}(TD)^{-0.0178}(BC)^{-0.3423}(PD)^{0.1658}(GAP)^{-0.0364}(F_p)^{-0.0030}(E)^{-0.0493} (P_c)^{0.0967}(P_u)^{0.8577}(\delta_0)^{-0.9948}] \quad (5.10)$$

those presented in Figures B-1(c), B-2(b), B-13 (a), and B-13 (b), even though exact match is not achieved, the predicted and FEM results show very good correlations.

The comparisons of the FEM results with predicted three-parameter power model for FRP poles are shown in Figures C-1 through C-16 of Appendix C. It can be seen from these figures that the predicted curves give identical results in the elastic and show of a little difference in the post yield region. The better load-deflection prediction equation for FRP compared to that of steel is attributed to higher R^2 value for the FRP's rigidity parameter ($R^2 = 0.8974$), compared to that of steel ($R^2 = 0.8593$).

5.5 Error band and sensitivity analysis

A comparison of the actual behaviors and the predicted behaviors are conducted in order to investigate the error of the equation obtained from the regression analysis and how closely the values response. A perfect match would be a 1:1 ratio (error band), with a percent error of 0, and an R^2 value of 1, where every point along this line possesses the same actual and predicted values. The error band analyses for the ultimate load, reference plastic deflection, rigidity parameter, characteristic load, and initial stiffness for steel and FRP poles are shown in Figures D-1 through D-4 of Appendix D. As shown in these figures, the values were obtained within the + /- 20 % error, except for the case of rigidity parameter for steel poles which were obtained within the +/- 30 % error, with most points being closer or on the line with slope 1:1. The points on the graphs are the predicted results.

Sensitivity analysis refers to the evaluation of the response when a design parameter is modified. Thus, to identify the behavior of Equations 5.1 through 5.10 for ultimate load, reference plastic deflection, and rigidity parameter of steel and FRP poles, respectively, sensitivity analyses were conducted. Since the prediction equations are functions of geometric and force-related variables of the pole, it was decided to vary one variable at the time. Figures E-1 through E-9 and F-1 through F-9 of Appendices E and F show the sensitivity analyses for the ultimate load, reference plastic deflection, and rigidity parameter versus the geometric and force variables of the steel and FRP

poles, respectively. The slope of each graph shows the sensitivity of the dependent parameter to the variation of the respective independent parameter. The ultimate load for steel poles is highly sensitive to the variation of the pole length, pole thickness at the bottom, outer diameter at bottom of pole, and yield stress as shown in Figures E-1(a) and (d), E-2(b), and E-3(d). Whereas the shallow slope of Figures E-2(c) and E-2(d) imply that the ultimate load for steel poles is least sensitive to the variation of the outer diameter at top of pole and bolt circle. The steep slope of Figures E-4(a), E-5(a) and (b), and E-6(d) shows that the reference plastic deflection for steel poles is highly sensitive to the variation of the pole length, nominal bolt diameter, pole diameter at the bottom, and yield stress. However, it can be seen from Figures E-4(b) and (c), and E-6(c) that the sensitivity of the reference plastic rotation for steel poles to the variation of the end-plate thickness, pole thickness at the top, and pretension load on bolts is low. As shown in Figures E-7 through E-9, the sensitivity of pole length, end-plate thickness, bolt diameter, and side length of end-plate is high for the values of rigidity parameter for steel poles, whereas the effect of variation of pole thickness at the top, bolt circle, GAP distance, and yield stress on the steel poles is insignificant. The sensitivity analysis of the ultimate load for FRP poles with respect to their geometric and force-related variables are shown in Figures F-1 through F-3. From these figures, it can be seen that the sensitivity of pole length, end-plate thickness, bolt diameter, bolt circle, and side-length of end-plate is higher than that of pole thickness at the top and bottom, pole diameter at the top and bottom, GAP distance, pretension load on bolts, and elastic modulus. The sensitivity analyses of the reference plastic deflection for FRP poles with respect to their geometric and force-related variables are presented in Figures F-4 through F-6. As shown in these figure, the trend of the reference plastic deflection for FRP poles is similar to that of the ultimate load. The sensitivity of the rigidity parameter for FRP poles to the variation of end-plate thickness, bolt diameter, pole diameter at the bottom, and bolt circle is more significant than that of the rigidity parameter to the variation of pole thickness at the top and bottom, GAP distance, pretension load on bolts, and elastic modulus as shown in Figures F-7 through F-9 of Appendix F.

5.6 Chapter summary

In this chapter, selected FEM test cases were used to develop regression equations for the parameters of the three-parameter model equation as functions of poles geometric and force-related variables. The independent variables were identified as parameter of three parameter model equations: ultimate load; reference plastic deflection; and rigidity parameter. The independent variables were the geometric and force-related variables of the steel and FRP poles including pole length, thickness, yield stress, etc. In obtaining regression equations, challenges were encountered for the value of multiple determination, R^2, for the rigidity parameters. Thus, a "characteristic load" concept was proposed the values of which were determined graphically. This characteristic load enhanced the values of the R^2 from $R^2 = 0.5508$ and $R^2 = 0.6633$ to $R^2 = 0.8539$ and $R^2 = 0.8974$ for steel and FRP poles, respectively.

Finally, error band and sensitivity analyses were conducted on the developed equations to determine the range of error and the behavior of each equation, respectively.

CHAPTER 6
SUMMARY AND CONCLUSION

6.1 Summary

The use of tapered hollow steel and FRP poles in structural engineering applications has been increased in past few decades. One application of these poles is to support CCTV cameras for which image stabilization is an important factor. Thus, deflection control and pole's stiffness become the major criteria for design. Due to lack of generalized design specification for pole design in departments of transportation in general, and Texas Department of Transportation in particular, this experimental and finite element study was undertaken to develop generalized load-deflection equations for steel and FRP poles.

A steel pole with an octagonal cross section and two circular cross sectional FRP poles were tested to determine their load-deflection characteristics. Test setup was designed to mimic the actual field condition and consisted of the test pole welded to an end-plate, which was bolted to a concrete base. Instrumentation consisted of a load cylinder, load cell, wire potentiometer, and digital data acquisition system. A pseudo cyclic loading history was applied to each test pole until failure and the load versus tip deflection plots were obtained. The failure mode for all the test specimens was determined to be excessive tip deflection. However, yielding of end-plate and superficial cracks at early loading (6,000 lbs (26,700 N)) was observed for steel and FRP poles, respectively. The first yield load in end-plate for the steel poles occurred at 450 lbs (2003 N). No yielding in any of the FRP poles was observed. A finite element model was developed using three-dimensional isoparametric solid elements, which included algorithms for contact, geometric, and material nonlinearities during the stress analysis. Since a plane of symmetry existed along a section through the longitudinal axis of the pole, one-half of the pole and its connection assembly were modeled. Three dimensional solid elements were used to model the entire pole, end-plate, bolt assemblage, and concrete base. Bilinear stress-strain curves were used for steel and

FRP. Transversely isotropic behavior of FRP pole was considered and the equivalent modulus was obtained for the analysis. The delamination of FRP poles was not modeled due to the fact that FRP poles are designed not to fail due to delamination. No delamination was observed during the experiments. Due to nonlinear system equation behavior, the full Newton-Raphson iteration was adopted and the convergence was obtained by using Hilbert L-2 norm coupled with equating external virtual work done to internal virtual strain energy. The FEM produced load-deflection plots that correlated well with the experimental results for most regions of loading. The maximum differences in load and deflection between the FEM and experimental results for the steel pole were 1.2 % and 2.5 %, respectively. Also, the maximum differences between FEM and experimental results for FRP poles were 2.3 % to 3.7 % and 1.2 % to 1.9 % for stresses and deflections, respectively. To further verify the developed models, the end-plate and wall thickness were varied one at the time while other geometric and force related variables were kept constant. The load-deflection plots showed that FEM models followed the trend that agrees with engineering intuition.

The mathematical models are used to curve fit the experimental load- deflection curves. There are several mathematical models used for representing the load-deflection curves of connections such as linear, bilinear, polynomial, Cubic B-spline, the three-parameter power, exponential, Ramberg-Osgood and Richard-Abbott models. Based on accuracy of three-parameter power model reported in literature (Abolmaali et al., 2004), for similar cases, three-parameter power model was adopted as a tool to develop prediction equations for load-deflection of steel and FRP poles. Geometric and force-related parameters of the pole were varied within their practical ranges, and based on the recommendation of the Texas Department of Transportation, matrices of test cases were developed. Fifty five test cases for steel and sixty one test cases for FRP poles were identified after careful consideration of all the varied parameters discussed above, which included elimination of impractical cases. Finite element analyses were conducted on the selected test cases and the three parameter power model equation was fitted to the data obtained from the FEM results. Selected FEM test cases were used to

develop regression equations for the parameters of the three-parameter model equation as functions of poles geometric and force-related variables. The independent variables were identified as parameter of three parameter model equations: ultimate load; reference plastic deflection; and rigidity parameter. The independent variables were the geometric and force-related variables of the steel and FRP poles including pole length, thickness, yield stress, etc. In obtaining regression equations, challenges were encountered for the value of multiple determination, R^2, for the rigidity parameters. Thus, a characteristic load concept was proposed, the value of which was determined graphically. This characteristic load enhanced the values of the R^2 from $R^2 = 0.5508$ to $R^2 = 0.8539$ for a steel pole and $R^2 = 0.6633$ to $R^2 = 0.8974$ for FRP poles. Finally, error band and sensitivity analyses were conducted on the developed equations to determine the range of error and the behavior of each equation, respectively.

6.2 Conclusion

In this study, the load-deflection behavior of tapered steel and FRP poles subjected to cantilever bending loads have been investigated experimentally and analytically. The followings are presented as conclusions based on the findings of this study:

- The experimental testing showed that the 25 ft (7.6 m) FRP pole long was more flexible than the shorter and steel pole was the most flexible of the three. This was due to the fact that steel pole's thickness was much less than that of the FRP poles.
- All three tested poles experienced excessive tip deflection and permanent bolt elongation in the tension region. However, no yielding of their end-plate was observed due to their relatively thick end-plate. Also, FRP poles failed without delamination.
- The use of three-dimensional FEM analysis can successfully predict the behavior of hollow tapered steel and FRP poles. The FEM analysis performed correlated well with the experiments. However, the nonlinear FEM pole model with bolt and contact model behaved slightly stiffer than the behavior of the

pole tested experimentally as expected. The FEM results showed deviation from the experimental results past the yield point. In the FEM model, the ultimate load was controlled by the excessive yielding of end-plate around the bolt holes.

- The FEM to experimental ultimate load ratios were 0.964 for steel pole, and 0.977 and 0.963 for 20 ft (6.1 m) and 25 ft (7.6 m) FRP poles, respectively. The FEM to experimental ultimate deflection ratios were 0.975 for steel pole, and 0.988 and 1.019 for 20 ft (6.1 m) and 25 ft (7.6 m) FRP poles, respectively.
- The concept of the "characteristic load" and the "characteristic displacement" was proposed in order to improve the values of coefficient of multiple determination, R^2, for parameter defining three-parameter power model significantly. The results of prediction equations with these values enhanced the values of the R^2 for steel and FRP poles, and were fairly close to those of FEM tests selected.
- Based on the error band analysis for the ultimate load, reference plastic deflection, and rigidity parameter, the errors between the results obtained from FEM and prediction equations were obtained within +/- 20 % error, with most points being closer or on the line with slope 1:1 (i.e. no error).
- Based on the regression analysis for steel poles, it was clear that with increasing pole thickness at the top and bottom, increasing pole diameter at the bottom, and increasing yield stress, the ultimate load capacity of a steel pole increases. Increasing pole length, bolt circle, and yield stress increased the reference plastic deflections, and the increment of end-plate thickness, side length, bolt diameter, and pole diameter at the top and bottom of the pole significantly increases the rigidity parameter, n.
- Based on the regression analysis for FRP poles, the effect of variation of pole length, end-plate thickness, bolt diameter, bolt circle, and side-length of end-plate was highly sensitive to ultimate load and reference plastic deflection. The

sensitivity of the rigidity parameter to the variation of end-plate thickness, bolt diameter, pole thickness at the bottom, and bolt circle was significant.

- The prediction equation developed was capable of predicting the load-deflection plots with high accuracy within the limitation of the independent parameters selected.
- Based on the experimental testing, FEM analysis, and prediction equations, it was concluded that the predicted equations adequately predict the behavior of the tapered hollow steel and FRP poles and should be used for the design of poles subject to cantilever bending loads within the limitation of the parameters selected.

6.3 Recommendations

Based on the experimental and analytical studies conducted on steel and FRP poles, some subsequent efforts to advance this knowledge are suggested as follows:

- Further experimental tests need to be conducted on steel and FRP pole to study failure mode analysis or other pole applications. Especially, experimental tests for the local buckling and delamination require further investigation.
- The ranges of variables in this study are mostly based on TX DOT specification. It is recommended that variables from other state department of transportations and international to be considered for selecting of test cases.
- Different FRP material to be tested. Examples of which are: S-glass/epoxy composite; E-glass/vinyl ester composite; and Carbon/polyester.
- The effect of the pole height on the failure mode to be studied. This means that experiments to be conducted for very short and very tall poles to verify the failure modes.
- Equation obtained from numerous tests conducted on pole with the help of ANSYS, and regression analysis needs to be modified taking into consideration wide range of independent variables for the pole.

- The accuracy of predicted rigidity parameter is much lower than the accuracy associated with the ultimate load or reference plastic deflection in the prediction equations. Efforts are needed to propose another conceptually similar one.
- The prediction equation presented in this study can be further developed into engineering design equations which can be used directly by structural design engineers and manufacturer. Step-by-step procedures and guidelines for tapered steel and FRP poles can be developed.
- Cyclic testing should be investigated to ascertain the type of dynamic loading that best presents actual wind conditions, and to establish a base of qualifying tests for each pole configuration.
- To satisfy the design practice, creep and fatigue behaviors of steel and FRP poles should be investigated.

APPENDIX A

COMPARISON OF PARAMETERS
OBTAINED FROM FEM AND PREDICTION EQUATIONS

Table A. 1 Parameters obtained from FEM and prediction equations of steel cases

Test ID	FEM P_u	Pred* P_u	$R_{F/P}$** P_u	FEM δ_0	Pred δ_0	$R_{F/P}$ δ_0	FEM n	Pred n	$R_{F/P}$ n
S20-0.5-0.1-0.15-0.75-9-4-2-36-12-11-28	1595.5	1794.1	0.8893	19.3	18.5	1.0434	3.37	1.84	1.8323
S20-1-0.15-0.15-0.75-7-4-2-40-10-9.5-25	1338.7	1402.5	0.9545	22.0	21.2	1.0346	4.73	3.63	1.3039
S20-1-0.15-0.15-1-7-3-2.75-45-10.5-9.5-51	1515.6	1600.9	0.9467	22.8	24.6	0.9240	2.55	3.01	0.8459
S20-1-0.15-0.15-1.25-11-5-2.75-40-15.5-14-55	3066.1	3236.5	0.9473	13.3	13.2	1.0012	7.80	3.24	2.4072
S25-0.75-0.15-0.2-1.25-12-6-2.75-45-16.5-15-70	4925.7	4409.8	1.1170	24.3	22.0	1.1045	1.52	2.12	0.7157
S25-0.75-0.3-0.3-0.75-7-5-2.75-36-10-10-28	2242.0	2407.1	0.9314	41.8	36.5	1.1451	1.64	1.64	0.9989
S25-1-0.15-0.15-1-8-5-2.5-40-11.5-11-45	1444.4	1472.4	0.9810	21.2	23.6	0.8975	2.94	3.83	0.7664
S25-1-0.15-0.2-0.75-7-4-2-50-10-9-25	1758.7	1723.1	1.0207	45.4	41.3	1.1003	4.30	3.03	1.4181
S25-1-0.1-0.2-1.25-11-6-3-55-15.5-14.5-70	2718.1	2631.8	1.0328	43.9	43.6	1.0076	2.75	2.81	0.9808
S25-1-0.15-0.2-1-10-6-2.5-40-14-13-35	2337.4	2463.6	0.9488	15.1	15.0	1.0125	4.97	3.99	1.2458
S30-0.75-0.15-0.15-1.25-12-7-2.5-40-16.5-15-35	2569.8	2420.9	1.0615	26.1	21.6	1.2095	4.30	3.81	1.1275
S30-0.75-0.2-0.2-1.5-14-6-3.5-36-19-17-85	4300.6	4521.4	0.9512	21.5	21.5	0.9997	1.45	1.92	0.7593
S30-1-0.15-0.15-1.25-11-6-3.25-40-15.5-15-50	2125.2	1973.3	1.0770	25.5	26.9	0.9487	7.92	5.35	1.4805
S30-1.25-0.15-0.15-1-7-4-2.75-45-10.5-10-40	1007.0	996.4	1.0106	39.5	42.4	0.9314	4.06	5.76	0.7041
S35-1-0.2-0.2-1.25-11-7-3-40-15.5-17-70	2589.4	2488.3	1.0406	34.2	35.4	0.9664	3.51	4.46	0.7859
S35-1-0.3-0.3-1.75-12-6-3.75-50-18-17-100	6277.7	6174.2	1.0168	36.4	41.4	0.8805	1.48	2.26	0.6538
S35-1.25-0.15-0.2-1.5-12-8-3.5-36-17-16.5-90	2731.1	2476.0	1.1030	22.6	25.6	0.8812	2.90	4.61	0.6288
S35-1.25-0.2-0.3-1.25-11-6-3.5-50-15.5-15-100	4686.1	4293.0	1.0916	55.4	57.4	0.9646	2.94	2.99	0.9825
S35-1.5-0.2-0.3-1.25-11-6-3-45-15.5-14-80	3998.6	4109.2	0.9731	50.1	44.6	1.1241	4.31	2.89	1.4904
S35-1.75-0.3-0.3-1-7-4-3-55-10.5-11-45	2324.9	2228.6	1.0432	89.7	87.3	1.0276	2.67	4.66	0.5735

Pred* = Parameter obtained from prediction equations.

$R_{F/P}$** = Ratio of parameter obtained from FEM to parameter obtained from prediction equations.

Table A. 1– *Continued.*

Test ID	FEM P_u	Pred P_u	$R_{F/P}$ P_u	FEM δ_0	Pred δ_0	$R_{F/P}$ δ_0	FEM n	Pred n	$R_{F/P}$ n
S40-1-0.2-0.2-1.25-12-6-3-50-16.5-15-65	3318.3	3173.9	1.0455	56.6	55.7	1.0156	3.44	3.47	0.9900
S40-1-0.2-0.3-1.25-11-7-3-45-15.5-14-80	4900.2	3749.8	1.3068	47.1	52.6	0.8949	1.00	2.18	0.4605
S40-1-0.3-0.2-1.5-12-6-3.75-40-17-17-95	2712.7	3126.3	0.8677	38.5	42.8	0.8996	3.82	3.28	1.1648
S40-1.25-0.2-0.2-1.25-11-6-3.5-36-16-15-55	2072.8	1950.4	1.0628	31.5	44.2	0.7139	2.23	5.11	0.4366
S40-1.25-0.2-0.25-1.5-14-6-3.5-40-19-18-90	4328.3	4182.2	1.0349	39.0	36.8	1.0598	4.49	3.52	1.2765
S40-1.5-0.2-0.25-1.75-12-6-3.75-45-18-18-128	3350.5	3458.6	0.9687	48.8	45.3	1.0777	7.27	4.68	1.5524
S40-1.5-0.25-0.25-1.5-16-9-3.25-45-22-20-80	6536.2	6251.1	1.0456	38.5	38.6	0.9966	4.39	4.39	1.0008
S40-1.5-0.25-0.3-1.25-12-7-2.75-45-16.5-16-50	5114.0	4278.1	1.1954	31.9	48.2	0.6619	1.25	3.80	0.3278
S45-1-0.2-0.25-1.25-12-5-3-36-16.5-14.5-65	2595.7	2720.0	0.9543	47.1	52.9	0.8895	1.79	2.29	0.7834
S45-1-0.25-0.25-1.5-12-5-3.25-50-17-17.5-85	3562.0	3629.1	0.9815	75.1	69.4	1.0815	3.76	3.22	1.1679
S45-1-0.3-0.3-1.5-12-5-3.5-50-17-19-85	4125.7	4325.8	0.9538	78.6	77.7	1.0111	4.62	3.17	1.4583
S45-1.25-0.2-0.2-1.25-11-4-2.75-36-16-16-50	1578.9	1736.7	0.9091	55.2	55.6	0.9931	5.04	4.99	1.0114
S45-1.25-0.2-0.3-1.5-12-6-3.5-36-17-17-103	3010.5	3059.1	0.9841	49.4	49.0	1.0082	2.56	3.01	0.8520
S45-1.25-0.3-0.2-1.25-11-8-3-50-15.5-14.5-80	2540.2	2959.8	0.8582	62.6	62.1	1.0078	5.46	4.11	1.3277
S45-1.5-0.2-0.2-1.25-11-8-3-40-15.5-15-80	2029.4	2033.1	0.9982	52.1	48.9	1.0664	3.98	5.48	0.7256
S45-1.5-0.3-0.3-1.75-13-8-4-40-19-18-130	4025.0	4634.3	0.8685	47.5	45.11	1.0525	6.81	3.31	2.0580
S45-1.5-0.3-0.4-1.25-11-6-3.75-50-16-14-55	5205.5	4739.0	1.0984	87.0	92.20	0.9434	2.26	3.05	0.7416
S45-1.75-0.2-0.25-1.5-12-7-4-45-18-16-110	3092.3	3339.9	0.9259	57.9	49.91	1.1606	7.57	5.51	1.3738
S50-1-0.2-0.25-1.5-14-7-3.5-45-19-17.5-75	3238.7	3641.6	0.8894	62.0	62.71	0.9893	13.24	3.25	4.0815
S50-1.25-0.15-0.2-1.5-12-7-3.25-40-17-15-65	1980.7	1896.3	1.0445	61.7	49.51	1.2456	6.96	4.83	1.4403

Table A.1– *Continued.*

Test ID	FEM P_u	Pred P_u	$R_{F/P}$ P_u	FEM δ_0	Pred δ_0	$R_{F/P}$ δ_0	FEM n	Pred n	$R_{F/P}$ n
S50-1.25-0.2-0.2-1.25-11-6-3.5-40-15.5-15-70	1843.6	1724.0	1.0694	65.6	71.27	0.9202	2.86	5.23	0.5466
S50-1.25-0.3-0.4-1-11-6-3-36-15-14-40	3081.8	3332.9	0.9247	92.0	83.65	1.0999	3.66	2.40	1.5239
S50-1.5-0.25-0.25-2-18-9-4.25-45-26-26-105	6215.9	5657.5	1.0987	59.8	50.64	1.1804	14.62	6.88	2.1240
S50-1.5-0.3-0.3-2-18-10-4.5-45-26-26-140	7880.8	7380.2	1.0678	58.9	53.59	1.0983	6.27	5.19	1.2072
S50-1.75-0.3-0.3-1-7-5-3-50-10.5-9.5-60	1531.3	1643.9	0.9315	139.0	126.10	1.1023	2.66	3.63	0.7309
S50-1.75-0.3-0.2-1.75-14-7-4-50-20-18-120	3578.4	3886.7	0.9207	63.5	63.45	1.0012	7.15	5.67	1.2612
S55-1.25-0.3-0.2-1.25-11-5-3-36-15.5-14-80	3364.5	1904.6	1.7665	78.2	72.07	1.0849	2.08	3.21	0.6478
S55-1.5-0.2-0.2-1.5-12-8-3.5-36-17-16-80	1767.5	1757.9	1.0055	53.0	52.71	1.0047	3.49	5.85	0.5972
S55-1.75-0.25-0.25-2-15-9-4.5-36-22-21-140	3459.2	3402.0	1.0168	51.0	47.40	1.0757	3.18	5.77	0.5506
S60-1.25-0.2-0.25-1.5-16-9-3.25-50-22-19.5-85	3338.6	4199.0	0.7951	64.7	84.74	0.7634	4.61	4.66	0.9906
S60-1.5-0.2-0.3-1-7-5-3.5-40-10.5-10.5-50	813.4	874.8	0.9298	159.0	149.04	1.0669	15.87	5.19	3.0612
S60-1.5-0.3-0.3-1.75-14-8-3.5-36-20-18-120	3476.3	3827.0	0.9084	55.3	57.53	0.9611	1.95	3.01	0.6473
S60-1.75-0.25-0.25-1.5-16-8-3.5-36-22-19-95	3397.5	3575.4	0.9503	64.8	64.20	1.0094	5.06	4.68	1.0815
S60-1.75-0.3-0.3-1.5-12-8-3.5-36-17-15.5-103	2697.7	2833.7	0.9520	60.5	67.37	0.8981	1.53	3.54	0.4320
S60-1.75-0.3-0.3-1.75-16-8-3.5-40-23-21-110	4579.5	4897.6	0.9350	74.1	66.28	1.1174	4.93	4.36	1.1296

Table A. 2 Parameters obtained from FEM and prediction equations of FRP cases

Test ID	FEM P_u	Pred P_u	$R_{F/P}$ P_u	FEM δ_0	Pred δ_0	$R_{F/P}$ δ_0	FEM n	Pred n	$R_{F/P}$ n
F20-0.5-0.2-0.2-0.75-6-3.5-1.5-8-7.5-28-4.5	531.7	535.8	0.9923	155.3	152.6	1.0178	5.97	6.12	0.9760
F20-0.75-0.25-0.275-0.75-7.5-5-1.75-10-10-25-3.5	1196.6	1119.5	1.0689	58.0	55.9	1.0372	3.02	3.91	0.7743
F20-0.75-0.275-0.25-0.75-8-5.5-1.5-10-9-10-4	922.5	896.8	1.0286	37.7	36.8	1.0239	4.86	5.49	0.8855
F20-0.75-0.275-0.3-1-8-3.5-2.5-10.7-10.5-40-4.5	1647.5	1612.0	1.0220	66.6	65.8	1.0115	4.31	5.23	0.8243
F20-0.75-0.3-0.3-1-8-5-2.5-10.7-10.2-40-5	1485.5	1476.9	1.0058	44.9	43.0	1.0435	4.27	3.82	1.1177
F20-1-0.25-0.225-1-10-7-2.5-13.5-12-50-4.5	1705.7	1747.7	0.9759	32.5	34.2	0.9520	4.07	4.24	0.9608
F25-0.5-0.25-0.25-1-8-4.5-2.5-10.6-10-45-5.5	861.4	759.8	1.1337	62.6	58.1	1.0773	2.99	3.72	0.8035
F25-0.75-0.275-0.25-1.25-10-6-2.75-13.2-13-70-4.5	1658.6	1735.3	0.9558	61.1	63.5	0.9624	4.57	4.52	1.0108
F25-0.75-0.3-0.3-0.75-7-4-2-9.5-8.5-28-5	675.3	705.4	0.9573	59.7	62.3	0.9589	4.83	4.53	1.0652
F25-0.75-0.3-0.325-0.75-9.5-5-1.75-12-10.5-20-4.5	796.6	853.9	0.9329	33.8	36.9	0.9161	4.73	4.32	1.0953
F25-1-0.275-0.275-1-7.5-4.5-2.5-10-10-51-5.5	1274.1	1546.7	0.8238	78.9	99.1	0.7957	5.49	5.95	0.9221
F25-1-0.325-0.35-1-8.5-5.5-2.25-11.5-10.5-40-5	1541.0	1561.7	0.9868	61.8	61.0	1.0131	5.79	4.63	1.2517
F25-1.25-0.3-0.325-1-10-6-2-13.5-12.5-35-5	2174.0	2156.1	1.0083	58.5	57.5	1.0167	4.56	4.75	0.9594
F30-0.75-0.275-0.275-1-8-4-2.5-10.6-10-40-3.5	1012.9	947.3	1.0693	157.3	150.5	1.0451	11.00	8.23	1.3359
F30-0.75-0.35-0.35-1.125-8.5-5-2.5-11.5-10.5-45-3.5	1156.6	1143.7	1.0113	117.2	114.1	1.0268	5.94	6.11	0.9722
F30-1-0.3-0.275-1-9-5-2.25-11.5-11-45-5	1357.2	1321.1	1.0273	98.4	95.4	1.0309	7.65	7.03	1.0881
F30-1-0.325-0.3-1.25-11-6-2.5-14.5-13.5-71-4	1926.9	1923.4	1.0018	89.4	90.2	0.9915	6.23	6.35	0.9798
F30-1-0.325-0.325-1.125-12-7-2.25-16-14-56-5.5	1637.4	1673.5	0.9784	43.3	44.1	0.9816	4.58	3.83	1.1970
F30-0.75-0.3-0.3-1-9-4-2.5-12-11-40-4.5	996.8	1006.2	0.9907	93.6	92.5	1.0122	5.99	5.93	1.0099
F35-0.75-0.325-0.35-1-10-5.5-2.5-13.7-13.5-51-4	1120.3	1119.8	1.0004	101.4	100.8	1.0060	3.17	3.49	0.9089
F35-1.25-0.35-0.35-1.125-12-7.5-2.5-16-15-48-5	2079.4	2020.1	1.0294	76.4	74.2	1.0304	4.54	4.37	1.0390

Table A. 2 – *Continued.*

Test ID	FEM P_u	Pred P_u	$R_{F/P}$ P_u	FEM δ_0	Pred δ_0	$R_{F/P}$ δ_0	FEM n	Pred n	$R_{F/P}$ n
F35-1-0.275-0.275-1.125-12-6.5-2.75-16-15-50-3.5	1568.2	1545.2	1.0149	111.4	109.9	1.0140	6.33	5.99	1.0584
F35-1-0.3-0.3-1.25-12-7-2.5-16.2-15.7-56-5	1872.7	1904.0	0.9836	86.0	85.6	1.0046	5.37	4.18	1.2833
F35-1-0.35-0.35-1-10-5-2.5-13.5-12.5-41-4.5	1270.5	1275.8	0.9959	105.5	104.8	1.0073	5.70	5.34	1.0671
F35-1.25-0.325-0.325-1.5-13-8-3-17.5-16-90-4	2669.4	2739.8	0.9743	103.3	106.4	0.9707	6.27	6.34	0.9891
F35-1.25-0.35-0.325-1.25-12-7-2.75-16-14.5-65-5.5	2065.9	2060.3	1.0027	80.0	77.1	1.0376	6.27	5.25	1.1935
F35-1.25-0.35-0.35-1.125-12-7.5-2.5-16-15-48-5	2079.4	2020.1	1.0294	76.4	74.2	1.0304	4.54	4.37	1.0390
F35-1.5-0.375-0.375-1-13-8-2-17-15.5-45-5.5	2295.9	2140.2	1.0728	58.1	54.9	1.0581	4.46	4.10	1.0868
F40-0.75-0.3-0.3-1-10.5-5-2.5-14-12.5-40-5	753.5	790.1	0.9538	3.1	3.1	0.9983	2.66	2.44	1.0866
F40-1-0.275-0.3-1.125-11-5.5-2.75-14.5-13-50-4	1204.7	1213.9	0.9924	143.5	145.7	0.9847	7.60	7.94	0.9572
F40-1-0.3-0.325-1.25-12.5-6-3-16.5-15-60-3.5	1587.0	1570.1	1.0108	140.1	139.0	1.0082	8.29	7.34	1.1297
F40-1-0.325-0.325-1-9-4.5-2.25-12-10.5-45-5	915.2	909.4	1.0063	147.1	145.1	1.0134	7.31	7.89	0.9265
F40-1-0.35-0.325-1.5-12-6.5-3.25-16.5-15-95-4	1854.5	1841.7	1.0069	144.3	142.9	1.0097	5.94	6.36	0.9340
F40-1.25-0.375-0.35-1-10.5-6-2.5-14-12.5-43-5.5	1331.9	1281.7	1.0392	102.5	98.5	1.0408	5.30	5.63	0.9417
F40-1.25-0.375-0.375-1.5-14-7.5-3-18.5-16.5-85-4	2551.8	2521.3	1.0121	114.3	113.5	1.0063	7.01	6.89	1.0167
F45-1-0.325-0.35-1.125-12.5-5-2.5-16.2-14.5-40-5	1227.5	1242.1	0.9882	119.9	120.3	0.9964	6.69	6.81	0.9814
F45-1-0.35-0.375-1.5-14-7.5-3.5-18.2-16.2-85-5.5	1877.0	1810.0	1.0370	96.3	90.7	1.0619	5.13	5.23	0.9802
F45-1-0.4-0.4-1.25-13-6.5-2.75-17.5-15-50-4	1296.4	1368.1	0.9476	110.4	123.2	0.8961	5.25	5.84	0.8995
F45-1.25-0.375-0.4-12.5-6-2.75-16.5-14.5-55-4.5	1738.7	1704.3	1.0202	142.9	138.5	1.0319	8.67	7.48	1.1579
F45-1.5-0.4-0.4-1.5-16-10-3-20-18-95-4.5	2992.6	2902.5	1.0310	97.1	96.0	1.0114	5.31	6.76	0.7856
F50-0.75-0.35-0.35-1.125-12-5-2.5-16-15-45-4	932.2	917.9	1.0156	165.9	161.6	1.0267	4.18	5.39	0.7754

Table A. 2 – *Continued.*

Test ID	FEM P_u	Pred P_u	$R_{F/P}$ P_u	FEM δ_0	Pred δ_0	$R_{F/P}$ δ_0	FEM n	Pred n	$R_{F/P}$ n
F50-1-0.35-0.375-1.5-14-7-3.5-19-17-75-4.5	1644.3	1679.8	0.9789	145.8	143.8	1.0143	5.63	5.58	1.0097
F50-1-0.375-0.4-1.25-16.5-9-2.75-21-19.5-71-3.5	1626.4	1652.5	0.9842	98.7	98.7	0.9994	5.05	4.54	1.1141
F50-1.125-0.375-0.375-1.25-16.5-9-2.75-21-19-90-4	1695.9	1693.8	1.0013	91.0	90.8	1.0023	5.09	4.88	1.0436
F50-1.5-0.4-0.425-1.75-16-9-3.75-22.5-21-93-4	3651.8	3548.3	1.0292	178.9	174.8	1.0234	4.83	5.42	0.8914
F50-1.25-0.4-0.425-1.75-16-8-3.5-22.5-21-93-4	3016.9	3048.6	0.9896	167.5	167.9	0.9976	4.88	5.05	0.9675
F50-1.125-0.375-0.375-1.75-16-8-3.5-22.5-21.5-108-3.5	2784.5	2769.3	1.0055	191.0	189.4	1.0087	4.56	5.15	0.8845
F50-1.5-0.4-0.4-1.5-17.5-9-3.75-23-20-79-3.5	2816.3	2761.7	1.0197	96.2	93.6	1.0278	4.95	5.21	0.9503
F55-1-0.45-0.45-1.25-16-8.5-2.75-20-18.5-45-3.5	1327.1	1499.5	0.8850	111.0	123.7	0.8974	5.71	5.33	1.0714
F55-1.25-0.425-0.45-1.5-18-10-3.25-24-22-103-4	2394.2	2426.2	0.9868	111.8	111.1	1.0054	4.96	4.16	1.1919
F55-1.25-0.45-0.475-1.25-15.5-8-2.75-19.5-17.5-71-5.5	1743.5	1724.4	1.0111	95.5	93.8	1.0179	4.98	4.94	1.0074
F55-1.125-0.45-0.45-1.5-14-6-3.5-18.5-17.5-60-4	2078.2	1983.0	1.0480	232.5	223.7	1.0394	8.32	7.23	1.1508
F55-1.5-0.375-0.4-1.75-16-8.5-3.25-22-19-85-5	2636.5	2731.5	0.9652	157.7	162.9	0.9683	7.00	6.83	1.0250
F55-1.5-0.45-0.425-1.5-18-10.5-3.5-24-21-90-4.5	2655.1	2513.6	1.0563	108.7	102.4	1.0615	4.22	4.84	0.8714
F60-1-0.425-0.45-1.5-16-8-3.25-22-19.5-85-5	1626.7	1601.5	1.0157	115.8	127.1	0.9112	2.14	3.86	0.5551
F60-1.25-0.45-0.45-1.75-17.5-9-3.5-23.5-22-101-4	2642.0	2690.2	0.9821	179.1	179.5	0.9976	7.22	5.41	1.3357
F60-1.5-0.425-0.4-2-18-9.5-3.75-24-22-90-5	3387.0	3412.1	0.9926	179.2	183.7	0.9753	6.22	6.89	0.9028
F60-1.5-0.425-0.425-1.75-16.5-8-3.5-21.5-20-67-5.5	3013.5	2920.1	1.0320	190.3	190.2	1.0003	7.00	7.35	0.9522
F60-1.125-0.45-0.45-1.5-17-7.5-3.5-21.5-19-103-3.5	1796.1	1792.1	1.0022	165.5	166.0	0.9972	7.28	7.65	0.9514
F60-1.125-0.475-0.5-1.5-15-6.5-3.25-20-18.5-95-3.5	1935.6	1910.7	1.0130	235.0	233.0	1.0085	6.44	6.69	0.9623
F60-1.25-0.5-0.5-2-20-11.5-4-27-24-79-4.5	3126.2	3179.3	0.9833	124.2	123.5	1.0057	4.44	4.33	1.0259
F60-1.5-0.45-0.45-2-20-10-4.25-27-25-110-4	3806.6	3923.5	0.9702	173.8	177.8	0.9772	6.72	5.93	1.1324

APPENDIX B

PLOTS OF FEM MODEL AND PREDICTED EQUATION MODEL FOR STEEL POLES

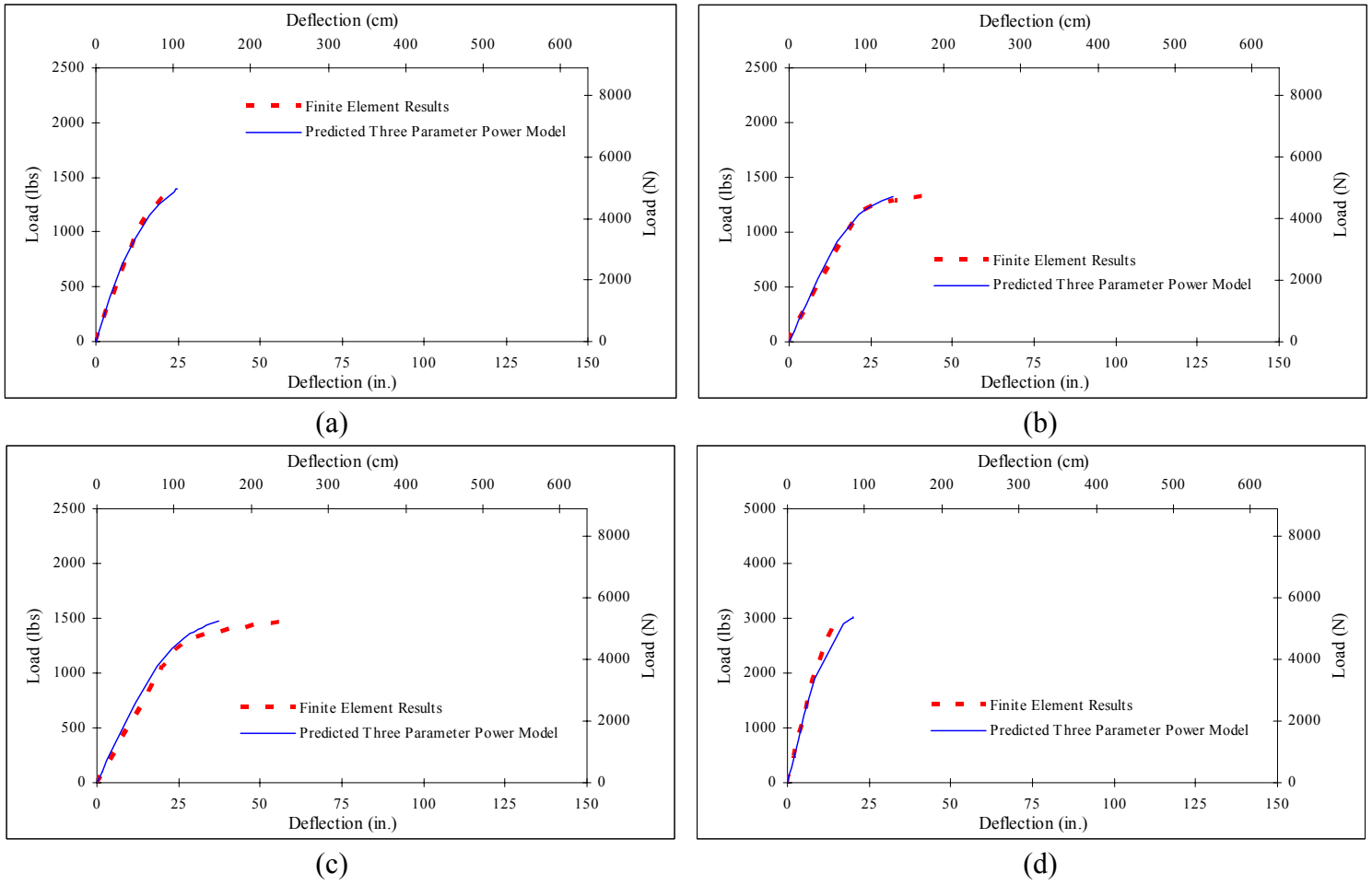

Figure B-1 Comparison of FEM model and predicted equation model for steel poles:
(a) S20-0.5-0.1-0.15-0.75-9-4-2-36-12-11-28; (b) S20-1-0.15-0.15-0.75-7-4-2-40-10-9.5-25;
(C) S20-1-0.15-0.15-1-7-3-2.75-45-10.5-9.5-51; (d) S20-1-0.15-0.15-1.25-11-5-2.75-40-15.5-14-55

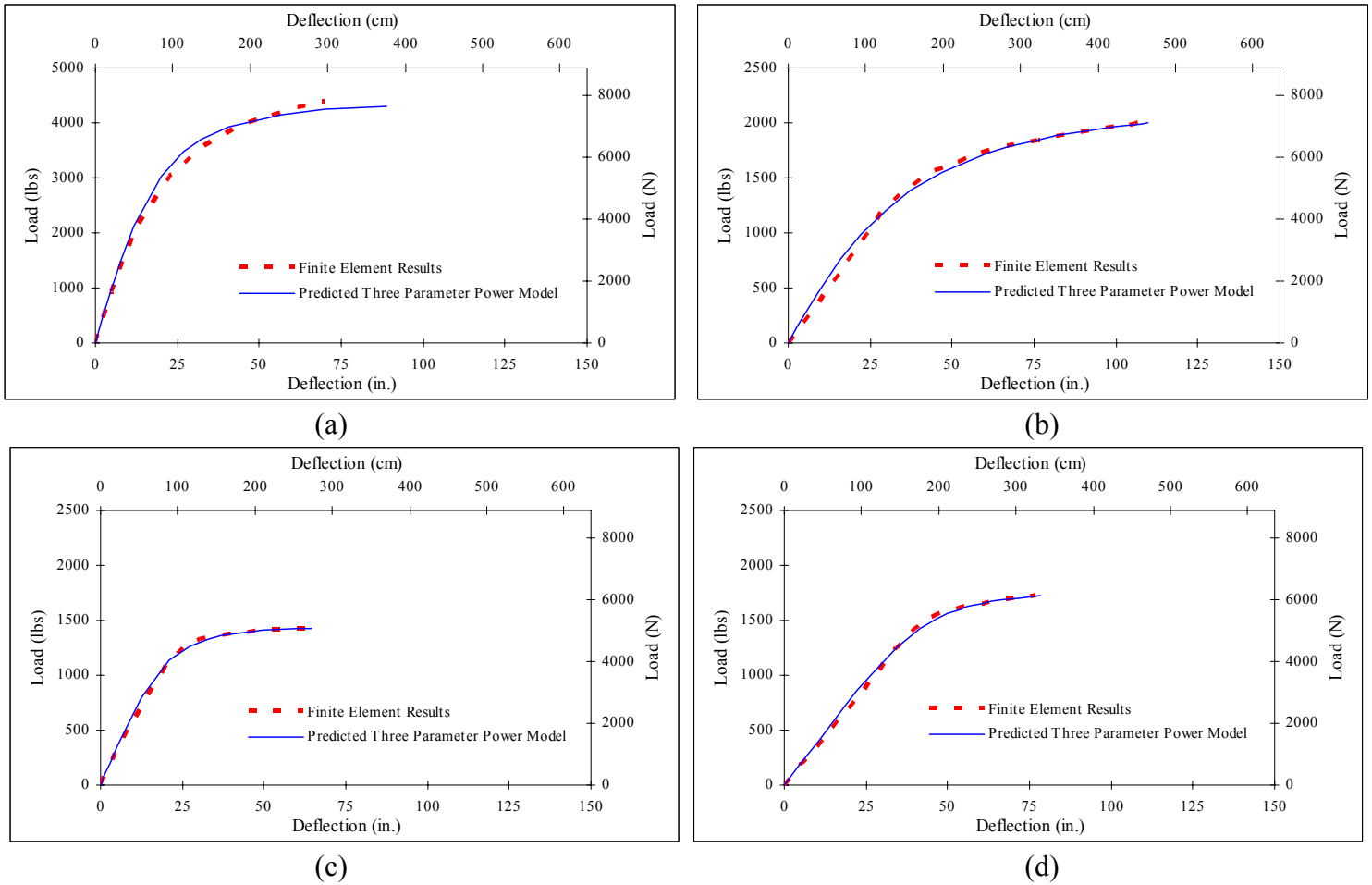

Figure B-2 Comparison of FEM model and predicted equation model for steel poles:
(a) S25-0.75-0.15-0.2-1.25-12-6-2.75-45-16.5-15-70; (b) S25-0.75-0.3-0.3-0.75-7-5-2.75-36-10-10-28;
(C) S25-1-0.15-0.15-1-8-5-2.5-40-11.5-11-45; (d) S25-1-0.15-0.2-0.75-7-4-2-50-10-9-25

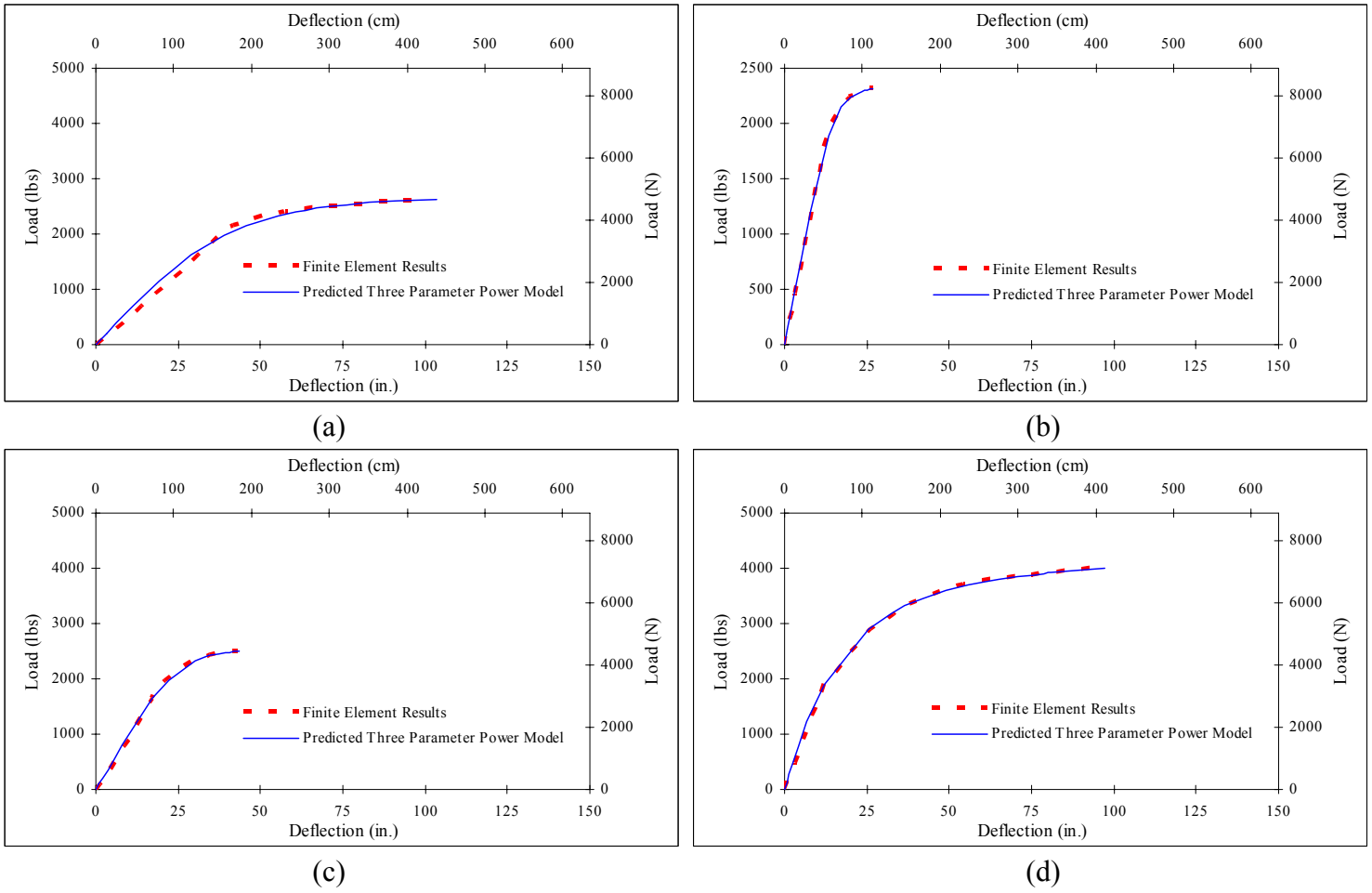

Figure B-3 Comparison of FEM model and predicted equation model for steel poles:
(a) S25-1-0.1-0.2-1.25-11-6-3-55-15.5-14.5-70; (b) S25-1-0.15-0.2-1-10-6-2.5-40-14-13-35;
(C) S30-0.75-0.15-0.15-1.25-12-7-2.5-40-16.5-15-35; (d) S30-0.75-0.2-0.2-1.5-14-6-3.5-36-19-17-85

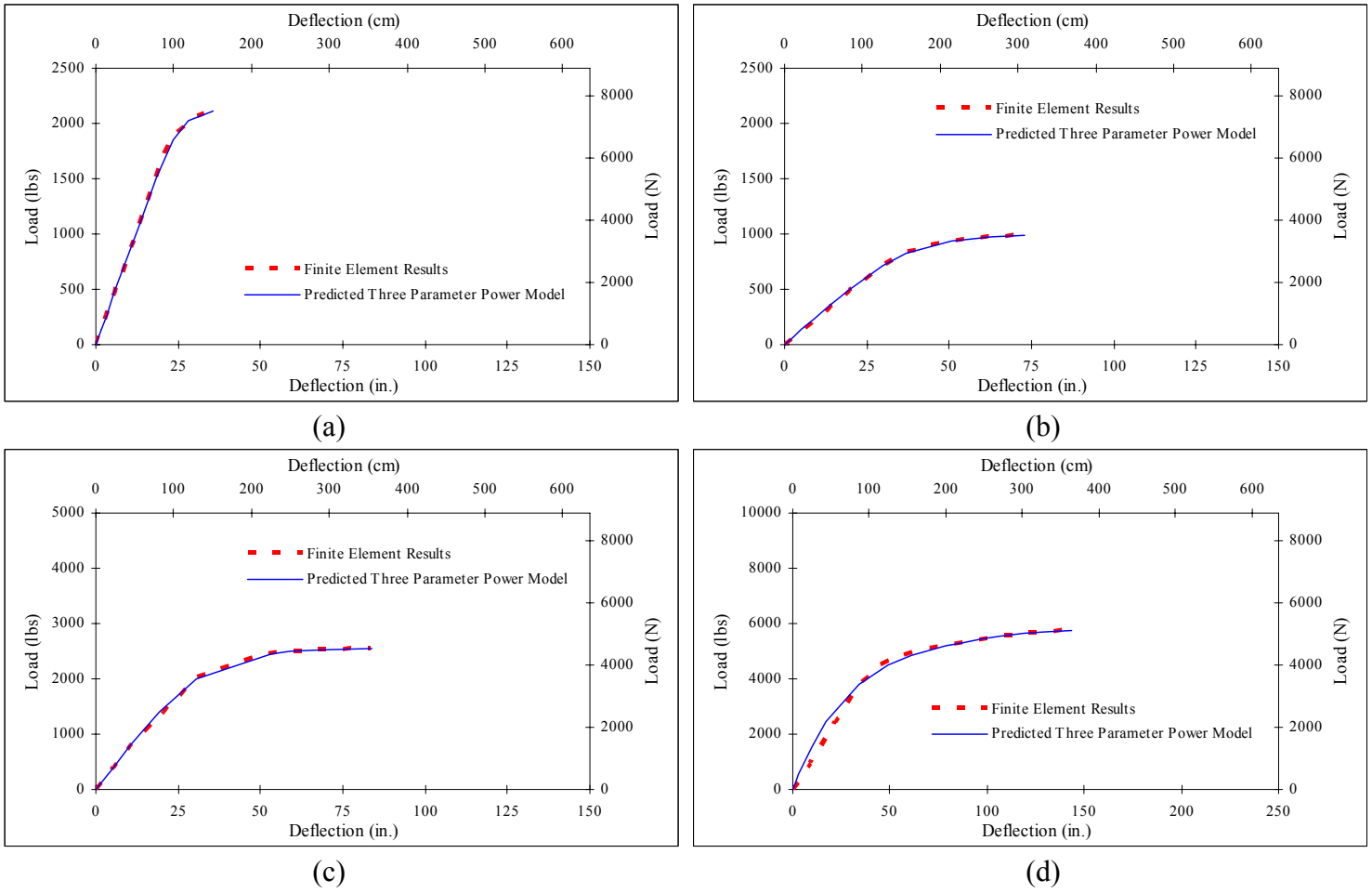

Figure B-4 Comparison of FEM model and predicted equation model for steel poles:
(a) S30-1-0.15-0.15-1.25-11-6-3.25-40-15.5-15-50; (b) S30-1.25-0.15-0.15-1-7-4-2.75-45-10.5-10-40;
(C) S35-1-0.2-0.2-1.25-11-7-3-40-15.5-17-70; (d) S35-1-0.3-0.3-1.75-12-6-3.75-50-18-17-100

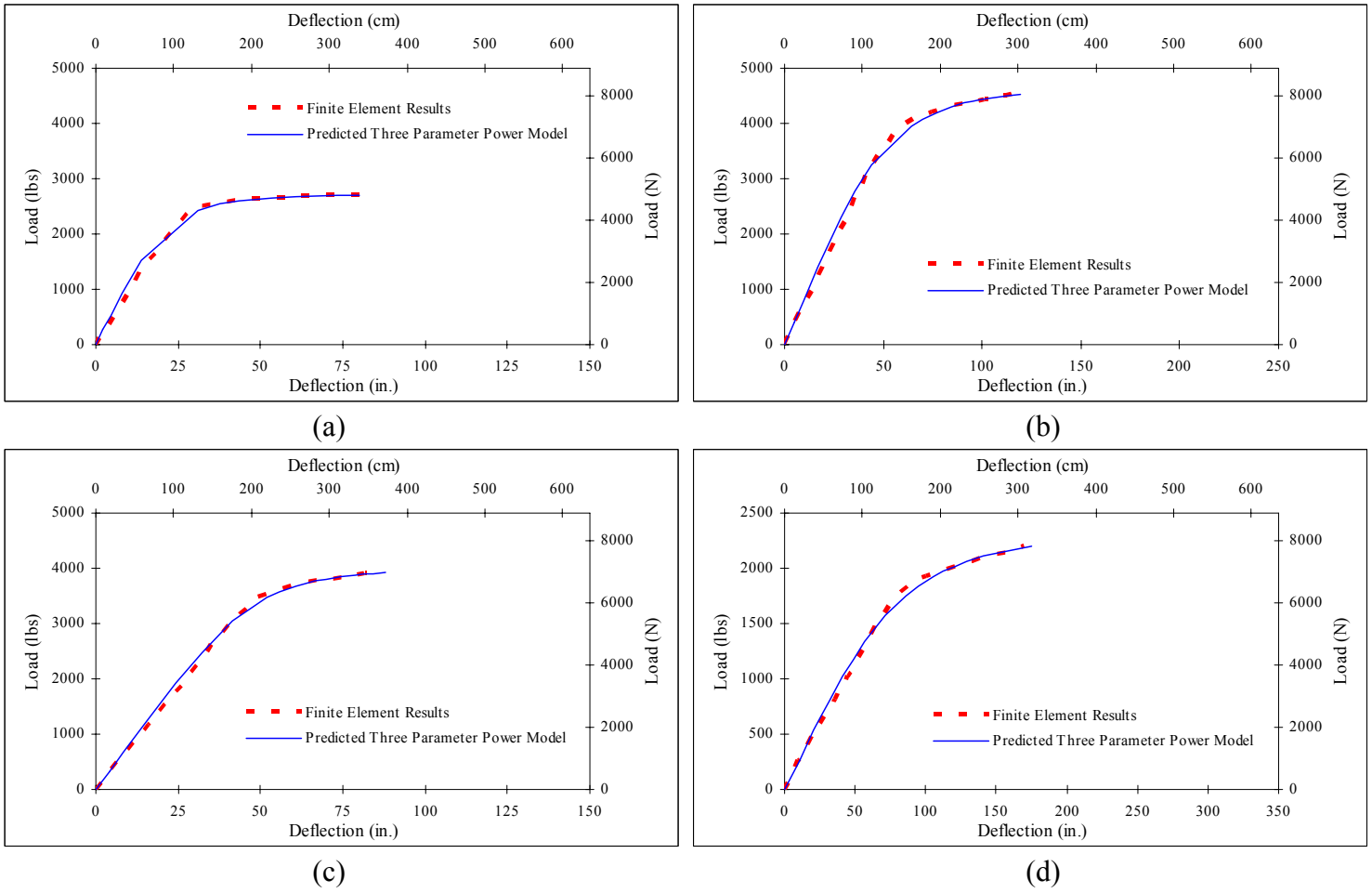

Figure B-5 Comparison of FEM model and predicted equation model for steel poles:
(a) S35-1.25-0.15-0.2-1.5-12-8-3.5-36-17-16.5-90; (b) S35-1.25-0.2-0.3-1.25-11-6-3.5-50-15.5-15-100;
(C) S35-1.5-0.2-0.3-1.25-11-6-3-45-15.5-14-80; (d) S35-1.75-0.3-0.3-1-7-4-3-55-10.5-11-45

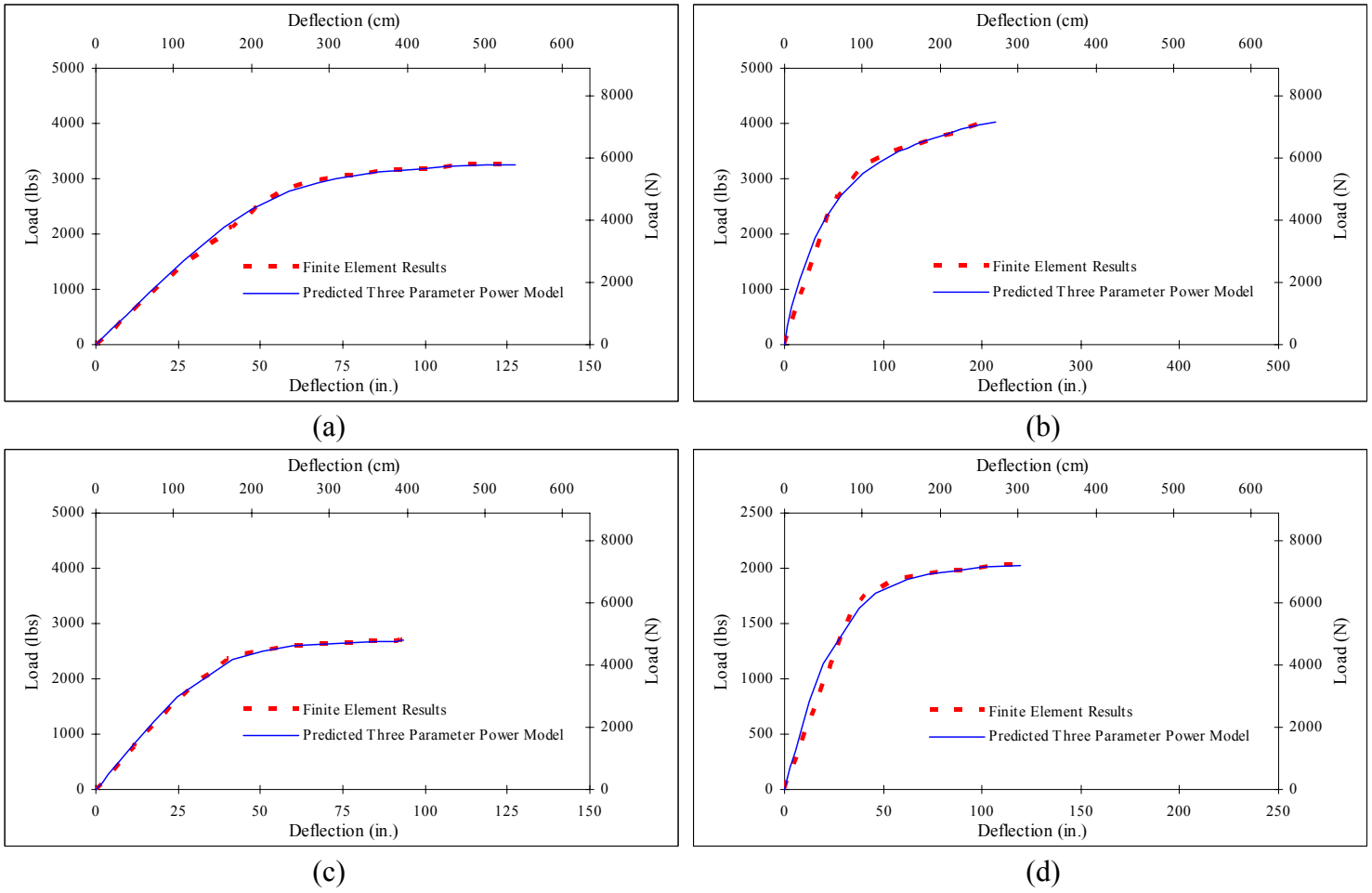

Figure B-6 Comparison of FEM model and predicted equation model for steel poles:
(a) S40-1-0.2-0.2-1.25-12-6-3-50-16.5-15-65; (b) S40-1-0.2-0.3-1.25-11-7-3-45-15.5-14-80;
(C) S40-1-0.3-0.2-1.5-12-6-3.75-40-17-17-95; (d) S40-1.25-0.2-0.2-1.25-11-6-3.5-36-16-15-55

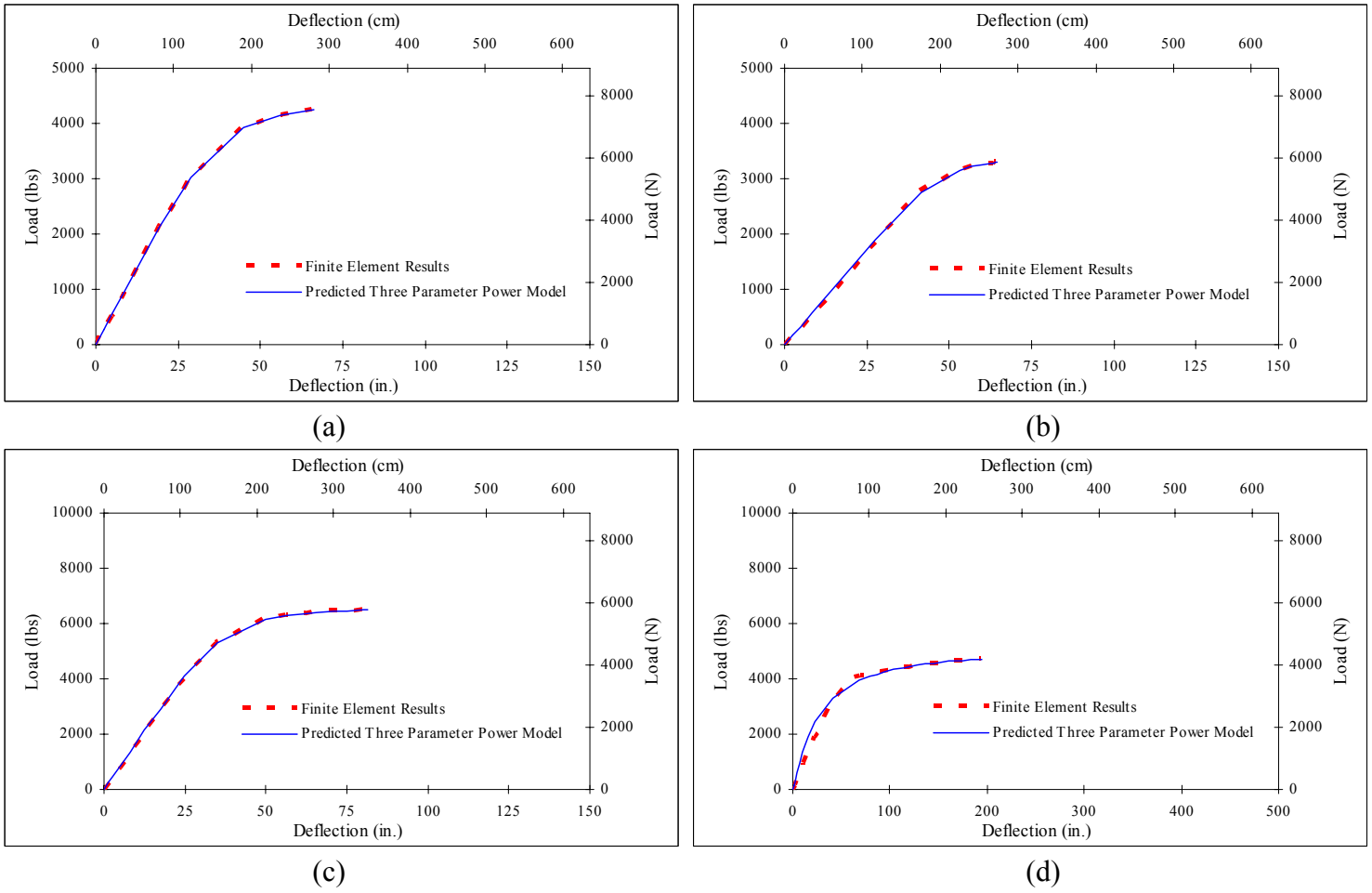

Figure B-7 Comparison of FEM model and predicted equation model for steel poles:
(a) S40-1.25-0.2-0.25-1.5-14-6-3.5-40-19-18-90; (b) S40-1.5-0.2-0.25-1.75-12-6-3.75-45-18-18-128;
(C) S40-1.5-0.25-0.25-1.5-16-9-3.25-45-22-20-80; (d) S40-1.5-0.25-0.3-1.25-12-7-2.75-45-16.5-16-50

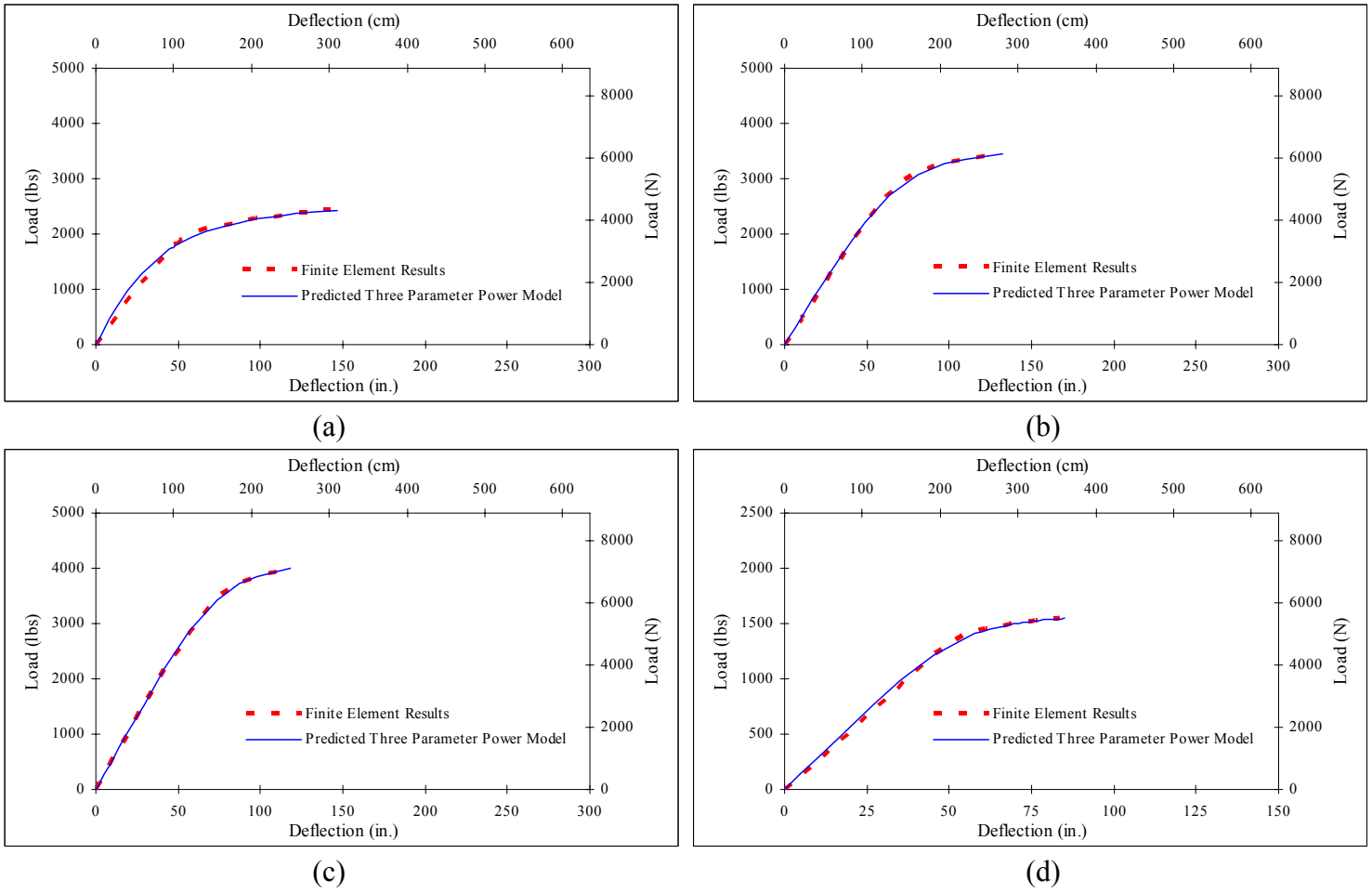

Figure B-8 Comparison of FEM model and predicted equation model for steel poles:
(a) S45-1-0.2-0.25-1.25-12-5-3-36-16.5-14.5-65; (b) S45-1-0.25-0.25-1.5-12-5-3.25-50-17-17.5-85;
(C) S45-1-0.3-0.3-1.5-12-5-3.5-50-17-19-85; (d) S45-1.25-0.2-0.2-1.25-11-4-2.75-36-16-16-50

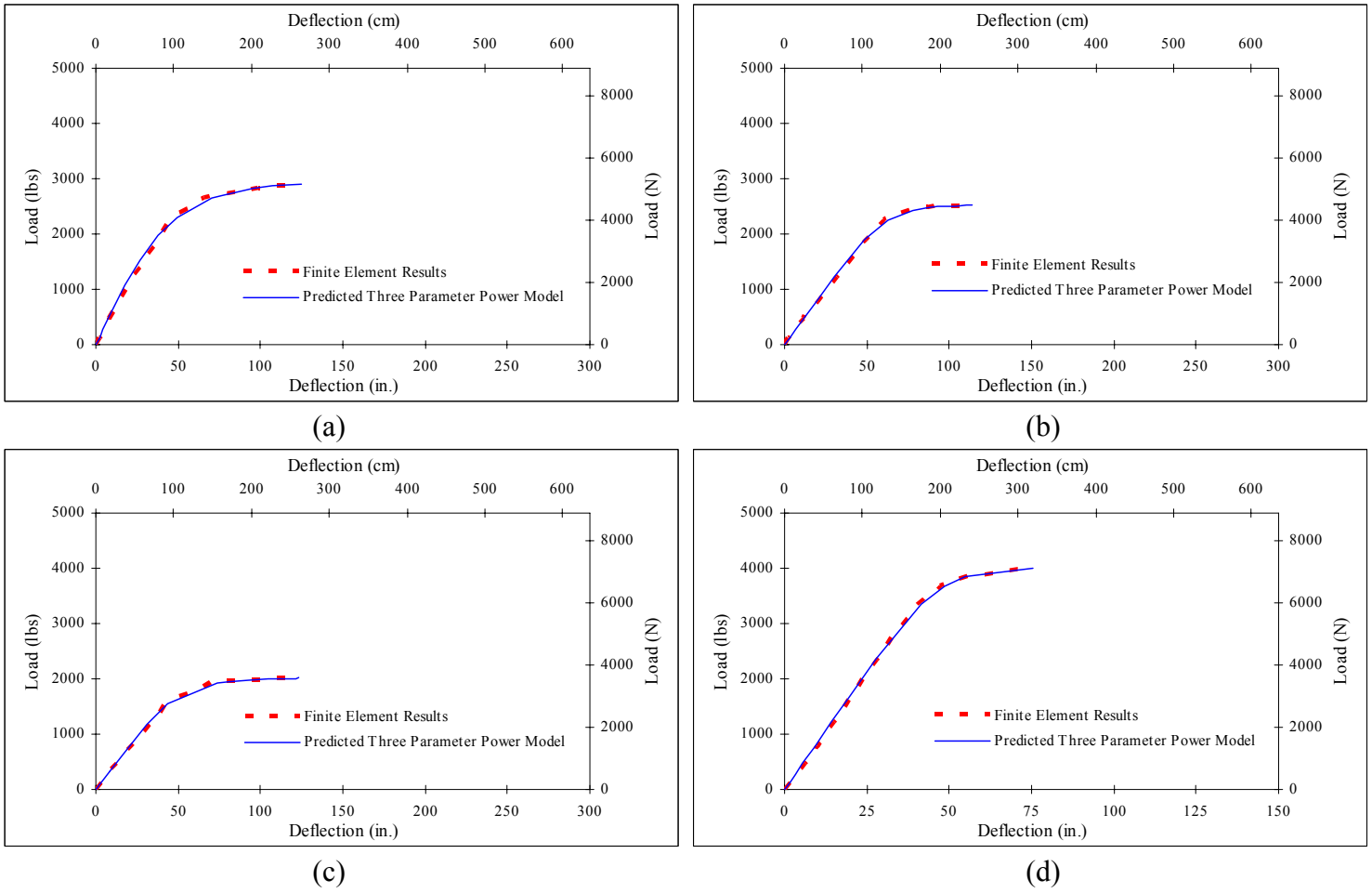

Figure B-9 Comparison of FEM model and predicted equation model for steel poles:
(a) S45-1.25-0.2-0.3-1.5-12-6-3.5-36-17-17-103; (b) S45-1.25-0.3-0.2-1.25-11-8-3-50-15.5-14.5-80;
(C) S45-1.5-0.2-0.2-1.25-11-8-3-40-15.5-15-80; (d) S45-1.5-0.3-0.3-1.75-13-8-4-40-19-18-130

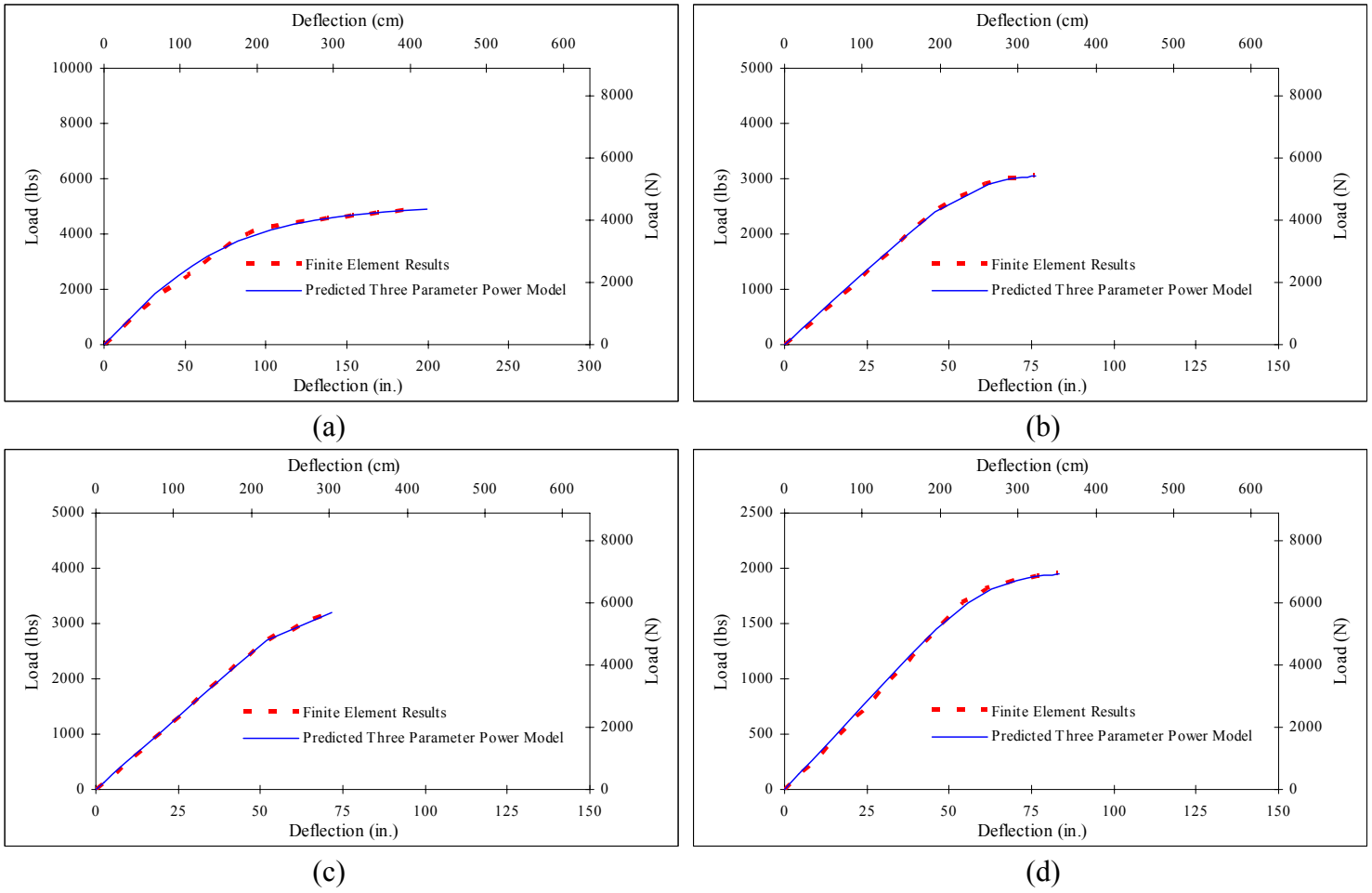

Figure B-10 Comparison of FEM model and predicted equation model for steel poles:
(a) S45-1.5-0.3-0.4-1.25-11-6-3.75-50-16-14-55; (b) S45-1.75-0.2-0.25-1.5-12-7-4-45-18-16-110;
(C) S50-1-0.2-0.25-1.5-14-7-3.5-45-19-17.5-75; (d). S50-1.25-0.15-0.2-1.5-12-7-3.25-40-17-15-65

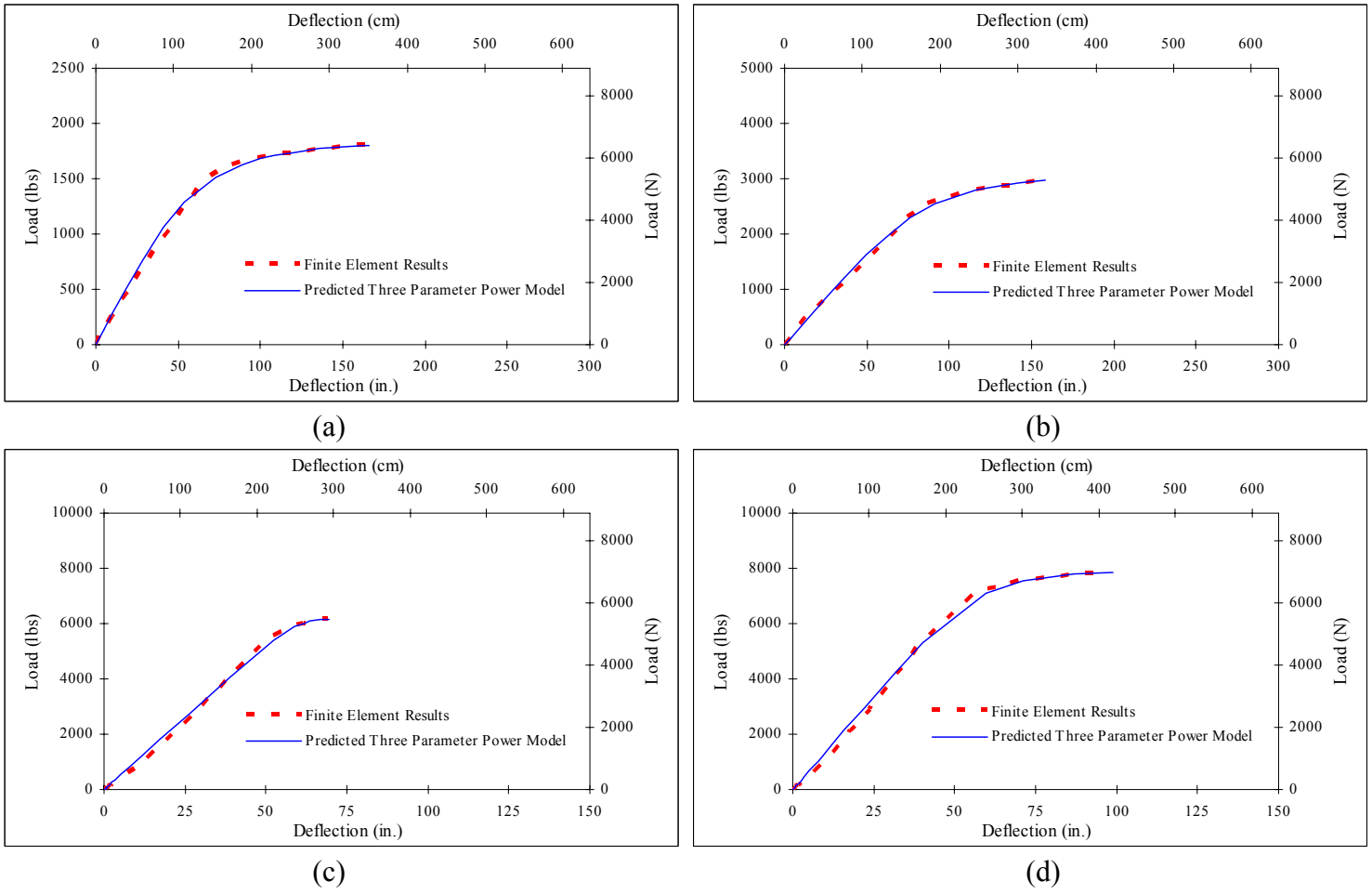

Figure B-11 Comparison of FEM model and predicted equation model for steel poles:
(a) S50-1.25-0.2-0.2-1.25-11-6-3.5-40-15.5-15-70; (b) S50-1.25-0.3-0.4-1-11-6-3-36-15-14-40;
(C) S50-1.5-0.25-0.25-2-18-9-4.25-45-26-26-105; (d) S50-1.5-0.3-0.3-2-18-10-4.5-45-26-26-140

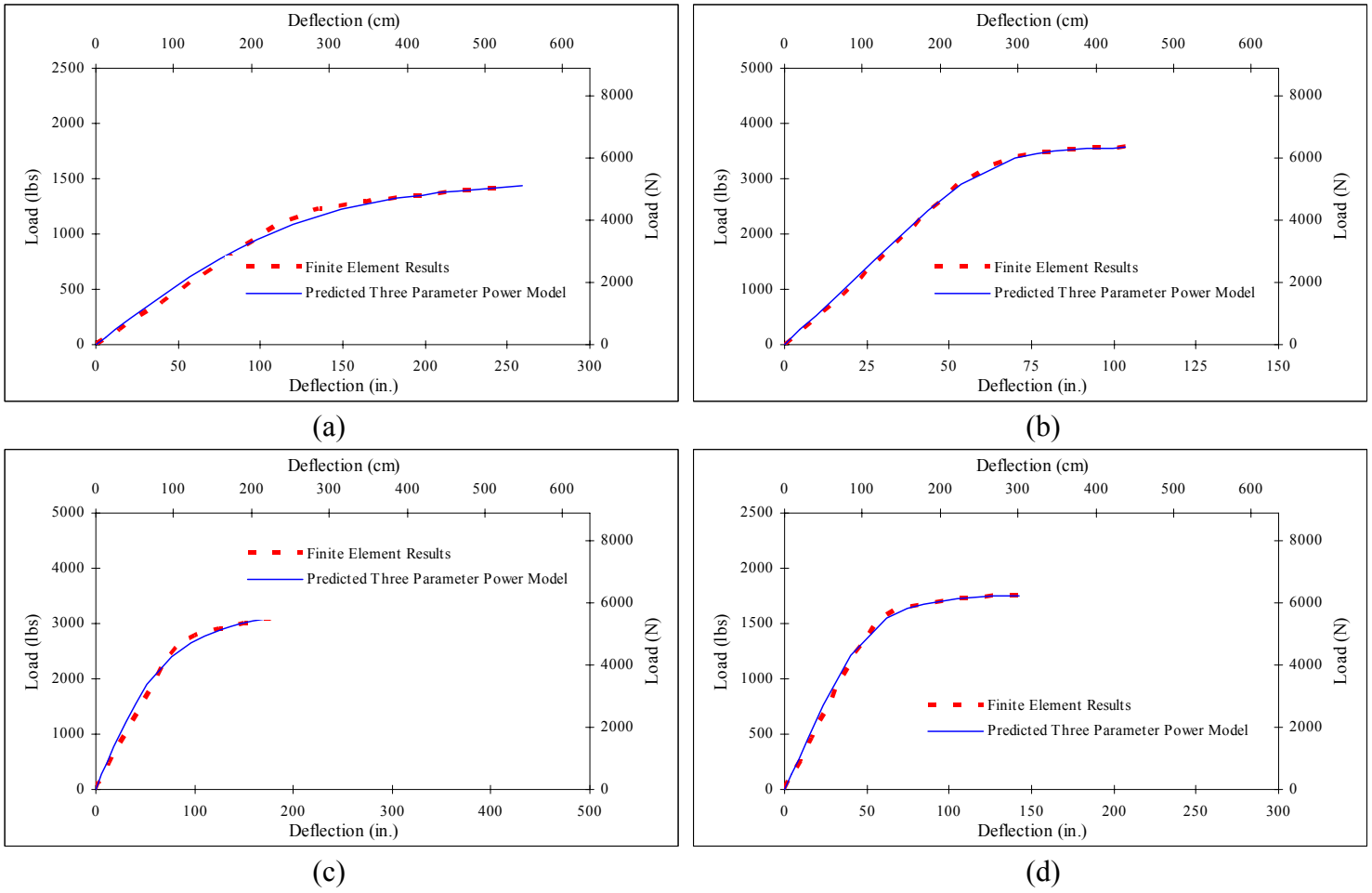

Figure B-12 Comparison of FEM model and predicted equation model for steel poles:
(a) S50-1.75-0.3-0.3-1-7-5-3-50-10.5-9.5-60; (b) S50-1.75-0.3-0.2-1.75-14-7-4-50-20-18-120;
(C) S55-1.25-0.3-0.2-1.25-11-5-3-36-15.5-14-80; (d) S55-1.5-0.2-0.2-1.5-12-8-3.5-36-17-16-80

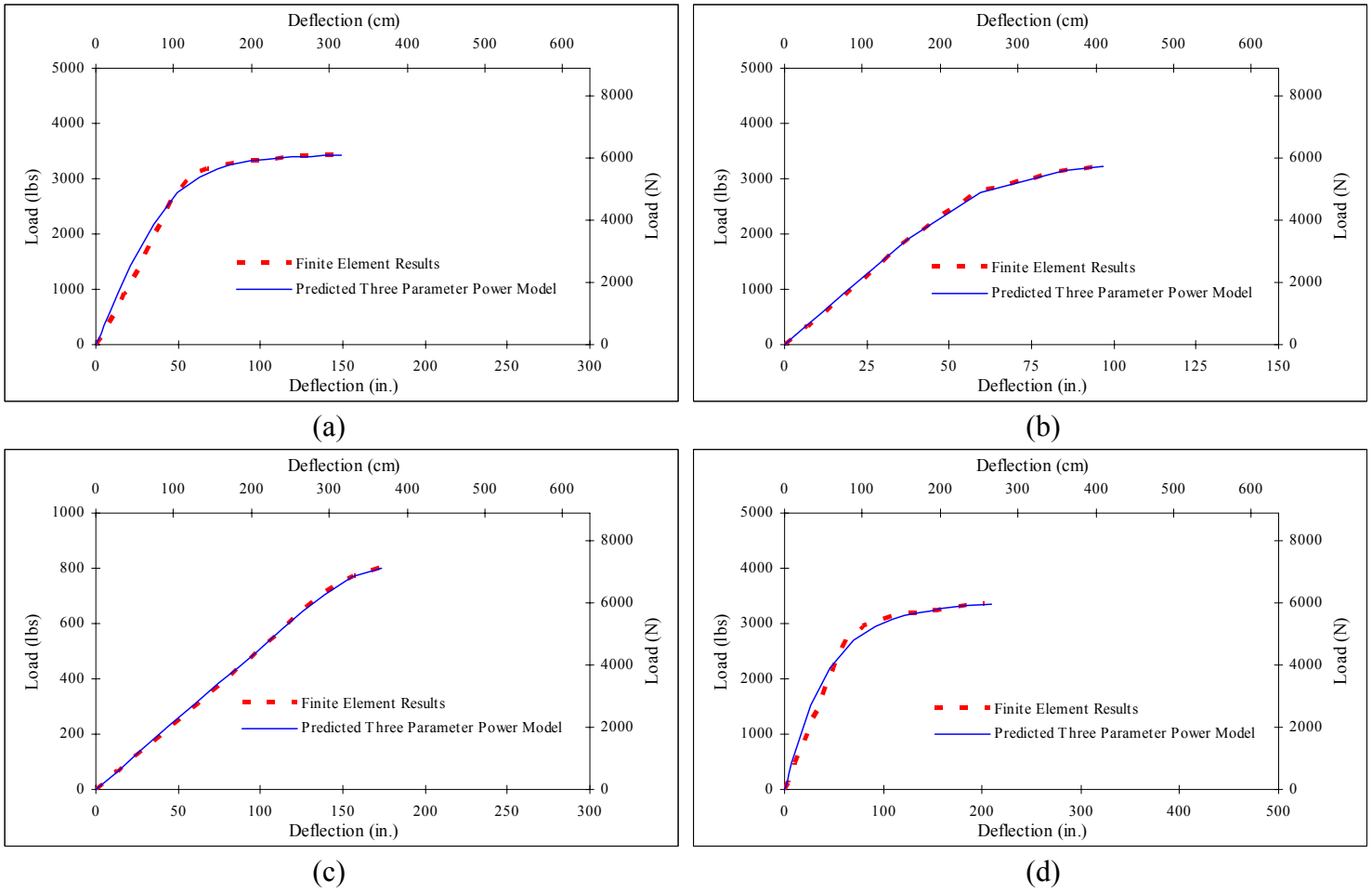

Figure B-13 Comparison of FEM model and predicted equation model for steel poles:
(a) S55-1.75-0.25-0.25-2-15-9-4.5-36-22-21-140; (b) S60-1.25-0.2-0.25-1.5-16-9-3.25-50-22-19.5-85;
(C) S60-1.5-0.2-0.3-1-7-5-3.5-40-10.5-10.5-50; (d) S60-1.5-0.3-0.3-1.75-14-8-3.5-36-20-18-120

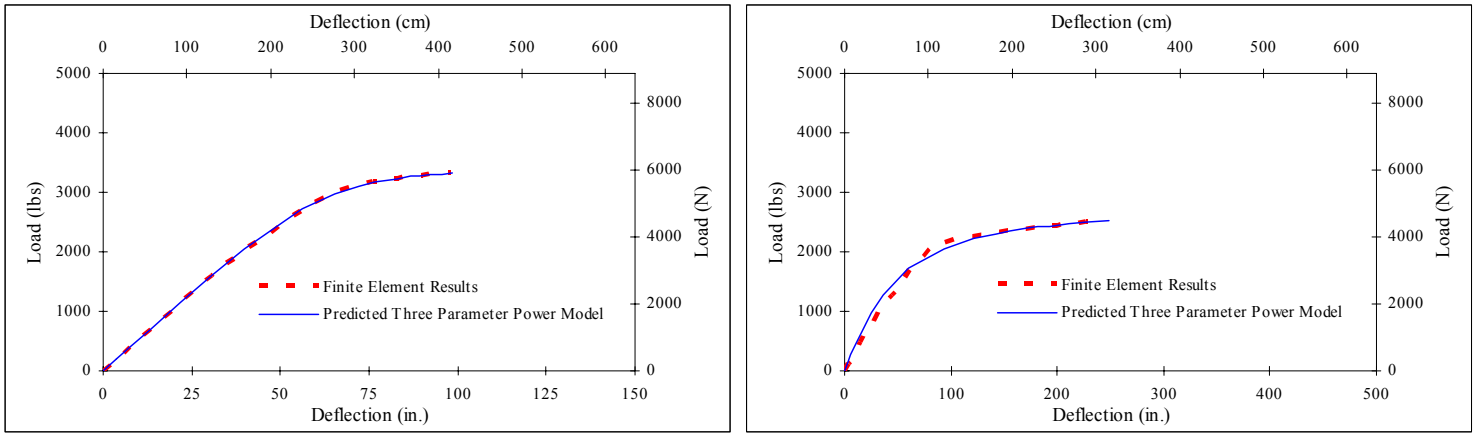

(a)

(b)

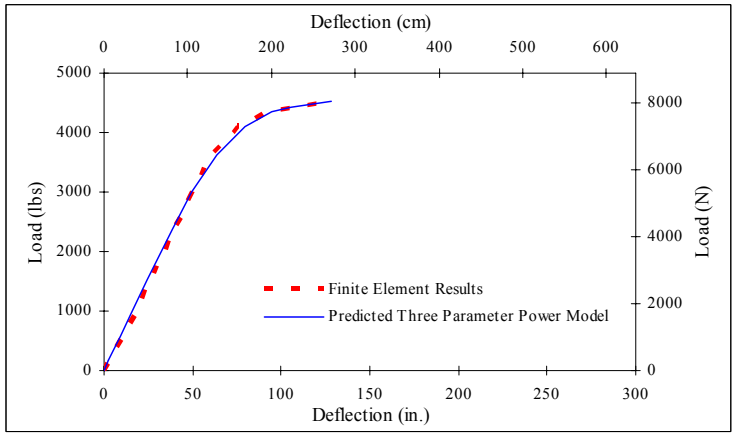

(c)

Figure B-14 Comparison of FEM model and predicted equation model for steel poles:
(a) S60-1.75-0.25-0.25-1.5-16-8-3.5-36-22-19-95; (b) S60-1.75-0.3-0.3-1.5-12-8-3.5-36-17-15.5-103;
(C) S60-1.75-0.3-0.3-1.75-16-8-3.5-40-23-21-110

APPENDIX C

PLOTS OF FEM MODEL AND PREDICTED EQUATION MODEL FOR FRP POLES

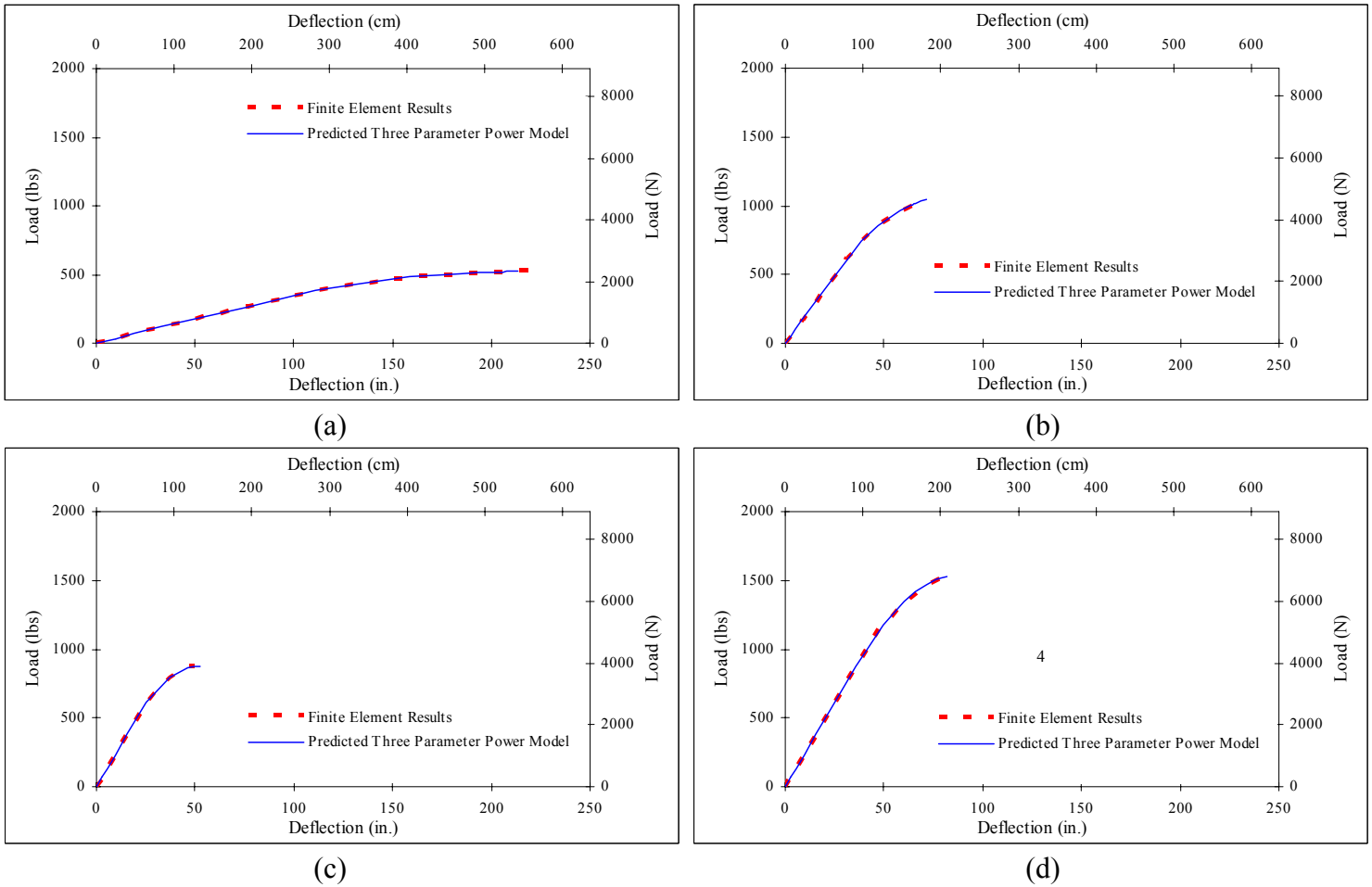

Figure C-1 Comparison of FEM model and predicted equation model for FRP poles:
(a) F20-0.5-0.2-0.2-0.75-6-3.5-1.5-8-7.5-28-4.5; (b) F20-0.75-0.25-0.275-0.75-7.5-5-1.75-10-10-25-3.5;
(c) F20-0.75-0.275-0.25-0.75-8-5.5-1.5-10-9-10-4; (d) F20-0.75-0.275-0.3-1-8-3.5-2.5-10.7-10.5-40-4.5

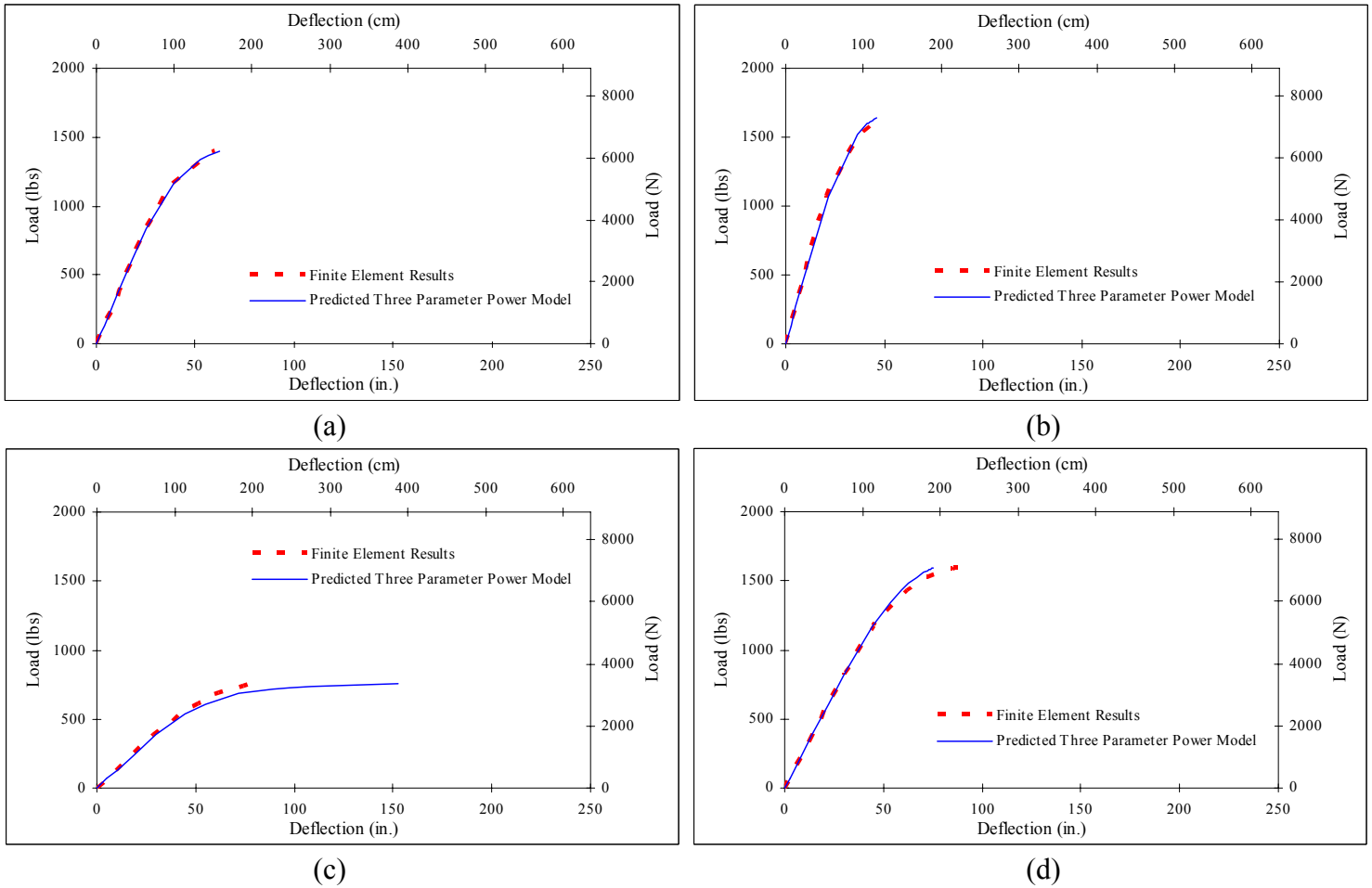

Figure C-2 Comparison of FEM model and predicted equation model for FRP poles:
(a) F20-0.75-0.3-0.3-1-8-5-2.5-10.7-10.2-40-5; (b) F20-1-0.25-0.225-1-10-7-2.5-13.5-12-50-4.5;
(c) F25-0.5-0.25-0.25-1-8-4.5-2.5-10.6-10-45-5.5; (d) F25-0.75-0.275-0.25-1.25-10-6-2.75-13.2-13-70-4.5

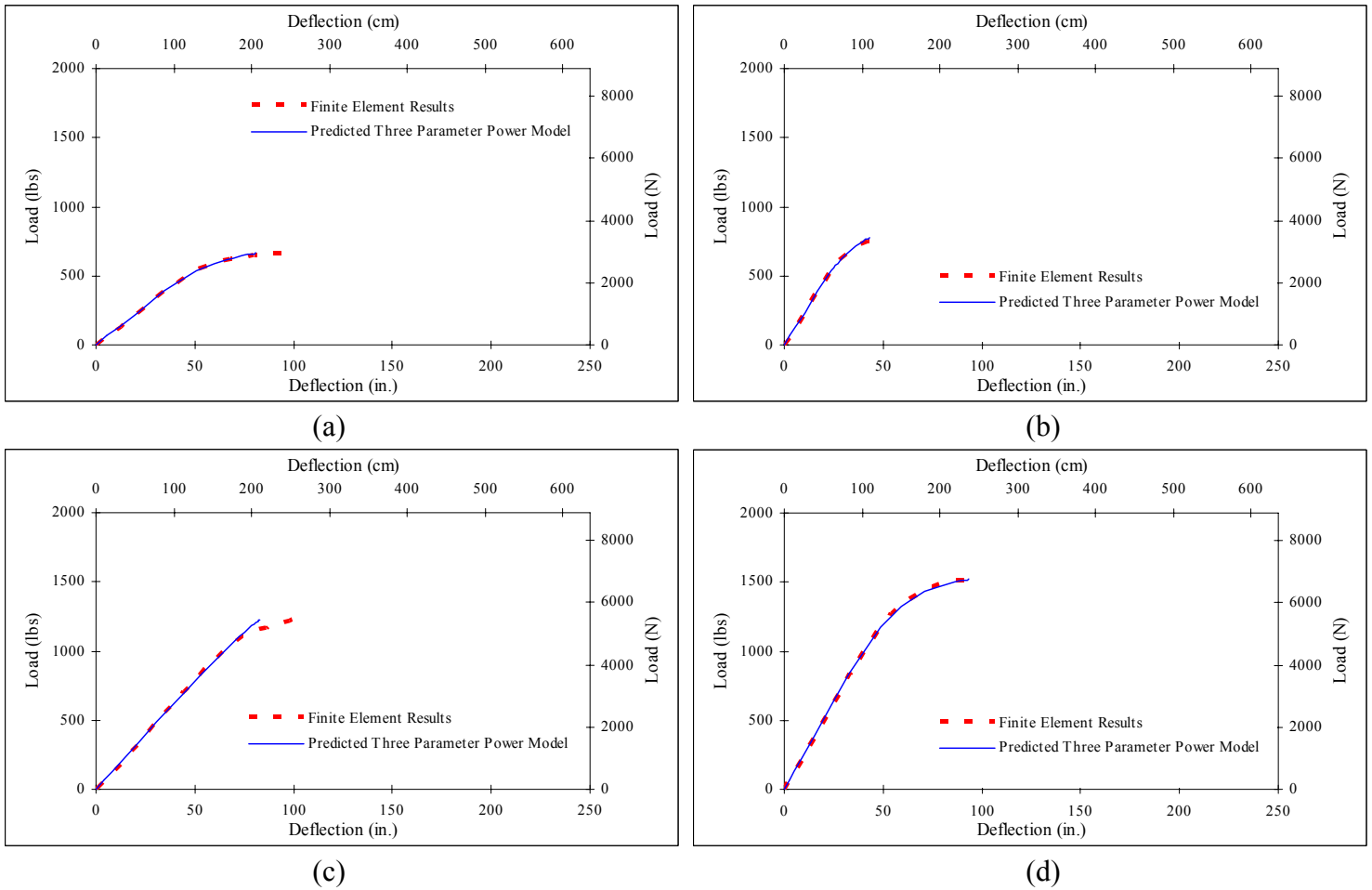

Figure C-3 Comparison of FEM model and predicted equation model for FRP poles:
(a) F25-0.75-0.3-0.3-0.75-7-4-2-9.5-8.5-28-5; (b) F25-0.75-0.3-0.325-0.75-9.5-5-1.75-12-10.5-20-4.5;
(c) F25-1-0.275-0.275-1-7.5-4.5-2.5-10-10-51-5.5; (d) F25-1-0.325-0.35-1-8.5-5.5-2.25-11.5-10.5-40-5

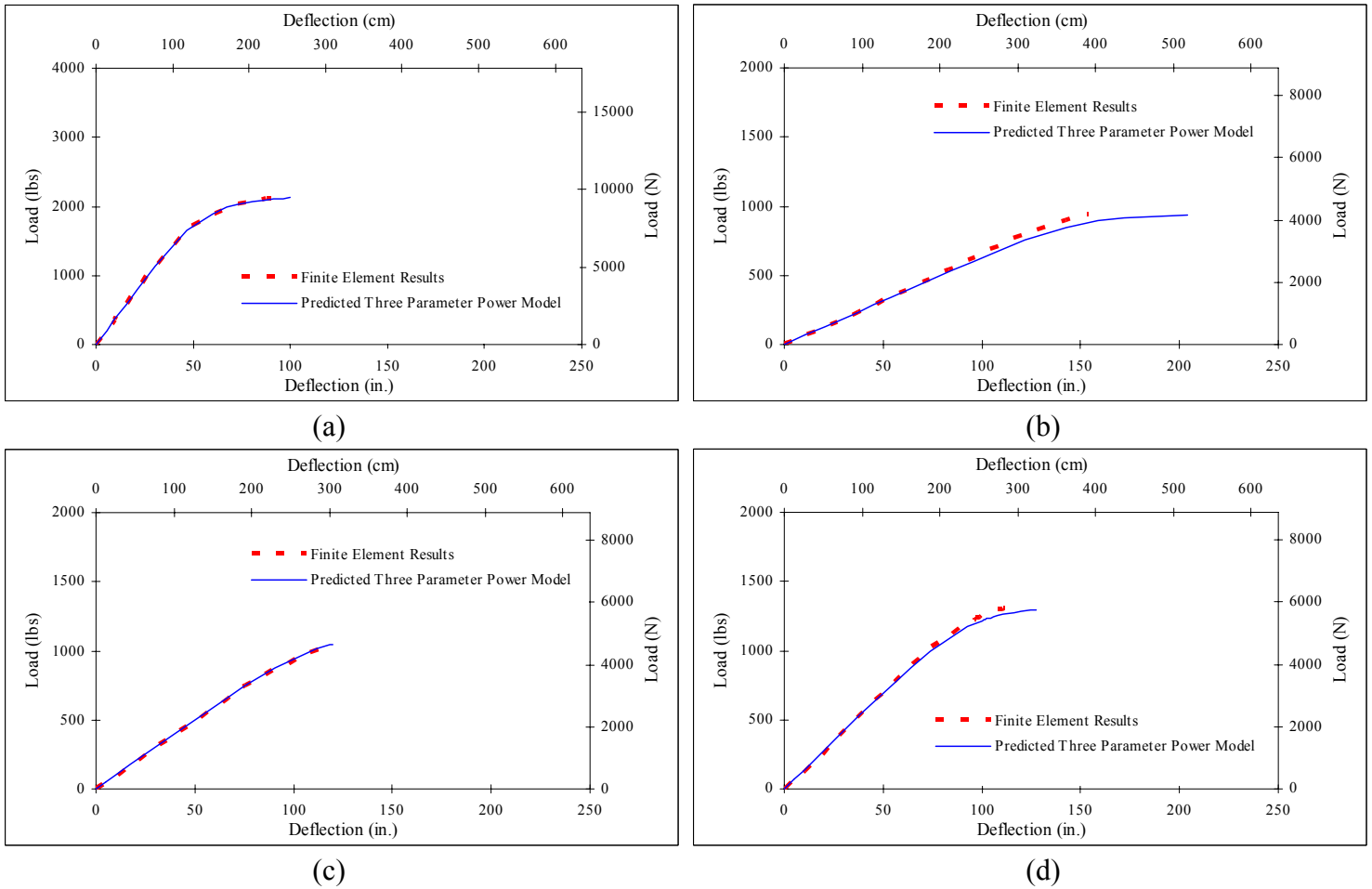

Figure C-4 Comparison of FEM model and predicted equation model for FRP poles:
(a) F25-1.25-0.3-0.325-1-10-6-2-13.5-12.5-35-5; (b) F30-0.75-0.275-0.275-1-8-4-2.5-10.6-10-40-3.5;
(c) F30-0.75-0.35-0.35-1.125-8.5-5-2.5-11.5-10.5-45-3.5; (d) F30-1-0.3-0.275-1-9-5-2.25-11.5-11-45-5

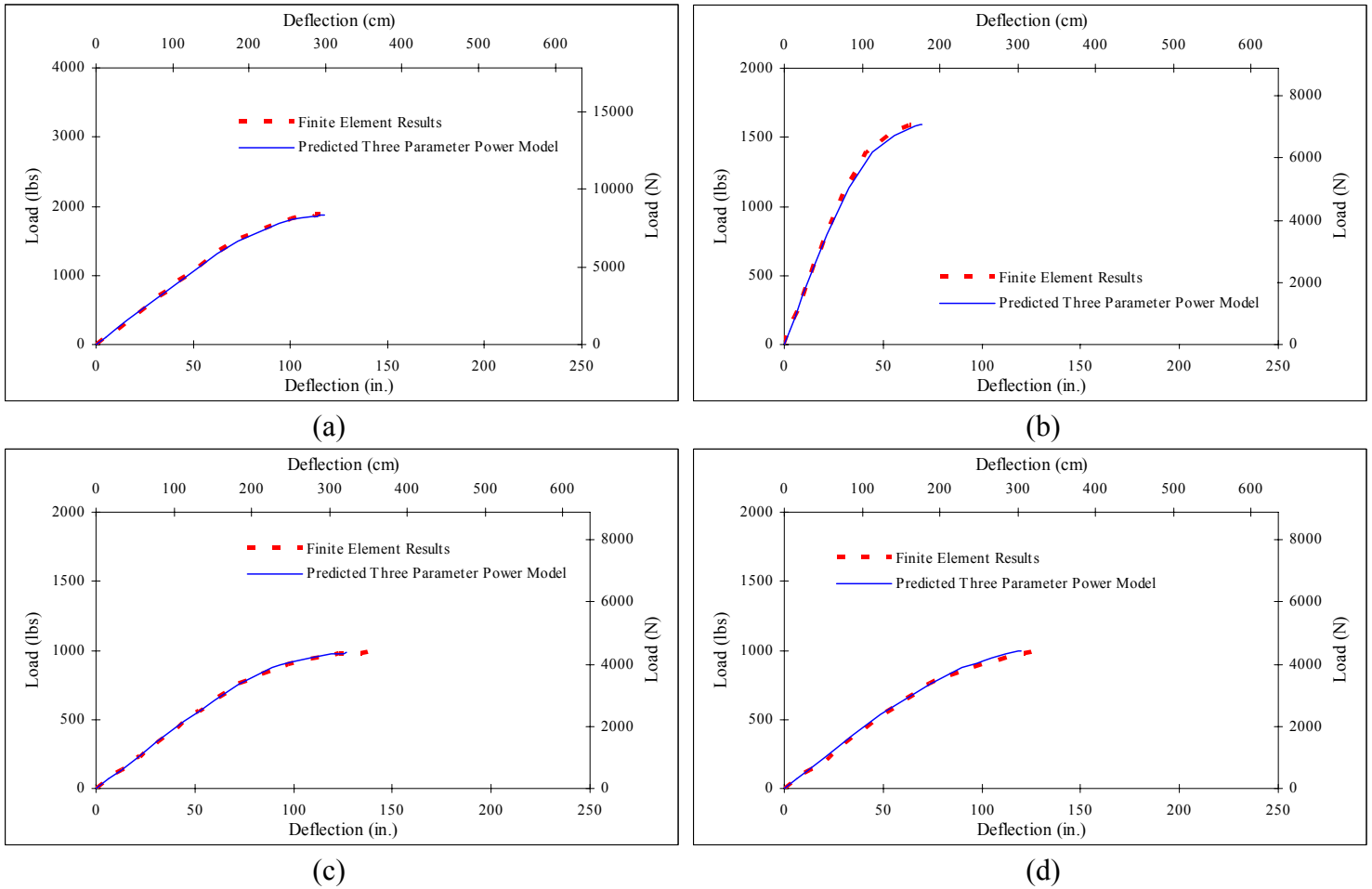

Figure C-5 Comparison of FEM model and predicted equation model for FRP poles:
(a) F30-1-0.325-0.3-1.25-11-6-2.5-14.5-13.5-71-4; (b) F30-1-0.325-0.325-1.125-12-7-2.25-16-14-56-5.5;
(c) F30-0.75-0.3-0.3-1-9-4-2.5-12-11-40-4.5; (d) F35-0.75-0.325-0.35-1-10-5.5-2.5-13.7-13.5-51-4

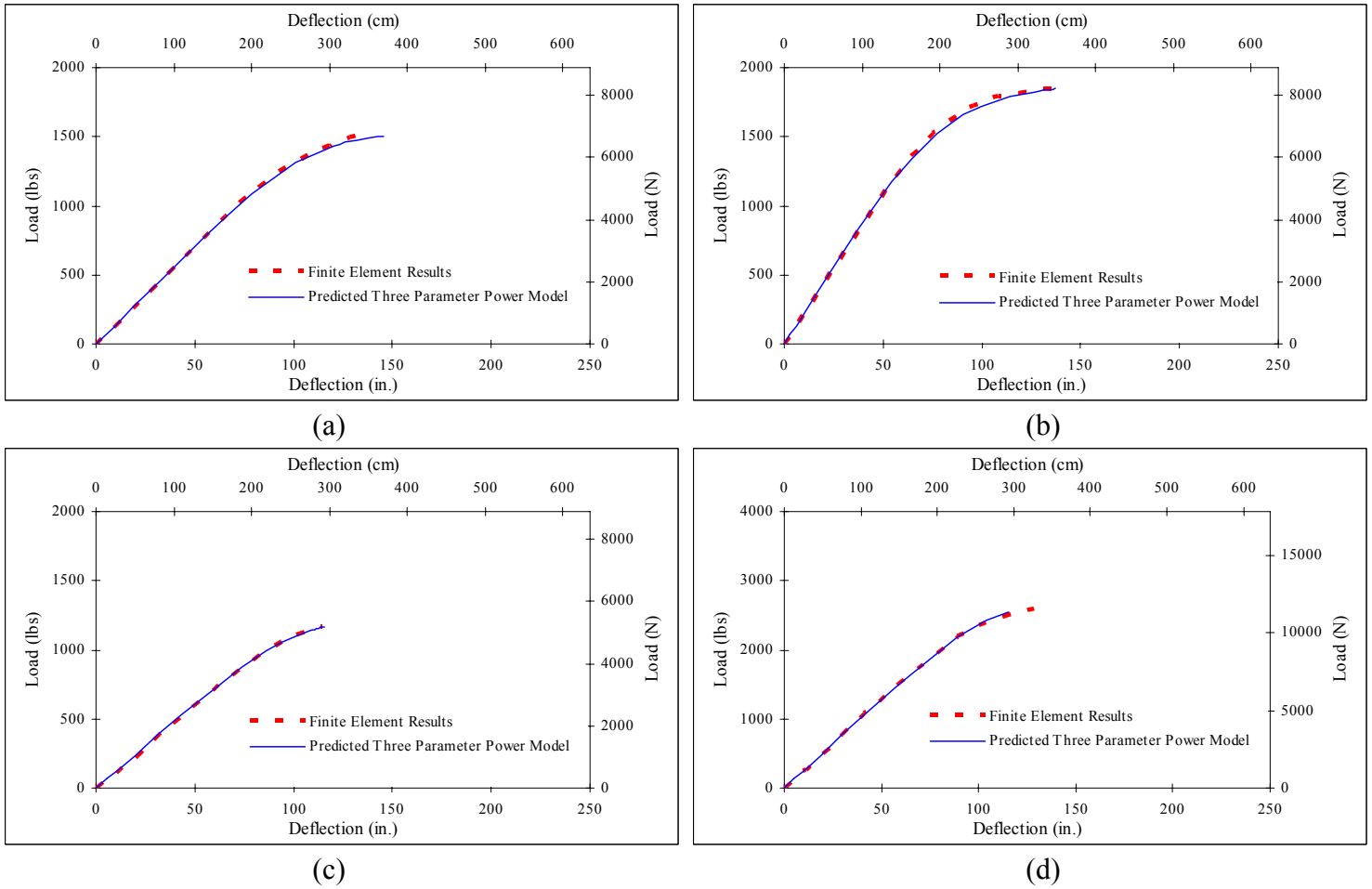

Figure C-6 Comparison of FEM model and predicted equation model for FRP poles:
(a) F35-1-0.275-0.275-1.125-12-6.5-2.75-16-15-50-3.5; (b) F35-1-0.3-0.3-1.25-12-7-2.5-16.2-15.7-56-5;
(c) F35-1-0.35-0.35-1-10-5-2.5-13.5-12.5-41-4.5; (d) F35-1.25-0.325-0.325-1.5-13-8-3-17.5-16-90-4

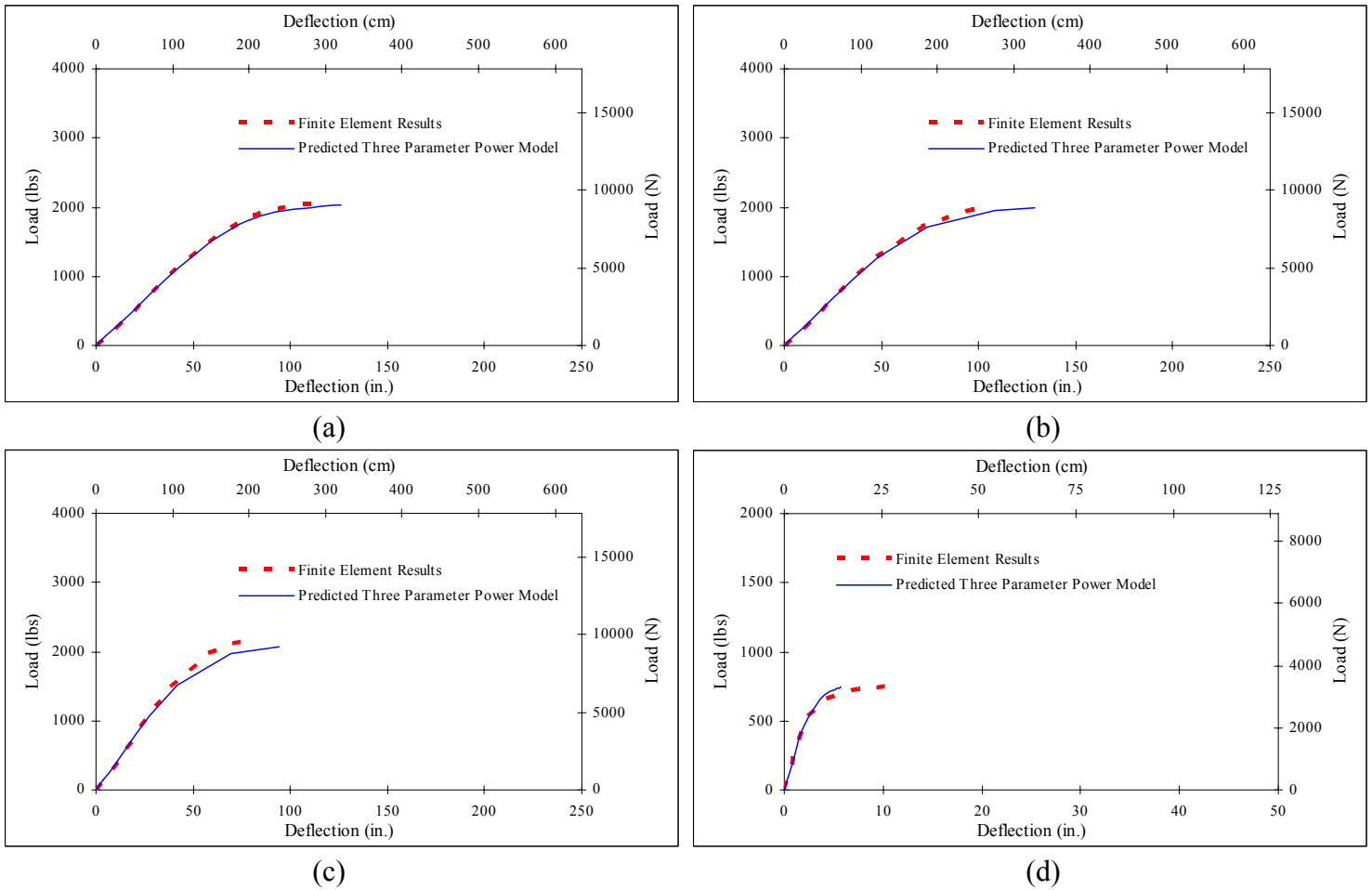

Figure C-7 Comparison of FEM model and predicted equation model for FRP poles:
(a) F35-1.25-0.35-0.325-1.25-12-7-2.75-16-14.5-65-5.5; (b) F35-1.25-0.35-0.35-1.125-12-7.5-2.5-16-15-48-5;
(c) F35-1.5-0.375-0.375-1-13-8-2-17-15.5-45-5.5; (d) F40-0.75-0.3-0.3-1-10.5-5-2.5-14-12.5-40-5

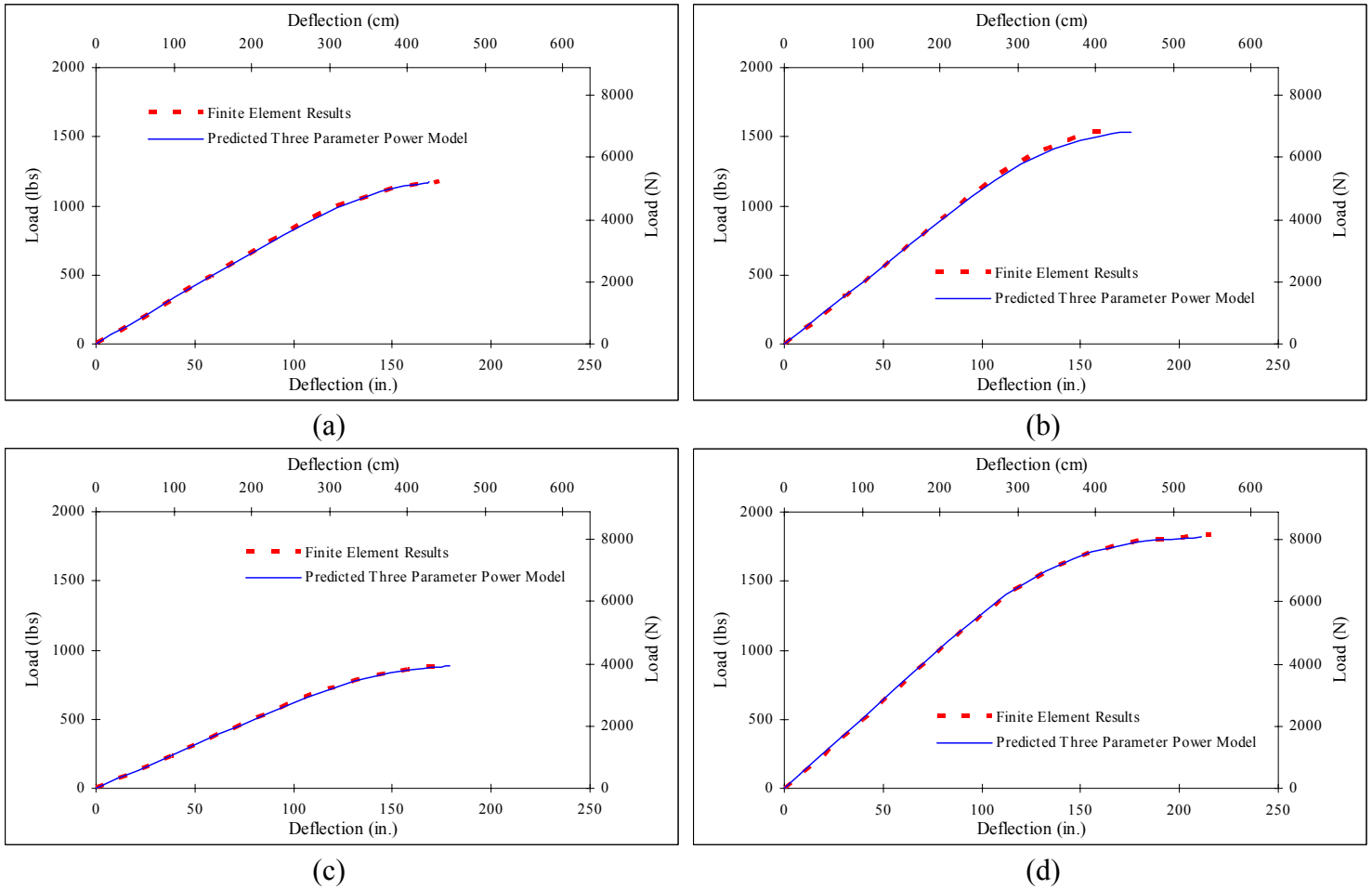

Figure C-8 Comparison of FEM model and predicted equation model for FRP poles:
(a) F40-1-0.275-0.3-1.125-11-5.5-2.75-14.5-13-50-4; (b) F40-1-0.3-0.325-1.25-12.5-6-3-16.5-15-60-3.5;
(c) F40-1-0.325-0.325-1-9-4.5-2.25-12-10.5-45-5; (d) F40-1-0.35-0.325-1.5-12-6.5-3.25-16.5-15-95-4

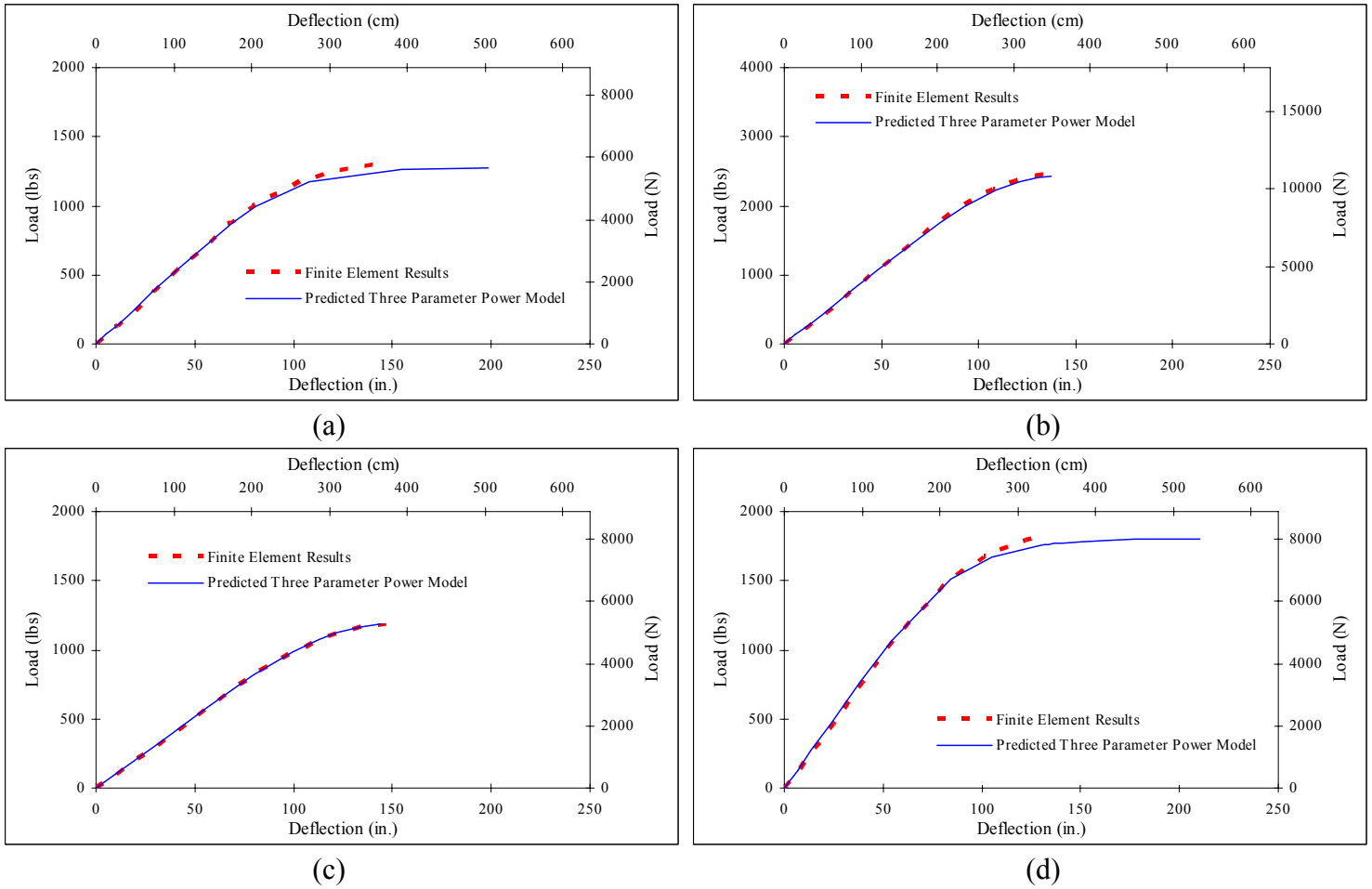

Figure C-9 Comparison of FEM model and predicted equation model for FRP poles:
(a) F40-1.25-0.375-0.35-1-10.5-6-2.5-14-12.5-43-5.5; (b) F40-1.25-0.375-0.375-1.5-14-7.5-3-18.5-16.5-85-4;
(c) F45-1-0.325-0.35-1.125-12.5-5-2.5-16.2-14.5-40-5; (d) F45-1-0.35-0.375-1.5-14-7.5-3.5-18.2-16.2-85-5.5

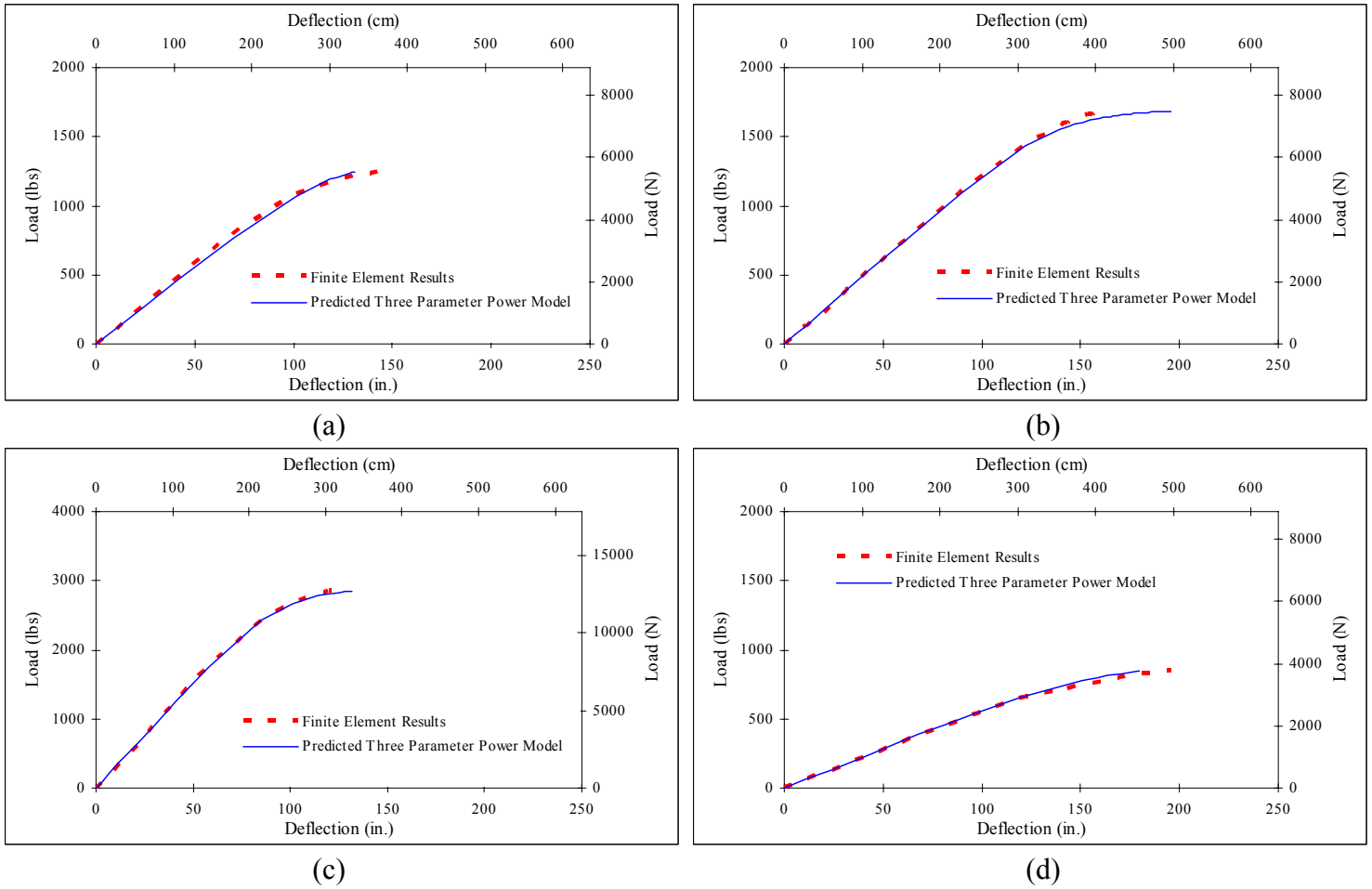

Figure C-10 Comparison of FEM model and predicted equation model for FRP poles:
(a) F45-1-0.4-0.4-1.25-13-6.5-2.75-17.5-15-50-4; (b) F45-1.25-0.375-0.4-12.5-6-2.75-16.5-14.5-55-4.5;
(c)F45-1.5-0.4-0.4-1.5-16-10-3-20-18-95-4.5; (d) F50-0.75-0.35-0.35-1.125-12-5-2.5-16-15-45-4

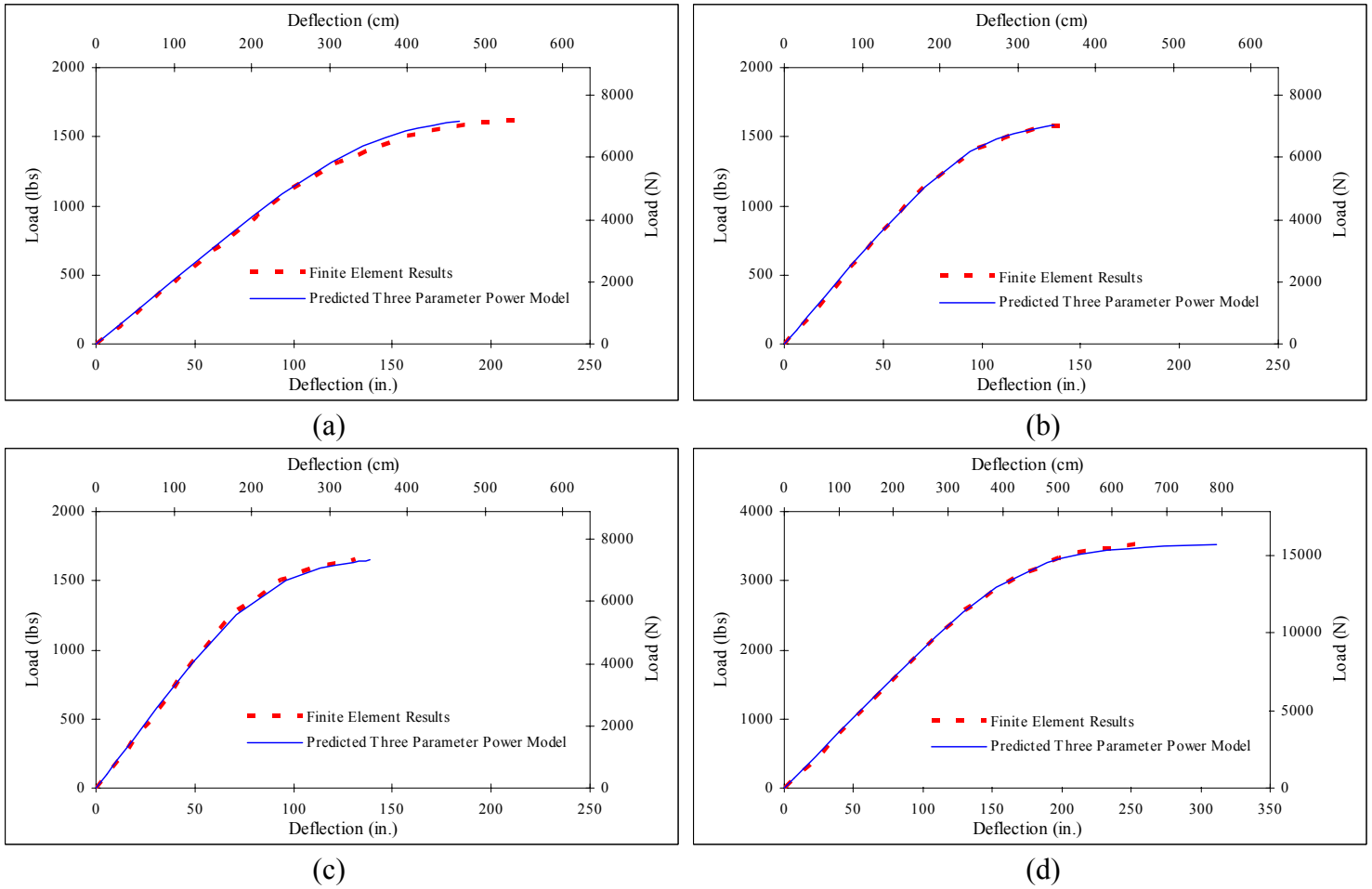

Figure C-11 Comparison of FEM model and predicted equation model for FRP poles:
(a) F50-1-0.35-0.375-1.5-14-7-3.5-19-17-75-4.5; (b) F50-1-0.375-0.4-1.25-16.5-9-2.75-21-19.5-71-3.5;
(c) F50-1.125-0.375-0.375-1.25-16.5-9-2.75-21-19-90-4; (d) F50-1.5-0.4-0.425-1.75-16-9-3.75-22.5-21-93-4

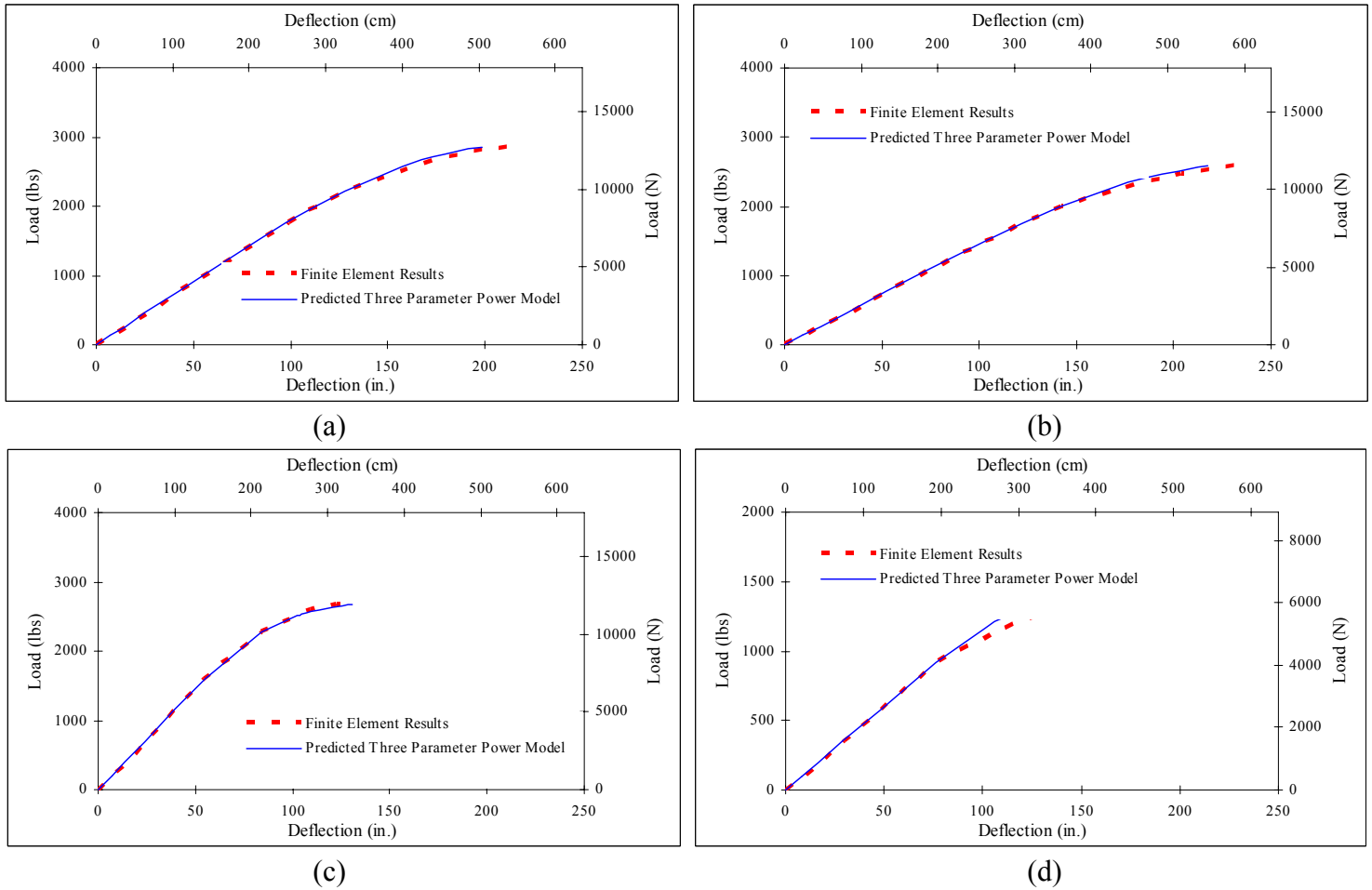

Figure C-12 Comparison of FEM model and predicted equation model for FRP poles:
(a) F50-1.25-0.4-0.425-1.75-16-8-3.5-22.5-21-93-4; (b) F50-1.125-0.375-0.375-1.75-16-8-3.5-22.5-21.5-108-3.5;
(c) F50-1.5-0.4-0.4-1.5-17.5-9-3.75-23-20-79-3.5; (d) F55-1-0.45-0.45-1.25-16-8.5-2.75-20-18.5-45-3.5

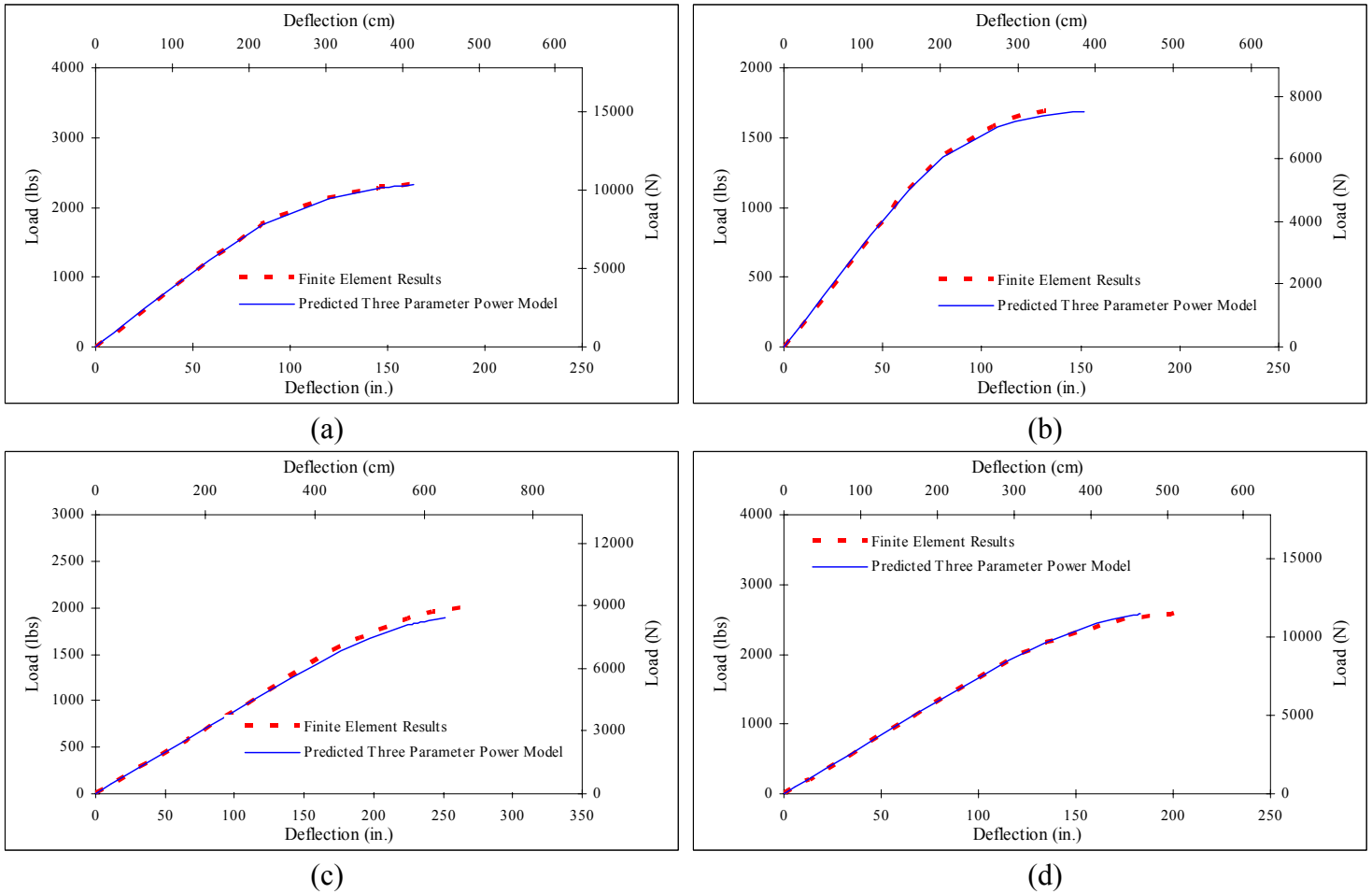

Figure C-13 Comparison of FEM model and predicted equation model for FRP poles:
(a) F55-1.25-0.425-0.45-1.5-18-10-3.25-24-22-103-4; (b) F55-1.25-0.45-0.475-1.25-15.5-8-2.75-19.5-17.5-71-5.5;
(c) F55-1.125-0.45-0.45-1.5-14-6-3.5-18.5-17.5-60-4; (d) F55-1.5-0.375-0.4-1.75-16-8.5-3.25-22-19-85-5

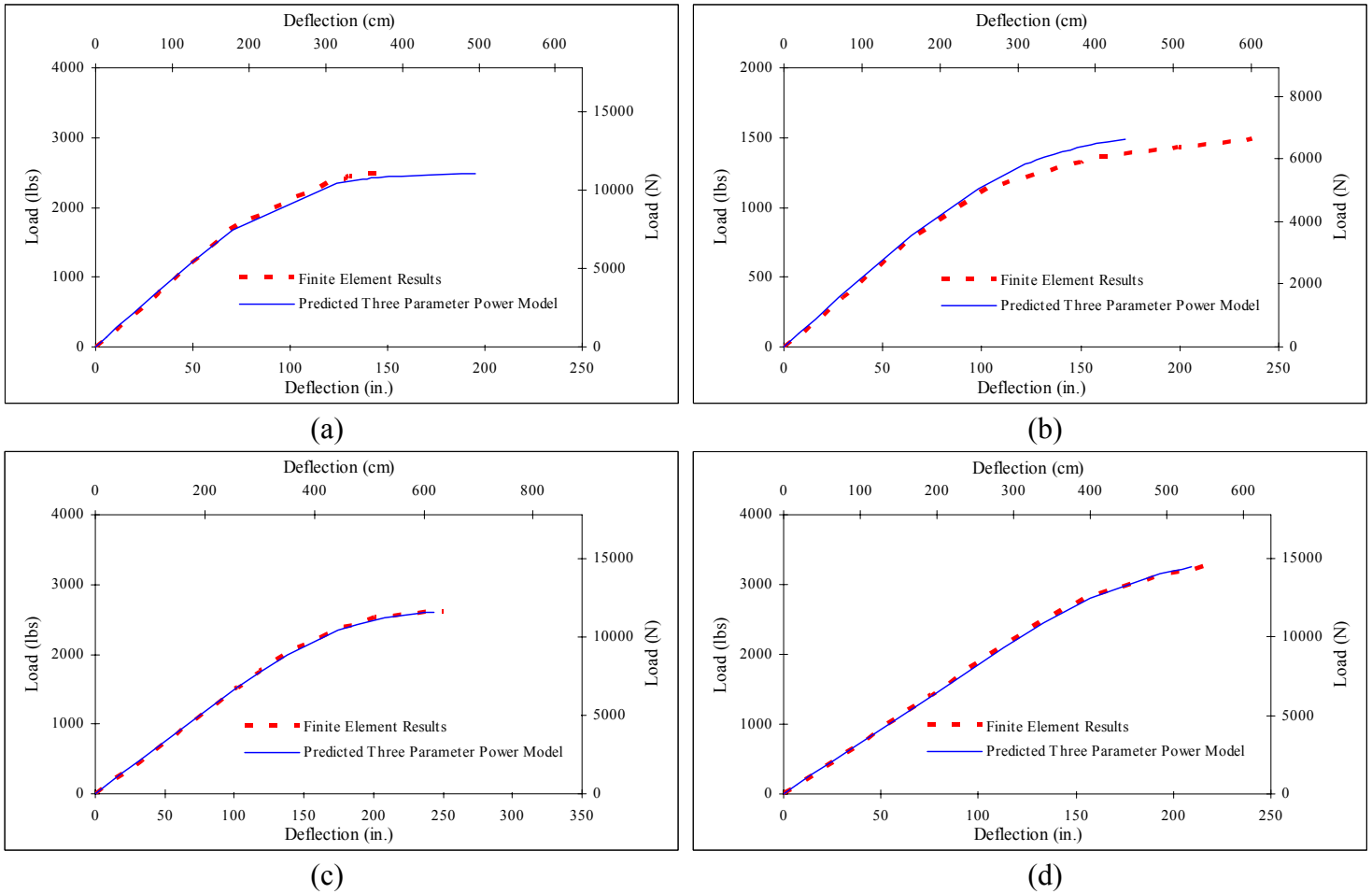

Figure C-14 Comparison of FEM model and predicted equation model for FRP poles:
(a) F55-1.5-0.45-0.425-1.5-18-10.5-3.5-24-21-90-4.5; (b) F60-1-0.425-0.45-1.5-16-8-3.25-22-19.5-85-5;
(c) F60-1.25-0.45-0.45-1.75-17.5-9-3.5-23.5-22-101-4; (d) F60-1.5-0.425-0.4-2-18-9.5-3.75-24-22-90-5

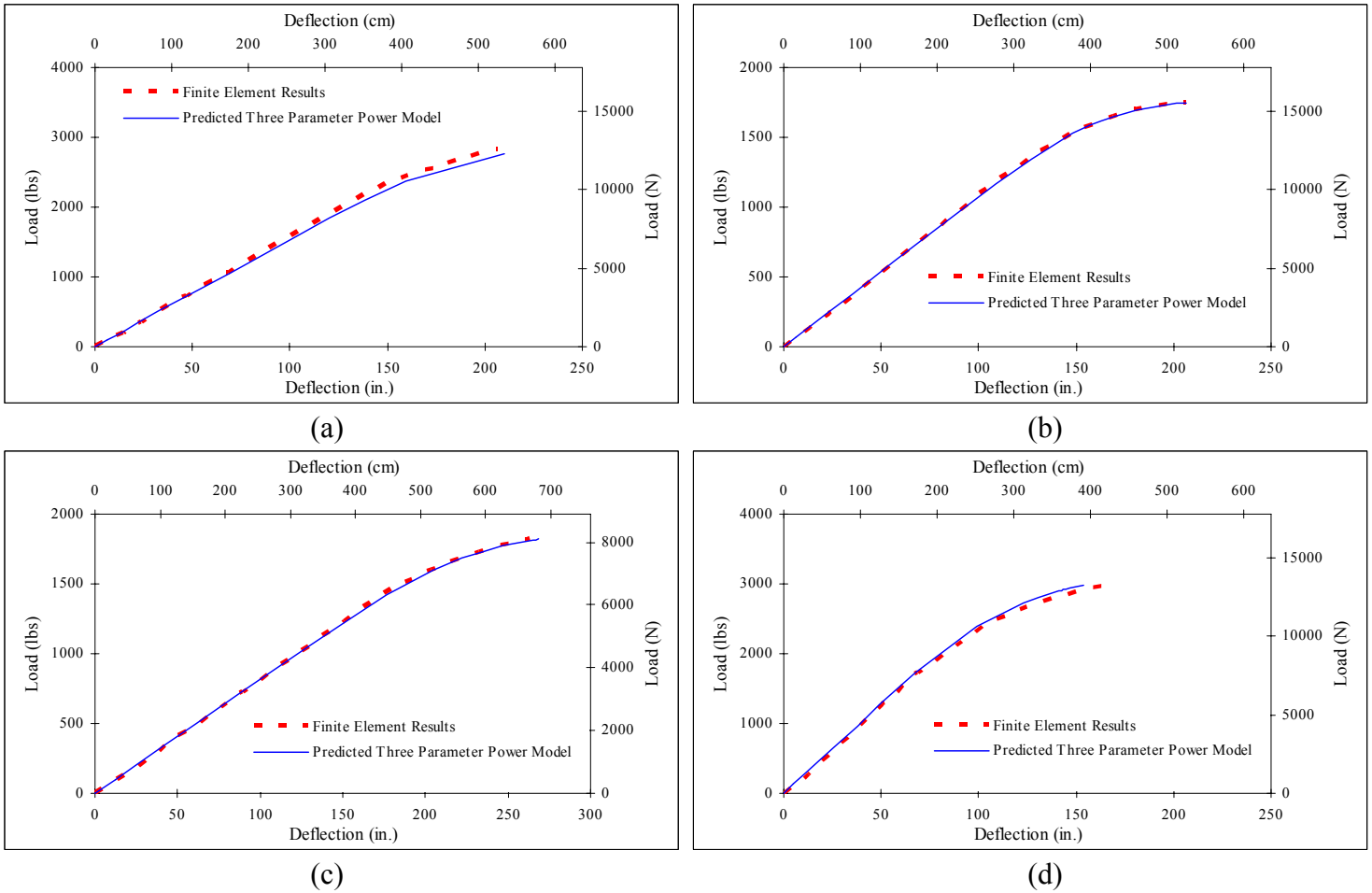

Figure C-15 Comparison of FEM model and predicted equation model for FRP poles:
(a) F60-1.5-0.425-0.425-1.75-16.5-8-3.5-21.5-20-67-5.5; (b) F60-1.125-0.45-0.45-1.5-17-7.5-3.5-21.5-19-103-3.5;
(c) F60-1.125-0.475-0.5-1.5-15-6.5-3.25-20-18.5-95-3.5; (d) F60-1.25-0.5-0.5-2-20-11.5-4-27-24-79-4.5

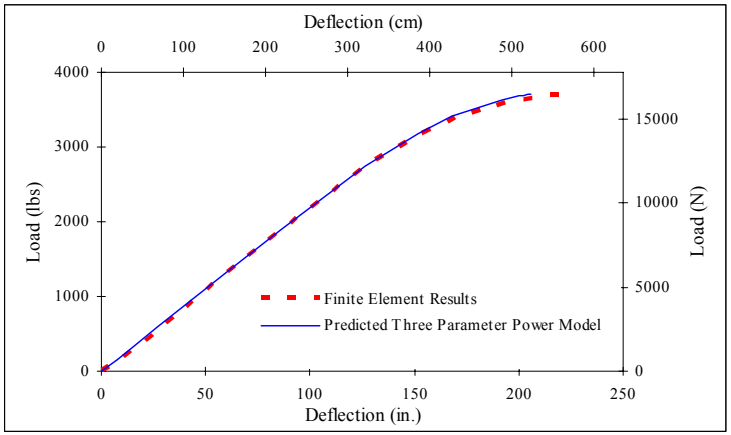

Figure C-16 Comparison of FEM model and predicted equation model for FRP poles: F60-1.5-0.45-0.45-2-20-10-4.25-27-25-110-4

APPENDIX D

ERROR BAND PLOTS

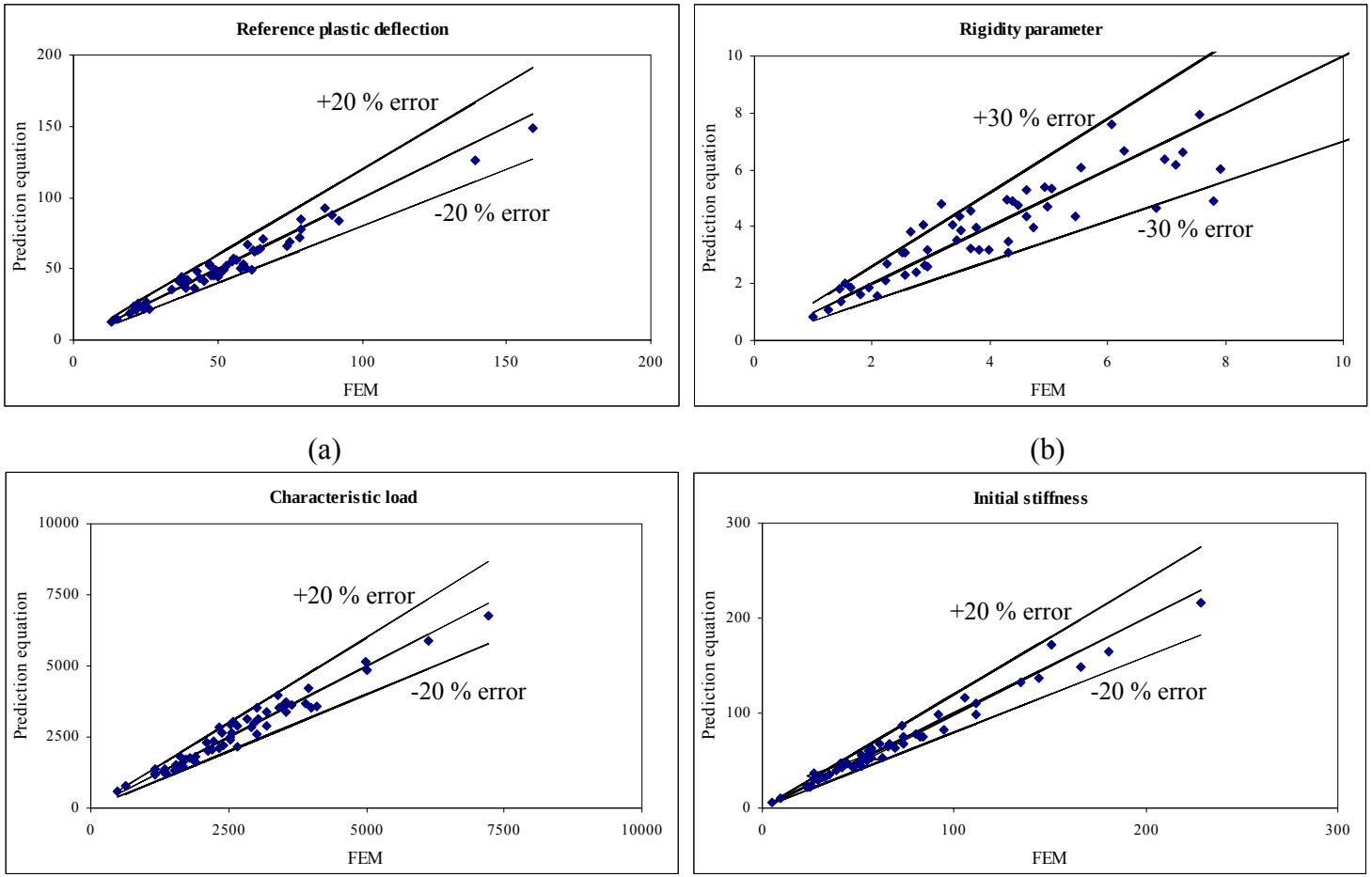

Figure D-1 Error band analysis for steel poles:
(a) Reference plastic deflection; (b) Rigidity parameter;
(c) Proposed characteristic load; (d) Initial stiffness

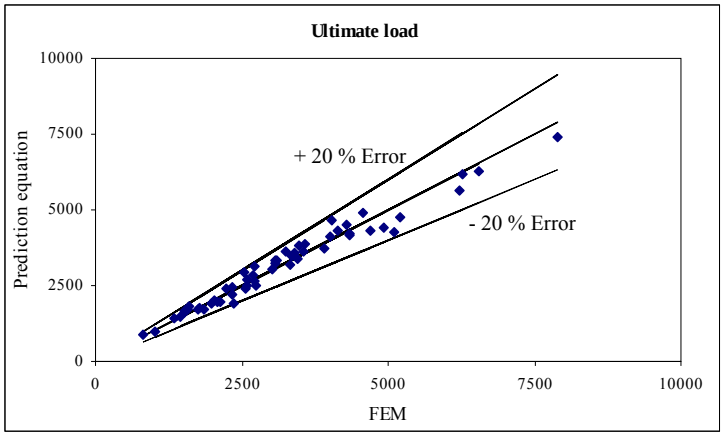

Figure D-2 Error band analysis for steel poles: Ultimate load

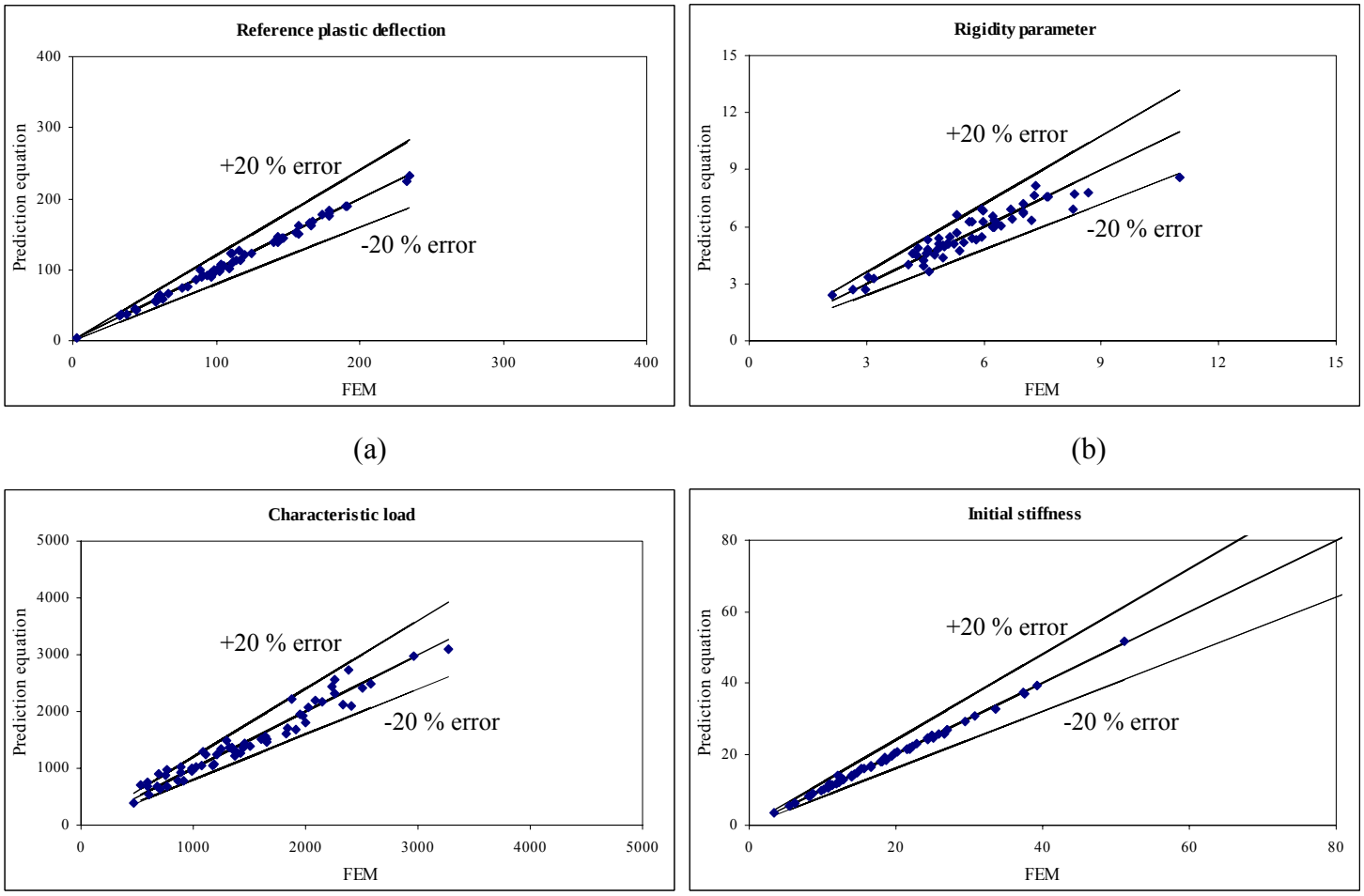

Figure D-3 Error band analysis for FRP poles:
(a) Reference plastic deflection; (b) Rigidity parameter;
(c) Proposed characteristic load; (d) Initial stiffness

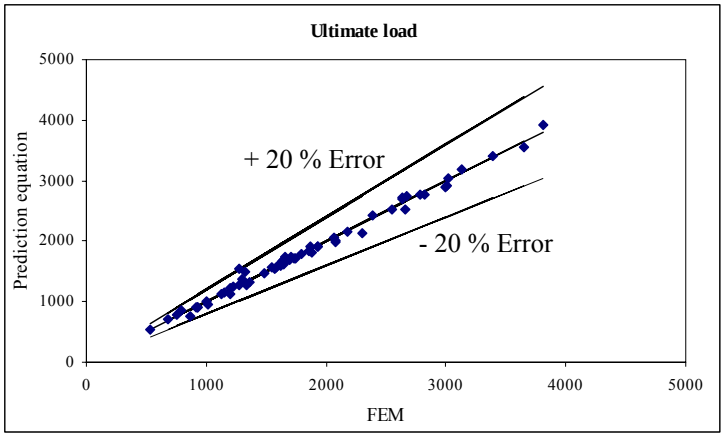

Figure D-4 Error band analysis for FRP poles: Ultimate load

APPENDIX E

SENSITIVITY PLOTS FOR STEEL POLES

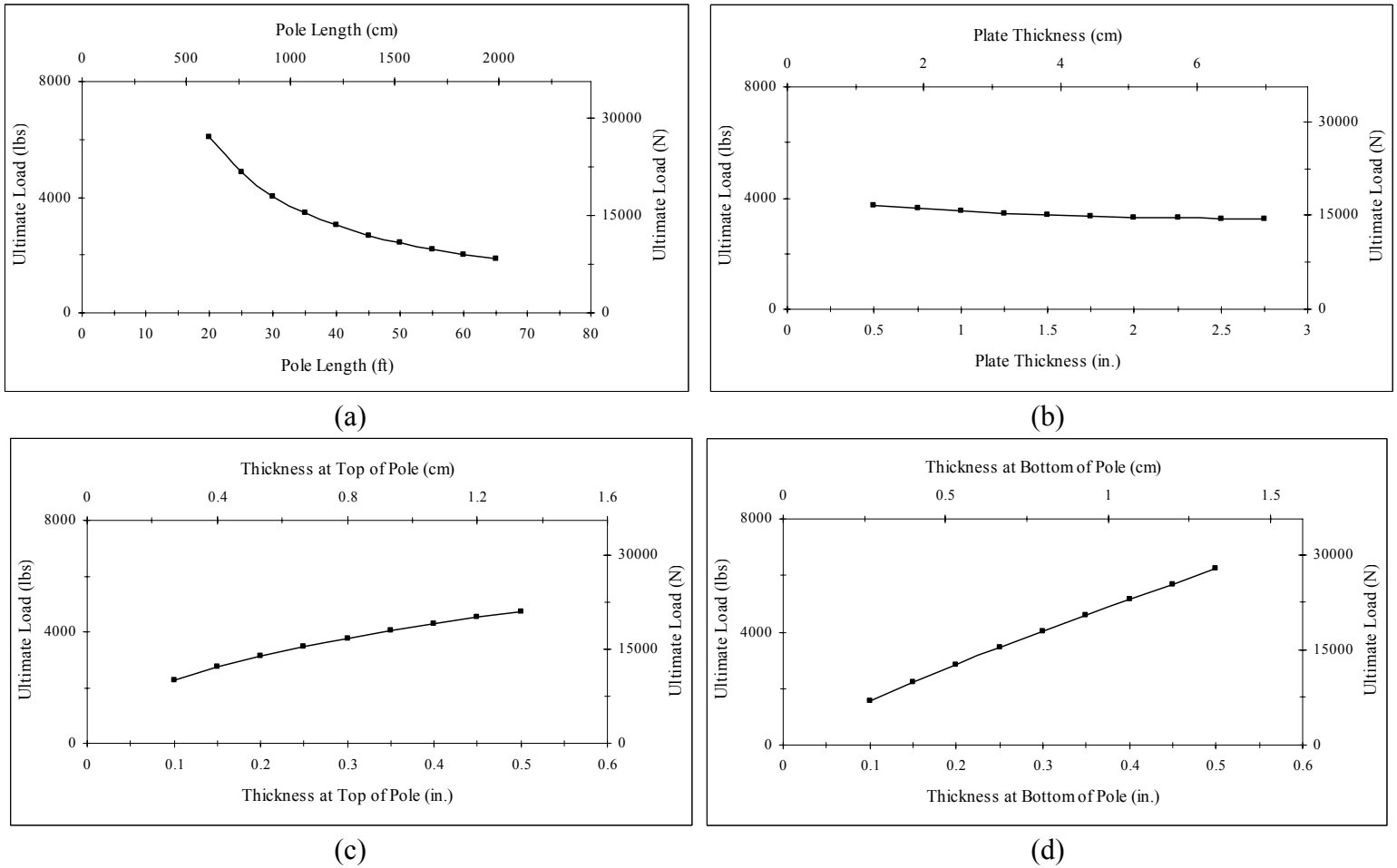

Figure E-1 Sensitivity plots of ultimate load vs. L, PT, TT, and BT for steel poles:
(a) Ultimate load vs. pole length; (b) Ultimate load vs. plate thickness;
(c) Ultimate load vs. thickness at top of pole; (d) Ultimate load vs. thickness at bottom of pole

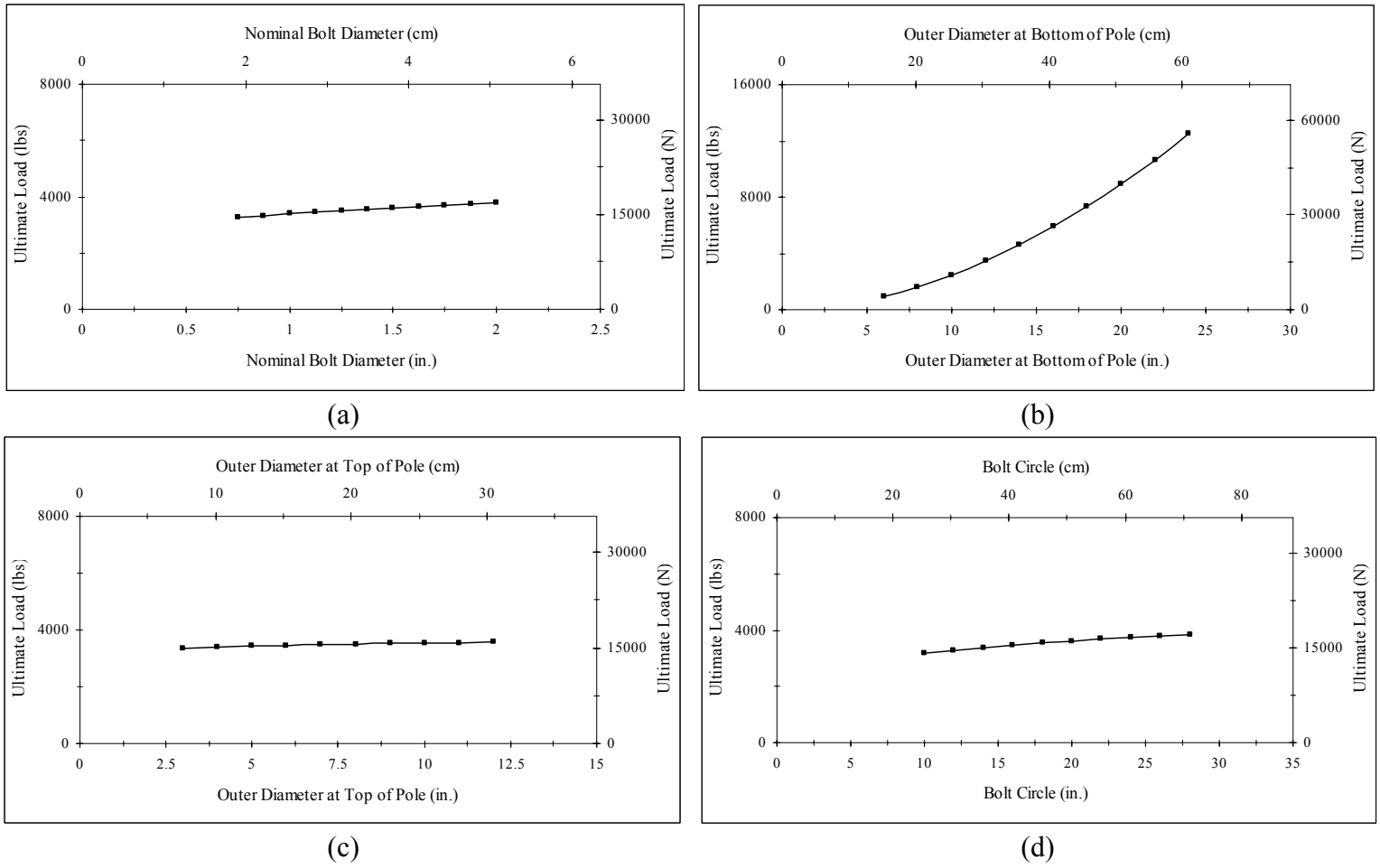

Figure E-2 Sensitivity plots of ultimate load vs. DB, BD, TD, and BC for Steel poles:
(a) Ultimate load vs. nominal bolt diameter; (b) Ultimate load vs. outer diameter at bottom of pole;
(c) Ultimate load vs. outer diameter at top of pole; (d) Ultimate load vs. bolt circle

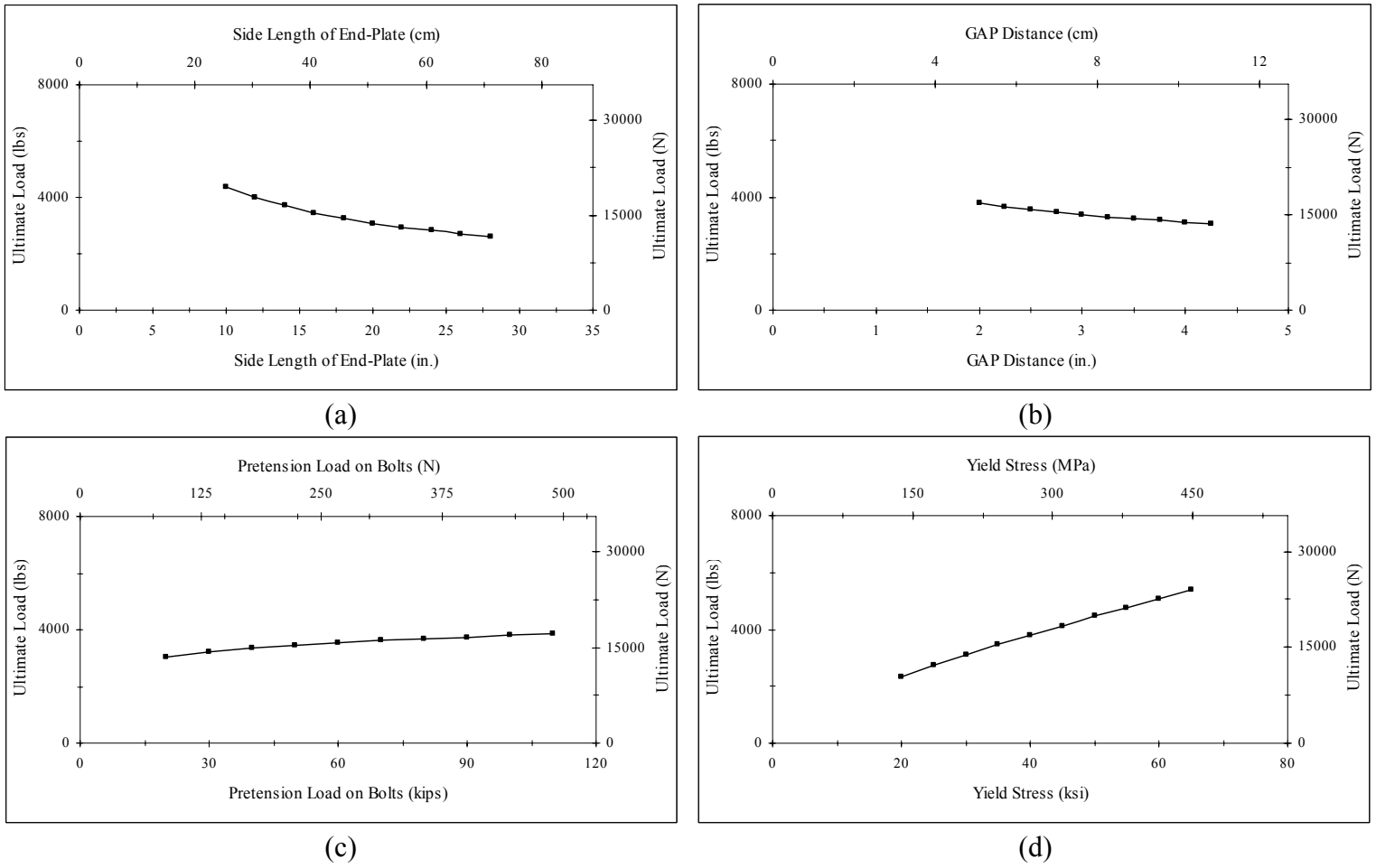

Figure E-3 Sensitivity plots of ultimate load vs. PD, GAP, F_p, and F_y for steel poles: (a) Ultimate load vs. side length of end-plate; (b) Ultimate load vs. GAP distance; (c) Ultimate load vs. pretension load on bolts; (d) Ultimate load vs. yield stress

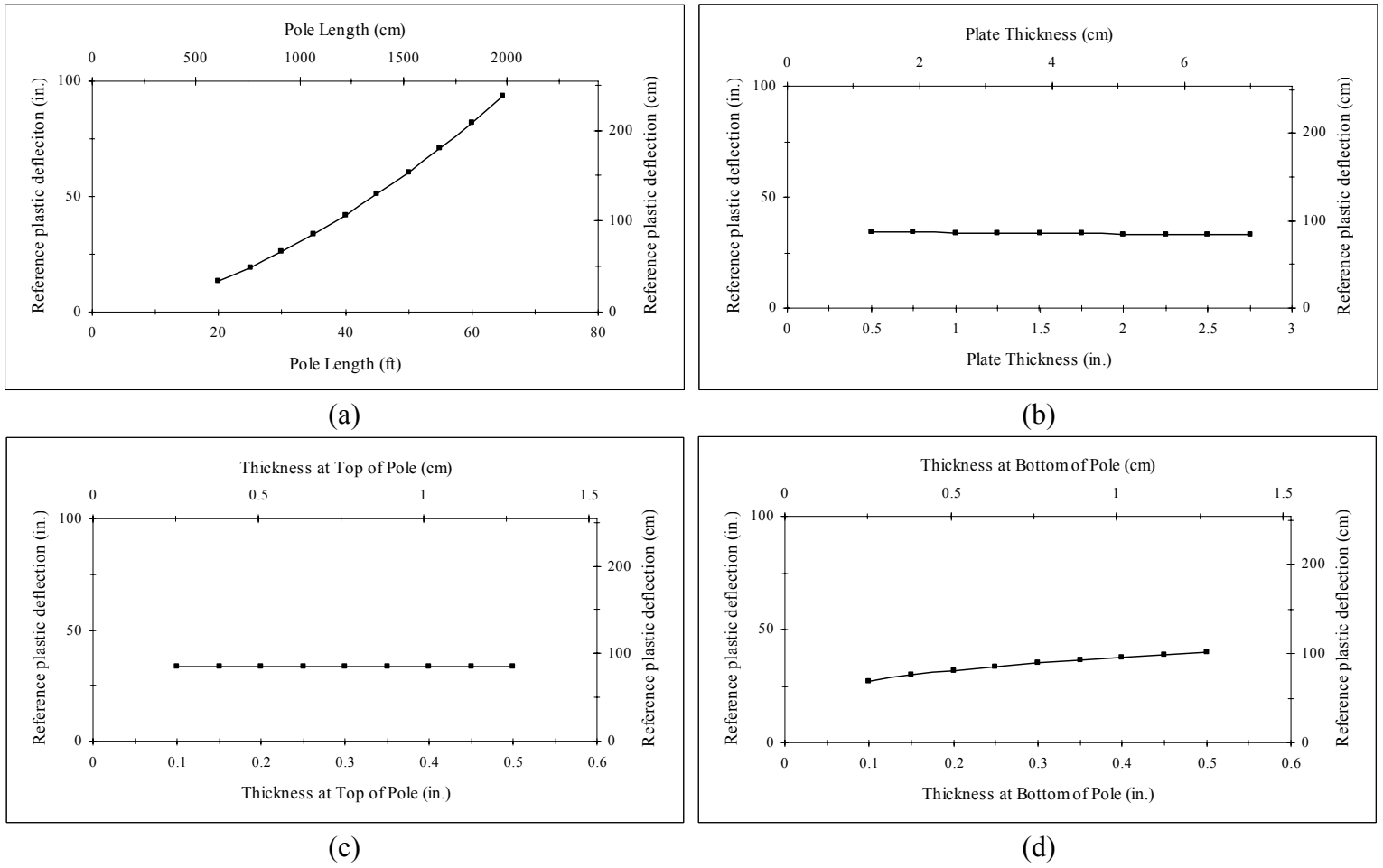

Figure E-4 Sensitivity plots of reference plastic deflection vs. L, PT, TT, and BT for steel poles:
(a) δ_0 vs. pole length; (b) δ_0 vs. plate thickness;
(c) δ_0 vs. thickness at top of pole; (d) δ_0 vs. thickness at bottom of pole

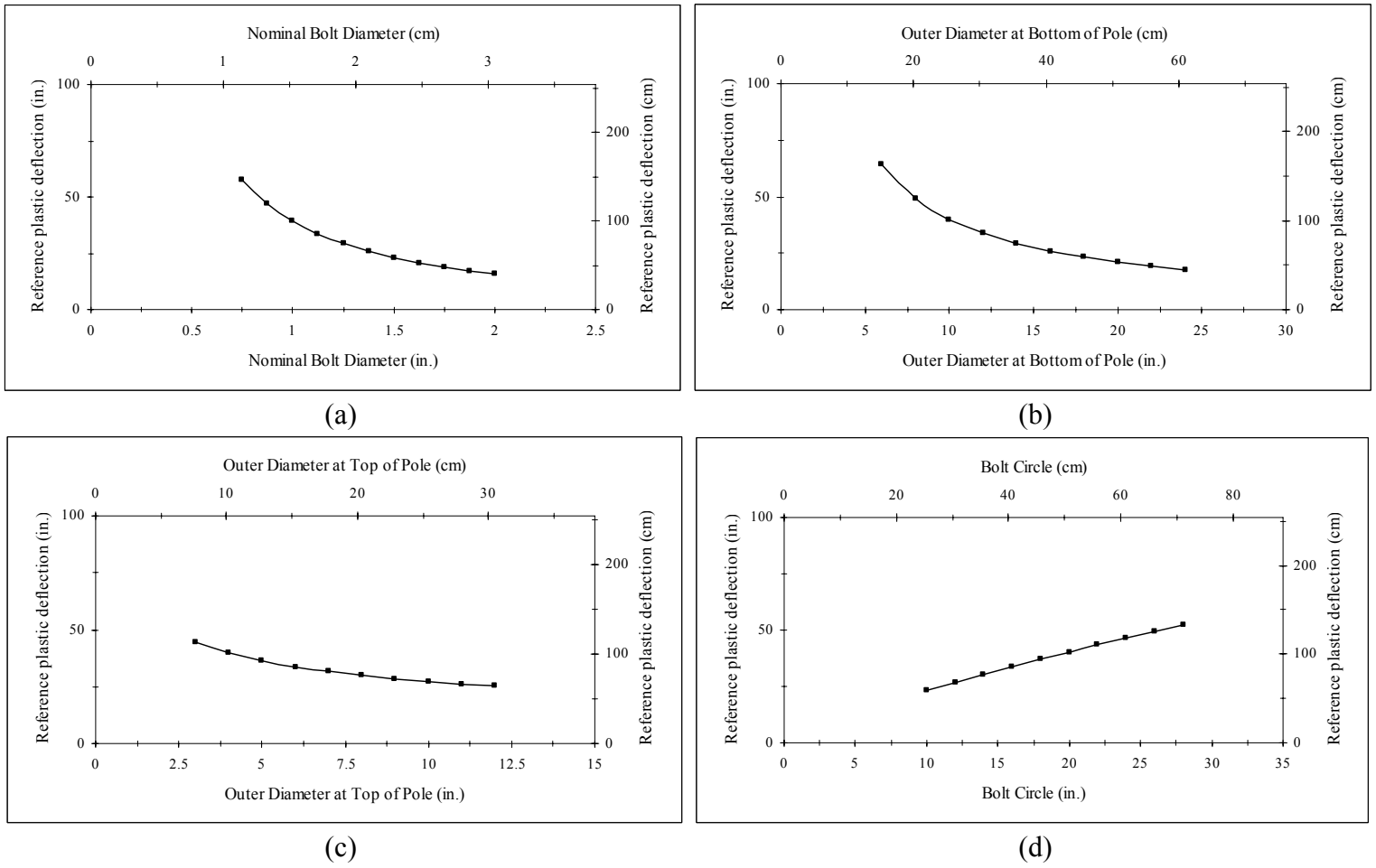

Figure E-5 Sensitivity plots of reference plastic deflection vs. DB, BD, TD, and BC for steel poles:
(a) δ_0 vs. nominal bolt diameter; (b) δ_0 vs. outer diameter at bottom of pole;
(c) δ_0 vs. outer diameter at top of pole; (d) δ_0 vs. bolt circle

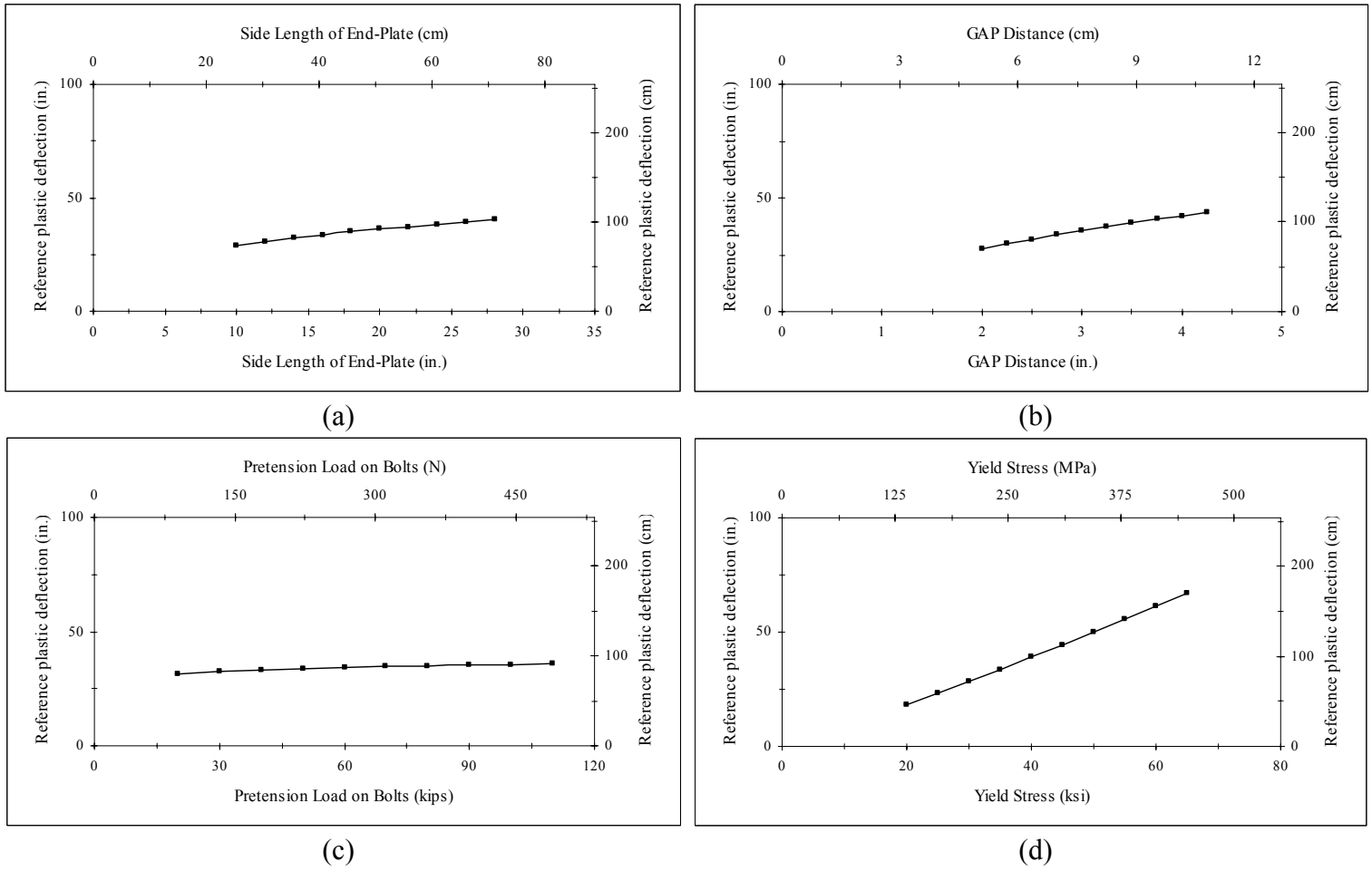

Figure E-6 Sensitivity plots of reference plastic deflection vs. PD, GAP, F_p, and F_y for steel poles:
(a) δ_0 vs. side length of end-plate; (b) δ_0 vs. GAP distance;
(c) δ_0 vs. pretension load on bolts; (d) δ_0 vs. yield stress

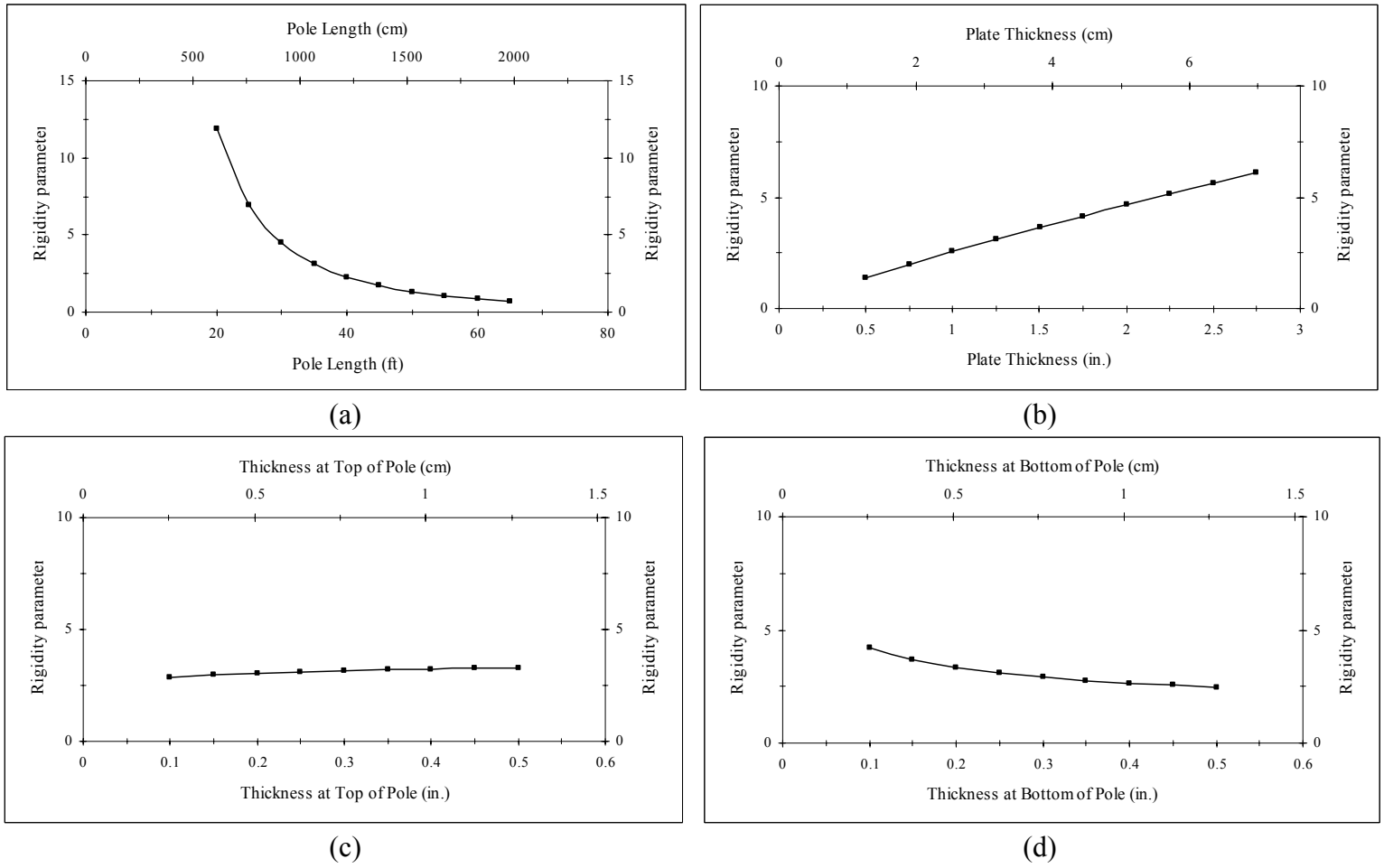

Figure E-7 Sensitivity plots of rigidity parameter vs. L, PT, TT, and BT for steel poles:
(a) Rigidity parameter vs. pole length; (b) Rigidity parameter vs. plate thickness;
(c) Rigidity parameter vs. thickness at top of pole; (d) Rigidity parameter vs. thickness at bottom of pole

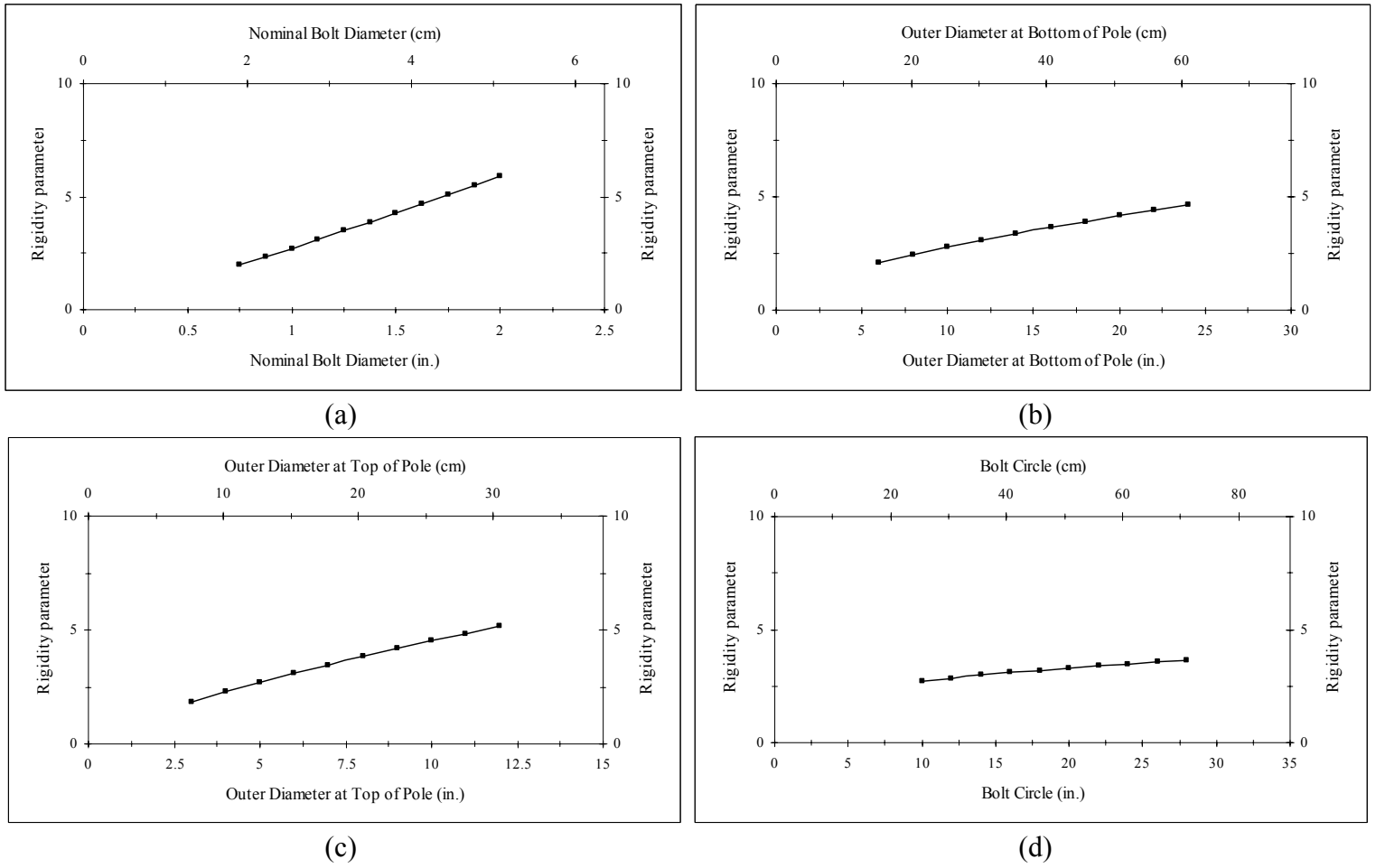

Figure E-8 Sensitivity plots of rigidity parameter vs. DB, BD, TD, and BC for steel poles:
(a) Rigidity parameter vs. nominal bolt diameter; (b) Rigidity parameter vs. outer diameter at bottom of pole;
(c) Rigidity parameter vs. outer diameter at top of pole; (d) Rigidity parameter vs. bolt circle

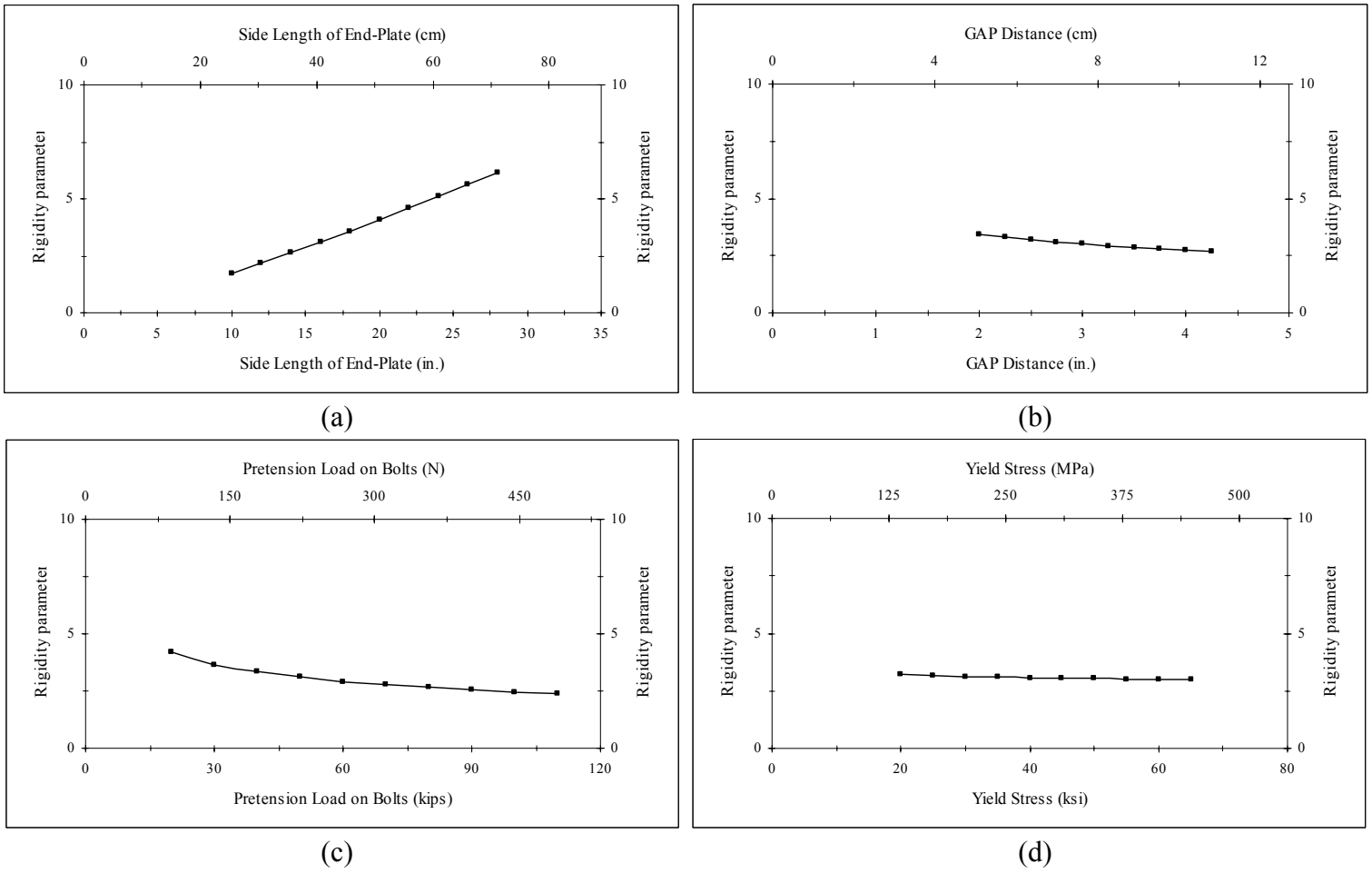

Figure E-9 Sensitivity plots of rigidity parameter vs. PD, GAP, F_p, and F_y for steel poles:
(a) Rigidity parameter vs. side length of end-plate; (b) Rigidity parameter vs. GAP distance;
(c) Rigidity parameter vs. pretension load on bolts; (d) Rigidity parameter vs. yield stress

APPENDIX F

SENSITIVITY PLOTS FOR FRP POLES

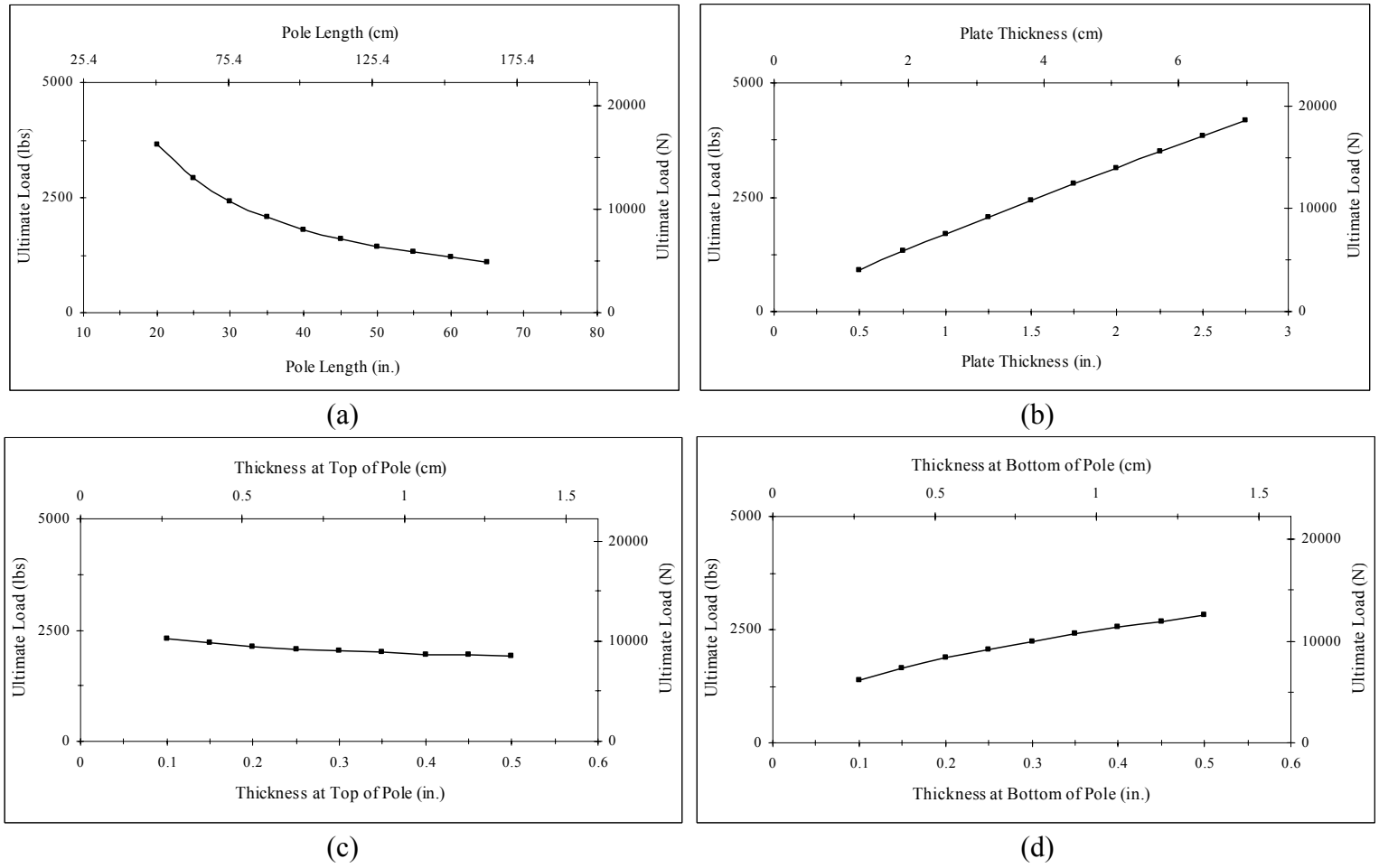

Figure F-1 Sensitivity plots of ultimate load vs. L, PT, TT, and BT for FRP poles:
(a) Ultimate load vs. pole length; (b) Ultimate load vs. plate thickness;
(c) Ultimate load vs. thickness at top of pole; (d) Ultimate load vs. thickness at bottom of pole

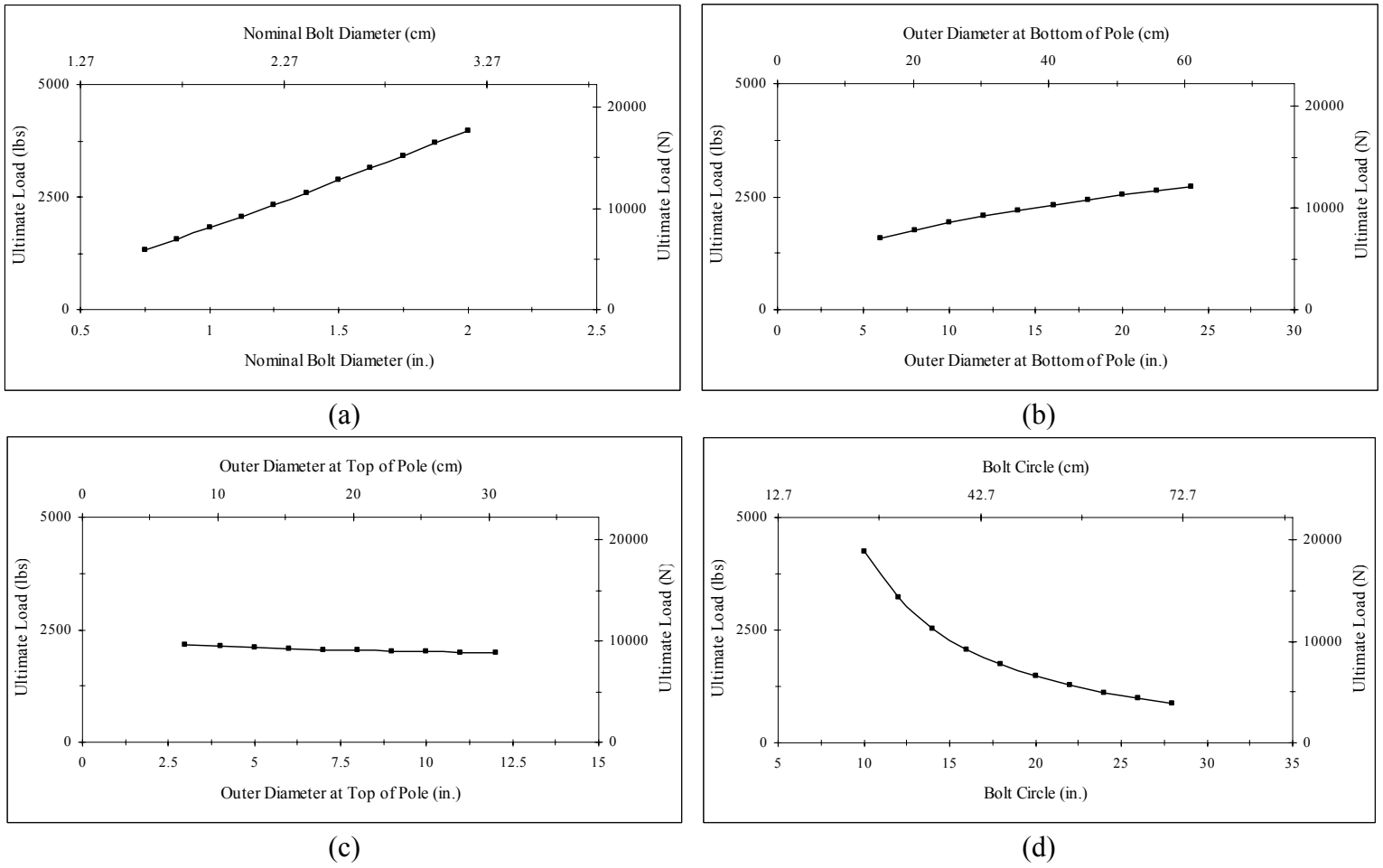

Figure F-2 Sensitivity plots of ultimate load vs. DB, BD, TD, and BC for FRP poles:
(a) Ultimate load vs. nominal bolt diameter; (b) Ultimate load vs. outer diameter at bottom of pole;
(c) Ultimate load vs. outer diameter at top of pole; (d) Ultimate load vs. bolt circle

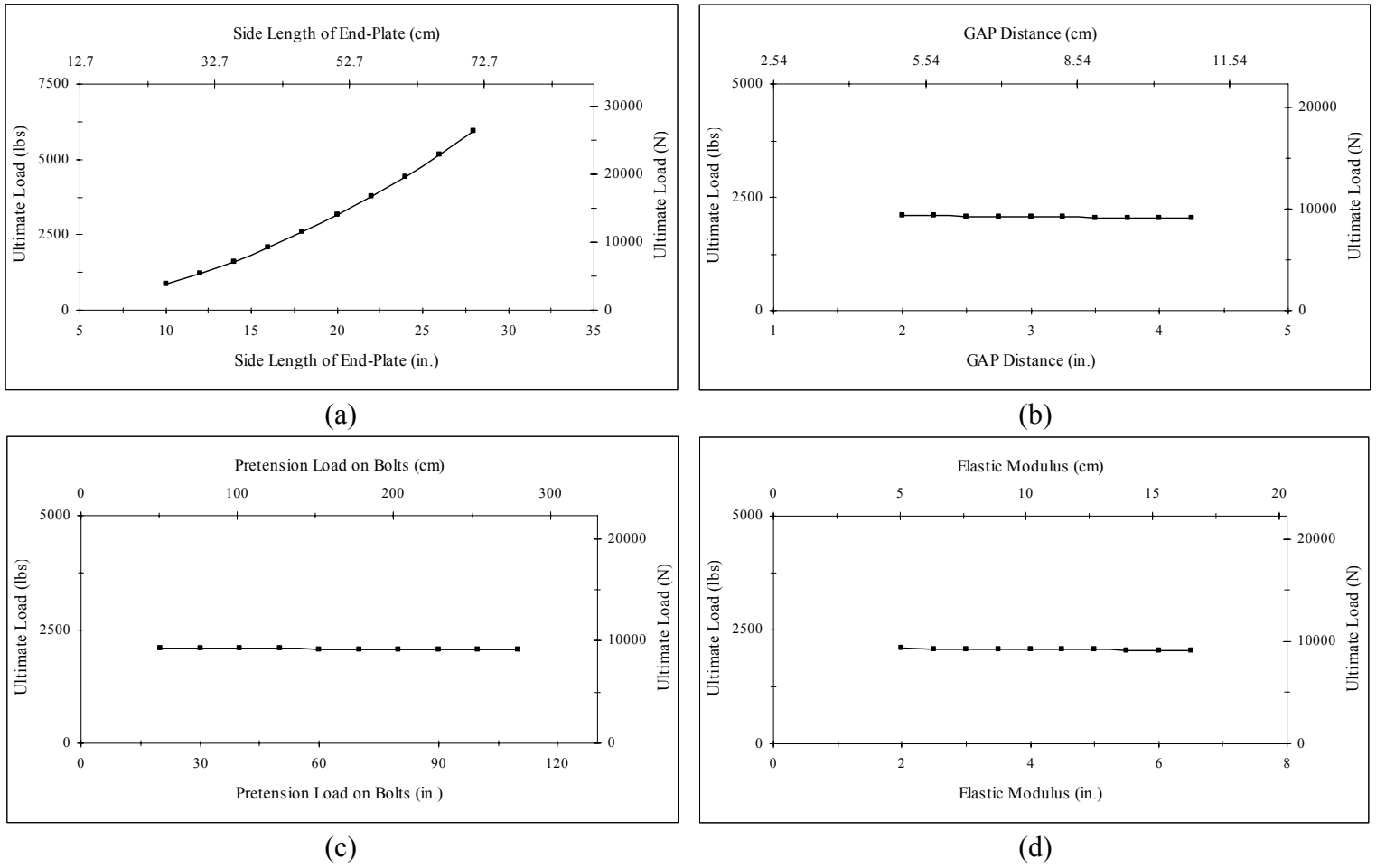

Figure F-3 Sensitivity plots of ultimate load vs. PD, GAP, F_p, and E for FRP poles: (a) Ultimate load vs. side length of end-plate; (b) Ultimate load vs. GAP distance; (c) Ultimate load vs. pretension load on bolts; (d) Ultimate load vs. elastic modulus

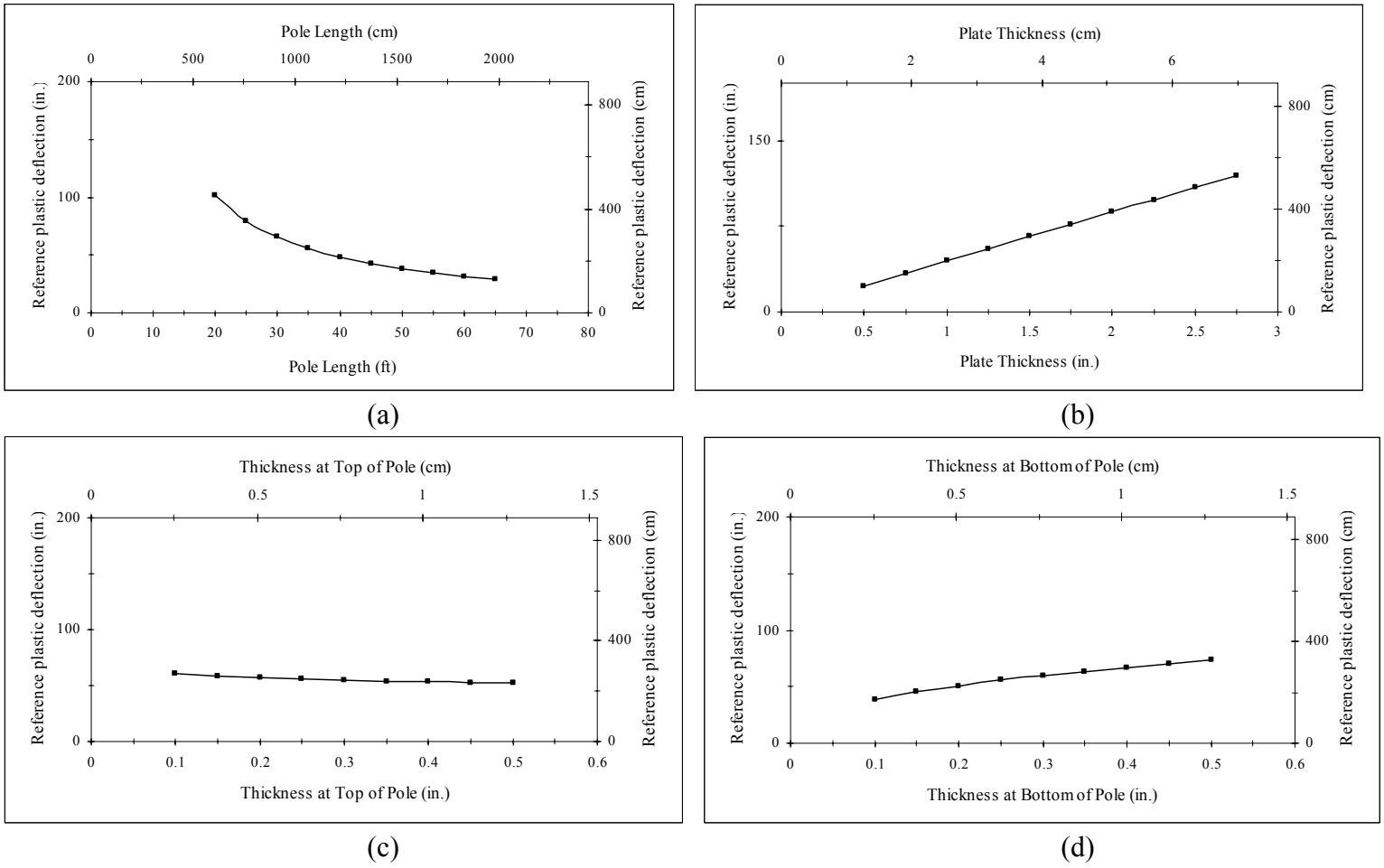

Figure F-4 Sensitivity plots of reference plastic deflection vs. L, PT, TT, and BT for FRP poles:
(a) δ_0 vs. pole length; (b) δ_0 vs. plate thickness;
(c) δ_0 vs. thickness at top of pole; (d) δ_0 vs. thickness at bottom of pole

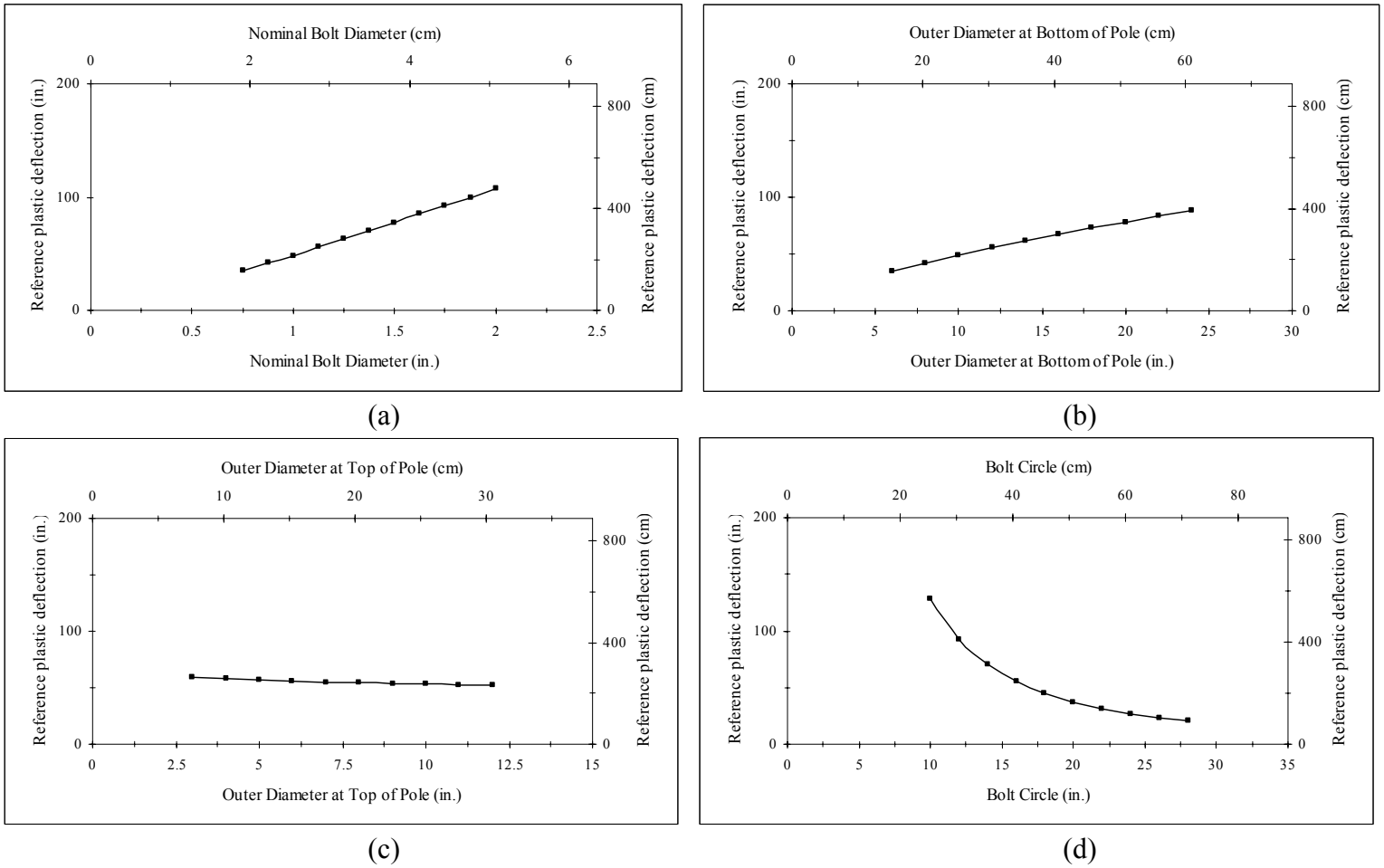

Figure F-5 Sensitivity plots of reference plastic deflection vs. DB, BD, TD, and BC for FRP poles:
(a) δ_0 vs. nominal bolt diameter; (b) δ_0 vs. outer diameter at bottom of pole;
(c) δ_0 vs. outer diameter at top of pole; (d) δ_0 vs. bolt circle

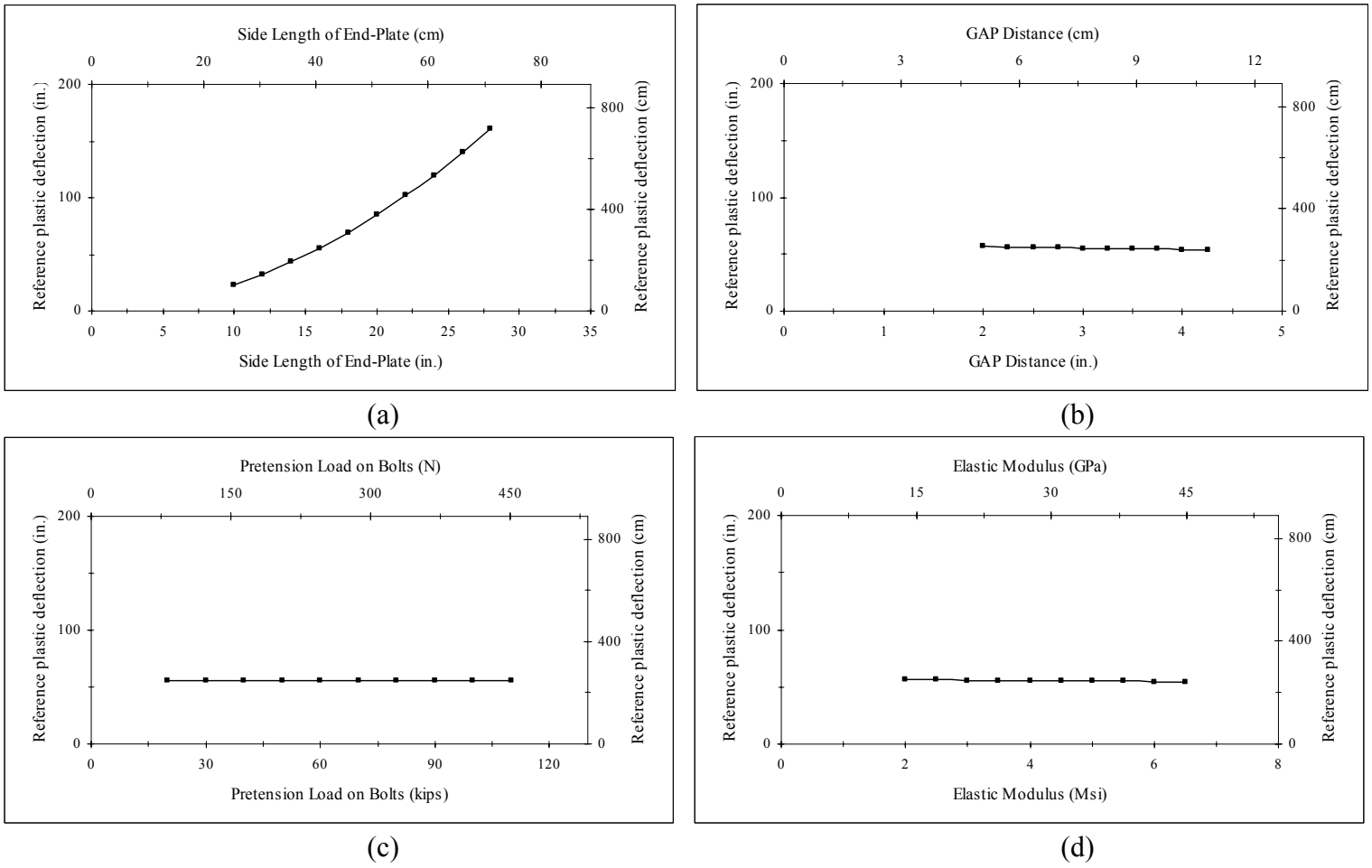

Figure F-6 Sensitivity plots of reference plastic deflection vs. PD, GAP, F_p, and E for FRP poles:
(a) δ_0 vs. side length of end-plate; (b) δ_0 vs. GAP distance;
(c) δ_0 vs. pretension load on bolts; (d) δ_0 vs. elastic modulus

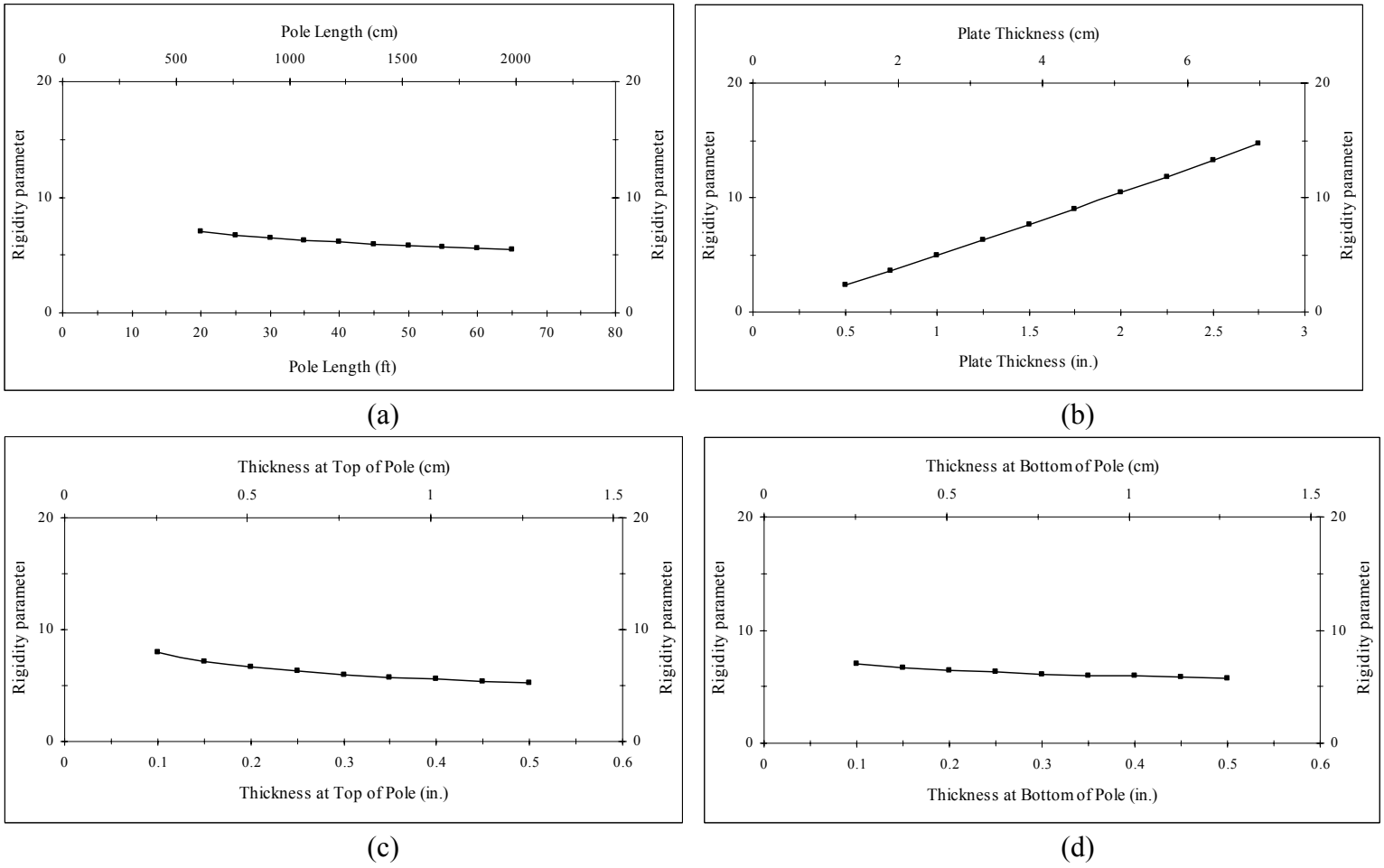

Figure F-7 Sensitivity plots of rigidity parameter vs. L, PT, TT, and BT for FRP poles:
(a) Rigidity parameter vs. pole length; (b) Rigidity parameter vs. plate thickness;
(c) Rigidity parameter vs. thickness at top of pole; (d) Rigidity parameter vs. thickness at bottom of pole

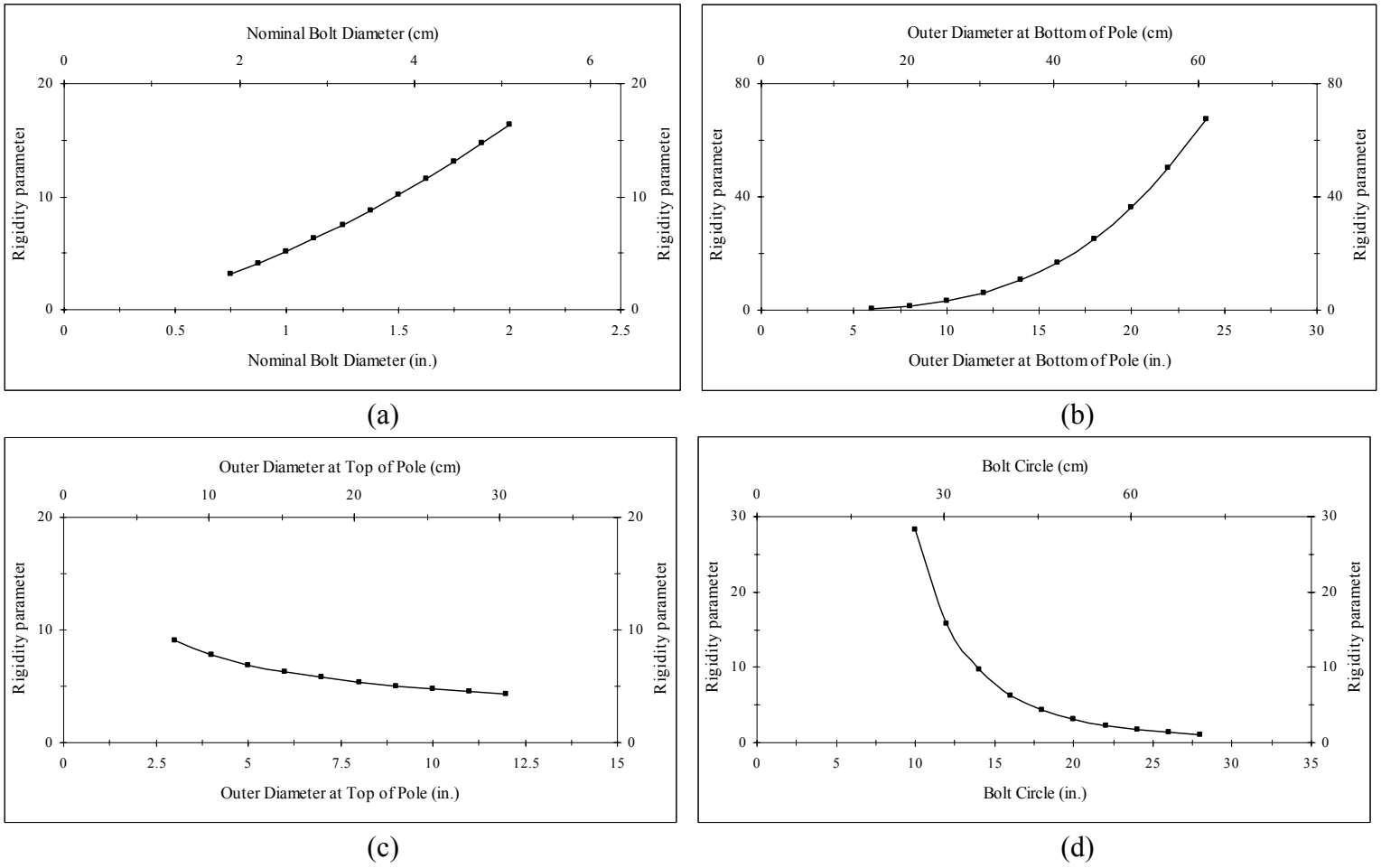

Figure F-8 Sensitivity plots of rigidity parameter vs. DB, BD, TD, and BC for FRP poles:
(a) Rigidity parameter vs. nominal bolt diameter; (b) Rigidity parameter vs. outer diameter at bottom of pole;
(c) Rigidity parameter vs. outer diameter at top of pole; (d) Rigidity parameter vs. bolt circle

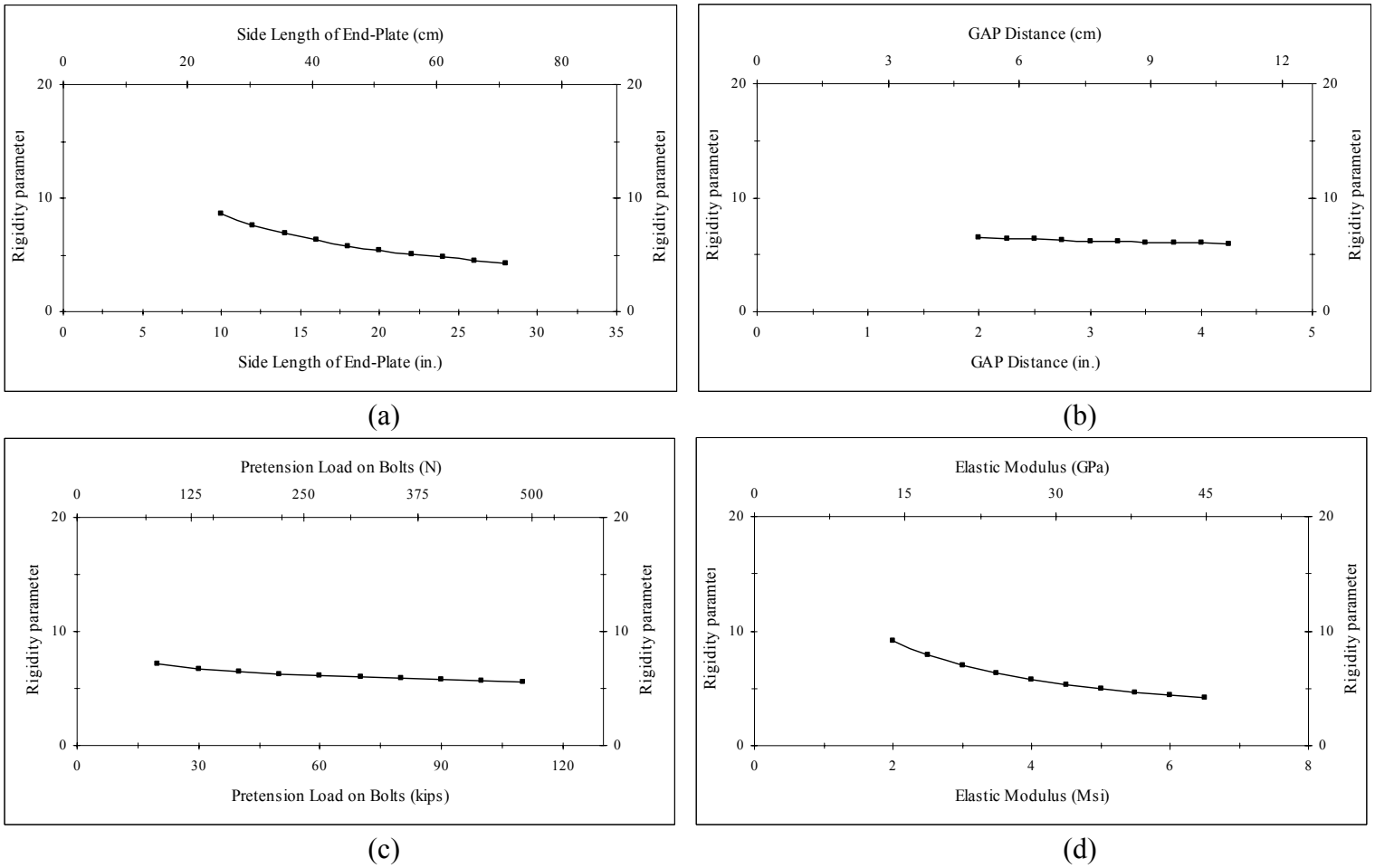

Figure F-9 Sensitivity plots of rigidity parameter vs. PD, GAP, F_p, and E for FRP poles:
(a) Rigidity parameter vs. side length of end-plate; (b) Rigidity parameter vs. GAP distance;
(c) Rigidity parameter vs. pretension load on bolts; (d) Rigidity parameter vs. elastic modulus

REFERENCES

AISC (1999), Load and resistance factor design specification for structural steel building, American Institute of Steel Construction, Chicago, IL.

ANSI 05.1 (1992), American national standard for wood poles specifications and dimensions, American National Standards Institute, New York, NY.

ANSYS (2004), user manual, Release 9.0, Canonsburg, PA.

ASTM (2005), D1036-99, Standard Test Methods of Static Tests of Wood Poles, American Society for Testing and Materials, West Conshohocken, PA.

FHWA, Federal Highway Administration, Washington, DC.

IEEE (2002), National Electrical Safety Code, Institute of Electrical and Electronic Engineers, Piscataway, NJ.

"Composite utility poles may eliminate toxic waste." Reinforced Plastics, Vol. 42, No. 6, June 1998, pp. 6.

"RSI installs first modular composite utility pole." Reinforced Plastics, Vol. 49, No. 1, January 2005, pp. 7.

Abolmaali, A., Matthys, J. H., Farooqi, M., and Choi, Y. (2004 a). "Development of moment-rotation model equations for flush end-plate connection." Journal of Constructional Steel Research, In Press, Corrected Proof, Available online 14 June 2005.

Abolmaali, A., Yuan, R. L., Choi, Y., and Shah, A., (2004 b). "Stiffness Characteristics of Closed Circuit Television Camera Steel Poles." Proceedings of the 84th Transportation Research Board Conference, January 9-13, on CD Rom.

Ang, K. M., and Morris, G. A. (1984). "Analysis of three-dimensional frame with flexible beam-column connections." Canadian Journal of Civil Engineering, Vol. 11, pp. 245-254.

Attiogbe, E., and Morris, G. (1991). "Moment-rotation functions for steel connections." Journal of Structural Engineering, Vol. 117, No. 6, pp. 1703-1718.

Azizinamini, A. (1985). "Cyclic characteristics of bolted semi-rigid steel beam to column connections." Ph.D. thesis, University of South Carolina, Columbia.

Bahaari, M. R., and Sherbourne, A. N. (1997). "Finite element prediction of end plate connection behavior." Journal of Structural Engineering, Vol. 123, No. 2, pp. 165-175.

Bahaari, M. R., and Sherbourne, A. N. (2000). "Behavior of eight-bolt large capacity endplate connections." Computers and Structures, 77, pp. 315-325.

Baniotopoulous, C. C., and Abdalla, K. M. (1995). "Sensitivity analysis results on the separation problem of bolted steel column-to-column connections." International Journal of Solids and Structures, Vol. 32, No. 2, pp. 251-265.

Bathe, K. J. (1996). "Finite element procedures." Prentice-Hall, Upper Saddle River, NJ.

Belgacem, F. B., Hild, P., and Laborde, P. (1998). "The mortar finite elemnt method for contact problems." Mathematical Computer Modeling, Vol. 28, No. 4-8, pp. 263-271

Boresi, A. P., Schmidt, R. J., and Sidebottom, O. M. (1993). "Advanced Mechanics of Material." Fifth Edition, John Willey & Sons, New York.

Chen, W. F., and Kishi, N. (1987). "Moment-rotation relation of top- and seat-angle connections." Proceedings of the International Colloquium on Bolted and Special Connection, Moscow.

Chen, W. F., Goto, Y., and Liew, J. Y. (1996). "Stability design of semi-rigid frames." John Wiley & Sons, New York.

Chen, W. F., and Han, D. J. (1988). "Plasticity for structural engineering." Springer-Verlag Publications, New York.

Choi, C. K., and Chung, G. T. (1996). "A gap element for three-dimensional elasto-plastic contact problems." Computers and Structures, Vol. 61, No. 6, pp. 1155-1167.

Chung, K. F., and Ip, K. H. (2001). "Finite element investigation on the structural behavior of cold-formed steel bolted connections." Engineering Structures, Vol. 23, pp. 1115-1125.

Chutima, S., and Blackie, A. P. (1996). "Effect of pitch distance, row spacing, end distance and bolt diameter on multi-fastened composite joints." Composites Part A, Vol. 27, 2, pp. 105-110.

Citipitioglu, A. M., Haj-Ali, R. M., and White, D. W. (2002). "Refined 3D finite element modeling of partially-restrained connections including slip." Journal of constructional Steel Research, 58, pp. 995-1013.

Colson, A., and Louveau, J. M. (1983). "Connections incidence on the inelastic behavior of steel structures." Proceedings of the Euromech Colloquium, October, pp. 174.

Crisfield, M. A. (1997). "Non-linear Finite element Analysis of Solids and Structures." John Wiley & Sons, New York.

Daniel, I. M., and Ishai, O. (2005). "Engineering Mechanics of Composite Materials." Second Edition, Oxford University Press.

Dicleli, M. (1997). "Computer-aided optimum design of steel Tubular telescopic pole structures." Computers & Structures, Vol. 62, No. 6, pp. 961-973.

Frye, M. J., and Morris, G. A. (1975). "Analysis of flexibly connected steel frames." Canadian Journal of Civil Engineers, Vol. 2, pp. 280-291.

Fu, Gongkang, and Boulos, S. J. (1996). "Finite element analysis of irregular thick plates for signal pole design." Computers and Structures, Vol. 58, No. 1, pp. 221-232.

Gantes, C. J., and Lemonis, M, E. (2003). "Influence of equivalent bolt length in finite element modeling of T-stub steel connections." Computers and Structures, Vol. 81, pp. 595-604.

Gun, H. (2004). "Boundary element analysis of 3-D elasto-plastic contact problems with friction." Computers and Structures, Vol. 82, pp. 555-566.

Guyot, N., Kosior, F., and Maurice, G. (2000). "Coupling of finite elements and boundary elements methods for study of the frictional contact problem." Computer Methods in Applied Mechanics and Engineering, Vol. 181, pp. 147-159

Harte, A. M., and Cann, D. M. (2001). "Finite element modeling of the semi-rigid behavior of pultruded FRP connections." Journal of Materials Processing Technology, Vol. 119, pp. 98-103.

Huang, D. Y., and Stallings, J. M. (1994). "Finite element analysis of bolted flange connections." Computers and Structures, Vol. 51, No. 5, pp. 521-533.

Huang, Y., and Leu, D. (1995). "Finite element analysis off contact problems for a sheet metal bending process." Computers and Structures, Vol. 57, No. 1, pp. 15-27.

Ibrahim, S., Polyzois, D., and Hassan, S. K. (2000). "Development of glass fiber reinforced plastic poles for transmission and distribution lines." Canadian Journal of Civil Engineering, Vol. 25, No. 2, pp. 850-858.

Ibrahim, S., and Polyzois, D. (1999). "Ovalization analysis of fiber-reinforced plastic poles." Composite Structures, 45, pp. 7-12.

Jones, R. M. (1999). "Mechanics of Composite Material." Second Edition, Taylor & Francis.

Jones, S. W., Kirby, P. A., and Nethercot, D. A. (1980). "Effect of semi-rigid connections on steel column strength." Journal of Constructional Steel Research, Vol. 1, No. 1, pp. 38-46.

Jones, S. W., Kirby, P. A., and Nethercot, D. A. (1981). "Modeling of semi-rigid connection behavior and its influence on steel column behavior." in Joints in Structural Steelwork, Pentech Press, London, pp. 5.73-5.78.

Keating, P. B., James, R. W., Richards, J. H., and Rinehart, A. J. (2004). "Supplement laboratory testing to extend scope of proposed standard method of tighting of anchor bolts." TXDOT Contract No. 46-MTIA005, TTI SL No. 409090, February.

Kishi, N., and Chen, W. F. (1990). "Moment-rotation relations of semi-rigid connections with angles." Journal of Structural Engineering, ASCE, Vol. 116, No. 7, pp. 1813-1834.

Kishi, N., Chen, W. F., Goto, Y., and Matsuoka, K. G. (1991). "Applicability of three-parameter power model to structural analysis of flexibly jointed frames." Proceedings of Mechanics Computing in 1990's and Beyond, Columbus, Ohio.

Kishi, N., Chen, W. F., Matsuoka, K. G., and Nomachi, S. G. (1988a). "Moment-Rotation Relation of Top- and Seat-Angle with Double Web-Angle Connections." Proceedings of the State-of-the-Art Workshop on Connections and the Behavior, Strength and Design of Steel Structures, pp. 121-134.

Kish, N., Chen, W. F., Matsuoka, K. G., and Nomachi, S. G. (1988b). "Moment-rotation relation of single/double web-angle connections." Proceedings of the State-of-the-Art Workshop on Connections and the Behavior, Strength and Design of Steel Structures, pp. 135-149.

Kishi, N., Ahmed, A., Yabuki, N., and Chen, W. F. (2001). "Nonlinear finite element analysis of top- and seat-angle with double web-angle connections." Structural Engineering and Mechanics, Vol. 12, No. 2, pp. 201-214.

Krishnamurthy, N., and Graddy, D. E. (1976). "Correlation between 2- and 3-dimensional finite element analysis of steel bolted end-plate connections." Computers and Structures, Vol. 6, pp. 381-389.

Krishnamurthy, N., Huang, H. T., Jefferey, P. K., and and Avery, L. K. (1979). "Analytical M-θ Curves for End-Plate Connections." Journal of Structural Engineering. ASCE, Vol. 105, No. ST1, pp. 133-145.

Krishnamurthy, N. (1980). "Modeling and prediction of steel bolted connection behavior." Computers and Structures, Vol. 11, pp. 75-82.

Kocer, F. Y., and Arora, J. S. (1996). "Optimal design of steel transmission poles." Journal of Structural Engineering, November, pp. 1347-1356.

Kocer, F. Y., and Arora, J. S. (1997). "Standardization of steel pole design using discrete optimization." Journal of Structural Engineering, March, pp. 345-349.

Komuro, M., and Kishi, N. (2003). "Quasi-static loading tests on moment-rotation behavior of top- and seat-angle connections." STESSA Conference, pp. 329-334.

Kukreti, A. R., Murray, T. M., and Abolmaali, A. (1987). "End-plate connection moment-rotation relationship." Journal of Constructional Steel Research, Vol. 8, pp. 137-157.

Kukreti, A. R., Murray, T. M., and Ghassemieh, M. (1989). "Finite element modeling of large capacity stiffened steel tee-hanger connections." Computers and Structures, Vol. 32, pp. 409-422.

Kulak, G. L., and Birkemoe, P. C. (1993). "Field studies of bolt pretension." Journal of Steel Research, Vol. 25, pp. 95-106.

Lacoursiere, B. (1999). "Steel utility poles: Advantages and application." IEEE Conference Paper, No. 99B2.

Lin, Z. M. (1995). "Analysis of pole-type structures of fiber-reinforced plastics by finite element method," Ph.D. Dissertation, University of Manitoba, Canada.

Lui, E. M., and Chen, W. F. (1986). "Analysis and behavior of flexibly jointed frames." Engineering Structures, Vol. 8, No. 2, pp. 107-118.

McDonald, J. R., Mehta, K. C., Oler, W. W., and Pulipaka, N. (1995). "Wind load effects on signs, luminaries and traffic signal structures." Texas Tech University Research Study, No. 11-5-92-1310.

McClure, G., Boire, L., and Carriere, J. C. (1992). "Applications of advanced composite materials in overhead power lines and telecommunications structures." Advanced Composite in Bridges and Structures, First International Conference. pp. 543-549.

Morozov, E. V. (2004). "Mechanics and analysis of fabric composites and structures." AUTEX Research Journal, Vol. 4, No.2, pp. 60-71.

Myslinski, A. (1997). "Mixed finite element approach for shape optimal design of large displacement contact problems." Computers and Structures, Vol. 64, No. 1-4, pp. 595-602.

Naughton, B. P., Panhuizen, F., and Venmeulen, A. C. (1985). "The elastic properties of chopped strand mat and woven roving in g.r.laminea." Journal of Reinforced Plastics and Composites, Vol. 4, No. 2, pp. 195-204.

Oldfield, M., Ouyang, H., and Mottershead, J. (2003). "Modeling and simulation of bolted joints under harmonic excitation." Materials Science Forum, Vol. 440-441, pp. 421-428.

Peyrot, A. H. (1982). "Large deflection analysis of beams, pipes, or poles." Engineering Structures, Vol. 4, pp. 11-16.

Pilkey, W. D. (1994). "Stress, Strain, and Structural Matrices." John Wiley & Sons, New York.

Piluso, V, Faella, C., and Rizzano, G. (2001). "Ultimate behavior of bolted T-stubs. I: Theoretical model." Journal of Structural Engineering, Vo. 127, No. 6, pp. 686-693.

Polyzois, D., Ibrahim, S., and Raftoyiannis, I. G. (1999). "Performance of fiber-reinforced plastic tapered poles under lateral loading." Journal of Composites Materials, Vol. 33, No. 10, pp. 941-960.

Polyzois, D., Raftoyiannis, I. G., and Ibrahim, S. (1998). "Finite elements method for the dynamic analysis of tapered composite poles." Composite Structures, 43, pp. 25-34.

Raj, N. S., Dattaguru, B., Krishnamurthy, T., and Ramamurthy, T. S. (1987). "Analysis of flange joints with elastic bolt." Nuclear Engineering Design, Vol. 100, pp. 41-48.

Ramberg, W., and Osgood, W. R. (1943). "Description of stree-strain curves by three parameters." Technical Note 902, Washington, DC: National Advisory Connittee for Aeronautics.

Reddy, J. N. (1993). "Introduction to the finite element method." McGraw-Hill Science, Second Edition.

Richard, R. M. and Abbott, B. J., (1975). "Versatile elastic-plastic stress-strain formula." Journal of the Engineering Mechanics Division, ASCE, Vol.101, No. EM4, pp 511-515.

Richard, R. M., Gillet, P. E., Kriegh, J. D., and Lewis, B. A. (1980). "The analysis and design of single plate framing connections." AISC Engineering Journal, Second Quarter, pp. 38-52.

Shenoi, R. A., and Wellicome, J. F. (1993). "Composite materials in maritime structures." Vol. 1: Fundamental Aspects, Cambridge University Press.

Solberg, J. M., and Papadopoulos, P. "A finite element method for contact/impact." Finite Elements in Analysis and Design, Vol. 30, pp. 297-311.

Stallings, J. M., and Hwang, D. Y. (1992). "Modeling pretensions in bolted connections." Computers and Structures, Vol. 45, No. 4, pp. 801-803.

Statik, H., Gebeken, N., and Binder, B. (1992). "Nonlinear three dimensional finite element contact analysis of bolted connections in steel frames." International Journal of Numerical Methods in Engineering, Vol. 34, No. 11, pp. 3122-3136.

Sherbourne, A. N., and Bahaari, M. (1997). "Finite element prediction of end plate bolted connection behavior. I: Parametric study." Journal of Structural Engineering, Vol. 123, No. 2, pp. 157-164.

Sommer, W. H. (1969). "Behavior of welded-header-plate connections." M. S. thesis, University of Toronto.

Stallings, J. M., and Hwang, D. Y. (1992). "Modeling pretensions in bolted connections." Computers and Structures, Vol. 45, No. 4, pp. 801-803.

Tsai, S. W., and Wu, E. M. (1971). "A general theory of strength for anisotropic material." Journal of Composites Materials, Vol. 5, pp. 58-80.

Wanzek, T., and Gebbeken, N. (1999). "Numerical aspects for the simulation of end plate connections." Report of Working Group 6 – Numerical simulation of semi-rigid connections by the finite element method, Brussels, Luxembourg, pp. 13-31.

Wu, F. S., and Chen, W. F. (1990). "A design model for semi-rigid connections." Engineering Structures, Vol. 12, No. 2, pp. 88-97.

Yang, J. G. (1997). “Double angle framing connections subjected to shear and tension.” Ph. D. thesis, Virginia Polytechnic Institute and State University, Blacksburg, VA.

Yee, Y. L., and Melchers, R. E. (1986). “Moment-rotation curves for bolted connections.” Journal of Structural Engineering, ASCE, Vol. 112, No. ST3, pp. 615-635.

Yang, J. G., Murray, T. M., and Plaut, R. H. (2000). “Three-dimensional finite element analysis of double angle connections under tension and shear.” Journal of Constructional Steel Research, Vol. 54, pp. 227-244.

Yorgun, C., Dalc1, S., and Altay, G. A. (2004). “Finite element modeling of bolted steel connections designed by double channel.” Computers and Structures, 82, pp. 2563-2571.

Vanderbilt, M. D., and Criswell, M. E. (1987). “Analysis and design of single-pole transmission structures.” Computers and Structures, Vol. 28, No. 4, pp. 551-562.

Zhu, C. (1995). “A finite element–mathematical programming method for elasto–plastic contact problems with friction.” Finite Elements in Analysis and Design, Vol. 20, pp. 273-282.